Expression of photosynthetic genes and possible regulatory mechanisms in the single-cell C_4 species, *Bienertia sinuspersici*

by

Makoto Yanagisawa

A thesis

presented to the University of Waterloo

in fulfilment of the

thesis requirement for the degree of

Doctor of Philosophy

in

Biology

Waterloo, Ontario, Canada, 2012

AUTHOR'S DECLARATION

I hereby declare that I am the sole author of this thesis. This is a true copy of the thesis, including any required final revisions, as accepted by my examiners.

I understand that my thesis may be made electronically available to the public.

_____

Makoto Yanagisawa

ABSTRACT

Bienertia sinuspersici is one of three terrestrial plants identified to perform C_4 photosynthesis in a single chlorenchyma cell by compartmentation of organelles and photosynthetic enzymes. This thesis describes a study on the distribution of photosynthetic proteins and their corresponding transcripts in an attempt to understand the regulatory mechanisms underlying their differential accumulation in two types of chloroplast. The patterns of photosynthetic enzymes and transcripts accumulation in developing leaves were examined by using immunolocalization and *in situ* hybridization. The polypeptides of Rubisco large subunit (RbcL) and pyruvate Pi dikinase (PPDK) accumulate equally in all chloroplasts before the formation of two intracellular cytoplasmic compartments: the central (CCC) and peripheral (PCC) cytoplasmic compartment. The differential accumulation of these enzymes is not completed until the mature stage, indicating that the transition from C_3 to C_4 photosynthesis occurs at the very late stage of leaf development. In mature chlorenchyma cells, RbcL accumulates 20-fold more in the CCC than in the PCC while PPDK demonstrates a concentration gradient that is lowest in chloroplasts in the center of the CCC and highest in the PCC chloroplasts. The pattern of *rbcL* transcript accumulation follows that of its polypeptides in developing leaves, suggesting the expression of this gene is controlled at the transcriptional and/or mRNA stability level. The quantitative real-time PCR results of *rbcL* transcripts from isolated chloroplasts of each compartment further supported this observation. Bioinformatics tools were used to predict possible structual motifs on *rbcL* mRNA as an attempt to speculate on their role in its distribution and identify the presence of secondary structures in the 5' untranslated region (UTR) that may function in the regulation of gene expression. Detailed examination of the ultrastructure of the unique intracellular organization in the single-cell C_4 system showed various vesicles in close proximity to chloroplasts in both compartments in mature

chlorenchyma cells of *B. sinuspersici* under H_2O_2 treatments. To further understand the biogenesis of these vesicles, imunolocalization and transient expression of green fluorescent protein (GFP) experiments were performed. These studies identified stroma-filled tubules (stromules) as the structure that participates in the formation of sequestering vesicles (autophagosomes) containing cytosol and organelles. Fluorescent microscopic analyses using autophagosome-specific and autophagic vacuole markers only showed partial overlapping of two fluorescent signals. These results suggest that the formation of autophagosome and autophagic vacuole occur independently. The contribution of stromules to autophagosome formation and the involvement of chloroplastic envelopes in this process provide another level of regulation in the compartmentation of photosynthetic enzymes in single-cell C_4 system. Collectively, the findings in this thesis enhance our overall understanding on the development and function of single-cell C_4 photosynthesis.

ACKNOWLEDGEMENTS

I would like to thank my supervisor, Dr. Simon Chuong for his guidance and support during this project. His continuous support both inside and outside school made my student life easier in Canada.

I would also like to thank members of my advisory committee, Drs. Barb Moffatt, Frederique Guinel, and Susan Lolle for their valuable advice. Thanks to Drs. Ken Wilson and Shirley Tang for being on my committee.

Thanks to the faculty and staffs of the Department of Biology for their assistance. Special thanks to Dale, Lynn, Janet, and Linda for their continuous support.

Thanks to former and current members of the Chuong's and Moffatt's lab: Terry, Sarah, Jen, Ishari, Sang, Katja, Tony, and Yong for the valuable discussion and encouragement.

Finally, I would like to thank my family, Yumiko and Mai, for their patience and support. Thanks to my parents for their ongoing support.

TABLE OF CONTENTS

LIST OF FIGURES

LIST OF ABBREVIATIONS

ABD2	Actin binding domain 2
ATG	Autophagy-related gene
ATP	Adenosine triphosphate
BS	Bundle sheath
BSA	Bovine serum albumin
CAB	Chlorophyll a/b binding protein
CAM	Crassulacean acid metabolism
CCC	Central cytoplasmic compartment
CCCI	Central cytoplasmic compartment inner region
CCCO	Central cytoplasmic compartment outer region
CS	Cell stabilizing
DIG	Digoxigenin
EGFP	Enhanced green fluorescent protein
ER	Endoplasmic reticulum
FAA	Formaldehyde - acetic acid - alcohol
GFP	Green fluorescent protein
H_2O_2	Hydrogen peroxide
M	Mesophyll
ME	Malic enzyme
NAD	Nicotinamide adenine dinucleotide
NADP	Nicotinamide adenine dinucleoside phosphate
NLS	Nuclear-localization signal

NR	Neutral red
OAA	Oxaloacetate
PAS	Pre-autophagosmal structure
PCR	Polymerase chain reaction
PEG	Polyethyleneglycol
PEP	Phospho*enol*pyruvate
PEPC	Phospho*enol*pyruvate carboxylase
PEP-CK	Phosphoenolpyruvate carboxykinase
3-PGA	3-phosphoglycerate
PI3K	Phosphatidylinositol-3-phosphate kinase
PPDK	Pyruvate, Pi dikinase
PS	Photosystem
psaB	Photosystem I core reaction center protein-encoding gene
psbA	Photosystem II D1 protein-encoding gene
psbO	Photosystem II associating 80 kD protein-encoding gene
PTS1	Peroxisomal-targeting signal 1
qPCR	Quantitative polymerase chain reaction
RACE	Rapid amplification of cDNA ends
RbcL	Ribulose 1,5-bisphosphate carboxylase/oxygenase large subunit
RbcS	Ribulose 1,5-bisphosphate carboxylase/oxygenase small subunit
RCB	Ribulose 1,5-bisphosphate carboxylase/oxygenase-containing body
ROS	Reactive oxygen species
RT	Reverse transcription
Rubisco	Ribulose 1,5-bisphosphate carboxylase/oxygenase

SAV	Senescence associate vacuole
SCV	Stroma-containing vesicle
TBST	Tris buffer saline with Tween 20
TEM	Transmission electron microscopy
TIP	Tonoplast intrinsic protein
TOR	Target-of-rapamycin
TP	Transit peptides
UTR	Untranslated region
VPS	Vacuolar-protein-sorting

CHAPTER 1. INTRODUCTION

1.1.1 Photosynthesis

Photosynthesis is the only mechanism that can convert energy derived from the sun into carbohydrates using CO_2 and water. Moreover, photosynthetic organisms have the ability to assimilate CO_2 into the organic matter that is essential for all living organisms. Depending on the CO_2 assimilation process, photosynthesis can be divided into three groups: C_3 photosynthetic carbon fixation (C_3), C_4 photosynthetic carbon fixation (C_4) and Crassulacean acid metabolism (CAM). C_4 species dominate tropical and sub-tropical regions while CAM plants are found in hot and arid conditions. According to Sage (2004), about 250,000 plant species are C_3, in contrast to 30,000 CAM and 7,500 C_4 species. Nevertheless, about 30% of terrestrial primary productivity is contributed by C_4 plants on a global basis (Gillon and Yakir, 2001). C_4 and CAM photosynthesis evolved from C_3, and they have similar biochemistries with respect to the CO_2 assimilation processes. In this thesis, C_3, C_4, and novel single-cell C_4 photosynthesis will be discussed.

1.1.2 C_3 and C_4 photosynthesis

The majority of land plants perform C_3 photosynthesis. These plants fix atmospheric CO_2 directly using ribulose 1,5-bisphosphate carboxylase/oxygenase (Rubisco), producing a 3-carbon compound, 3-phosphoglycerate (3-PGA). One major disadvantage of C_3 photosynthesis is that Rubisco is a dual functional enzyme where CO_2 and O_2 are competitive substrates;

Rubisco not only reacts with CO_2 by the carboxylase activity but also with O_2 by the oxygenase activity (Fig. 1.1). While carboxylase activity leads to net carbon assimilation, oxygenase activity leads to the release of CO_2 from fixed carbohydrate without producing energy, a process known as photorespiration. Photorespiration is a metabolically wasteful process which reduces net CO_2 fixation and productivity in C_3 plants by as much as 40% (Ku et al., 1996). On the other hand, C_4 plants have evolved a mechanism which raises the CO_2 concentration at the site of Rubisco, preventing the oxygenase activity and thus reducing photorespiration. Most C_4 plants, such as maize, sugarcane, and *Amarantus*, have leaves containing two morphologically distinct photosynthetic cell types, the bundle sheath (BS) and mesophyll (M) cells, which have different roles in CO_2 fixation (Fig. 1.2). The arrangement of these two cell types in C_4 leaves is known as Kranz anatomy (Hatch, 1987) and has become the hallmark feature associated with C_4 plants for more than forty years. In the C_4 photosynthetic pathway, atmospheric CO_2 is initially fixed in M cells. After CO_2 enters the M cells, carbonic anhydrase hydrates it to bicarbonate. The bicarbonate is converted to a 4-carbon acid, oxaloacetate (OAA), by phosphoenolpyruvate carboxylase (PEPC) in the cytosol of M cells; OAA is further reduced to malate or transaminated to aspartate. These C_4 acids are transported from the M cells to the BS cells via plasmodesmata where they are decarboxylated to release CO_2. C_4 photosynthesis can be divided into three biochemical subtypes based on the means by which CO_2 is released from C_4 acids. In the NADP-malic enzyme (NADP-ME) type C_4 pathway (e.g. maize), OAA is mainly reduced to malate by NADP-malate dehydrogenase in the chloroplast. The malate is transported to the BS cell chloroplast where NADP-ME decarboxylates it to pyruvate. In the NAD-malic enzyme (NAD-ME) (e.g. pigweed, *Amaranthus*) and phosphoenolpyruvate carboxykinase (PEP-CK) (e.g. guinea grass, *Panicum maximum*) types, OAA is transaminated to aspartate by aspartate aminotransferase in the cytosol.

Figure 1.1 Schematic representation of Rubisco fixation of CO_2 and O_2 in C_3 photosynthetic pathway

CO_2 and O_2 diffuse into a mesophyll cell and a chloroplast. Two molecules of 3-PGA are produced when CO_2 is fixed with RuBP by the carboxylase activity of Rubisco **(A)** while one molecule of 3-PGA and phosphoglycolate are produced when O_2 is fixed with RuBP by the oxygenase activity of Rubisco **(B)**. The phosphoglycolate is processed through the photorespiration pathway leading to the CO_2 release by using chemical energies including ATP and $NADH_2$. RuBP, ribulose 1,5-bisphosphate; Rubisco, ribulose 1,5-bisphosphate carboxylase/oxygenase; 3-PGA, 3-phosphoglycerate.

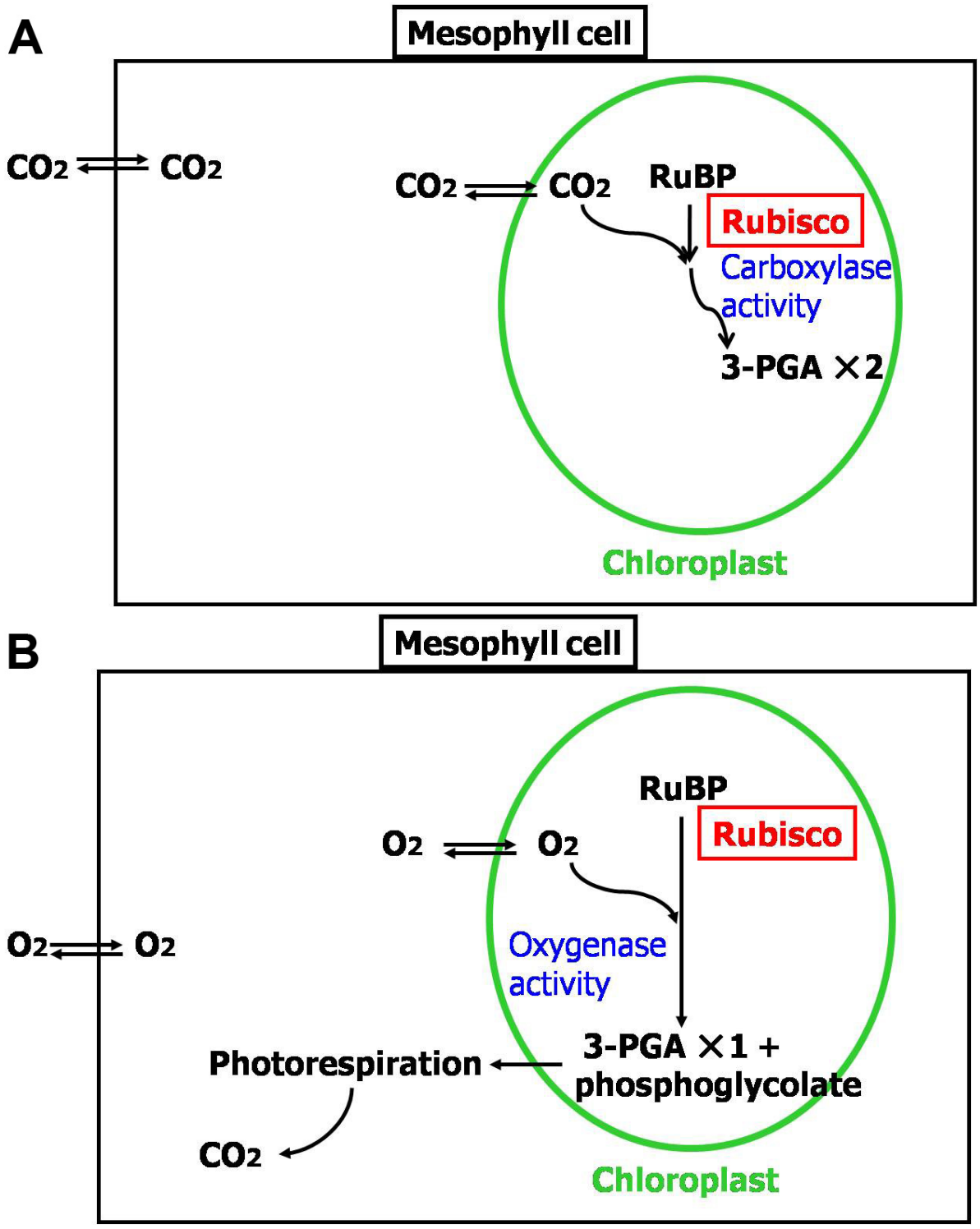
A
Mesophyll cell
CO2 ⇌ CO2
CO2 ⇌ CO2
RuBP
Rubisco
Carboxylase activity
3-PGA ×2
Chloroplast
B
Mesophyll cell
O2 ⇌ O2
O2 ⇌ O2
RuBP
Rubisco
Oxygenase activity
3-PGA ×1 + phosphoglycolate
Photorespiration
CO2
Chloroplast

Figure 1.2 Schematic representation of Kranz-type C_4 photosynthetic pathway (NAD-ME subtype)

Atmospheric CO_2 that enters the mesophyll cell is converted to HCO_3^- by CA, and combined with PEP to form a 4-carbon acid OAA by PEPC. OAA is transaminated to aspartate in the cytosol of the mesophyll cell by aspartate aminotransferase (Aspartate-AT). Aspartate is transported to the bundle sheath cell mitochondria and is converted to OAA. OAA is then reduced to malate, and malate is decarboxylated by mitochondrial NAD-ME producing pyruvate and CO_2. The released CO_2 diffuses into the chloroplast and fixed into 3-PGA by Rubisco. Pyruvate is converted by alanine aminotransferase (Alanine-AT) to alanine in the bundle sheath cell, and transported back to the mesophyll cell. In the mesophyll cytosol, ananine is transaminated to pyruvate. Pyruvate is then converted to PEP by PPDK in the mesophyll chloroplast. CA, carbonic anhydrase; PEPC, phosphoenolpyruvate carboxylase; OAA, oxaloacetate; MDH, malate dehydrogenase; ME, malic enzyme; Rubisco, ribulose 1,5-bisphosphate carboxylase/oxygenase; 3-PGA, 3-phosphoglycerate; PEP, phosphoenolpyruvate; PPDK, pyruvate Pi dikinase.

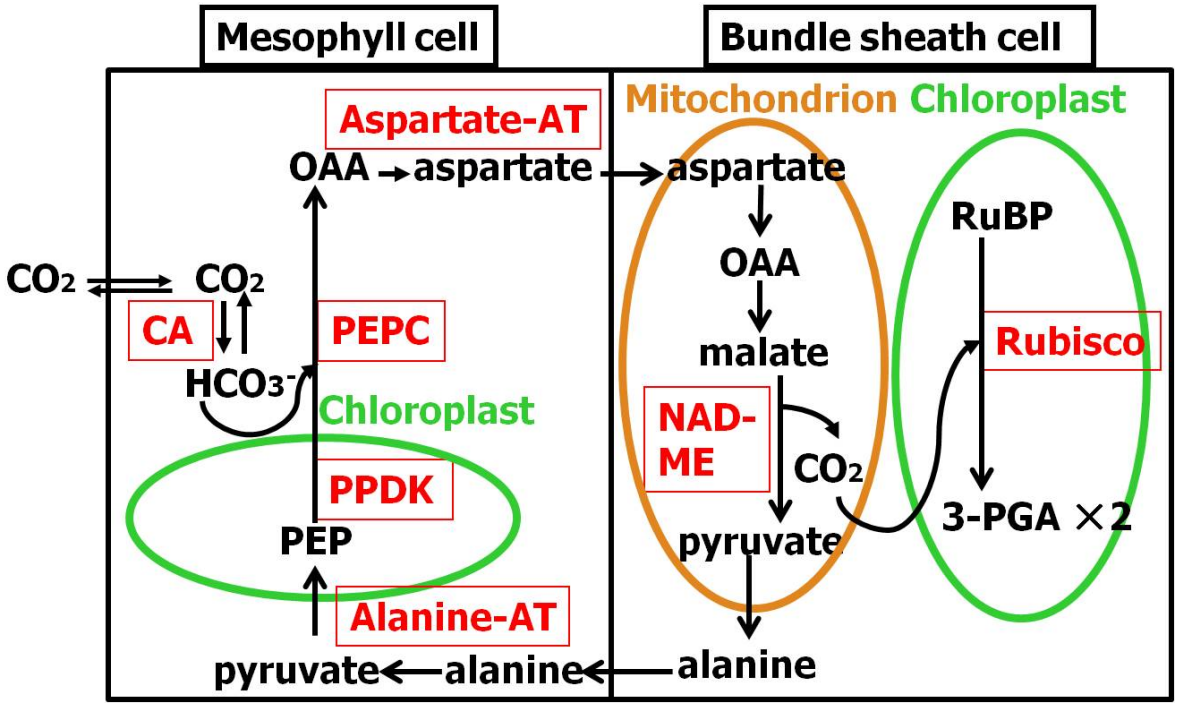
Mesophyll cell
Bundle sheath cell
Mitochondrion
Chloroplast
Aspartate-AT
OAA
aspartate
aspartate
OAA
malate
NAD-ME
CO2
pyruvate
RuBP
Rubisco
3-PGA ×2
CO2
CO2
CA
PEPC
HCO3-
Chloroplast
PPDK
PEP
Alanine-AT
pyruvate
alanine
alanine

In the BS cell, decarboxylation is catalyzed by NAD-ME or PEP-CK which are located in the mitochondrion or cytosol, respectively. In all cases, the released CO_2 is finally re-fixed by Rubisco in the BS chloroplasts. The C_3 products released from C_4 acid decarboxylation, either pyruvate (by ME) or PEP (by PEP-CK), are returned to the M cell. Pyruvate Pi dikinase (PPDK) in the M chloroplast is responsible for the conversion of pyruvate to PEP, the substrate for PEPC; PPDK requires two ATP equivalents for this reaction. The regenerated PEP is used for the fixation of another CO_2 molecule.

In addition to the distinct anatomical differences, key C_4 enzymes are also strictly confined to specific cell types. This enzyme localization in two different cell types makes the CO_2 concentration mechanism functional. Although these C_4 enzymes are present in C_3 plants, the enzyme activities are very low, and their localizations are different. C_4 enzymes play different roles in C_3 plants and are not related to the CO_2 concentrating mechanism as in C_4 plants (Ku *et al*., 1996; Sheen, 1999; Sage, 2004). For instance, PEPC provides OAA in the citric acid cycle, PPDK has been suggested to supply PEP in the shikimate pathway for lignin biosynthesis, and NADP-ME functions in a defense mechanism (see Doubnerová and Ryšlavá 2011 and references therein).

1.1.3 Advantages in C_4 photosynthesis

As mentioned above, photorespiration is a major problem in C_3 plants. The rate of photorespiration increases under high light and temperature conditions because the Rubisco specificity for CO_2 decreases (Brooks and Farquhar, 1985), the solubility ratio of CO_2 to O_2 decreases (Ku and Edwards, 1977), and stomata tend to close as temperature increases. In order to overcome photorespiration, especially in response to the drastic decrease of atmospheric CO_2

over geological time (Sage, 2004), C_4 plants have evolved a CO_2 concentration mechanism along with a modification in leaf anatomy (Kranz anatomy) which prevents the oxygenase activity of Rubisco through elevated CO_2 concentration in BS chloroplasts (Hatch, 1987). With the CO_2 concentration mechanism, C_4 plants show advantages under high light and temperature conditions, where C_3 plants suffer from increased photorespiration. In fact, C_4 plants dominate the flora of hot and arid regions. Furthermore, the photosynthetic light saturation point of C_4 plants is much higher than that of C_3 plants, meaning that C_4 plants can convert more light energy into chemical energy such as NADPH and ATP under high light conditions. In contrast, under excess light, many C_3 plants suffer from photoinhibition and photo-oxidation (Demmig-Adams and Adams III, 1992). However, these advantages in C_4 plants diminish under low temperatures because some enzymes, especially PPDK, lose their activity so that the plants cannot maintain an effective C_4 pathway. For C_3 plants growing at low temperatures, photorespiration is largely decreased and imposes no serious limitation to their growth. The CO_2 concentration mechanism in C_4 plants also increases water use efficiency by avoiding a wide stomatal opening, and thus reduces water loss during photosynthesis, and increases nitrogen use efficiency. C_4 photosynthesis, therefore, has a higher capacity for CO_2 assimilation under current ambient CO_2 concentration, warm, and high light environments. These advantages make it possible for C_4 crops to produce more biomass and yield than C_3 crops (Sage, 2004).

1.1.4 Introducing C_4 photosynthesis into C_3 plants

Plant biologists are interested in expressing C_4 photosynthetic traits in C_3 crops for enhanced photosynthetic capacity and productivity (Sheen, 1999; Matsuoka et al., 2001; Häusler et al., 2002; Miyao, 2003; Miyao et al., 2011; Raines, 2006; Sage and Sage, 2009; Furbank, 2011;

Peterhansel, 2011). In order to introduce a functional C_4 pathway in C_3 plants, initial attempts have been made to overexpress genes encoding C_4 enzymes in C_3 plants in the past 25 years. Such attempts so far have been focused on C_4 biochemistry because very little is known about the Kranz anatomy at the molecular level, such as differentiation mechanisms of the M cell and the BS cell.

C_4 biochemistry has been well studied and several key C_4 enzymes have been successfully introduced in C_3 plants. For instance, the intact maize PEPC gene including exons, introns and its own promoter and terminator is transformed into rice; the transgenic plants show significant (up to 110-fold) increases in expression and enzyme activity without causing any deleterious effects on growth (Ku et al., 1999). In another study, the maize PPDK gene with exons and introns, and its own promoter and terminator, is introduced into rice (Fukayama et al., 2001). The PPDK activity in transgenic rice plants increases up to 40-fold, relative to that of the wild type. However, when maize PPDK cDNA fused with its own or the *chlorophyll a/b binding protein* (*Cab*) promoter is used for transformation, PPDK activity only increases slightly (up to 5-fold). The authors proposed that the presence of introns and/or terminator sequences is required for the efficient expression of PPDK. Takeuchi et al. (2000) introduced maize NADP-ME cDNA using rice *Cab* or 35S promoter into rice. NADP-ME produced from rice *Cab* promoter shows high NADP-ME activity as compared to the wild type (up to 70-fold increase). However, NADP-ME transgenic rice produced using the 35S promoter shows a similar activity to the wild type. A decrease in growth and bleaching in leaves are observed in transgenic rice with the *Cab* promoter and high levels of expression, but not in transgenic rice with the 35S promoter. It appears that a higher expression level of NADP-ME in the C_3 M chloroplasts resulted in a higher severity of photoinhibition or photo-oxidation in the transgenic rice (Takeuchi et al., 2000). More recently, four key C_4 enzymes PEPC, PPDK, NADP-ME and NADP malate dehydrogenase are

simultaneously overexpressed in rice leaves, and the transgenic rice shows slightly enhanced photosynthetic rates (Taniguchi et al., 2008). However, the increased photosynthetic rates do not appear to be attributed to the CO_2 concentrating mechanism.

It has been hypothesized that a functional C_4 pathway could raise the CO_2 concentration in the C_3 M chloroplasts, where Rubisco is located, so that photosynthesis is increased and photorespiration suppressed. However, simple overexpression of C_4 enzymes in C_3 M cells has some problems. One major concern is that the CO_2 released by overexpressed decarboxylation enzymes could easily leak from the chloroplast to the cytoplasm. Another concern is that overexpressed PEPC in cytoplasm could fix CO_2 which has just been decarboxylated in the chloroplast and diffused back to the cytoplasm. The discovery of a new type of C_4 photosynthesis suggested a possibility to overcome these problems.

Previously, three terrestrial plants capable of performing C_4 photosynthesis in a single cell without the Kranz anatomy, *Bienertia cycloptera* (Freitag and Stichler, 2000; Voznesenskaya et al., 2002), *Bienertia sinuspersici* (Akhani et al., 2005) and *Suaeda aralocaspica* (Voznesenskaya et al., 2001), have been reported. The authors named these plants as "single-cell C_4 species" as compared to the typical Kranz-type C_4 plants. These single-cell C_4 species are annual plants and grow in central Iran (*B. cycloptera*), around Persian Gulf (*B. sinuspersici*) or, in Central Asia (*S. aralocaspica*) (Voznesenskaya et al., 2001; Akhani et al., 2005). The C_4 biochemistry and associated organelles are spatially separated within a single photosynthetic cell in these plants. These plants offer an alternative strategy for introducing C_4 systems in C_3 plants without the need for Kranz anatomy. However, neither the developmental processes nor the gene regulatory systems for the intracellular spatial compartmentation of the C_4 pathway in these plants have been characterized.

1.1.5 C_4 biochemistry and enzyme localization in single-cell C_4 species

In *Suaeda aralocaspica*, there is a spatial compartmentation of the carboxylation, decarboxylation and re-fixation processes in a single M cell with dimorphic chloroplasts located at opposite ends of the cells (Voznesenskaya et al., 2001). Atmospheric CO_2 is initially fixed by PEPC, in the cytoplasm of the outer region of the cell, into C_4 acids which are transported to the inner region where decarboxylation takes place; the released CO_2 is then fixed by Rubisco, located in the chloroplasts of the inner region of the cell. The locations where the carboxylation and decarboxylation processes occur are separated by a large central vacuole. The C_3 product, pyruvate, released from decarboxylation is then transported to the chloroplasts in the outer region for regeneration to PEP (Voznesenskaya et al., 2001). This unique physical arrangement of biochemical steps appears to be able to prevent CO_2 leakage after C_4 acid decarboxylation.

Similar to *S. aralocaspica*, *Bienertia cycloptera* and *Bienertia sinuspersici* also perform C_4 photosynthesis in individual chlorenchyma cells. In the Bienertia system, the single-cell C_4 pathway is achieved by the spatial separation of a central cytoplasmic compartment (CCC) enriched in mitochondria and granal chloroplasts and a peripheral cytoplasmic compartment (PCC) lacking mitochondria and having agranal chloroplasts (Fig. 1.3; Voznesenskaya et al., 2002). The initial fixation of atmospheric CO_2 occurs in the cytoplasm of the PCC where PEPC is located, and the C_4 acid produced is diffused to the CCC by transvacuolar cytoplasmic channels. Decarboxylation is carried out by NAD-ME in mitochondria in the CCC, and the released CO_2 is refixed by Rubisco in chloroplasts surrounding the mitochondria in the CCC. The C_3 product is returned to the chloroplasts in the PCC where enriched PPDK regenerates PEP (Voznesenskaya et al., 2002; Offermann et al., 2011). The chloroplasts in the PCC and CCC are

Figure 1.3 Schematic representation of single-cell C_4 photosynthetic pathway (*Bienertia* system)

A central cytoplasmic compartment (CCC) and a peripheral cytoplasmic compartment (PCC) are separated by the single large vacuole and connected by cytoplasmic channels. CO_2 diffused into the PCC is initially fixed into a 4-carbon acid by PEPC and transported to CCC through cytoplasmic channels. In mitochondria at the center of CCC, the 4-carbon acid malate is decarboxylated by NAD-ME producing a 3-carbon compound pyruvate and releasing CO_2. The released CO_2 is fixed into 3-PGA by Rubisco in chloroplasts surrounding mitochondria. Pyruvate moves back to the PCC chloroplasts where PPDK regenerates to phosphoenol pyruvate; PEPC, phosphoenolpyruvate carboxylase; ME, malic enzyme; Rubisco, ribulose 1,5-bisphosphate carboxylase/oxygenase; PPDK, pyruvate Pi dikinase; 3-PGA, 3-phosphoglycerate.

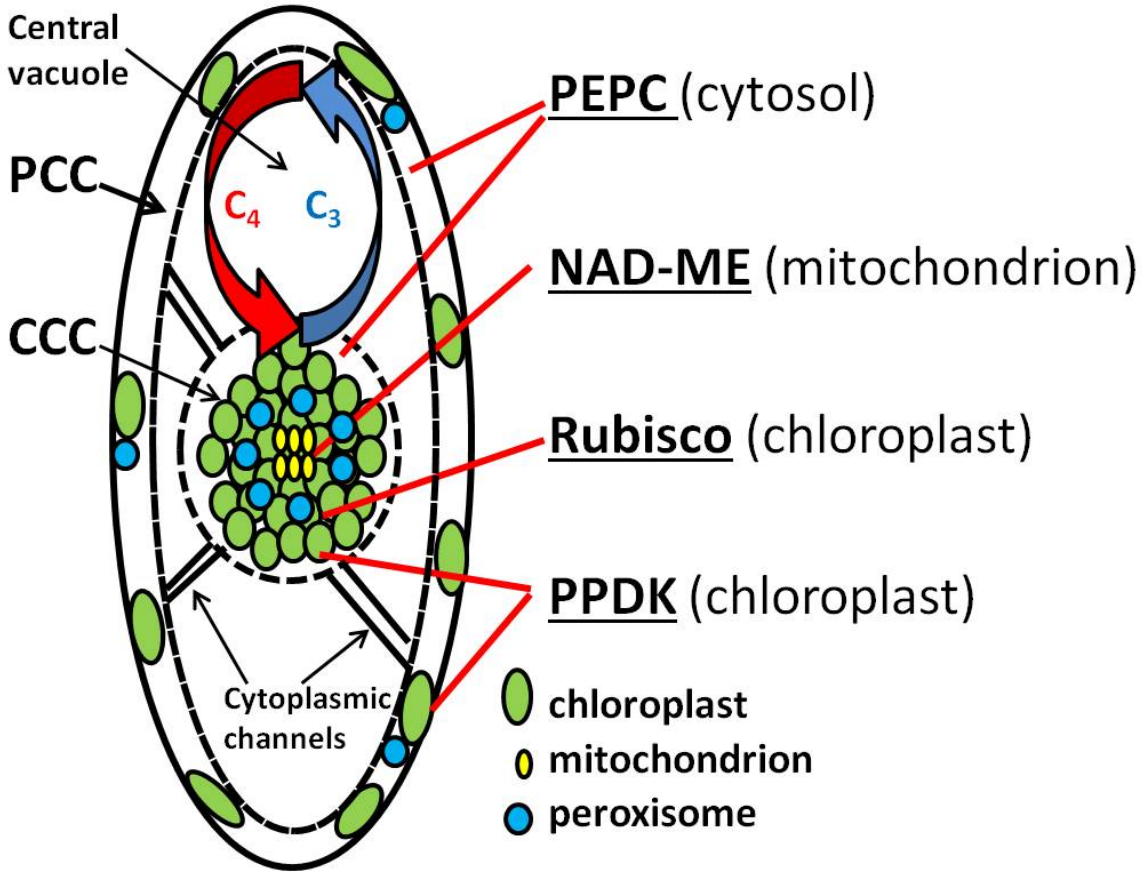
Central vacuole
PCC
CCC
C4
C3
Cytoplasmic channels
PEPC (cytosol)
NAD-ME (mitochondrion)
Rubisco (chloroplast)
PPDK (chloroplast)
chloroplast
mitochondrion
peroxisome

thought to be functionally analogous to the M and BS cells, respectively, in Kranz-type C_4 plants.

1.1.6 Regulation of C_4 gene expression in maize and *Amaranthus*

The localization of C_4 enzymes and mRNAs during leaf development has been well studied in maize and *Amaranthus*, monocot and dicot C_4 plants, respectively, with Kranz anatomy. In maize, *Rubisco* transcripts accumulate in the earliest stage of development where its polypeptides are undetectable (Martineau and Taylor, 1985). In contrast, the accumulation of *PEPC* and *NADP-ME* transcripts coincide with the accumulation of their corresponding polypeptides (Langdale et al., 1988). Moreover, their mRNAs and proteins accumulate after the differentiation of the M and BS cells, and are localized in a cell-specific manner. The cell-specific accumulation of C_4 enzymes has been proposed to occur by transcriptional regulation (Hibberd and Covshoff, 2010). The expression of maize *PEPC* is thought to be regulated by DNA methylation (Langdale et al., 1991), histone modification (Danker et al., 2008), and *trans*-acting factors binding to its promoter region (Taniguchi et al., 2000). The *PPDK* transcripts accumulate mostly in M cells, but are also detectable in BS cells of mature maize leaves (Sheen and Bogorad, 1987a). Further studies on maize *PPDK* revealed that important regulatory elements for the M-cell-specific localization are present in its promoter region (Matsuoka and Numazawa, 1991; Nomura et al., 2000)

In *Amaranthus*, both transcripts and polypeptides of the Rubisco large subunit (RbcL) are detected in the initial stage of leaf development (Wang et al., 1992, 1993b). However, the transcripts and polypeptides of Rubisco are localized not only in the BS cells but in the M cells as well. *PEPC* and *PPDK* transcripts are abundant in leaf primordia although corresponding

polypeptides are not detected (Ramsperger et al., 1996). Non-cell-specific accumulation of these transcripts remains in later developmental stages, while their polypeptides increase and show cell-specific accumulation. The *PPDK* transcripts disappear from the BS cell, followed by the *PEPC* transcripts. The authors mentioned that the localization of PEPC and PPDK appears to be regulated at post-transcriptional level in C_4 dicot *Amaranthus* unlike in C_4 monocot maize. The NAD-ME polypeptides show cell-specific accumulation ahead of their transcripts in early stages of leaf development (Long and Berry, 1996). The *NAD-ME* transcripts disappear from the M cells at earlier stages than the Rubisco transcripts.

These studies suggest that cell-specific localization is regulated independently among the photosynthetic enzymes and also among species. Moreover, the cell-specific gene expression of these enzymes is differentially regulated during leaf development; in the earlier stage it is regulated at the post-transcriptional level and in the later stage it is regulated at the transcriptional level (Martineau and Taylor, 1985; Sheen and Bogorad, 1987b; Langdale et al., 1988, 1991; Matsuoka and Numazawa, 1991; Wang et al., 1992, 1993b; Long and Berry, 1996; Ramsperger et al., 1996; Nomura et al., 2000; Taniguchi et al., 2000; McCormac et al., 2001; Danker et al., 2008; Hibberd and Covshoff, 2010).

1.1.7 C_4 enzyme localization during leaf development in single-cell C_4 species

The localization of C_4 enzymes during leaf development has been reported in the two single-cell C_4 species, *S. aralocaspica* (Voznesenskaya et al., 2003) and *B. cycloptera* (Voznesenskaya et al., 2005). In *S. aralocaspica*, Rubisco accumulates in all chloroplasts in the cell during the early stage of leaf development. Chloroplast-specific localization of Rubisco correlates with the partitioning of chloroplasts in two different compartments of the chlorenchyma cell as well as

their morphological differentiation. PEPC accumulates throughout the cytoplasm and does not show specific compartmentation in any leaf developmental stages. PPDK accumulates in very low amounts in chloroplasts of young leaves. Its expression increases and specifically localizes in the chloroplasts in the distal part of the cell in the late stage of development. NAD-ME is undetectable in the early stages of developmental, but it is found in mitochondria concentrating in the proximal end of the cell in mature leaves (Voznesenskaya et al., 2003).

In *B. cycloptera*, the localization of these key C_4 enzymes and Rubisco during leaf development is quite similar to that in *S. aralocaspica*, except organelles are compartmentalized in a different region of the chlorenchyma cell. Rubisco and NAD-ME are located in the CCC, and PPDK accumulates specifically in the PCC chloroplasts. PEPC is detected in the cytoplasm throughout the cell (Voznesenskaya et al., 2005). In *B. sinuspersici*, the accumulation of various proteins and transcripts of developing leaves under different light conditions was determined by using immunoblot and real-time PCR analyses (Lara et al., 2008). The authors described that a substantial amount of Rubisco accumulates in the early stage of leaf development whereas PEPC and PPDK are low until the late stage. Because the accumulation of transcripts mostly correlates to that of their proteins, they suggest transcriptional control is involved in the developmental regulation of photosynthesis. In this study, total proteins and transcripts are isolated from leaf extracts. However, to determine the accumulation of photosynthetic enzymes and their transcripts in dimorphic chloroplasts, alternative methods, such as the separation of the two types of chloroplasts or quantification of the protein accumulation *in situ*, are required. Recently, a method for chloroplast isolation from each compartment of chlorenchyma cells in *B. sinuspersici* has been established by Offermann et al. (2011). The immunoblot analysis using proteins extracted from dimorphic chloroplasts indicated that RbcL level was 3.5-times higher in CCC than in PCC chloroplasts (Offermann et al., 2011). This result seems to underestimate the

difference of the RbcL accumulation in two types of chloroplasts based on the immunolocalization studies in *B. cycloptera* (Voznesenskaya et al., 2005) and *B. sinuspersici* (Chuong et al., 2006). There might be room for improvement in either the chloroplast separation method or the quantification method, or both of them. Although the localization and accumulation of photosynthetic enzymes during leaf development in the single-cell C_4 species have been well-studied (Voznesenskaya et al., 2004, 2005; Lara et al., 2008), the quantitative distribution of proteins and their transcripts in dimorphic chloroplasts has not been characterized.

1.1.8 Current progress in the C_4 photosynthesis research

Recently, several high throughput proteomic analyses of maize seedling leaf have been performed. Approximately 400 proteins of maize M and BS chloroplast stroma are quantitatively compared by using three independent methods: two-dimensional gel electrophoresis, cleavable isotope coded affinity tag, and liquid chromatography electrospray mass spectrometry (Majeran et al., 2005). The authors conclude that the accumulation of NADPH in the M chloroplasts and a shortage of NADPH in the BS chloroplasts result in the metabolic differentiation in many cases. In addition, differential functions in M and BS chloroplasts are often attributed to differential expression of isoforms. Similarly, membrane proteins in maize M and BS chloroplasts are comparatively analyzed (Majeran et al., 2008). In the study, the differential accumulation of proteins related to the electron transport chain including PSI and PSII are found. Moreover, the PEP transporter is more abundant in M chloroplast envelopes, and two isoforms of malate transporters are preferentially accumulated each M and BS chloroplast envelopes.

More recently, another proteomic analysis is performed using the maize leaf blade, which shows differentiation of M and BS cells along a developmental gradient from the base of the

blade to the tip (Majeran et al., 2010). The C_4 differentiation in the maize leaf blade is classified into five transition phases based on structural features and metabolic processes found by the proteomic analysis: in Phase 1, cells are not differentiated into M and BS cells and lack of the photosynthetic apparatus; in Phase 2, the formation of Kranz anatomy is visible and cells start differentiating into M and BS, but the accumulation of photosynthetic proteins is low; in Phase 3, the expression of proteins for chloroplast biogenesis is maximized, and cells become photoautotrophic; in Phase 4, cell walls of BS cells are thickened, and C_4 photosynthetic proteins start accumulating; in Phase 5, cells are completing C_4 differentiation, and proteins for chloroplast biogenesis are reduced.

As well as proteomic studies, transcriptome analyses have been conducted to examine gene expressions in C_4 plants. More than 25,000 genes in the maize leaf blade are analyzed using Illumina sequencing (Li et al., 2010). In many cases, differential accumulation of transcripts in M and BS cells corresponds to the accumulation of proteins reported by previous proteomic studies (Majeran et al., 2005, 2008; Friso et al., 2010). Furthermore, about 180 transcription factors are found to be differentially expressed in M and BS cells. Another transcriptomic research has been carried out using closely related C_3 and C_4 *Cleome* plants (Bräutigam et al., 2011). Because *Cleome* is phylogenetically closely related to *Arabidopsis*, the well-annotated *Arabidopsis* genome can be used for studies of *Cleome* (Brown et al., 2005). By 454 sequencing, more than 13,000 transcripts are detected in mature leaves, and about 600 transcripts are differentially regulated between C_3 and C_4 *Cleome* plants. These studies reveal the complexity of metabolic processes and the gene regulation involved in C_4 differentiation and also give many new entry points for studying C_4 photosynthesis.

1.1.9 Rubisco and its transcripts

Rubisco is the most abundant protein in the world. Rubisco contributes to the process of CO_2 fixation in cyanobacteria, algae, and plants. This enzyme is a hexadecamer composed of eight large subunits encoded by a plastid gene and eight small subunits encoded by a family of two or more nuclear genes (DeRocher et al., 1993; Khrebtukova and Spreitzer, 1996; Schwarte and Tiedemann, 2011). Although much work on this enzyme at the biochemical and molecular levels has been done in the last two decades (Spreitzer and Salvucci, 2002; Parry et al., 2003, 2008; Andersson, 2008; Patel and Berry, 2008), the regulatory mechanisms of this enzyme distribution in C_4 plants have yet to be elucidated.

The transcript of *rbcL* basically has two forms with different lengths in the 5' untranslated region (UTR) generated by alternative processing. In tobacco, the premature mRNA has an 182 bp 5'UTR (-182) whereas the mature mRNA has a 59 bp (-59) 5'UTR (Serino and Maliga, 1998). Although the length of the 5'UTR varies slightly between species, processing of the 5'UTR to around -60 is considered to be necessary for mRNA stabilization and efficient translation. However, a third form of *rbcL* mRNA has been observed in barley (Reinbothe et al., 1993) and *Amaranthus* (McCormac et al., 2001) with processing sites at -94 and -103, respectively. These intermediate forms appear to be present under illuminated or stress conditions. Reinbothe et al. (1993) proposed that the intermediate form (-103) is untranslatable and could compete with the mature form (-59), and repress the translation rate of *rbcL*. Despite being an essential enzyme in photosynthesis, Rubisco has yet to be studied at the transcript level in *B. sinuspersici* as only a quantitative analysis of the transcripts in developing leaves has been performed by Lara et al. (2008). Therefore, analysis of the *rbcL* transcript sequence using bioinformatics tools may help elucidate its regulation in the single-cell C_4 system.

1.1.10 Translational and post-translational control of RbcL

Although the differential distribution of RbcL protein in C_4 plants has been proposed to be mainly regulated at the post-transcriptional level (Patel et al., 2006; Patel and Berry, 2008), other levels of regulation such as translational and post-translational cannot be ruled out. In the green algae *Chlamydomonas reinhardtii*, the translation of *rbcL* is stalled when the level of reactive oxygen species (ROS) is high (Shapira et al., 1997; Irihimovitch and Shapira, 2000). Cohen et al. (2005) proposed that the conformation of RbcL protein is altered by oxidation causing to the exposure of its RNA binding sites which might bind *rbcL* transcripts arresting the translation, and leading to the auto-regulation of the *rbcL* expression. Moreover, Wostrikoff and Stern (2007) demonstrated that the translation of RbcL is auto-regulated in tobacco by the assembly status of RbcL polypeptides. The authors proposed that unassembled RbcL exposes a repressor motif which may be hidden when they are assembled. It is possible that this repressor motif is the RNA binding site described by Cohen et al. (2005). Post-translational modification of RbcL proteins which may facilitate their subsequent degradation has also been suggested. For example, RbcL proteins are site-specifically cleaved in naturally senescing leaves and upon ROS treatment, making RbcL susceptible to further degradation (Desimone et al., 1996; Ishida et al., 1997, 1998, 1999; Kokubun et al., 2002; Nakano et al., 2006). Furthermore, the RbcL turnover outside chloroplasts through the transportation of cargo from chloroplasts to the central vacuole has been suggested; the cargo is called Rubisco-containing body (RCB) (Chiba et al., 2003; Ishida et al., 2008) or Rubisco vesicular body (Prins et al., 2008). Although these studies have been performed in C_3 plants such as wheat and tobacco, the results suggest that RbcL turnover might also contribute to the differential accumulation of RbcL in C_4 species, including *B. sinuspersici*. To test this hypothesis, the chloroplast physiology and morphology need to be examined.

1.1.11 Plastids

Plastids are double-membrane bound organelles containing a fluid called stroma. A chloroplast is one form of plastids specifically found in photosynthetic tissues and cells of photoautotrophic organisms. The precursor of all types of plastids is called a proplastid. It can differentiate into various forms including the chloroplast containing the green colored pigment chlorophylls, the chromoplast containing various colored pigments including carotenoids, the amyloplast containing starch for long-term storage, and the elaioplast containing a large amount of lipid. In chloroplasts, the light reaction of photosynthesis occurs on flattened membrane compartments called thylakoids. These thylakoids make stacks called grana, where the light harvesting complex II and photosystem (PS) II proteins accumulate (Andersson and Anderson, 1980). On the other hand, PSI and ATPase are mainly located in the unstacked region, the thylakoid lamella, which connects the grana.

Because plastids are of endosymbiotic origin and derived from cyanobacteria, each plastid has its own genome as well as transcriptional and translational machinery (Woodson and Chory, 2008). The plastid genome size is 110 – 200 kb depending on the species and consists of a mixture of circular, linear and branched DNA (Sugiura, 1995; Oldenburg and Bendich, 2004). Plastid genes encode 100-200 proteins for general maintenance of the organelle and photosynthesis (Rivas et al., 2002). The former includes the β-subunit of RNA polymerase and initiation factor 1, and the latter includes RbcL and the *psbA* product, PSII D1 protein. Although chloroplasts contain about 3000 proteins, over 95% of them are encoded by the nucleus (Leister, 2003). Therefore, crosstalk between chloroplasts and the nucleus has been considered to be important for developmental and environmental control of the expression of chloroplast protein-encoding genes (Woodson and Chory, 2008). Furthermore, the interaction of plastids with other organelles

including mitochondria and endoplasmic reticulum (ER) has been observed in *Arabidopsis*, tobacco, and *Nicotiana benthamiana* (Kwok and Hanson, 2004a; Holzinger et al., 2007; Schattat et al., 2011). Interestingly, these organellar interactions were seen with plastids of altered morphology.

1.1.12 Plastid morphology and stromules

Plastids have been known to form membrane dilations, protrusions, extensions devoid of thylakoid membranes. Tubule structures named "stromules" because they are stroma-filled tubules (Köhler and Hanson, 2000). Although stromules have been observed in the early 1960s, using light and electron microscopy, they were considered as artifacts or abnormal traits (Weier and Thomson, 1962; Wildman et al., 1962; Shalla, 1964; Köhler and Hanson, 2000). However, the visualization of platids using green fluorescent protein (GFP) facilitated the re-discovery of stromules by Köhler et al. (1997). Since then, a number of laboratories have reported the morphology of stromules using various GFP-expressing transgenic plants such as tobacco, petunia, spinach, rice, tomato and *Arabidopsis* (Tirlapur et al., 1999; Shiina et al., 2000; Arimura et al., 2001; Pyke and Howells, 2002). In addition, fluorescent microscopic analyses have revealed that stromules are double-membrane structures having both outer and inner envelopes (Gray et al., 2001; Holzinger et al., 2008; Hanson and Sattarzadeh, 2008). Typical stromules range from 0.3 to 0.8 μm in diameter whereas a length up to 50 μm has been reported (Arimura et al., 2001; Gray et al., 2001; Hanson and Sattarzadeh, 2011). Holzinger et al. (2007) have defined stromules and protrusions based on the radius and the length of the plastid extensions. A wide range of stromule shapes have been observed in previous studies including simple tubules,

branches, loops and vesicles (Köhler and Hanson, 2000; Pyke and Howells, 2002; Gunning, 2005; Schattat et al., 2011).

1.1.13 Stromule movement

Various movements of stromules have been observed by using video microscopy (Gunning, 2005). Gunning explained that some stromules extend, retract, anchor, change directions, connect to other plastids and even break off as vesicles. In addition, Gunning (2005) mentioned that stromules mostly extend following cytoplasmic streaming, but some can grow against the flow.

Mechanisms of stromule movements have also been studied. Studies using inhibitors of cytoskeleton have revealed the association of stromules with actin microfilaments (Kwok and Hanson, 2003). In addition, hypocotyl epidermal cells of transgenic *Arabidopsis* expressing GFP fused to the actin binding protein talin exhibits direct interactions between stromules and actin cytoskelton (Kwok and Hanson, 2004a). Recently, two groups demonstrated that at least myosin XI is involved in the formation and the movement of stromules interacting with the actin cytoskeleton (Natesan et al., 2005; Sattarzadeh et al., 2009). Furthermore, Schattat et al. (2011) described that stromules move along channels between ER tubules. This finding suggests that the ER guides stromule directions and possibly provides the new membranes required for the stromule extension.

1.1.14 Stromule distribution

Stromules have been observed in different tissues and cell types. Stromules are more frequent in cells from non-photosynthetic tissues such as petals and roots although they are also found in leaf M cells which have fewer numbers and shorter forms (Köhler and Hanson, 2000). The distribution of stromules and chlorophyll autofluorescence signals in callus cells induced from leaf explants suggests that the frequency of stromules increases as chlorophyll contents decreases (Köhler and Hanson, 2000). Similarly, stromules are not detected in pericarp cells from the young and green tomato fruit while vesicle-like stromules are often observed in the ripe and red fruit (Pyke and Howells, 2002). Waters et al., (2004) described that stromule length is negatively correlated with plastid density, and the frequency of stromules is controlled by the differentiation status of plastids; for instance, inhibiting chloroplast differentiation from proplastids increases stromules whereas increasing chloroplastic components such as chlorophyll and thylakoid membranes reduces stromules.

1.1.15 Potential functions of stromules

Although the morphology and distribution of stromules have been well studied, their functions are not well understood. Several possible functions have been suggested, such as increasing the surface area of chloroplast envelopes, transporting materials between plastids and other organelles, transmitting signals to the nucleus, and discarding or recycling plastid contents (Hanson and Sattarzadeh, 2011). For examples, in rice chlorenchyma cells, 95 % of the cell periphery is occupied by chloroplasts and stromules (Sage and Sage, 2009). The authors hypothesized that stromules increase the surface area of chloroplasts to enhance CO_2 conductance and re-capture of CO_2 released by photorespiration.

Previous studies demonstrated that proteins exchange via stromules of two connected plastids (Köhler et al., 1997; Tirlapur et al., 1999; Köhler and Hanson, 2000; Gunning, 2005). However, transporting materials between plastids may not be the main function of stromules because most plastids are not connected by stromules (Shiina et al., 2000; Natesan et al., 2005; Hanson and Sattarzadeh, 2011). Stromules also interact with other organelles such as nuclei, mitochondria and ER (Kwok and Hanson, 2004b; Sage and Sage, 2009; Schattat et al., 2011). Close contacts between nuclei and plastids with stromules are found in rapidly dividing and growing cells such as suspension cells and etiolated hypocotyls (Kwok and Hanson, 2004b). Stromules extending outwards to the plasma membrane from perinuclear plastids indicate that they may enhance intercellular trafficking of macromolecules, especially related to the membrane biogenesis. Based on the close association of stromules and ER, Schattat et al. (2011) suggest the exchange of lipids and metabolites between these organelles.

There has been no direct evidence of the exchange of materials between chloroplasts and other organelles through stromules. Nevertheless, protein complexes as large as 550 kD (Rubisco) can traffic through stromules (Kwok and Hanson, 2004c). However, GFP-labelled plastid DNA and ribosomes are not detected in stromules (Howells et al., 2012). This study suggests that transportation of genetic information through stromules and protein synthesis in stromules unlikely occur.

Several lines of evidence indicate a potential role of stromules in stress response. Stromules are induced by various stress treatments such as high temperature, drought and salt stress (Holtinger et al., 2007; Gray et al., 2012). Moreover, application of stress-related plant hormones such as abscisic acid, methyl jasmonate and ethylene precursor also induces stromules (Gray et al., 2012).

The hypothesized role of stromules in recycling plastid contents has been supported by the observation of RCBs, which are detected away from chloroplasts, in the cytoplasm and in the central vacuole of senescing leaf cells in wheat (Chiba et al., 2003). Prins et al. (2008) proposed that oxidized Rubisco binds to the chloroplast envelopes where stromules and vesicles form for the transportation of stromal contents to vacuoles. Moreover, colocalization of the stroma-targeting red fluorescent protein DsRed and GFP fused to ATG8, which is localized to autophagosomes, in RCBs in the central vacuole suggests that chloroplast-derived RCBs are transported into the vacuole via autophagic pathway (Ishida et al., 2008). It is possible that the accumulation of photosynthetic proteins including Rubisco in the single-cell C_4 system might be controlled by the post-translational turnover via stromules through autophagic pathways.

1.1.16 Autophagy

Autophagy is a process responsible for the degradation of cytosolic and organellar materials for nutrient recycling and removal of undesirable components in eukaryotes. Although there are several types of autophagy, two main autophagic pathways have been described in plants: microautophagy and macroautophagy (Bassham et al., 2006). Microautophagy involves direct engulfment of cytoplasmic contents by invagination of the tonoplast followed by their release inside the vacuole. This process often occurs during the deposition or mobilization of storage proteins in developing seeds or during seed germination (Levanony et al., 1992; Toyooka et al., 2001). Macroautophagy is a process whereby a portion of cytoplasm including organelles is sequestered into a double- or multi-membrane structure called an autophagosome. Subsequently, the autophagosome is transported into the lysosome in mammals or into vacuoles in yeast and plants for hydrolysis and degradation by proteases. Finally, the degraded products such as amino

acids are re-allocated and recycled (for plant autophagy see reviews: Thompson and Vierstra, 2005; Bassham et al., 2006; Bassham, 2007, 2009; Kwon and Park, 2008; Reumann et al., 2010).

1.1.17 Process in autophagy

Many autophagy-related genes (ATG) were initially discovered by molecular and genetic analysis in yeast and have been found to be conserved in mammals and plants (Meijer et al., 2007). Over the past decades, significant progress was made in describing molecular events in autophagy (Fig. 1.4; Thompson and Viestra, 2005; Yang and Klionsky, 2009; Rabinowitz and White, 2010; Weidberg et al., 2011). Autophagy initiated from environmental and developmental signals affects the target-of-rapamycin (TOR) kinase. TOR kinase phosphorylates ATG13, blocking the association with ATG1 kinase. The ATG1 and ATG13, association occurs when TOR kinase is inhibited, which leads to the ATG1 complex formation including ATG11, ATG17, and VAC8 proteins. The ATG1 complex activates the vacuolar-protein-sorting (VPS) 34-phosphatidylinositol-3-phosphate kinase (PI3K) complex including ATG6, ATG14 and other factors. The VPS34-PI3K complex interacts with the transmembrane ATG9 protein at the pre-autophagosomal structure (PAS) and initiates vesicle nucleation. Ubiquitination-like processes are required for autophagosome formation through ATG8 and ATG12 activation. In this pathways, the C-terminal of ATG8 is first cleaved by the cysteine protease ATG4. Both ATG8 and ATG12 are then activated by the E1-like activating enzyme ATG7. The active ATG8 and ATG12 behave as ubiquitin tags that deliver the PAS to the E2-like conjugating enzymes ATG3 and ATG10, respectively. ATG8 is attached to phosphatidylethanolamine, and ATG12 is conjugated to ATG5. The ATG12-ATG5 assembly then associates with ATG16, guiding ATG8-PE to the PAS. The VPS-PI3K complex and the ATG12 complex dissociate from mature autophagosomes.

Figure 1.4 Schematic model of the autophagosome formation and its molecular machinery

This figure is adapted from Thompson and Vierstra (2005) with modifications. TOR kinase controls formation of the ATG1 complex (**A**). The active TOR phosphorylates ATG13, preventing it from binding to ATG1. When TOR is inactive, ATG13 is dephosphrylated, leading to the ATG1-ATG13 assembly and the formation of the ATG1 complex which contains ATG11, ATG17, and VAC8. VPS34-PI3K is activated by the ATG1 complex and associates with the pre-autophagosomal structure (PAS) with other components ATG2, ATG6, ATG9, ATG14, and VPS15 (**B**). Elongation of PAS requires two ubiquitination-like systems: 1) ATG4 cleaves the C-terminal of ATG8; 2) ATG8 and ATG12 are activated by ATG7; 3) ATG8 and ATG12 are conjugated to their respective targets, phosphatidylethanolamine (PE) and ATG5, mediated by the E2-like enzymes ATG3 and ATG10, respectively; 4) the ATG12-ATG5 conjugate further interacts with ATG16 (**C**). The association of ATG12 complex and ATG8-PE with PAS leads to the PAS elongation (**D**). The VPS34-PI3K complex and the ATG12 complex dissociate from mature autophagosomes. ATG, autophagy-related gene; TOR, target-of-rapamysin; VPS, vacuolar-protein-sorting; PI3K, phosphatidylinositol-3-phosphate kinase.

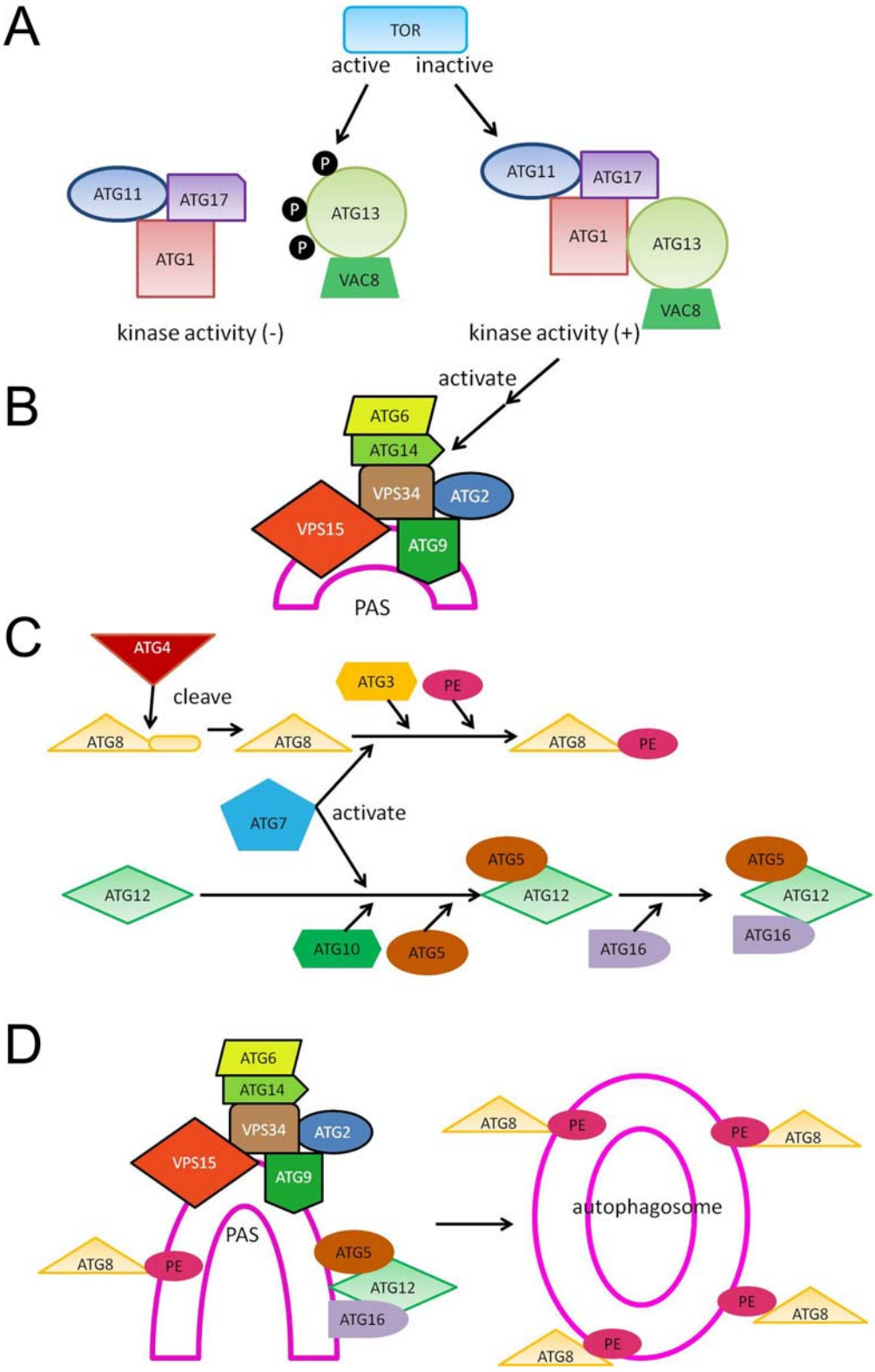
A
TOR
active
inactive
ATG11
ATG17
ATG1
P
P
P
ATG13
VAC8
kinase activity (-)
ATG11
ATG17
ATG1
ATG13
VAC8
kinase activity (+)
B
activate
ATG6
ATG14
VPS34
ATG2
VPS15
ATG9
PAS
C
ATG4
cleave
ATG8
ATG8
ATG3
PE
ATG8
PE
ATG7
activate
ATG12
ATG5
ATG12
ATG10
ATG5
ATG16
ATG5
ATG12
ATG16
D
ATG6
ATG14
VPS34
ATG2
VPS15
ATG9
PAS
ATG8
PE
ATG5
ATG12
ATG16
ATG8
PE
PE
ATG8
autophagosome
PE
ATG8
ATG8
PE

1.1.18 Autophagy in plants

In plants, autophagy is induced under nutrient-limiting conditions such as carbon and nitrogen starvation (Aubert et al., 1996; Moriyasu and Ohsumi, 1996; Doelling et al., 2002; Yoshimoto et al., 2004), during developmentally programmed events such as senescence (Hanaoka et al., 2002; Wada et al., 2009), and in response to oxidative stress and pathogen attack (Liu et al., 2005; Xiong et al., 2007b; Patel and Dinesh-Kumar, 2008). Although autophagy was initially thought to be associated with stress-related processes, recent studies have provided evidence to suggest it serves in important housekeeping roles by removing damaged or unwanted organelles and ubiquinated aggregates too large for the 26S proteosome (Inoue et al., 2006; Xiong et al., 2007a; Ishida et al., 2008; Johansen and Lamark, 2011; Vanhee et al., 2011; Youle and Narendra, 2011).

Plant-specific autophagy has also been reported, in which RCBs derived from chloroplasts are transferred to the vacuole for degradation in senescing or carbon-deprived leaves of wheat and *Arabidopsis* (Chiba et al., 2003; Ishida et al., 2008; Wada et al., 2009; Izumi et al. 2010). In a study using tobacco miniprotoplasts in which the central vacuoles are removed from protoplasts, Yano et al. (2007) found cytoplasmic materials in newly-formed vacuoles in the presence of cysteine protease inhibitor E-64d. Since the *de novo* vacuole generation is not inhibited by autophagy inhibitors such as 3-Methyladenine, wortmannin, or LY294002, the authors proposed that different types of autophagy could be involved in this vacuole biogenesis. Similarly, chloroplast-containing cell specific lytic vacuoles have been observed in naturally senescing *Arabidopsis* leaves, and are termed senescence-associated vacuoles (SAVs) (Otegui et al., 2005). Their presence in M protoplasts of *Arabidopsis* mutant in the *atapg/atg7-1*, encoding the E1-like activating enzyme ATG7, indicates that the biogenesis of the SAV is independent from the ATG-dependent autophagic pathway.

1.1.19 Origin of autophagosome membranes

Although autophagy was discovered over 40 years ago, the origin of autophagosomes and their membranes is not clearly understood. In yeast, the PAS containing ATG proteins plays a central role in autophagosome formation (Suzuki et al., 2001; Kawamata et al., 2008; Suzuki and Ohsumi, 2010). Several lines of research suggest that the endoplasmic reticulum (ER) or trans-Golgi network is responsible for autophagosome generation (Young et al., 2006; Axe et al., 2008). Recent research using electron 3D tomography showed interconnections between ER and premature-autophagosome membranes in mammalian cells (Hayashi-Nishino et al., 2009; Ylä-Anttila et al., 2009). However, more recently, Hailey et al. (2010) reported that the outer membrane of mitochondria is utilized for autophagosome biogenesis during starvation in rat kidney cells. Furthermore, the involvement of the plasma membrane in mammal has been suggested by Ravikumar et al. (2010) showing the localization of Atg16L1, which is asscociated with pre-autophagosomal structures as a part of an ATG12-ATG5 complex, to plasma membrane, autophagosomes, and clathrin-coated structures. These findings imply that various organelles contribute to autophagosome formation depending on the situation. Although the molecular machinery involved in autophagy is similar among eukaryotes including mammals, yeasts and plants, it is also possible that different organisms have established novel pathways for autophagosome formation using different organelles as a source of membrane.

1.2 Goals and objectives for this research

The goal of my PhD research was to gain a better understanding of the mechanisms regulating photosynthetic enzyme distribution in the novel single-cell C_4 plant, *Bienertia sinuspersici*. The possible regulatory mechanisms responsible for the differential enzyme accumulation at multiple

levels including post-transcriptional and post-translational controls were studied. In addition, the unique anatomical arrangement of this model species offers advantages in the study of autophagy. The findings from this research will enrich our understanding on C_4 photosynthesis and could eventually help in the introduction of C_4 traits into C_3 crops.

The following specific objectives were addressed:

-To elucidate the distribution of photosynthetic proteins in dimorphic chloroplasts of *B. sinuspersici* at different leaf developmental stages at fine resolution.

-To investigate whether the distribution and relative abundance of transcripts of photosynthetic genes correlate to those of proteins.

-To predict possible secondary structures in the Rubisco large subunit (*rbcL*) mRNA, which change the conformation depending on the conditions.

-To investigate possible roles of autophagy in the differential enzyme accumulation in *B. sinuspersici*.

-To examine whther membranes of chloroplasts and stromules are involved in the formation of autophagic organelles in plant mesophyll cells under oxidative stress.

CHAPTER 2. MATERIALS AND METHODS

2.1 Plant material

B. sinuspersici was grown as previously described (Lung et al., 2011). *B. sinuspersici* was propagated by vegetative cuttings. Shoot branches of healthy plants were excised, surface-sterilized with 0.5% (v/v) bleach, and cultured on Murashige-Skoog basal medium (Murashige and Skoog, 1962) containing Gamborg's vitamins (Sigma, cat. no. M0404), 3% (w/v) sucrose, and 0.7% (w/v) agar until the formation of adventitious roots. Rooted plants were transferred to 6-inch pots and gradually acclimatized to greenhouse conditions under low light for 4 weeks. Acclimatized plants were then transferred to controlled-environment chambers (Conviron Ltd., Winnipeg, Canada) with day/night temperatures of 25/18 ^{o}C and a photoperiod of 14/10 h under moderate light (ca. 350 μmol m^{-2} s^{-1}). Three- to four-month-old plants were used for all experiments except for senescing leaves which were obtained from plants older than ten months. *Arabidopsis thaliana* ecotype Columbia was grown in soil (1:1 Sunshine mix of LG3 and LC1) in chambers at 120 μmol m^{-2} s^{-1} at 21 °C with a photoperiod of 16/8 h.

2.2 Immunolocalization

Various developmental stages of leaves of *B. sinuspersici* were studied by the analysis of youngest (0.1 cm in length), young (0.2 cm in length), intermediate (0.5 - 0.6 cm in length), intermature (1.0 - 1.2 cm in length) and mature leaves (more than 2.0 cm in length). For fixation one-half (young and intermediate) or one-third (intermature and mature) from the tip of the leaf was used to uniform cell developmental stages, with an exception of the youngest leaf for which

the whole leaf was used. Leaf samples were fixed in 1.25% (v/v) glutaraldehyde and 2% (v/v) paraformaldehyde in 50 mM PIPES buffer, pH 7.2, containing 0.3 M mannitol at 4 ^{o}C overnight. The fixed leaf was washed with the same buffer without the fixatives, dehydrated through an ethanol series and embedded in LR White resin (London Resin Company Ltd., Berkshire). Sections (60 -80 nm thick) were made on an ultramicrotome and collected on 150 mesh nickel grids. Sections were treated with TBST-BSA containing 25 mM Tris-HCl, pH7.5, 150 mM NaCl, 0.1% (v/v) Tween 20, and 1% (w/v) bovine serum albumin (BSA) for 1 h, and then incubated with anti-catalase (courtesy of Robert Mullen, 1:20 dilution), anti-Rubisco large subunit (Agrisera, Sweden, cat. no. AS03 037, 1:1,000), anti-*Zea mays* PPDK (courtesy of Chris Chastain, 1:1,000), anti-PsbO (33 kD protein in the oxygen evolving complex associated with PSII; courtesy of Marilyn Griffith, 1:1,000), anti- *Zea mays* cytochrome f (Agrisera, Sweden, cat. no. AS08 306, 1:100), or anti- *Zea mays* PEPC (Chemicon, Canada, cat. no. AB1829, 1:1,000) at 4 ^{o}C overnight. All antibodies were purified antigen in rabbit except for anti-catalase which was raised in mouse. After washing with TBST-BSA, sections were incubated with 10 nm gold conjugated anti-rabbit IgG (Sigma-Aldrich, Oakville) for 1 h. Sections were sequentially washed with TBST-BSA, TBST, and H_2O, and then stained with uranyl acetate and lead citrate.

To observe the response to oxidative stress, chlorenchyma cells of *B. sinuspersici* leaves were isolated as described previously (Lung et al., 2011). Briefly, leaves of *B. sinuspersici* were gently pressed by using a mortar and pestle in a cell stabilizing (CS) solution containing 25 mM HEPES-KOH (pH 6.5), 5 mM KCl, 1 mM $CaCl_2$, and 1 M mannitol. *Arabidopsis* leaves were excised and transferred into the CS solution containing 0.4 M instead of 1 M mannitol. Primary antibodies used for immunolabeling were anti-Rubisco large subunit (1:1,000), anti-PPDK (1:1,000), anti-catalase (1:20 dilution), or anti- PEPC (1:1,000). Very low background labelling was observed in the negative control in which sections were treated as described above except

that the treatment with primary antibodies was omitted.

2.3 RNA extraction and RACE

Total RNA was extracted from *B. sinuspersici* mature leaves using a modified protocol of the LiCl precipitation method (Sambrook et al., 1989). Leaves were ground to fine powder with a mortar and pestle in liquid nitrogen. Leaf powders were further grounded in pre-warmed RNA extraction buffer containing 100 mM LiCl, 1% sodium dodecyl sulphate (SDS), 100 mM Tris-HCl (pH 9.0) and 10 mM EDTA, and mixed with equal volume of phenol. RNA was precipitated by 2 M LiCl for 6 hours followed by ethanol for overnight at -20 ^{o}C. *Arabidopsis* leaf RNA was extracted using TRIzol Reagent (Invitrogen, Burlington, Canada, cat. no. 15596-026) according to the manufacturer's instructions. After being ground in liquid nitrogen using a mortar and pestle, leaf powders were mixed with 500 ml of TRIzol Reagent. One-third volume of chloroform was added to the mixture, mixed, and centrifuged at 18,000 *g* for 15 min. The aqueous layer was transferred to a new tube and mixed with an equal volume of isopropanol. RNA was pelleted at 18,000 *g* for 10 min at 4 ^{o}C, washed with 70% ethanol, air-dried, and resuspended in diethylpyrocarbonate treated water.

First-strand cDNA was synthesized from total RNA by using Protoscript II RT-PCR Kit (New England BioLabs, Ipswich, MA) according to the manufacturer's instructions. The first-strand cDNA was used as a template for polymerase chain reaction (PCR). Primers for PCR were designed using the known sequences of other C_4 plants, except for *PEPC*, the sequences of which can be obtained from GeneBank (Lara et al., 2006; Accession# 108782493) for the two single-cell C_4 species. Partial sequences of *RbcL*, *RbcS*, *PPDK*, *NAD-ME* were amplified by using primers, BcRbLF3 and BcRbLR4, BcRbSF2 and BsRbSR2, BsPPDKF4 and BsPPDKR4,

BsNADF2 and BsNADR3, respectively (see Appendix for primer sequences). The amplified fragments obtained from PCR were sequenced and confirmed as the target sequences by a BLAST search (National Center for Biotechnology Information). Both 5' and 3' cDNA ends were identified by rapid amplification of cDNA ends (RACE) using FirstChoice RLM-RACE (Ambion, Austin, TX). The RACE procedure was repeated until the full-length cDNA with both 5' and 3' ends were obtained. Gene-specific primers used for RACE were as following: for *RbcL*, BcRbL5'O, BcRbL3'O, BsRbcL5'O2, and BsRbcL3'I2; for *RbcS*, BsRbSF2, BsRbS5'O, and BsRbS5'I; for *PPDK*, BsPPDK5'O, BsPPDK3'O, BsPPDK3'I, BsPPDKR5, BsPPDK5'I2, BsPPDK5'O3, BsPPDKF7, and BsPPDKF8; for *NAD-ME*, BsNAD5'O, BsNAD3'O, BsNAD5'O2, BsNAD3'O2, BsNAD3'I3, BsNADF3, SaNADF1, SaNADR1, and BsNADR4; for *PEPC*, BsPEPC5'I, and BsPEPC3'I (Appendix).

2.4 GFP constructs

EGFP constructs were generated by subcloning specific cDNA sequences into the pSAT6-35S::EGFP-N1 or pSAT6-35S::EGFP-C1 vectors (Chung et al., 2005) for *in vivo* localization analysis of various proteins. The transit sequences of NAD-ME and RbcS were predicted using the ChloroP Prediction Server (Emanuelsson et al., 1999). The *NAD-ME* transit sequence was amplified using the BsMEcdsF4NcoI and BsMETPR1BamHI primers and subcloned into the *Nco*I-*Bam*HI sites of pSAT6-35S::EGFP-N1. The *RbcS* transit sequence was amplified using BsRbcScdsF3NcoI and BsRbcSTPR2Sal primers, and subcloned into the *Nco*I-*Sal*I sites of pSAT6-35S::EGFP-N1. The full coding sequence of *RbcS* was also amplified using BsRbcScdsF3NcoI and BsRbcSMatR2BamHI primers, and subcloned into the *NcoI-BamHI* sites of pSAT6-35S::EGFP-N1. The coding sequence of *PEPC* was amplified using

BsPCcdsF4SacI and BsPCcdsR4KpnI, and subcloned into the *Sac*I-*Kpn*I sites of pSAT6-35S::EGFP-N1. The PPDK-encoding sequence was amplified using BsPKTPF2NcoI and BsPKMatR3BamHI primers and inserted into *NcoI-BamHI* sites of pSAT6-35S::EGFP-N1. Three *Arabidopsis* sequences were amplified from *Arabidopsis* leaf cDNA. The coding sequence of actin binding domain 2 (*ABD2*) of *Arabidopsis* fimbrin (Sheahan et al., 2004) was amplified using AtfABD2F1NcoI and AtfABD2R1BamHI primers, and subcloned into *NcoI-BamHI* sites of pSAT6-35S::EGFP-N1. The coding sequence of *Arabidopsis ATG8* was amplified using AtATG8aSalIF1 and AtATG8aBamHIR1 primers designed according to Yoshimoto et al. (2004), and subcloned into the *SalI-BamHI* sites of pSAT6-35S::EGFP-C1. The *Arabidopsis* RbcS-coding sequence was amplified using AtRbcSF1NcoI and AtRbcSR1BamHI, and inserted into the *NcoI-BamHI* sites of pSAT6-35S::EGFP-N1.

To generate the nuclear localization signal (NLS; Goldfarb et al., 1986)-EGFP and Lifeact (actin binding domain: Riedl et al., 2008)-EGFP fusion constructs, the EGFP coding sequence was amplified using the forward primer containing the simian virus 40 (SV40)-like nuclear localization signal (NLS: PKKKRKV: NLS-GFP-NcoI) or the actin binding domain (MGVADLIKKFESISKEE: Lifeact-GFP-NcoI) in-frame with the amino terminal of EGFP and the reverse primer containing the carboxyl terminal of EGFP (EGFPR2NotI). Each amplicon was subcloned into the *Nco*I-*Not*I sites of pSAT6-35S::EGFP-N1. Similarly, the EGFP-peroxisomal-targeting signal (PTS) 1 fusion construct was generated by PCR-amplifying the EGFP-encoding sequence using the forward primer containing the amino terminal of EGFP (SAT6-F3) and the reverse primer containing the PTS1 sequence incorporated in the 3' end (SKLR1). The amplicon was subcloned into the *Nco*I-*Bam*HI sites of pSAT6-35S::EGFP-C1. The construction of the talin-GFP plasmid (Kost et al., 1998) and the MAP4-GFP (Marc et al., 1998) plasmid has been described previously. Plasmid DNA of all constructs was purified using

the Plasmid DNA Minipreps Kit (BioBasic Inc. Ontario, Canada) and verified by DNA sequence analysis before being used in transient expression experiments.

2.5 Biolistic transformation of onion epidermal cells

Biolistic transformation of onion epidermal cells was used to confirm the functionalities of various EGFP constructs as described previously (Chuong et al., 2006). Briefly, 5 μg of plasmid was purified using the EZ-10 Spin Column Plasmid DNA Kit (BioBasic Inc. Ontario, Canada) and mixed with a suspension of 1 mg tungsten and 16 mM spermidine. After the mixture was thoroughly vortexed, 0.1 M $CaCl_2$ was added and DNA-coated tungsten was collected by a brief centrifugation. After washes with 70% and 100% ethanol, the tungsten was resuspended in 100% ethanol, and loaded onto a plastic macrocarrier disc. The DNA-coated tungsten was bombarded into onion epidermal cells from a distance of 10 cm using a Biolistic PDS-1000/He system (Bio-Rad, Mississauga, Canada) at a helium pressure of 1100 psi. The bombarded onion tissue was incubated on water-saturated filter paper in the dark overnight, and observed by using fluorescent microscopy.

2.6 Protoplast isolation and transfection

EGFP constructs were transfected into *B. sinuspersici* protoplasts by using a polyethyleneglycol (PEG)-mediated method as described previously (Lung et al., 2011). Briefly, isolated chlorenchyma cells of *B. sinuspersici* were incubated in an enzyme solution containing 1.5 % (w/v) cellulase Onozuka R10 (Yakult Honsha Co. Ltd., Tokyo, Japan) and 1% (w/v) BSA in 0.7 M sucrose CS solution for more than 3 hours in the dark without shaking. After collected the

protoplasts by centrifugation at 100 g for 2 minutes, these were incubated in W5 solution [2 mM MES (pH 5.7), 154 mM NaCl, 125 mM $CaCl_2$, 5 mM KCl] and kept on ice for 30 minutes. Protoplasts were resuspended in Mg/MES solution [0.4 M sucrose, 4 mM MES (pH 5.7), 15 mM $MgCl_2$] and plasmid DNA was added. The mixture was mixed well with 40 % PEG solution [0.4 M sucrose, 100 mM $CaCl_2$, 40 % (w/v) PEG 4000] by inverting for transfection and incubated at room temperature for 5 minutes. The transfection was stopped by adding W5 solution, and the mixture was kept at room temperature for 20 minutes. Settled protoplasts were resuspended in WI solution [0.7 M sucrose, 4 mM MES (pH 6.5), 5 mM KCl] and incubated at 23°C under low light (30 μmol m^{-2} sec^{-1}) overnight in a Petri plate.

Arabidopsis protoplast transfection was performed according to Yoo et al. (2007). Leaves of 3- to 4-week old *Arabidopsis* plants were cut into small strips and transferred in an enzyme solution containing 20 mM MES (pH 5.7), 1.5 % (w/v) cellulase R10, 0.4% (w/v) macerozyme R10 (Yakult Honsha Co. Ltd., Tokyo, Japan), 1% BSA, 0.4 M mannitol, 20 mM KCl, 10 mM $CaCl_2$. After vacuum infiltration for 30 minutes, leaves were continually digested in the dark for 3 hours. Protoplasts were released from leaves by gentle shaking and subjected to the procedures described above except that 0.4, 0.2, or 0.5 M mannitol was used in Mg/MES, PEG, or WI solution, respectively.

2.7 *In situ* hybridization

All constructs were made by subcloning specific DNA sequence into the pBluescript SK+ vector (Stratagene, La Jolla, CA), except the NAD-ME-encoding sequence which was inserted into pGEM-T easy vector (Promega, Madison, WI) for *in vitro* transcription. Coding sequences of *RbcL*, *RbcS*, *PEPC*, *PPDK*, *NAD-ME*, PSI core reaction center protein-encoding-gene *psaB*, PSII

D1 protein-encoding gene *psbA*, and *16S* rRNA were amplified by PCR from *B. sinuspersici* leaf cDNA or genomic DNA. The *RbcL* coding sequence was amplified using BsRbcLcdsF2BamH1 and BsRbcLcdsR2Sal1 primers, and inserted into the *Bam*HI-*Sal*I sites. The *RbcS* coding sequence was amplified using BsRbcScdsF1EcoRI and BsRbcScdsR1HindIII primers, and subcloned into the *EcoRI-HindIII* sites. The *PEPC* coding sequence was amplified using BsPEPCcdsF1ClaI and BsPEPCcdsR1SalI primers, and subcloned into the *ClaI-SalI* sites. The *PPDK* coding sequence was amplified using BsPPDKcdsF3BamHI and BsPPDKcdsR3SalI primers, and subcloned into the *BamHI-SalI* sites. The *NAD-ME* coding sequence was amplified using BsNADcdsF2Cla1 and BsNADcdsR2Sal1 primers, and subcloned into the T-overhang sites of pGEM-T easy. The *psaB* coding sequence was amplified by using BspsaBF2XhoI and BspsaBR2EcoRI primers, and inserted into the *Eco*RI-*Xho*I sites. The *psbA* coding sequence was amplified by using BspsbAF1XbaI and BspsbAR1BamHI primers, and inserted into the *Xba*I-*Bam*HI sites. The *16S* rRNA partial sequence was amplified using Bs16SF2XhoI and Bs16SR2BamHI primers, and inserted into the *Bam*HI-*Xho*I sites. All constructs were purified using the Plasmid DNA Minipreps Kit (BioBasic Inc., Ontario, Canada) and verified by DNA sequencing before *in vitro* transcription.

In situ hybridization was performed according to Langdale et al. (1987, 1988) with modifications. Two modified protocols were used for the fixation and the infiltration steps. In the first protocol, mature leaves and shoot tips were fixed in a FAA solution containing 50% (v/v) ethanol, 5% (v/v) acetic acid, and 3.7% (v/v) formaldehyde, vacuum infiltrated for 30 min, and incubated at 4ºC overnight. The fixed tissue was dehydrated through stepwise changes of 50, 70, 95 and 100% ethanol for two hours each, with additional incubation in fresh 100% ethanol overnight. The ethanol was replaced with xylene through changes of the mixture of xylene and ethanol (percentage of xylene and ethanol in the mixture: 25% and 75%, 50% and 50%, and 75%

and 25%, respectively) for one hour each, followed by incubation in 100% xylene for one hour repeated three times. Leaves were embedded in the high quality paraffin Paraplast Plus at 60ºC and were hardened in a plastic mold by immersing in ice water. In the second protocol, tissues were fixed in a solution containing 70% (v/v) ethanol and 30% (v/v) acetic acid instead of FAA, dehydrated, and infiltrated by tert-butyl alcohol in the replace of xylene as an attempt to obtain better preservation of cell structures. Sections (10 μm thick) were made on a rotary microtome and mounted onto silanated slides (Dako, Carpinteria, CA).

Mounted sections were deparaffinized in xylene for five minutes twice, and rehydrated through a 100, 95, 70, 50, and 30% ethanol series and through two changes of distilled water for five minutes each. Rehydrated sections were incubated in a solution containing 100 mM Tris-HCl (pH 8.0), 50 mM EDTA, and 2 μg/ml proteinase K at 37 ºC for 30 minutes to remove RNase. Digoxigenin-labeled (DIG; Roche, Manheim Germany) sense and anti-sense RNA probes were generated from the various pBluescript SK+ constructs by *in vitro* transcription reaction using T3 or T7 polymerase from MAXIscript kit (Ambion, Austin, TX) according to the manufacturers' instructions. The DIG-labeled RNA probes were full coding sequences of *rbcL* (1428 bp), r*bcS* (601 bp), *PEPC* (2910 bp), *PPDK* (2853 bp), *NAD-ME* (1872 bp), *psaB* (2205 bp), *psbA* (1062 bp), and a partial sequence of *16S* rRNA (606 bp). The DIG-probes were alkaline-hydrolyzed to small fragments (150-200 bp). Deparaffinized sections were prehybridized in the prehybridization medium containing 300 mM NaCl, 10 mM Tris-HCl (pH 6.8), 10 mM sodium phosphate (pH 6.8), 5 mM EDTA, 40% formamide (v/v), 10% dextran sulphate (w/v), 1 mg/ml tRNA, 10 mM dithiothreitol, and 0.1% RNase inhibitor (v/v) at 50 ºC for one hour, and then hybridized with the DIG-labeled RNA sense or antisense probes at 50 ºC overnight. Coverslips were used at the hybridization step to prevent evaporation. After the hybridization medium was removed, slides were washed twice in 2x SSC (150 mM NaCl, 150

mM sodium citrate), prewarmed at 37°C for 15 min, and then treated with 20 µg/ml RNase A in 10 mM Tris (pH 7.5), 1 mM EDTA, 500 mM NaCl at 37°C for 30 min. The slides were then washed as follow: 2x SSC for 1 h at room temperature; 1x SSC for 1 h at room temperature; 0.5x SSC for 30 min at 45°C; 0.5x SSC for 30 min at room temperature. To visualize the hybridized probes, slides were blocked in TBST [100 mM Tris-HCl (pH 7.5), 150 mM NaCl, 0.3% (v/v) Triton X100] with 2% (w/v) BSA (Sigma-Aldrich, St. Louis, MO) at room temperature for 30 minutes, followed by the incubation in blocking solution containing anti-DIG antisera (Roche, Manheim Germany) conjugated to alkaline phosphatase (1:300 dilution) in TBST-BSA for either 2 hours at room temperature or at 4 ºC overnight. Slides were washed twice in TBST with 1% BSA for 15 min at room temperature, twice in TBST for 15 min, then rinsed in detection buffer consisting of 100 mM Tris (pH 9.0), 100 mM NaCl, and 10 mM $MgCl_2$. The slides were developed in detection buffer with the addition of 175 µg/ml 1,5-bromo-4-chloro-3-indolyl-phosphate in dimethylformamide and 337.5 µg/ml 1,4-nitroblue tetrazolium chloride. Samples hybridized to mRNA of *rbcL*, *psaB*, *psbA*, or *16S* rRNA were counter-stained by 0.02% Safranin O to visualize cell structures unless otherwise specified.

2.8 Hydrogen peroxide treatment

For an oxidative stress treatment, *B. sinuspersici* chlorenchyma cells, and *Arabidopsis* leaves and protoplasts were incubated in CS solutions containing 20, 10, or 5 mM hydrogen peroxide (H_2O_2), respectively, for 2 h at room temperature. Different sets of samples were also incubated in CS solution without H_2O_2 as negative controls.

2.9 Neutral red staining

Chlorenchyma cells isolated from healthy, senescing, or H_2O_2-treated *B. sinuspersici* leaves were stained with 0.01% (w/v) Neutral red (NR) (Baker, Phillipsburg, NJ) for 30 min. *Arabidopsis* M protoplasts were stained with 0.005% (w/v) NR for 30 min. Samples were washed and fixed in a fixative solution containing 0.3 M mannitol, 50 mM PIPES (pH 7.2), 1.25% (v/v) glutaraldehyde and 2% (v/v) paraformaldehyde for 10 min.

2.10 Microscopic analyses

For ultrastructure and immunolocalization, images were taken from 25 cells in three different blocks using a Philips CM-10 transmission electron microscope (FEI Company) at an accelerating voltage of 60 kV and captured using an AMT16000 digital camera (AMT, Danvers, MA, USA). The number of gold particles was counted in chloroplasts in each image and the density of gold particles per area (μm) was calculated by using Image J (http://rsbweb.nih.gov/ij/), which was also used for all measurements of diameter of organelles.

In situ hybridization images were acquired using a Zeiss Axiophot microscope (Carl Zeiss Inc. Germany) equipped with a Q-Imaging digital camera (Quorum Technologies Inc. Guelph, Canada). EGFP signals in onion epidermal cells and *B. sinuspersici* protoplasts were detected and fluorescence micrographs were captured using a Zeiss AxioImager fluorescence microscope (Carl Zeiss Inc. Germany).

Images of live protoplasts expressing fluorescent fusion constructs were taken on 8-chamber Lab-Tek II chambered coverglass slides (Nalgene Nunc, Denmark) using an Olympus FV1000 confocal laser scanning microscope. Confocal images were acquired using a 40x objective lens at a digital resolution of 1,024 x 1,024. The confocal excitation and emission

wavelengths for chlorophyll autofluorescence were 649 nm and 666 nm, respectively. EGFP was excited at 488 nm and its emission detected at a bandpath 495-540 nm. All images were further processed and composed using Adobe Photoshop CS (Adobe Systems Incorporated, Seattle, WA). All experiments were repeated at least three times independently with similar results.

2.11 Semi quantitative RT-PCR

Total RNAs were extracted from *B. sinuspersici* leaves at various developing stages including youngest (0.1 cm in length), young (0.2 cm in length), intermediate (0.5 - 0.6 cm in length), intermature (1.0 - 1.2 cm in length) and mature (more than 2.0 cm in length) and cDNA was synthesized as described above. The amount of cDNA templates for PCR were normalized by *18S* rRNA products. Optimum PCR cycles were determined for each gene from exponential phase by checking spot density of products. PCR was performed by using gene-specific primers for *RbcS* (BsRbcSRTF1 and BsRbcSRTR2), *RbcL* (BsRbL3'I2 and BsRbLStop), *PEPC* (BsPEPCRTF1 and BSPEPC5'I), *PPDK* (BsPPDKRTF1 and BsPPDK5'O3), *NAD-ME* (BsNADRTF2 and BsNAD5'O2), and *18S* rRNA (18SrRNAF2 and 18SrRNAR) as an internal control with the following conditions [95°C for 30 sec, 60°C (62°C for *RbcS*) for 30 sec, 68°C for 45 sec: 29 cycles for *18S* rRNA and *RbcL*, 32 cycles for *RbcS* and *PEPC*, 34 cycles for *PPDK* and 40 cycles for *NAD-ME*]. A control without RT was used to eliminate possibility of genomic DNA contamination.

2.12 Chloroplast isolation and separation

Leaf protoplasts of *B. sinuspersici* were prepared as described above. To obtain total chloroplasts, protoplasts were broken by filtering through a 10 μm nylon mesh and loaded onto 40/85% (v/v) Percoll gradient containing 0.8 M sorbitol. Intact chloroplasts were purified by centrifugation at 4°C, 3,000 *g* for 10 min, washed in chloroplast suspension solution containing 20 mM Tricine-KOH (pH 8.4), 0.8 M sorbitol, 5 mM EDTA, 5 mM EGTA and 10 mM $NaHCO_3$, and pelleted at 750 *g* for 5 min. For CCC chloroplast isolation, protoplasts were loaded onto a 10 μm nylon mesh attached on a microfuge tube. The tube was centrifuged at 4°C, 100 *g* for 30 sec. Chloroplasts on the nylon mesh was collected and purified by a Percoll gradient. For PCC chloroplast separation, protoplasts were mixed with a same volume of 40% (w/v) PEG 4,000 (Sigma-Aldrich Canada, Oakville) solution containing 0.7 M sucrose and incubated on ice for 5 min. Three volumes of CS solution without osmoticum containing 25 mM HEPES-KOH (pH 8.4), 5 mM KCl and 1 mM $CaCl_2$ were added and the mixture was incubated on ice for 15 min. The protoplast solution was then mixed with a half volume of 0.2 M sucrose CS solution and kept on ice for 5 min. The mixture was centrifuged at 4°C, 300 g for 2 min. Chloroplasts were collected from the floating layer and purified by a Percoll gradient.

2.13 Western blot and silver staining

Purified chloroplasts were resuspended in 50 mM phosphate buffer and protein was extracted by adding 1% (w/v) SDS. Protein concentration was determined by the BCA Protein Assay Kit (Thermo Scientific, Rockford, IL) according to the manufacturer's instructions. Chloroplast extract was mixed with 6X SDS sample buffer containing 72 mM Tris-HCl (pH 6.5), 2.4% (w/v) SDS, 30% (v/v) glycerol, 0.12% (w/v) bromophenol blue, and 6% (v/v) 2-mercaptoethanol. Two

μg of protein was separated on a 12% SDS-polyacrylamide gel. For the western blot, protein was transferred to a nitrocellulose membrane electrophoretically, and probed with rabbit antibodies against PPDK (1:4,000), RbcL (1:5,000), maize cytochrome f (1:1000), PsaD (a core subunit of PSI; Agrisera, Sweden, cat. no. AS09 461, 1:500), or PsbO (1:5,000). Goat anti-rabbit IgG conjugated to horseradish peroxidase was used as a secondary antibody. The chemiluminescence signal was detected by using Amersham ECL Plus Western Blotting Detection System (GE Healthcare, Buckinghamshire, UK) according to the manufacturer's instruction. The quantification of immunoreactive bands was performed by using Image J (http://rsbweb.nih.gov/ij/). Silver staining was carried out according to the Vorum protocol (Mortz et al. 2001). For silver staining, after protein separation, the acrylamide gel was fixed in a solution containing 50% (v/v) methanol, 12% (v/v) acetic acid, and 0.05% (v/v) formaldehyde for 2 h or overnight at 4°C. The fixed gel was washed in 35% (v/v) ethanol, sensitized in 0.02% (w/v) sodium thiosulfate solution, and stained in a solution containing 0.2% (w/v) silver nitrate and 0.076% (v/v) formaldehyde. After rinsing in distilled water, colour was developed in a solution containing 6% (w/v) sodium carbonate, 0.05% (v/v) formaldehyde, and 0.0004% (w/v) sodiumthiosulfate. The reaction was stopped by adding a solution containing 50% (v/v) methanol and 12% (v/v) acetic acid.

2.14 RNA extraction and real-time qPCR

Total RNA was extracted from purified chloroplasts using TRIsol Reagent (Invitrogen, Burlington, Canada, cat. no. 15596-026) as described above. Contaminating genomic DNA was removed by DNA-free Kit (Ambion, Austin, TX) according to the manufacturer's instructions. The quantity and purity of the RNA were determined spectrophotometrically. The integrity of the

RNA was assessed by agarose electrophoresis. Single-strand cDNA was synthesized from 2 μg total RNA by using the Protoscript II RT-PCR Kit (New England BioLabs, Ipswich, MA) and random nonamer according to the manufacturer's instructions.

Primers for real-time quantitative PCR (qPCR) were designed by using Primer-BLAST program (National Center for Biotechnology Information) to produce amplicons of 121 to 167 bp. Secondary structures of amplicons were predicted by using Mfold version3.2 (Zuker, 2003) to avoid too many secondary structures. To determine relative expressions, *16S* rRNA was amplified using Bsq16SF2 and Bsq16SR2 primers; RbcL-encoding sequence was amplified using BsqRbcLF1 and BsqRbcLR1 primers; PsaB-encoding sequence was amplified using BsqpsaBF1 and BsqpsaBR1 primers; and PsbA-encoding sequence was amplified using and BsqpsbAR1 primers. Real-time quantitative PCR was performed in CFX96^{TM} Real time System (BioRad, Hercules, CA) using SsoFast^{TM} EvaGreen Supermix (BioRad, Hercules, CA) according to the manufacturer's instructions. The following conditions were used for real-time qPCR [95°C for 3 min, followed by 95°C for 10 sec, 60°C for 10 sec, 70°C for 20 sec: 40 cycles]. Single amplicon for each primer set was confirmed by a single peak in a melting curve and a single band on an agarose gel. Eight independent RNA samples were tested in duplicate for each primer set. Relative gene expression was calculated using the Pfaffl method (Pfaffl, 2001).

2.15 Multiple sequence alignment and generation of phylogenetic trees

In this study, analyses of *RbcL* nucleotide sequences were performed based on genomic sequences. Transcript sequences such as RbcL-encoding, 5'UTR, and 3'UTR sequences were determined by the annotated start and stop codons. Amino acid and nucleotide sequences of RbcL were aligned by sequence alignment programs ClustalW (Larkin et al., 2007), MUSCLE

(Edgar, 2004) and T-Coffee (Notredame et al., 2000). Phylogenetic trees were also generated from results of multiple sequence alignment by using ClustalW-Phylogeny (Larkin et al., 2007). Both amino acid and nucleotide sequences of *RbcL* were obtained from the Genebank Database as following: cyanobacteria *Synechococcus sp.* (Genebank accession No. NC007513) (CyRbcL); red algae *Galdieria partita* (AB018008) (RARbcL); green algae *Chlamydomonas reinhardtii* (NC005353) (GARbcL); a monocot C_3 plant *Oryza sativa* (NC008155) (OsRbcL); a monocot C_4 plant *Zea mays* (NC001666) (ZmRbcL); a dicot C_3 plant *Arabidopsis thaliana* (U91966) (AtRbcL); a dicot C_4 plant *Amaranthus hypochondriacus* (X51964) (AhRbcL); and a single-cell C_4 plant *Bienertia sinuspersici* (DQ499373.1 for the 5'UTR sequence) (BsRbcL). Color Align Conservation service in Sequence Manipulation Suite (Stothard, 2000) was used for the presentation of sequence alignment results from MUSCLE. Percent identities and consensus positions were calculated by AlignX program in Vector NTI (Invitrogen).

Both 3' and 5'UTR sequences were aligned independently by using MUSCLE. For UTR analysis, five higher plant species were included and cyanobacteria, red algae, and green algae were excluded. Additional species were monocot C_3 *Hordeum vulgare* (NC008590) (HvRbcL), dicot C_3 *Solanum tuberosum* (NC008096) (StRbcL), *Nicotiana tabacum* (NC001879) (NtRbcL) and *Spinacia oleracea* (NC002202) (SoRbcL). Different lengths of 5'UTR and 60 bp coding sequence were also aligned by using MUSCLE. Lengths of 5'UTR mature form and intermediate form in each species were determined by similarities to experimental evidences in tobacco (Serino and Maliga, 1998) and *Amaranthus* (McCormac et al., 2001), respectively.

2.16 Secondary structure analysis

Secondary structures of 3'UTR and different lengths 5'UTR of *RbcL* transcripts from various species were predicted by using Mfold (Zuker, 2003) and RNAfold (Hofacker, 2003). The same species used in multiple sequence alignment for UTR sequences were also analysed. Since there was no major inconsistencies between the results from the two programs, only data from RNAfold were shown. Alifold (Hofacker et al., 2002) was used to identify consensus secondary structures in these species. All programs were used with default settings.

CHAPTER 3: REGULATION OF PHOTOSYNTHETIC GENE EXPRESSION IN *BIENERTIA SINUSPERSICI*

3.1 Introduction

As described in Chapter 1, the distribution of photosynthetic enzymes are both developmentally and environmentally regulated in C_4 plants with varying the mode of regulation in different species. Although previous studies in single-cell C_4 species determined the shift in the abundance of the enzymes and transcripts in developing leaves (Voznesenskaya et al., 2004, 2005; Lara et al., 2008), further detailed analysis using immunolocalization at the electron microscope level and *in situ* hybridization would be helpful for a better understanding of the regulation of photosynthetic enzyme distribution in single-cell C_4 species.

Immunolocalization and *in situ* hybridization are powerful methods to determine the distribution of polypeptides and transcripts and they have been used extensively in studies on Kranz-type C_4 plants (Sheen, 1999; Edwards et al., 2001). Immunolocalization was also applied to single-cell C_4 species and successfully revealed the C_4 enzyme distribution (Voznesenskaya et al., 2001, 2002, 2003, 2005; Chuong et al., 2006). However, these immunological studies mainly analyzed the enzyme distribution at the light microscope level. High resolution study at the TEM level is especially important in the study of single-cell C_4 species because the enzyme

---

Part of the results described in this chapter have been published/accepted for publication as the following journal articles: Lung SC, Yanagisawa M, Chuong SDX (2011) Protoplast isolation and transient gene expression in the single-cell C_4 species, *Bienertia sinuspersici*. Plant Cell Rep. 30, 473-484; Lung SC, Yanagisawa M, Chuong SDX (2012) Isolation of dimorphic chloroplasts from the single-cell C_4 species *Bienertia sinuspersici*. Plant Method. In press.

compartmentation occurs at the sub-cellular level unlikeKranz-type C_4 plants which utilize two cell types. It was hypothesized that Furthermore, determination of transcript distribution by using *in situ* hybridization in single-cell C_4 is more challenging than that in Kranz-type C_4 since transcripts of nuclear-encoding genes such as *PEPC*, *PPDK*, and *NAD-ME* are localized in the cytosol of individual chlorenchyma cells.

It was hypothesized that the TEM analysis would elucidate the distribution of photosynthetic proteins in dimorphic chloroplasts of *B. sinuspersici* at fine resolution. In addition, the distribution of transcripts of photosynthetic genes would correlate those of the proteins. To address these hypotheses, the relative abundance of photosynthetic enzymes was examined by TEM analysis with immunolocalization in developing leaves of *B. sinuspersici*. The distribution and accumulation of cytosol- and chloroplast-transcribed transcripts of photosynthetic genes were determined by *in situ* hybridization, semi-quantitative RT-PCR, and real-time qPCR.

3.2 Results

3.2.1 Chlorenchyma cell development and organellar distribution

B. sinuspersici is an annual plant having succulent leaves (Fig. 3.1A; Akhani et al., 2005). The chlorenchyma cells from mature leaves contain two cytoplasimic compartments: a central cytoplasmic compartment (CCC) and a peripheral cytoplasmic compartment (PCC) (Fig. 3.1B; Voznesenskaya et al., 2002). In this study, leaves were divided into five developmental stages: youngest (0.1 cm), young (0.2 cm), intermediate (0.5 – 0.6 cm), intermature (1.0 – 1.2 cm), and mature (> 2 cm) (Fig. 3.1C). The leaves from each developmental stage were processed and observed using TEM. In youngest leaves, chlorenchyma cells are mainly occupied by nuclei and

Figure 3.1 A branch, chlorenchyma cell and five leaf developmental stages of *B. sinuspersici*

A branch of a four-month-old *B. sinuspersici* plant is shown **(A)**. A chlorenchyma cell was isolated from mature *B. sinuspersici* leaves, showing a central cytoplasmic compartment (CCC) and a peripheral cytoplasmic compartment separated by the central vacuole (cv) and connected by cytoplasmic channels **(B)**. Chloroplasts are scattered in the peripheral cytoplasmic compartment (PCh) or gathered in the CCC. Bars = 2 cm in **(A)**, 20 μm in **(B)**. Leaves of *B. sinuspersici* were divided into five developmental stages depending on the length; youngest (0.1 cm in length), young (0.2 cm in length), intermediate (0.5 - 0.6 cm in length), intermature (1.0 - 1.2 cm in length) and mature (more than 2.0 cm in length).

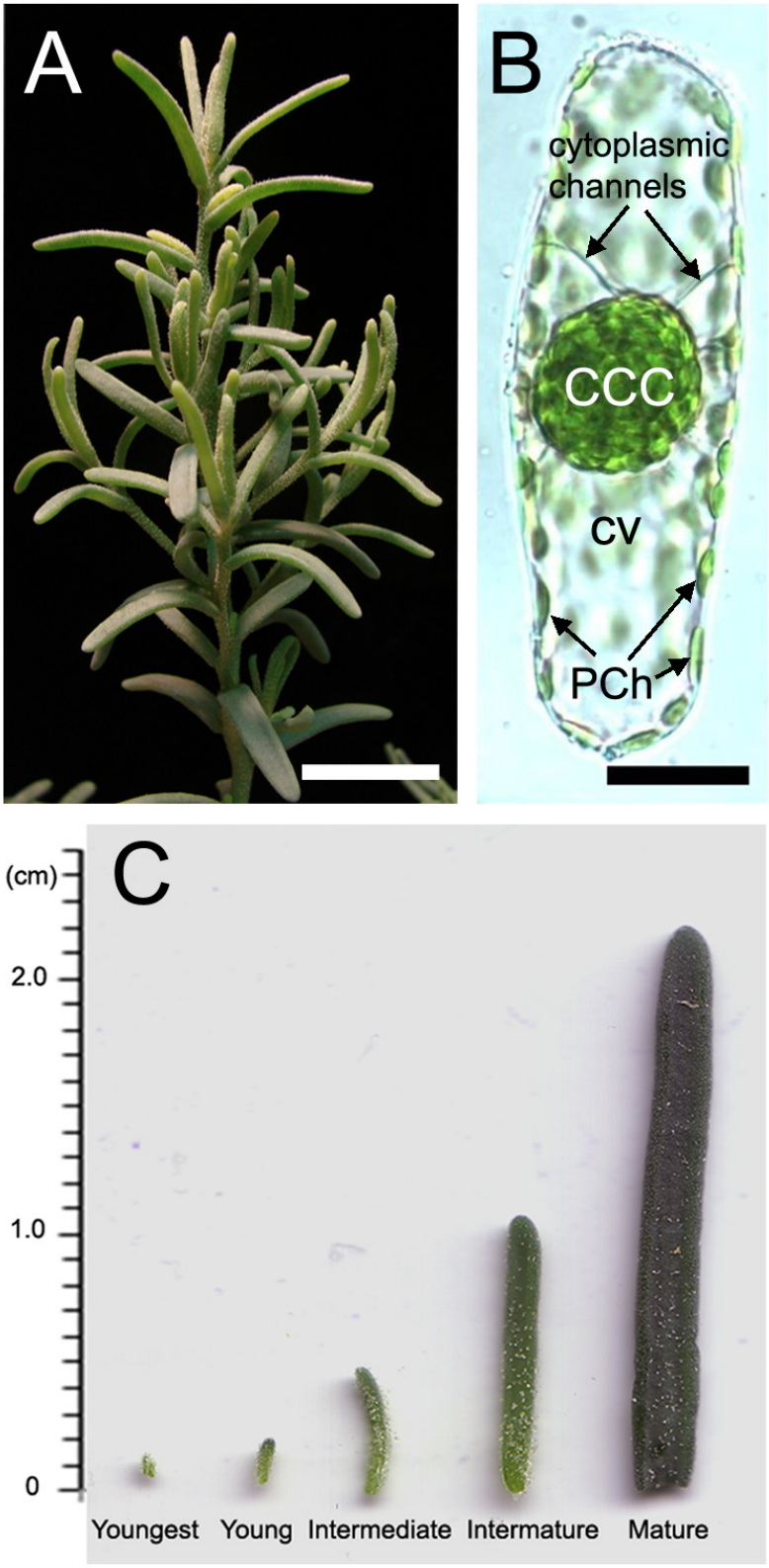
A
B
cytoplasmic
channels
CCC
CV
PCh
C
(cm)
2.0
1.0
0
Youngest
Young
Intermediate
Intermature
Mature

cytoplasm (Fig. 3.2A). There are several chloroplasts similar in morphology and small vacuoles in the cytoplasm. In young leaves, vacuoles developed and fused together pressing cytoplasm and chloroplasts either adjacent to the nucleus or along the cell wall (Fig. 3.2B). In intermediate leaves, there is the first evidence of the formation of the CCC in the center of cells (Fig. 3.2C). Intermature leaves show slightly extended chlorenchyma cells (Fig. 3.2D). In mature leaves, chlorenchyma cells are fully expanded and contain CCC and PCC chloroplasts morphologically distinct from each other (Fig. 3.2E). Chloroplasts in the CCC show well developed grana, particularly those localized in the outer layer of the CCC and contain large starch grains (Fig. 3.3A). Mitochondria and peroxisomes are also packed in this compartment. In previous studies, using rhodamine 123 staining some mitochondria are detected in the PCC associated with chloroplasts although the majority of mitochondria were localized in the CCC in the mature chlorenchyma cell of *B. sinuspersici* (Chuong et al., 2006; Lung et al., 2011). However, at the electron microscope level, no mitochondrion was found in the PCC. Instead, approximately 20% (20.1% ± 6%) of PCC chloroplasts were associated with peroxisomes and/or autophagosomes in ultra thin sections (60 – 80 nm) of mature leaves (Fig. 3.3B; see Chapter 5). To distinguish between peroxisomes and autophagosomes, anti-catalase antibody was used for the immunolocalization experiment. The labelling for catalase showed that the micro organelles having a single-membrane were indeed peroxisomes (Fig. 3.3C).

3.2.2 Immunolocalization

Previously, immunolocalization of RbcL and PPDK in chlorenchyma cells of mature *B. sinuspersici* leaf was shown at the light microscope level (Chuong et al., 2006). Offermann et al. (2011) also reported the relative amount of RbcL and PPDK in two types of chloroplasts

Figure 3.2 Transmission electron micrographs of chlorenchyma cells in developing leaves of *B. sinuspersici*

Leaves from various developmental stages were processed and observed using transmission electron microscopy (TEM). Images are chlorenchyma cells in youngest **(A)**, young **(B)**, intermediate **(C)**, intermature **(D)** and mature **(E)** leaves of *B. sinuspersici*. CCC, central cytoplasmic compartment; Ch, chloroplast; n, nucleus; v, vacuole; PCh, chloroplasts in the peripheral cytoplasmic compartment. Bars = 2 μm in **(A-D)**, 10 μm in **(E)**.

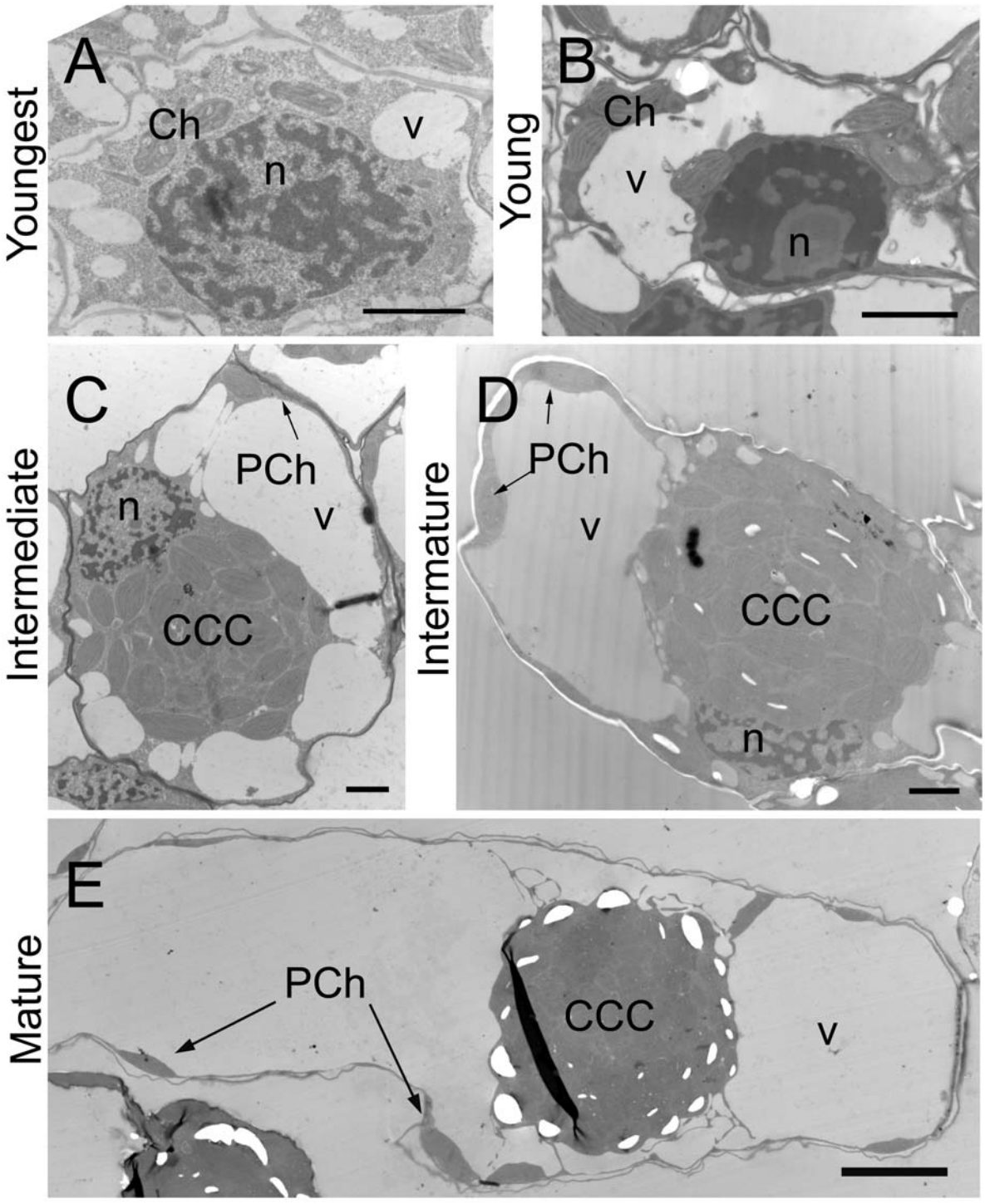
Youngest
A
Ch
n
v
Young
B
Ch
v
n
Intermediate
C
PCh
n
v
CCC
Intermature
D
PCh
v
CCC
n
Mature
E
PCh
CCC
v

Figure 3.3 Transmission electron micrographs of organelles in CCC and PCC

Mature *B. sinuspersici* leaves were observed using TEM. Mitochondria surrounded by chloroplasts are packed inside of the CCC and some autophagic organelles (arrows) are also visible in this compartment **(A)**. Autophagosomes are occasionally found associated with peripheral chloroplasts **(B)**. Peroxisomes are also detected in close proximity to the PCC chloroplasts as verified by immunolocalization studies using anti-catalase antibody **(C)**. CCC, central cytoplasmic compartment; PCC, peripheral cytoplasmic compartment; Ch, chloroplast; s, starch; m, mitochondrion; cv, central vacuole; ap, autophagosome; av, autophagic vacuole; p, peroxisome; cw, cell wall. Bars = 2 μm in **(A)**, 500 nm in **(B, C)**.

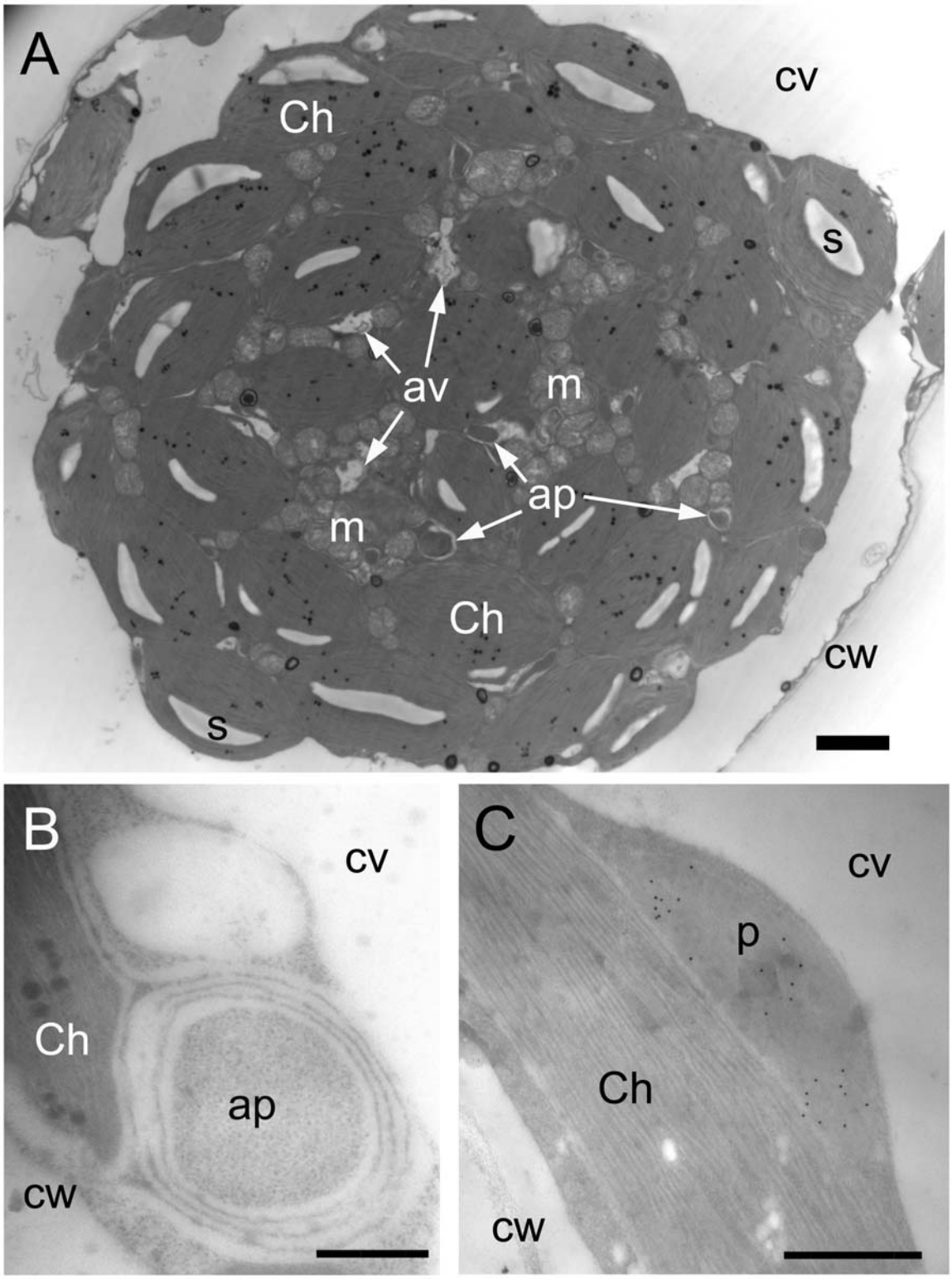
A
cv
Ch
s
av
m
ap
m
Ch
cw
s
B
cv
Ch
ap
cw
C
cv
p
Ch
cw

semi-quantitatively by isolating chloroplasts from the CCC and PCC compartments. However, quantitative analysis of these enzyme distributions in two types of chloroplasts with a high resolution is yet to be completed. To quantify the enzyme distribution at different developmental stages, I carried out immuno-gold labelling for RbcL (Fig. 3.4) and PPDK (Fig. 3.5) observed at the electron microscope level and calculated the density of gold particles (Fig. 3.6). In this analysis, the CCC chloroplasts were further divided into two groups: chloroplasts in the inner (CCC inner: CCCI chloroplasts) and outer region of the CCC (CCC outer: CCCO chloroplasts). Low labelling for RbcL was observed in cells of youngest leaves with very low density and gradually increased throughout the development with the exception of PCC chloroplasts in the mature leaves (Fig. 3.4K and 3.6). In the intermediate leaves, the CCC and the PCC were clearly evident (Fig. 3.2C). RbcL accumulates evenly in chloroplasts with slightly reduced amount in the PCC at intermediate and intermature leaves (Fig. 3.4C-H and 3.6). In mature leaves, the RbcL accumulated preferentially in the CCCI and CCCO chloroplasts, whereas it was scarce in the PCC chloroplasts (Fig. 3.4I-K and 3.6). The density of gold particles for RbcL in both CCCI and CCCO chloroplasts was more than twenty-fold in comparison to that in PCC chloroplasts in mature leaves (Fig. 3.6). The labelling for PPDK was rarely observed in youngest leaves (Fig. 3.5A). Although it accumulated in young leaves, unlike RbcL, the density of PPDK remain unchanged until the intermediate stage (Fig. 3.5B-E and 3.6). In intermature leaves, PPDK started showing a concentration gradient such that the density was low in the CCCI, moderate in the CCCO, and high in the PCC chloroplasts (Fig. 3.5F-H and 3.6). This gradient became more distinct in mature leaves showing approximately 2- and 6-fold more PPDK accumulation in the PCC than that in the CCCO and CCCI, respectively (Fig. 3.4I-K and 3.6).

In addition to Rubisco and C_4 enzymes, photosystem proteins are also known to differentially distribute in the M and BS cell in Kranz-type C_4 species (Majeran et al., 2008). To

Figure 3.4 Immunolocalization of RbcL in chloroplasts in developing leaves of *B. sinuspersici*

Leaf cross sections are from various developmental stages. Sections were probed with RbcL antiserum and then with a gold-conjugated secondary antibody. Images are transmission electron micrographs of chloroplasts in youngest **(A)**, young **(B)**, intermediate **(C-E)**, intermature **(F-H)**, and mature **(I-K)** leaves showing specific reaction of RbcL antibody. Starting from the intermediate stage, the CCC and PCC **(E, H, K)** are evident. Chloroplasts in the CCC were further divided into the inner layer of CCC (CCCI: **C, F, I**) and outer layer of CCC (CCCO: **D, G, J**). White arrows indicate gold particles **(A, B)**. RbcL, Rubisco large subunit; CCC, central cytoplasmic compartment; PCC, peripheral cytoplasmic compartment; s, starch; cv, central vacuole; cw, cell wall. Bars = 200 nm in **(A, B)**, 500 nm in **(C-K)**.

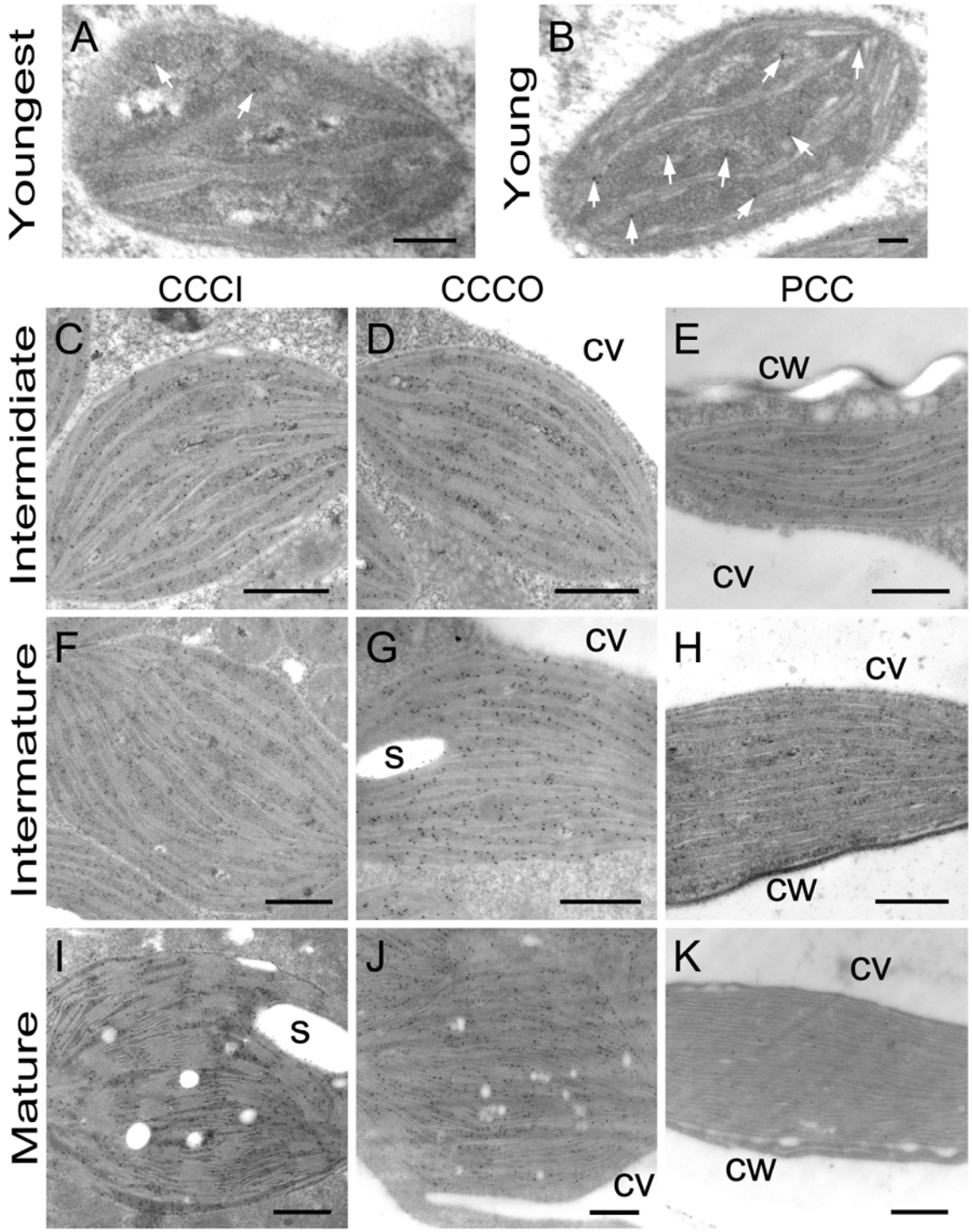
Youngest
A
B
Young
CCCI
CCCO
PCC
Intermidiate
C
D
cv
E
cw
cv
Intermature
F
G
cv
s
H
cv
cw
Mature
I
s
J
cv
K
cv
cw

Figure 3.5 Immunolocalization of PPDK in chloroplasts in developing leaves of *B. sinuspersici*

Leaf cross sections are from various developmental stages. Sections were probed with PPDK antiserum and then with a gold-conjugated secondary antibody. Images are transmission electron micrographs of chloroplasts in youngest **(A)**, young **(B)**, intermediate **(C-E)**, intermature **(F-H)**, and mature **(I-K)** leaves showing specific reaction of PPDK antibody. Starting from the intermediate stage, the CCC and PCC **(E, H, K)** are evident. Chloroplasts in the CCC were further divided into the inner layer of CCC (CCCI: **C, F, I**), and outer layer of CCC (CCCO: **D, G, J**). White arrows indicate gold particles **(B)**. CCC, central cytoplasmic compartment; PCC, peripheral cytoplasmic compartment; cv, central vacuole; cw, cell wall. Bars = 200 nm in **(A, B)**, 500 nm in **(C-K)**.

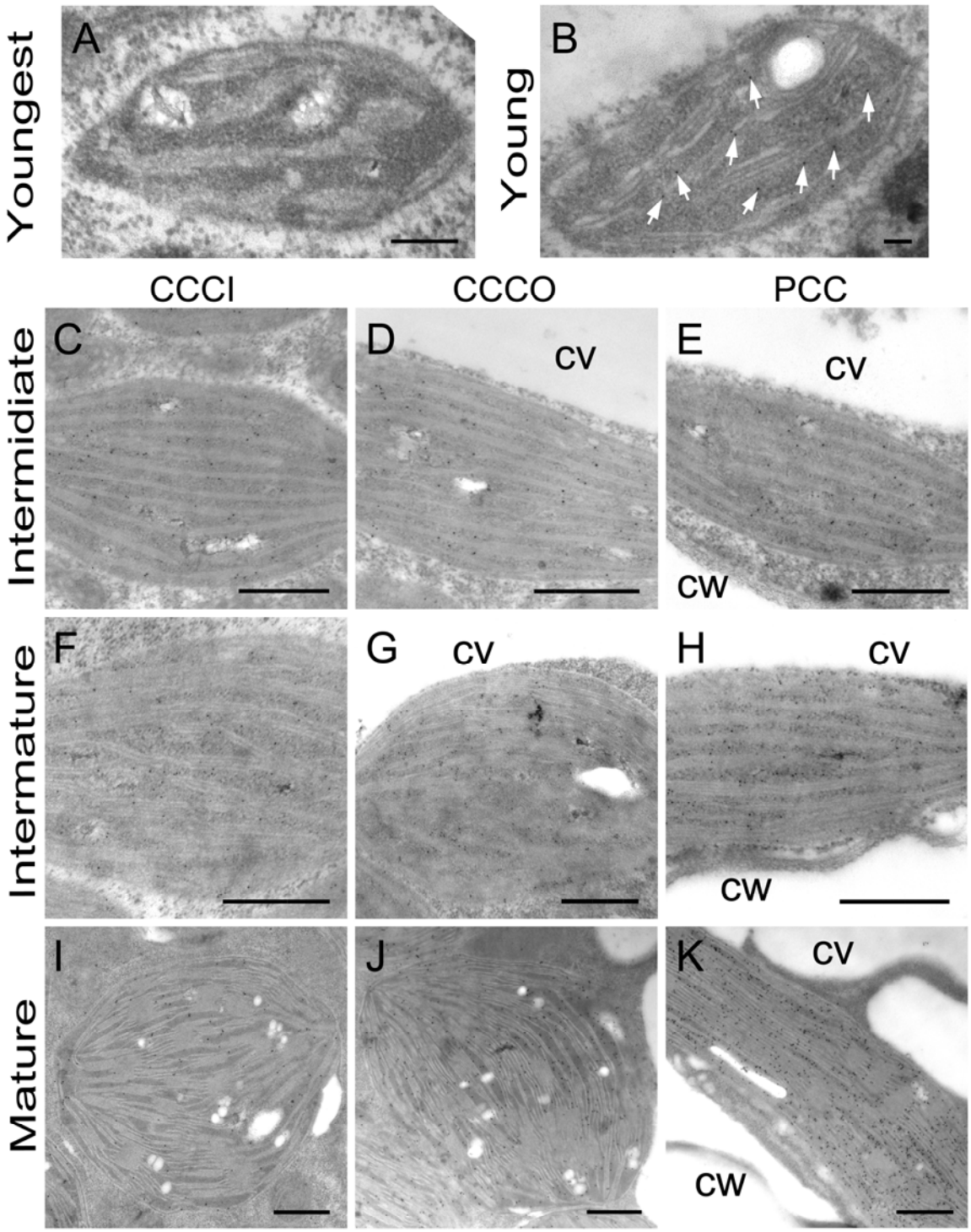
Youngest
A
Young
B
CCCI
CCCO
PCC
Intermidiate
C
D
cv
E
cv
cw
Intermature
F
G
cv
H
cv
cw
Mature
I
J
K
cv
cw

Figure 3.6 Quantification of RbcL and PPDK in chloroplasts in developing leaves of *B. sinuspersici* based on immunolocalization analyses

The number of gold particles per area (μm^2) was determined for RbcL and PPDK in developing leaves. Gold particles were counted and expressed nunber per area (μm^2) in chloroplasts in 25 cells from three different samples. Significance was determined by student *t*-test ($p < 0.01$). Different letters represent a significant difference (a and b for RbcL; a', b', and c' for PPDK). Error bars indicate standard errors. RbcL, Rubisco large subunit; CCCI, central cytoplasmic compartment inner region; CCCO, central cytoplasmic compartment outer region; PCC, peripheral cytoplasmic compartment.

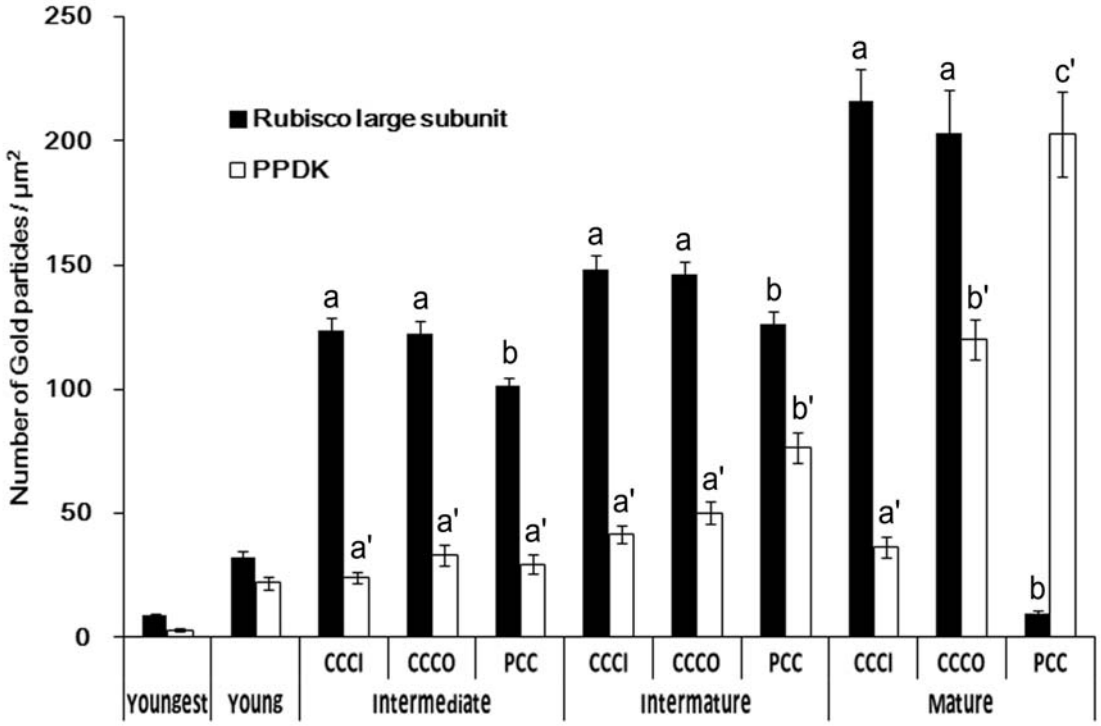
Number of Gold particles / µm²
250
200
150
100
50
0
Rubisco large subunit
PPDK
a
a'
a
a'
b
a'
a
a'
a
a'
b
b'
a
a'
a
b'
b
c'
CCCI
CCCO
PCC
CCCI
CCCO
PCC
CCCI
CCCO
PCC
Youngest
Young
Intermediate
Intermature
Mature

investigate the PSII distribution and accumulation in *B. sinuspersici*, I performed immunolocalization of PsbO which is a 33 kD protein in the oxygen evolving complex associated with the photosystem (PS) II reaction center. The distribution of cytochrome f in the two types of chloroplasts was also analyzed for comparison with the PsbO distribution because cytochrome f has been considered to be distributed equally between M and BS chloroplasts in the Kranz-type C_4 species maize (Majeran et al., 2008). The labelling for PsbO was observed mostly on the grana membrane (Fig. 3.7A, B and insets), whereas cytochrome f was distributed evenly to the grana membrane and stroma lamellae as expected (Fig. 3.7 D, E and insets). The density of PsbO in the CCCI and CCCO chloroplasts were 1.6-fold higher than in the PCC chloroplasts (Fig. 3.7C), while the density of cytochrome f was similar in all types of chloroplasts although it was slightly low in the CCCI chloroplasts (Fig. 3.7F).

3.2.3 Optimization of PEG-mediated protoplast transfection and *in vivo* protein localization analysis

All C-terminal EGFP-fusion constructs containing full-length or transit-peptide sequence of various cDNAs including *RbcS* and *PPDK* were generated for the *in vivo* protein localization analysis. All constructs were verified by DNA sequencing and their expression was confirmed by biolistc transformation of onion epidermal cells prior to transfection experiments (Fig. 3.8A-D). After verification by the biolistic transformation, EGFP-fusion constructs were transfected into chlorenchyma protoplasts of *B. sinuspersici*. Chlorenchyma protoplasts were prepared from 3- to 4-month old healthy leaves of *B. sinuspersici* (Fig. 3.8E). After cell wall digestion, the isolated protoplast still maintained two compartments showing CCC and PCC chloroplasts (Fig. 3.8F). I

Figure 3.7 Immunolocalization and quantification of PsbO and Cytochrome f in chloroplasts in mature leaves of *B. sinuspersici*

Immunolocalization and quantification of PsbO **(A-C)** and Cytochrome f **(D-F)** in mature leaves are shown. Images are transmission electron micrographs of CCC **(A and D)** and PCC **(B and E)** chloroplasts probed with PsbO and Cytochrome f antisera. Bars = 500 nm (100 nm in inset). Gold particles were counted and expressed number per area (μm^2) in chloroplasts in 25 cells from three different samples **(C and F)**. Error bars indicate standard errors. Significance was determined by student *t*-test ($p < 0.01$). Different letters represent a significant difference (a and b for PsbO; a' for cytochrome f). CCCI, central cytoplasmic compartment inner region; CCCO, central cytoplasmic compartment outer region; PCC, peripheral cytoplasmic compartment.

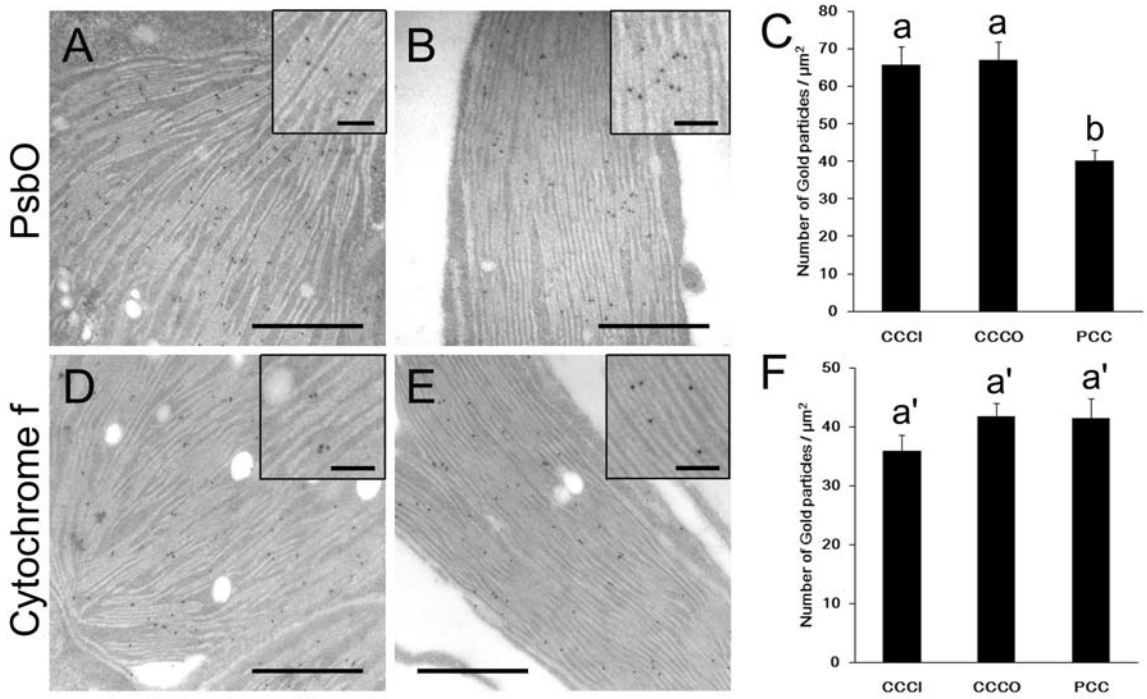
A
B
C
PsbO
Number of Gold particles / µm²
a
a
b
CCCI
CCCO
PCC
D
E
F
Cytochrome f
Number of Gold particles / µm²
a'
a'
a'
CCCI
CCCO
PCC

Figure 3.8 Transient expression of EGFP proteins in onion epidermal cells and *B. sinuspersici* chlorenchyma protoplasts

Biolistic transformation in onion epidermal cells shows signals of EGFP fused to an actin-binding domain, Lifeact **(A)**, a microtubule-binding protein, MAP4 **(B)**, a peroxisomal targeting signal **(C)**, or the transit peptides of NAD-ME **(D)**. Protoplasts were prepared from *B. sinuspersici* chlorenchyma cells **(E)**. Bright field (left panel), chlorophyll autofluorescence (middle panel) and merged images (right panel) of an individual protoplast are shown **(F)**. Bars = 10 µm **(A-D)**, 50 µm **(E)**, 20 µm **(F)**. NAD-ME, nicotinamide adenine dinucleotide malic enzyme

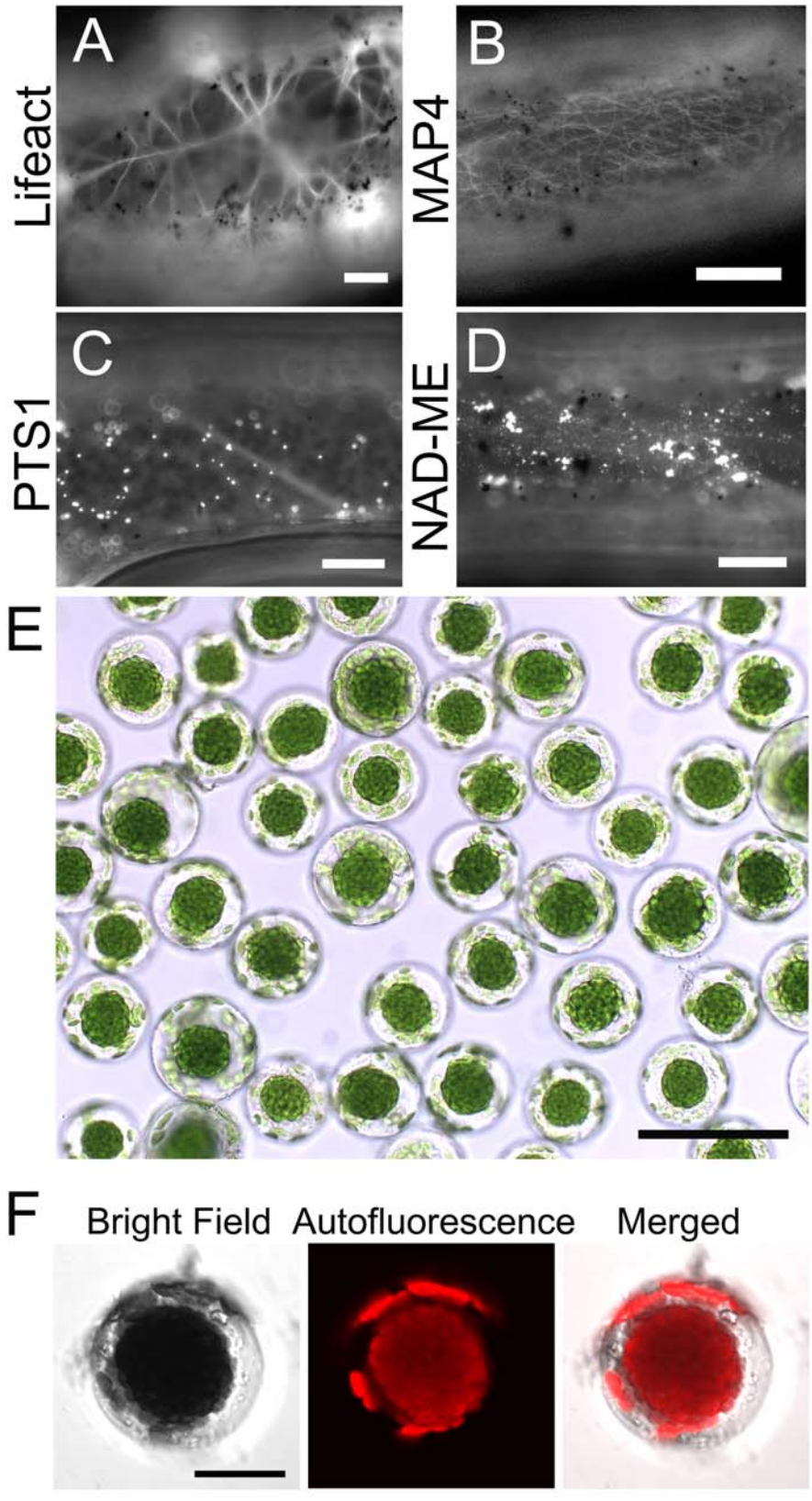
A
B
Lifeact
MAP4
C
D
PTS1
NAD-ME
E
F
Bright Field
Autofluorescence
Merged

empirically optimized the transfection conditions to obtain a high efficiency using the pSAT6-35S::EGFP-N1 plasmid (Chung et al., 2005). The optimized PEG-mediated transfection protocol was capable of providing a transfection efficiency of 50 – 90%, largely depending on plant conditions and EGFP constructs (Fig. 3.9A), an increase of more than ten-fold of the efficiency in the initial protocol (established by Shiu-Cheung Lung in our laboratory). Transfecting 1.5 X 10^4 protoplasts with 5 or 10 μg of plasmid DNA resulted in over 80% of protoplasts expressing the EGFP reporter gene (Fig. 3.9B). To further investigate whether protoplasts could be transfected using metabolically more inert osmotica, D-sorbitol or D-mannitol were substituted for sucrose included in transfection buffers (Fig. 3.9C). I found that the transfection efficiencies with different tested osmotica varied insignificantly, ranging from 77 to 84%. The transfection efficiency also apparently varied with the duration and conditions of post-transfection incubation. For examples, the maximum number of protoplasts expressing the reporter gene was achieved after 12-h incubation under low light intensity (30 μmol m^{-2} s^{-1}) or a prolonged 18-h in the dark incubation (Fig. 3.9D), whereas less than half of the protoplasts expressed the reporter gene after 12-h incubation in the dark.

To observe the *in vivo* localization of various proteins in *B. sinuspersici* chlorenchyma protoplasts, the optimized protocol of protoplast transfection was used. In the absence of targeting signal, EGFP protein resided mainly in the cytoplasm and diffused passively into the nuclei (Fig. 3.10A). The addition of a nuclear targeting signal (NLS) at the N-terminus, on the other hand, targeted the reporter protein exclusively to the nuclei (Fig. 3.10B). An extensive network of actin filament was visualized throughout the cytoplasm when an EGFP-fusion protein with talin, an actin-binding protein was used (Fig. 3.10C; Kost et al., 1998). Lifeact-EGFP (Riedl et al., 2008) and ABD2-EGFP (Sheahan et al., 2004) constructs were also used to compare the *in*

Figure 3.9 Protoplasts transiently expressing EGFP driven by the constitutive 35S promoter and transfection efficiencies under various conditions

Isolated protoplasts were transfected with 5 μg of pSAT6-35S::EGFP-N1 plasmid DNA and imaged under epifluorescence microscopy **(A)**. EGFP fluorescence (left panel), chlorophyll autofluorescence (middle panel) and a merged image (right panel) are shown. Bar = 20 μm. Effect of plasmid concentration **(B)**, various osmotica **(C)**, and light **(D)** on protoplast transfection efficiencies. Transfection efficiencies were determined as percentages of EGFP-expressing protoplasts over the total number of protoplasts (n > 100) randomly counted under epifluorescence microscopy. The depicted values represent means from at least four independent experiments. Error bars indicate standard errors.

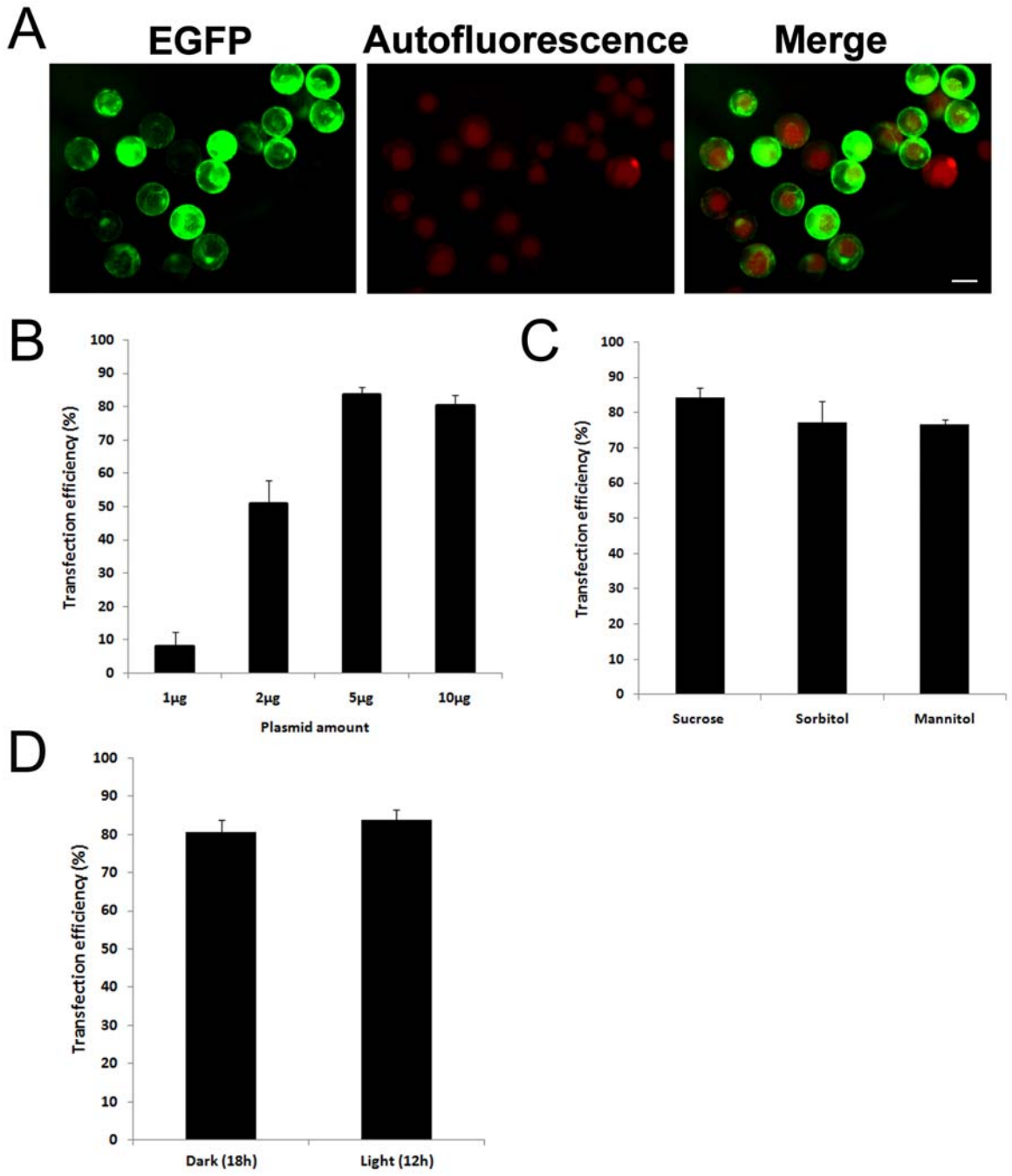
A
EGFP
Autofluorescence
Merge
B
Transfection efficiency (%)
100
90
80
70
60
50
40
30
20
10
0
1μg
2μg
5μg
10μg
Plasmid amount
C
Transfection efficiency (%)
Sucrose
Sorbitol
Mannitol
D
Transfection efficiency (%)
Dark (18h)
Light (12h)

Figure 3.10 Transient expression of EGFP fusion proteins localized to various subcellular organelles

Isolated protoplasts were transfected with 5 μg of DNA of various plasmid constructs for transient expression of EGFP-fusion proteins driven by the constitutive 35S promoter. Live protoplasts were visualized under confocal laser scanning microscopy. Each image shows a representative result from at least three independent experiments. EGFP fluorescence (*left panels* excitation at 488 nm and emission detected at 509 nm) chlorophyll autofluorescence (*middle panels* excitation at 649 nm and emission detected at 666 nm) and merged images (*right panels*) are shown. EGFP protein was either unmodified **(A)**, fused to a nuclear localization signal **(B)**, an actin-binding protein, talin **(C)**, a microtubule-binding protein, MAP4 **(D)**, or a peroxisomal targeting signal **(E)**. EGFP protein was also fused to PEPC **(F)**, the transit peptides (TP) of NAD-ME **(G)** or RbcS **(H)**, full-length PPDK **(I)** or RbcS **(J)**, an actin-binding domain, Lifeact **(K)** or ABD2 **(L)**. Bars = 20 μm. PEPC, phosphoenolpyruvate carboxylase; NAD-ME, nicotinamide adenine dinucleotide malic enzyme; RbcS, Rubisco small subunit.

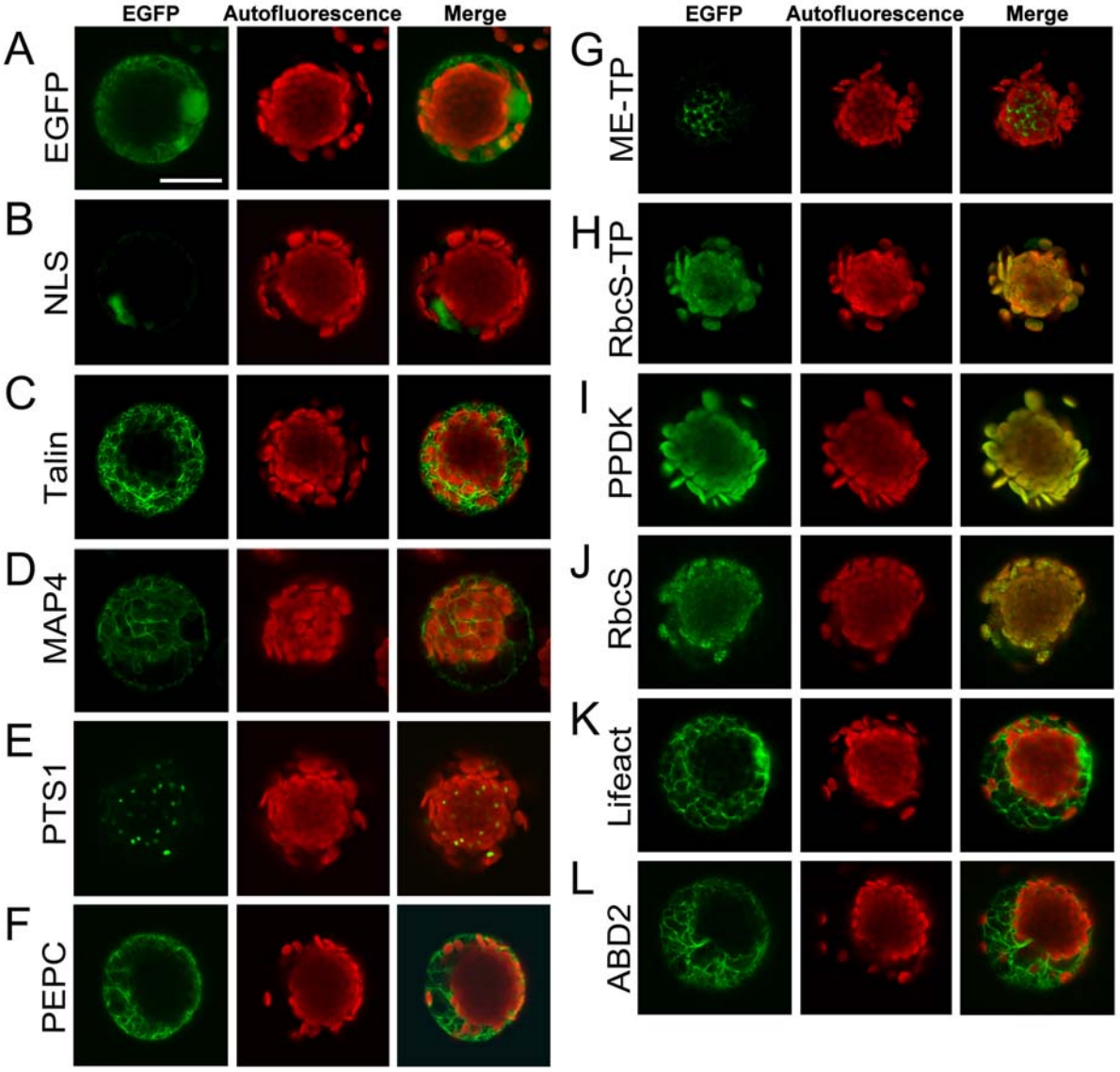
EGFP
Autofluorescence
Merge
A
EGFP
B
NLS
C
Talin
D
MAP4
E
PTS1
F
PEPC
G
ME-TP
H
RbcS-TP
I
PPDK
J
RbcS
K
Lifeact
L
ABD2

vivo organization of the actin cytoskeleton to that observed with EGFP-talin (Fig. 3.10K and L). These actin-targeting domains efficiently bound to actin filaments and the EGFP signals were comparable to that of the EGFP-talin. Similarly, EGFP-fusion with MAP4, a microtubule-associated protein (Marc et al., 1998), was used to examine the microtubule network in protoplasts (Fig. 3.10D). The inclusion of the Ser-Lys-Leu (SKL) tripeptide, a PTS1 (Gould et al., 1989), at the C-terminal tail of EGFP resulted in distinctive fluorescence-labeled peroxisomes, which were found more abundant in the CCC than the PCC (Fig. 3.10E; Chuong et al., 2006).

I also studied the subcellular localization of various photosynthetic and C_4 enzymes. EGFP–PEPC fusion protein was exclusively localized in the cytoplasm (Fig. 3.10F) and was excluded from passively diffusing into the nuclus due to its size (138 kDa) which exceeds the 90 – 110 kDa diffusion limit of the nuclear pores (Wang and Brattain, 2007). The mitochondrial targeting signal of NAD-ME targeted the reporter protein exclusively to the mitochondria in the CCC (Fig. 3.10G), whereas the transit peptides of RbcS guided the EGFP protein to chloroplast stroma in both CCC and PCC (Fig. 3.10H). In addition, EGFP constructs containing the full-length coding sequence of PPDK or RbcS were also transfected into protoplasts. The PPDK- and RbcS-EGFP signals were detected in both CCC and PCC chloroplasts (Fig. 3.10I and J, respectively). In addition, the full-length RbcS-EGFP fusion also accumulated in punctate structures at the peripheral of chloroplasts. In contrast to my immunolocalization results, there appeared to be no preferential accumulation of these proteins in two chloroplast types when their expression was driven by the constitutive 35S promoter.

3.2.4 Transcript localization analysis

Photosynthetic proteins are differentially distributed in dimorphic chloroplasts in mature leaves of *B. sinuspersici* as reported previously (Chuong et al., 2006) and as found in my immunolocalization studies. Therefore, it was expected that the distribution of their transcripts would correlate that of the proteins. Initially, the subcellular localization of *rbcL*, *rbcS*, *PEPC*, *PPDK* and *NAD-ME* transcripts in developing leaves was determined by *in situ* hybridization by using the first protocol (outlined in Materials and Methods). The approximate relative abundance of transcripts was estimated from the intensity of purple color. First, developing leaves of shoot tips were sectioned and the sections were hybridized to mRNAs to obtain a general idea of the transcript distribution. All tested transcripts were observed more abundantly in the adaxial side than in the abaxial side in developing leaves (Fig. 3.11 top panels). Next, the accumulation of each transcript was examined at different stages of development. Only *rbcL* transcripts were observed at very low level in the youngest leaves (Fig. 3.11A). The level of *rbcL* accumulation increased at the young stage when the CCC had not yet formed. At the intermediate stage, *rbcL* accumulated both in the CCC and PCC chloroplasts; however, *rbcL* was observed only in the CCC at the mature stage. *rbcS* and *PEPC* transcripts appeared in the cytosol at the young stage while *PPDK* and *NAD-ME* became detectable in the cytosol from the intermediate stage. Contrary to my expectations, the cellular localization of nuclear encoded transcripts such as *rbcS*, *PEPC*, *PPDK*, and *NAD-ME* did not change throughout the leaf age. Finally, *rbcL* or *PEPC* transcripts were hybridized to the longitudinal sections of intermature leaves to determine whether accumulation of the transcripts was different in the chlorenchyma cells from the base to the tip of the leaves. The *rbcL* transcript was detected in all chloroplasts of chlorenchyma cells at the base where the CCC has not completely formed. It was observed in the CCC and PCC

Figure 3.11 Accumulation and localization of various photosynthetic transcripts in developing leaves of *B. sinuspersici*.

Sections were prepared from shoot tips and mature leaves. Images are cross-sections of shoot tips (top panels) and enlarged images of leaves at various developmental stages (youngest, young, intermediate, and mature). Sections were hybridized with labelled sense *rbcL* (left panels: Sense) or antisense *rbcL, rbcS* **(A)**, *PEPC, PPDK,* or *NAD-ME* **(B)** RNA probes.. Specific hybridization is observed as a purple color. Scale bars = 300 μm in shoot tips, 20 μm in youngest and young leaves, 30 μm in intermediate and mature leaves. *rbcL*, Rubisco large subunit; *rbcS*, Rubisco small subunit; *PEPC*, phosphoenolpyruvate carboxylase; *PPDK*, pyruvate Pi dikinase; *NAD-ME*, nicotinamide adenine dinucleotide malic enzyme.

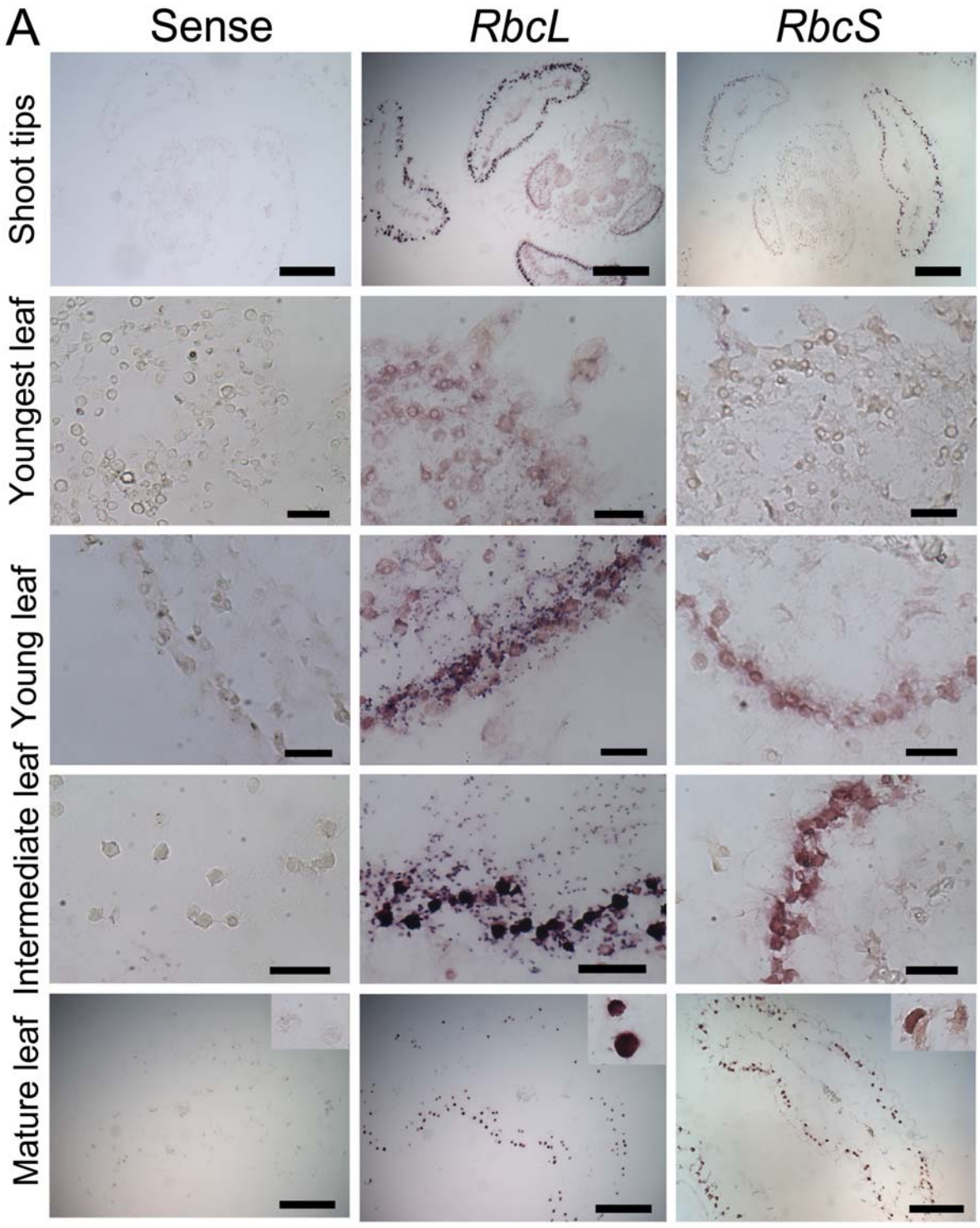
A
Sense
RbcL
RbcS
Shoot tips
Youngest leaf
Young leaf
Intermediate leaf
Mature leaf

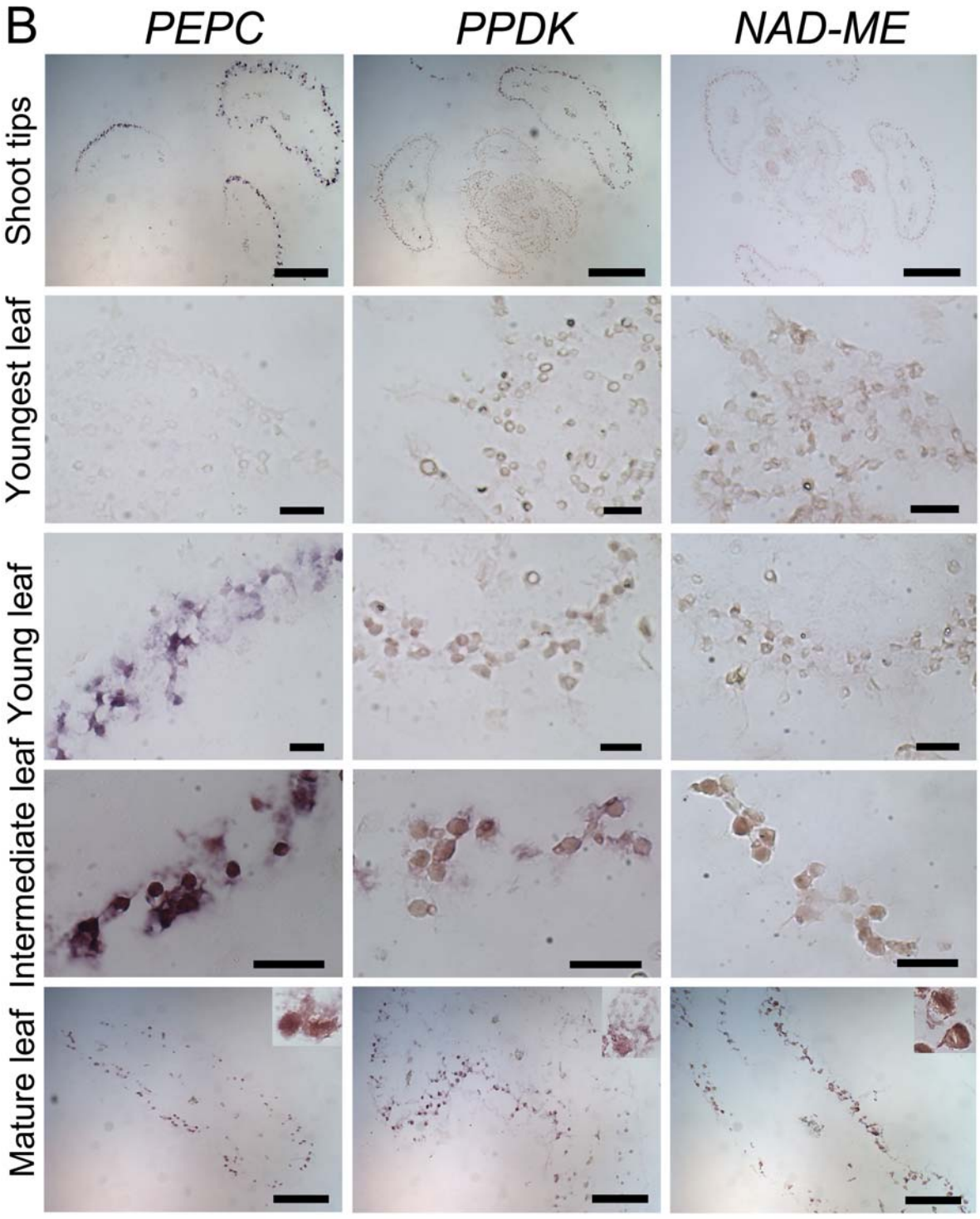
B
PEPC
PPDK
NAD-ME
Shoot tips
Youngest leaf
Young leaf
Intermediate leaf
Mature leaf

chloroplasts of chlorenchyma cells at the middle part while it was restricted in the CCC at the tip (Fig. 3.12A). Although the *PEPC* transcript did not show change in its localization, its abundance increased from the base to the tip (Fig. 3.12B). Since nuclear-encoded transcripts such as *PEPC*, *PPDK*, and *NAD-ME* are localized in cytosol and are difficult to trace with the resolution of *in situ* hybridization at the light microscope level, plastid-encoded transcripts were chosen for further detailed analysis. The subcellular localizations of *rbcL*, *psaB*, and *psbA* transcripts and *16S* rRNA in developing leaves of *B. sinuspersici* were determined by *in situ* hybridization using a different protocol (outlined in Materials and Methods; Fig. 3.13). Better preservation in cell structures was achieved by replacing the fixation solution FAA by the ethanol-acetic acid mixture and the infiltration solution xylene by tert-butyl alcohol. In addition, sections were counterstained with Safranin O after color development for a better visualization of cell structures. Sense strand of *rbcL* RNA was hybridized to leaf sections as negative controls, which only showed orange, pink, and red colors as a result of Safranin O staining (Fig. 3.13A-C). Note that the nucleus is the largest structure in the young leaves (Fig. 3.13 left panels) while the CCC forms and becomes the largest in the intermediate and mature leaves (Fig. 3.13 middle and right panels). In agreement with the results shown above, *rbcL* transcripts accumulated in all scattered chloroplasts that appeared as purple dots in young leaves where the CCC has not yet formed (Fig. 3.13D). In intermediate leaves, abundant *rbcL* mRNA was observed both in the CCC and PCC chloroplasts (Fig. 3.13E). However, majority of *rbcL* transcripts were localized in the CCC with a slight accumulation in the PCC chloroplasts in mature leaves (Fig. 3.13F). The PCC chloroplasts were barely visible without Safranin O counterstaining (Fig. 3.13F inset). In contrast to my expectations, *psaB* (Fig. 3.13G-I) and *psbA* transcripts (Fig. 3.13J- L) exhibited a distribution similar to that of the *rbcL* transcripts. The *16S* rRNA accumulated in similar amount in both the CCC and PCC throughout the leaf age

Figure 3.12 Accumulation of *rbcL* and *PEPC* transcripts in longitudinal sections of *B. sinuspersici* leaves

Longitudinal sections were prepared from an approximately 10-mm leaf. Sections were hybridized with labelled antisense *rbcL* **(A)** or *PEPC* **(B)** RNA probe. Micrographs are longitudinal-sections of the entire leaf (upper panels) and enlarged images of representative positions of the leaf (Base, Middle, and Tip: lower panels). Specific hybridization is observed as a purple color. Bars = 500 μm in upper panels, 100 μm in lower panels. *rbcL*, Rubisco large subunit. *PEPC*, phosphoenolpyruvate carboxylase.

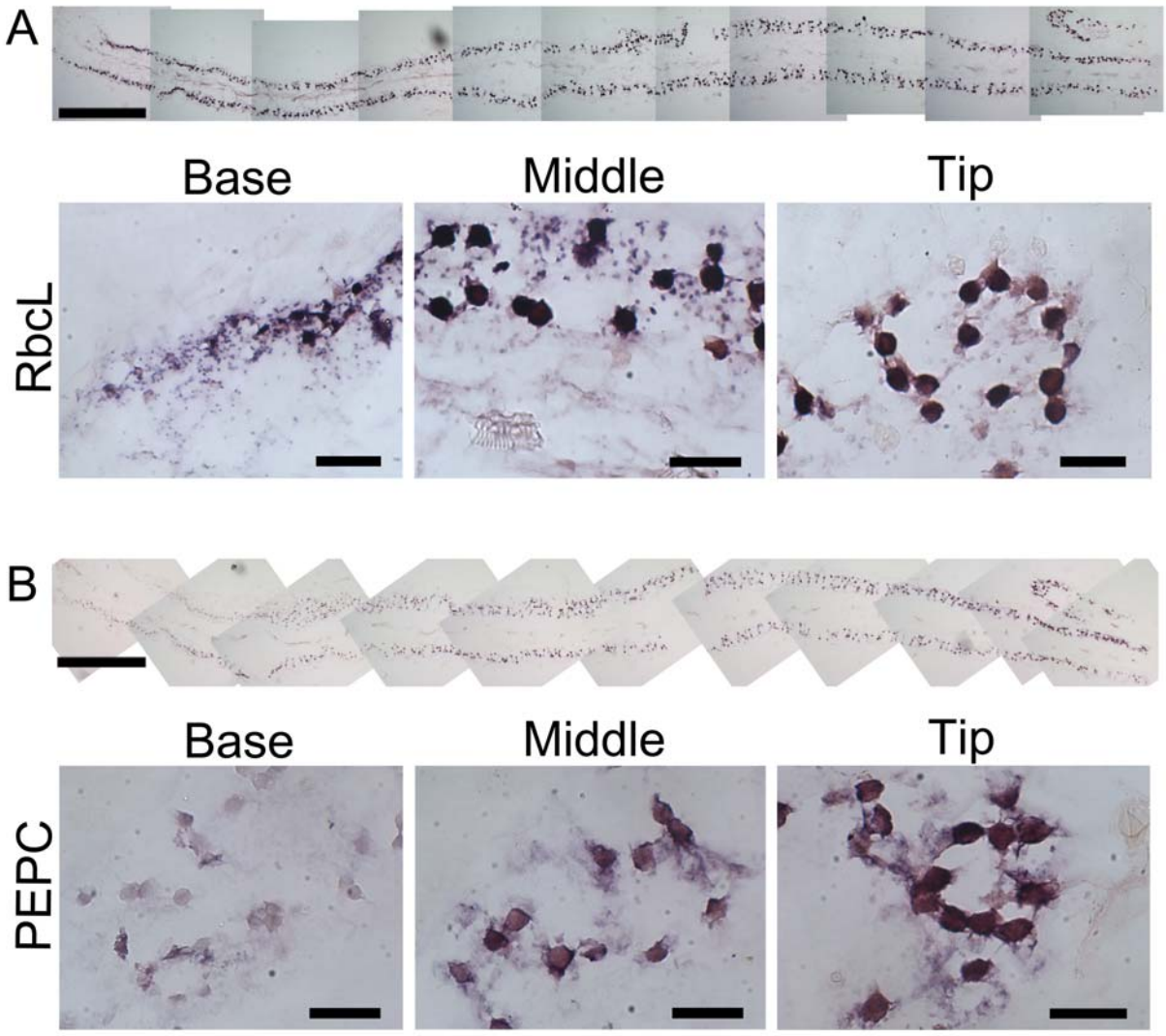
A
Base
Middle
Tip
RbcL
B
Base
Middle
Tip
PEPC

Figure 3.13 Chloroplastic transcript localization in chlorenchyma cells of developing *B. sinuspersici* leaves

Sections were prepared from shoot tips and mature leaves. Images are enlarged images of leaves at three developmental stages: young **(A, D, G, J, M)**, intermediate **(B, E, H, K, N)**, and mature **(C, F, I, L, O)**. Cross-sections were hybridized with labelled sense *rbcL* **(A-C)** or antisense *rbcL* **(D-F)**, *psaB* **(G-I)**, *psbA* **(J-L)** or *16S* **(M-O)** RNA probe. Sections were counter stained by safranine O for better visualization of cellular structures except for the inset image in **(F)**. A chlorenchyma cell is outlined by a dashed line in upper panels (**A-C**). Specific hybridization is observed as a purple color. CCC, central cytoplasmic compartment; PCh, chloroplasts in the peripheral cytoplasmic compartment (PCC); e, epidermal cells; ws, water storage cells; n, nuclei; *rbcL*, Rubisco large subunit. Bars = 20 μm.

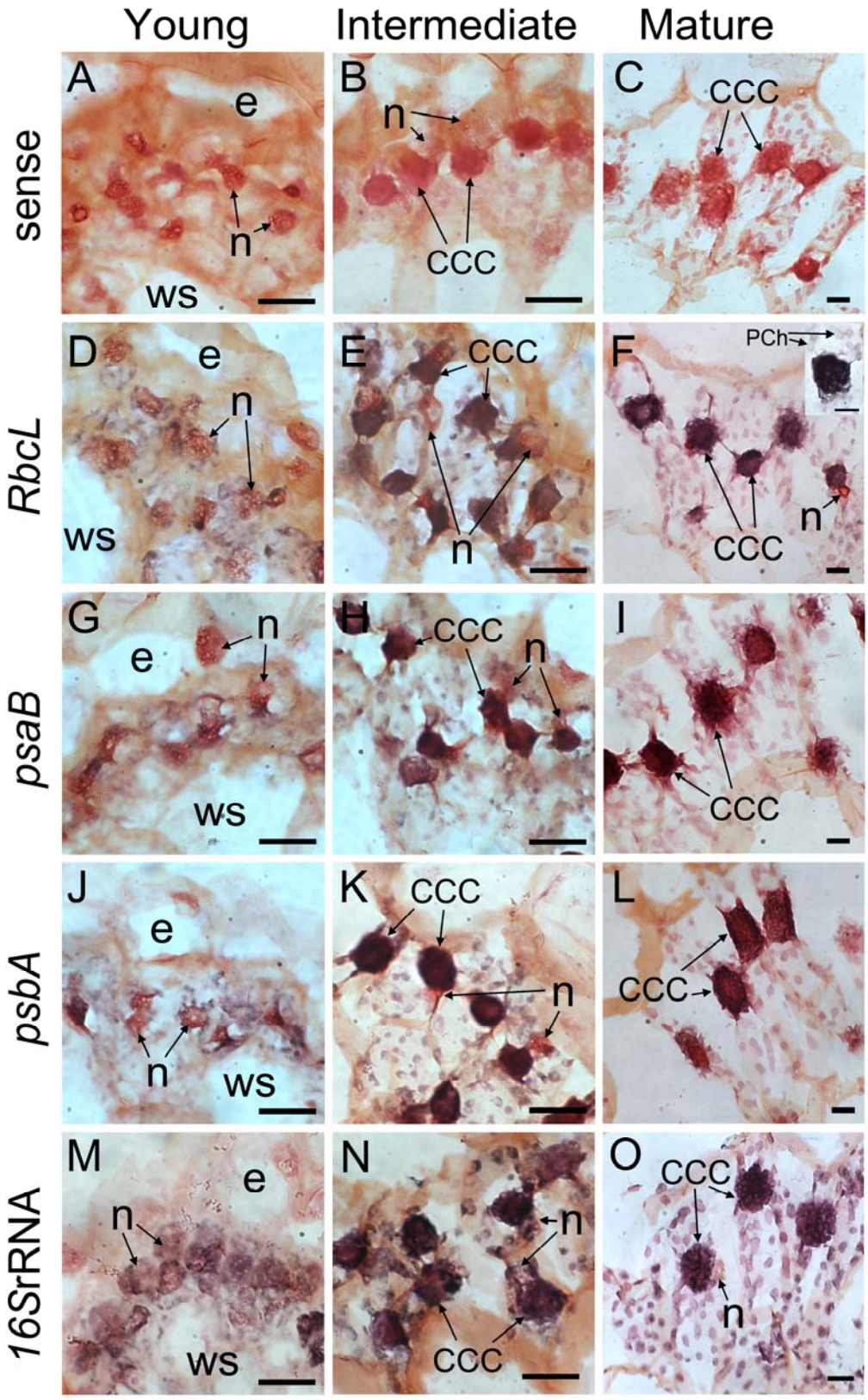
Young
Intermediate
Mature
sense
RbcL
psaB
psbA
16SrRNA
A
B
C
D
E
F
G
H
I
J
K
L
M
N
O
e
n
ws
CCC
PCh

indicating that this chloroplastic rRNA can be utilized as an internal control for the quantification of transcripts (Fig. 3.13M-O).

3.2.5 Semi-quantitative RT-PCR

To quantify the relative expression levels of *rbcS*, *rbcL*, *PEPC*, *PPDK* and *NAD-ME* transcripts in leaves at various developmental stages, I performed semi-quantitative RT-PCR. Total RNA was extracted from developing leaves divided into five stages by leaf length: youngest (0.1 cm), young (0.2 cm), intermediate (0.5 – 0.6 cm), intermature (1.0 – 1.2 cm), and mature (more than 2 cm). The amount of each synthesized cDNA was normalized by PCR-amplifying the cytosolic *18S* rRNA. All transcripts examined were present at low levels at the youngest stage and had increased in amount by the intermature stage (Fig. 3.14). In contrast to what was observed in the immunolocalization study of RbcL and PPDK, the accumulation of all transcripts decreased from intermature to mature leaves.

3.2.6 Chloroplast isolation from two compartments and quantification analyses

Since *in situ* hybridization was not suitable for a quantitative analysis, chloroplasts from the CCC and PCC were isolated and purified for further experiments. A method for separately isolating the two types of chloroplasts from mature *B. sinuspersici* leaves was first reported by Offermann et al. (2011). In this protocol, dimorphic chloroplasts are released from chlorenchyma protoplasts by the osmotic-shock treatment. Because the CCC maintains its structure after the lysis of protoplasts, the released CCC and PCC chloroplasts can be separated by the differential speed centrifugation. We used a different method to isolate two types of chloroplasts from

Figure 3.14 Quantitative analysis of photosynthetic transcripts in developing *B. sinuspersici* leaves by semi-quantitative RT-PCR

Total RNA was extracted from leaves at various developmental stages including youngest (0.1 cm in length), young (0.2 cm), intermediate (0.5 – 0.6cm), intermature (1.0 -1.2 cm), and mature (more than 2 cm). First-strand cDNA was synthesized from the total RNA and used as a template for RT-PCR. Gene specific cDNA of *rbcS*, *rbcL*, *PEPC*, *PPDK*, or *NAD-ME* was PCR amplified by using gene-specific primers described in Appendix. *18S* rRNA was used as an internal control. Images are representative results from at least three independent experiments. *rbcS*, Rubisco small subunit; *rbcL*, Rubisco large subunit; *PEPC*, phosphoenolpyruvate carboxylase; *PPDK*, pyruvate orthophosphate dikinase; *NAD-ME*, nicotinamide adenine dinucleotide malic enzyme.

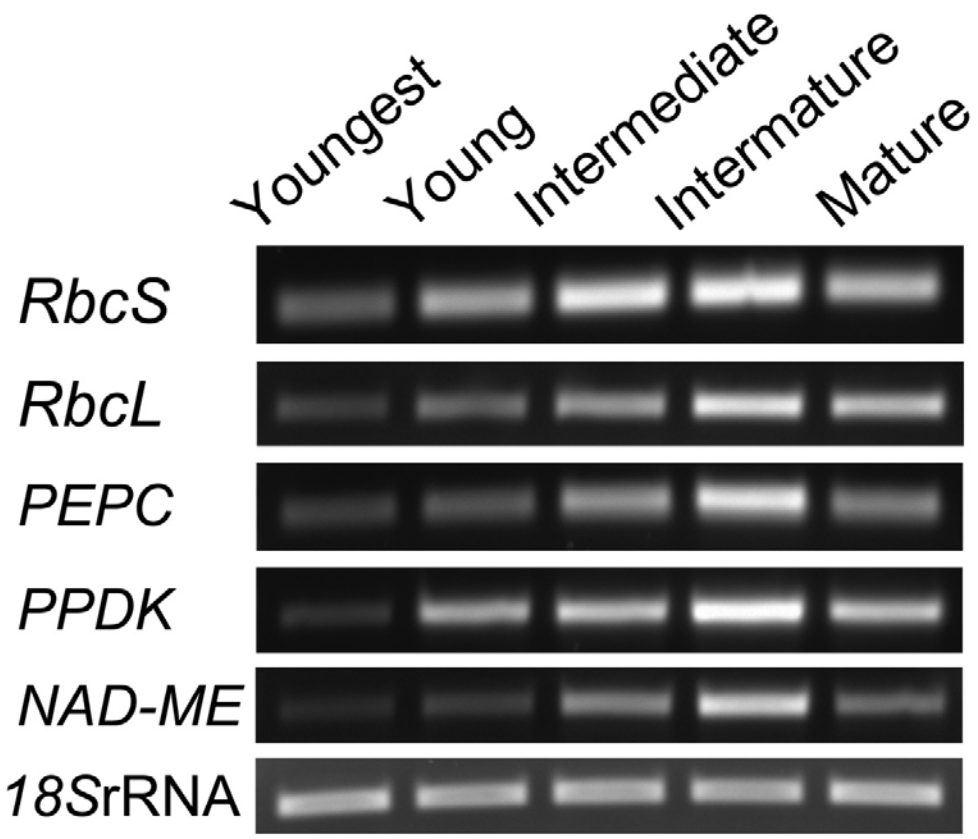
Youngest
Young
Intermediate
Intermature
Mature
RbcS
RbcL
PEPC
PPDK
NAD-ME
18SrRNA

mature *B. sinuspersici* leaves. In our protocol, the PCC chloroplasts were initially isolated along with the vacuole from chlorenchyma protoplasts by the osmotic-shock treatment (Lung et al. 2012). In addition, PEG was used to facilitate the vacuole separation from the protoplasts. The purity of PCC-associated vacuoles was confirmed using a light microscope for each preparation. The CCC structures were observed in non-ruptured protoplasts or attached to vacuoles before conditions were optimized (Fig. 3.15A; Initial protocol was developed by Shiu-Cheung Lung in our laboratry). First, the lysis of protoplasts was facilitated by adding 20% PEG in an isolation solution. Next, the centrifugation speed was incleased from 100 *g* to 300 *g* to make sure that CCC structures are settled and only PCC chloroplasts associated with vacuoles are in the floating layer. Finally, a higher yield of PCC chloroplasts was obtained by increasing the pH of the isolation solution from 7.2 to 8.4. Using this optimized protocol, the CCC chloroplast contamination was greatly reduced to less than 1%, indicating that less than one CCC structure was found per 100 vacuoles (Fig. 3.15B). The separated chloroplasts were purified by a Percoll gradient centrifugation. Proteins were extracted from isolated chloroplasts from each compartment and separated by the SDS-polyacrylamide gel electrophoresis. Western blot analysis showed relative amount of photosynthetic proteins in purified total, CCC and PCC chloroplasts (Fig. 3.15C). As expected, PPDK was more abundant in the PCC chloroplasts than those in the CCC. In contrast, the majority of RbcL was found in the CCC with only small amount observed in the PCC. These results agree with the immunogold results and the data reported by Voznesenskaya et al. (2002). I also examined the distribution of proteins associated with various components of the photosynthetic machinery such as the two photosystems and the electron transport chain in the chloroplast. Cytochrome f appeared equally abundant in both types of chloroplasts. There was not much difference in amount of PsbO in both chloroplasts with a slightly higher amount in the CCC. PsaD, a core subunit of photosystem I, appeared to be

Figure 3.15 Optimization of the procedure for chloroplast isolation from the PCC, and confirmation of the purity by immunoblot and silver staining analyses

PCC chloroplasts associated with vacuoles were released from protoplasts by osmotic shock. Significant contamination of CCC chloroplasts associated with vacuoles (black arrows) or in non-ruptured protoplasts (white arrows) is observed before optimization of the procedure **(A)** whereas CCC structures are rarely detected after conditions were optimized **(B)**. Bars = 50 μm. Proteins extracted from total, PCC, or CCC chloroplasts were separated by SDS polyacrylamide gel electrophoresis. Protein blots were probed with PPDK, RbcL, Cyt-f, PsbO, or PsaD antiserum, and the relative abundance of the proteins was expressed as a percentage of the amount in the total chloroplasts **(C)**. The silver staining method was also used to show equal loading of proteins in each lane **(D)**. Asterisks indicate estimated bands of PPDK (*), RbcL (**) and RbcS (***). Numbers at right indicate the molecular weight in kilodaltons. PCC, peripheral cytoplasmic compartment; CCC, central cytoplasmic compartment; SDS, sodium dodecyl sulphate; PPDK, pyruvate, Pi dikinase; RbcL, Rubisco large subunit; RbcS, Rubisco small subunit; Cyt-f, cytochrome f.

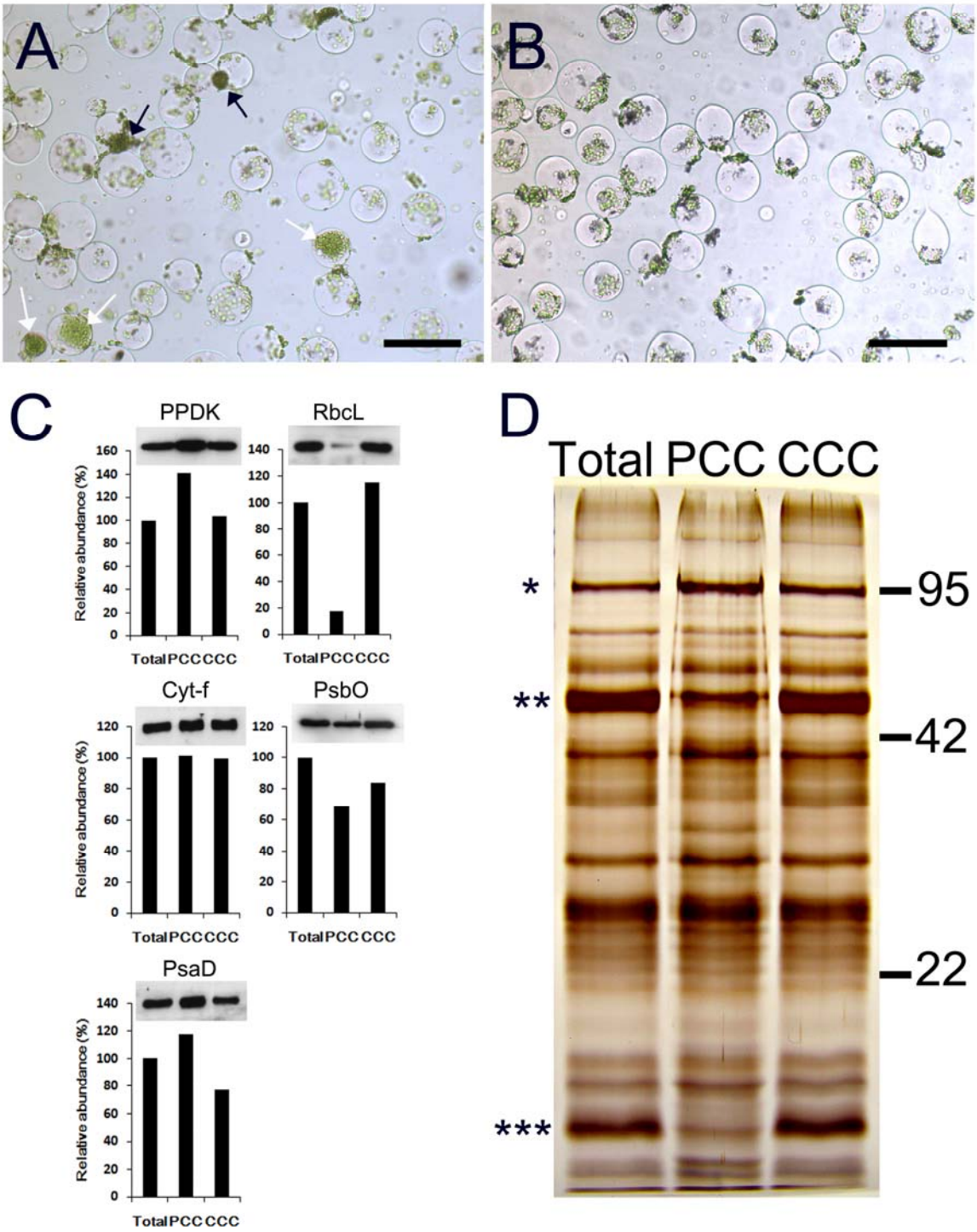
A
B
C
PPDK
RbcL
Cyt-f
PsbO
PsaD
Relative abundance (%)
Total PCC CCC
D
Total PCC CCC
*
**
***
95
42
22

more abundant in the PCC chloroplast than in the CCC chloroplast. To confirm equal loading and observe protein profile, extracts of chloroplasts were also separated on polyacrylamide gel and silver stained (Fig 3.15D). The intensity of some bands appeared to be very different between the PCC and CCC chloroplasts, including PPDK (*) and RbcL (**). Due to a lack of the antibody specific to RbcS, I was unable to confirm its distribution in the two types of chloroplasts. However, I assumed bands with three asterisks (***) as RbcS based on the estimated size and a great difference between the CCC and PCC chloroplasts.

To determine the relative total transcripts abundance in PCC and CCC chloroplasts, I extracted RNA from each type of purified chloroplasts, synthesized cDNA, and performed real-time qPCR using gene-specific primer sets for *rbcL*, *psaB* and *psbA*. Each gene was normalized by using Ct values of the plastid *16S* rRNA (Fig. 3.16). The *rbcL* transcripts accumulated approximately 4- and 7-fold more in total and CCC chloroplasts, respectively, than in the PCC chloroplasts (Fig. 3.16A). The expressions of *psaB* transcripts were approximately 7- and 8-fold higher in total and CCC chloroplasts, respectively, than that in the PCC chloroplasts (Fig. 3.16B). Similarly, the transcript levels for *psbA* were approximately 4- and 8-fold higher in total and CCC chloroplasts, respectively, than that in the PCC chloroplasts (Fig. 3.16C).

3.3 Discussion

3.3.1 Chlorenchyma cell development and organellar distributions

In the leaves of *B. sinuspersici*, cells are more developed and differentiated in the tip than those in the base region (Lara et al., 2008). Another single-cell C_4 species *Bienertia cycloptera* also show similar chlorenchyma cell development (Voznesenskaya et al., 2005). However, *B. cycloptera* exhibited small and multiple vacuoles at the young stage while

Figure 3.16 Relative abundance of chloroplastic transcripts in two types of chloroplasts in mature *B. sinuspersici* leaves by using real-time qPCR

Chloroplastic RNAs isolated from purified total, PCC, or CCC chloroplasts were used as a template and PCR amplified by using gene-specific primers for *rbcL* **(A)**, *psaB* **(B)**, and *psbA* **(C)** as described in Appendix. The means of results from triplicates of five independent RNA templates are shown. Each result was normalized by threshold cycle (Ct) values of *16S* rRNA. The fold differences in a particular transcript level relative to its amount in PCC chloroplast are shown. Error bars indicate standard errors. *rbcL*, Rubisco large subunit; PCC, peripheral cytoplasmic compartment; CCC, central cytoplasmic compartment.

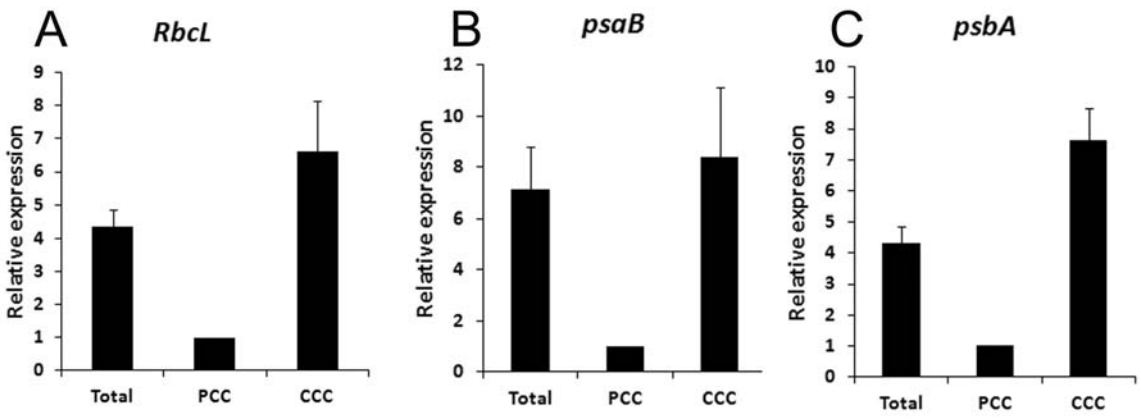
A
RbcL
Relative expression
0
1
2
3
4
5
6
7
8
9
Total
PCC
CCC
B
psaB
Relative expression
0
2
4
6
8
10
12
Total
PCC
CCC
C
psbA
Relative expression
0
1
2
3
4
5
6
7
8
9
10
Total
PCC
CCC

B. sinuspersici showed highly vacuolated cellular structures.at the same stage.

Peroxisomes were observed in both compartments. In plants, peroxisomes are involved in photorespiration, β-oxidation of fatty acid, the glyoxylate cycle, and the metabolism of ureides, indole-3-acetic acid, and jasmonic acid as well as the removal of H_2O_2 generated by catalase and other antioxidant enzymes (del Rio et al., 2006). In *B. sinuspersici* leaves, peroxisomes in the CCC and PCC are proposed to have different roles and mobility (Chuong et al., 2006). Since Rubisco accumulates mostly in the CCC chloroplasts, photorespiration, if any, should occur predominantly in the CCC where chloroplasts are in close proximity to mitochondria and peroxisomes. The PCC chloroplasts are also associated with peroxisomes but the absence of mitochondria and a low level of Rubisco make it impossible for photorespiration. Organelles located at the cell periphery might be more sensitive to environmental changes such as light intensity, temperature fluctuation, and CO_2 availability than those in the CCC. Therefore, it is possible that the PCC peroxisomes may function as a signal transmitter by receiving ROS produced in neighbouring chloroplasts and releasing H_2O_2 and nitric oxide which are known to function as signalling molecules (del Rio et al., 2006).

3.3.2 Immunolocalization of RbcL and PPDK in developing leaves

For terrestrial plants, the spatial compartmentation of enzymes is essential to perform C_4 photosynthesis in both Kranz-type and single-cell plants. However, the timing of the enzyme partitioning in different cells or compartments varies among C_4 species. In monocot C_4 maize and dicot C_4 *Atriplex rosea*, C_4 enzymes and Rubisco accumulate in a cell-specific manner throughout development in light-grown plants (Langdale et al., 1987; Dengler et al., 1995). In addition, the *rbcL* and *rbcS* transcripts accumulate before cell differentiation in maize (Langdale

et al., 1988). On the other hand, in another dicot C_4 *Amaranthus hypochondriacus*, *rbcL* and *rbcS* mRNA and proteins are found in both M and BS cells in 5 mm long leaves and the cell-specific accumulation of Rubisco is observed in 10 mm long leaves (Wang et al., 1992). The authors described that the amount of RbcL and RbcS proteins were quickly decreased from M cells and accumulated only in BS cells within 24 to 36 hours when leaves matured from 5 mm to 10 mm in length. My results suggest that the compartmentation of RbcL and PPDK occurs progressively at the late stage of development, between intermature (1.0 – 1.2 cm in length) and mature (> 2 cm in length) leaves in *B. sinuspersici* (Fig. 3.6). Notably, leaves of *B. sinuspersici* expand to 2 – 3 cm while fully expanded leaves of *A. hypochondriacus* reach 10 cm indicating that *B. sinuspersici*, unlike other C_4 plants, changes its mode of photosynthesis from C_3 to C_4 during leaf maturation in our growth conditions.

Being transcribed in different organelles, it is clear that the plastid-encoded RbcL and the nuclear-encoded PPDK are independently controlled in their distribution in single-cell C_4 plants. According to my results, RbcL accumulated slightly less in PCC chloroplasts as compared to CCCI and CCCO chloroplasts as soon as the two compartments formed in intermediate leaves while the differential accumulation of PPDK was first observed in intermature leaves (Fig. 3.6). These observations indicate that the accumulation of these proteins is regulated at different developmental stages. Although RbcL may be regulated at the transcriptional or mRNA stability level, PPDK appears to be controlled by a protein import and/or stability in two types of chloroplasts in a single chlorenchyma cell.

3.3.3 Immunolocalization of PsbO and Cytochrome f in mature leaves

The distribution of light harvesting complex II and PSII affects the development of grana stacks (Anderson, 1999; Adam et al., 2010). For instance, maize is known to develop dimorphic chloroplasts; M chloroplasts have well-developed grana and BS chloroplasts are deficient in grana (Edwards et al., 2004). Recent proteomic analysis in maize revealed that the content of PSII in BS cells is 55% lower than that in M cells (Majeran et al., 2008). Here, I showed that PsbO accumulated approximately 50% more in the CCC than in the PCC chloroplasts. Because PSII proteins including PsbO accumulate in the grana stack of thylakoid membranes, there should be a good correlation between the relative amount of PSII proteins and grana. This is supported by a previous study showing that the granal index is 1.5-fold higher in the CCC than in the PCC chloroplasts in closely related single-cell C_4 species *B. cycloptera* (Voznesenskaya et al., 2002). In addition, PPDK and PsbO polypeptides showed different accumulation patterns even though they are both nuclear-encoded (Fig. 3.6, 3.7C). Similarly, chloroplast-encoded RbcL and Cytochrome f did not show any correlation with their distribution (Fig. 3.6, 3.7F). These results suggest that the accumulation of each of these four polypeptides was controlled independently. This is also the case in Kranz-type C_4 plants in which each photosynthetic gene is expressed in a cell-specific manner using its own regulatory machinery (Sheen, 1999; Dengler and Taylor, 2000; Patel and Berry, 2008).

3.3.4 Optimization of the PEG-mediated protoplast transfection method and *in vivo* localization analysis of various proteins

For the *in vivo* protein subcellular localization analysis and the visualization of organellar dynamics, we established the PEG-mediated protoplast transfection protocol in *B. sinuspersici*

chlorenchyma cells (Lung et al., 2011). According to Yoo et al. (2007), a minimum transfection efficiency of 50% must be achieved in order to generate reproducible results from GFP expression experiments. Although the biolistic transformation method is useful to examine expression of GFP-fusion proteins in onion epidermal cells, it is not efficient for high transformation rates in chlorenchyma cells of *B. sinuspersici* or any plant cells using. Since our initial transfection protocol was inefficient with less than 5% of EGFP-expressing protoplasts, I have empirically optimized transfection conditions. I varied the ratio of amount of plasmid DNA to numbers of protoplast, the types and concentration of osmotica in transfection buffers, the duration of post-transfection incubation, and the effect of light during the incubation (Fig. 3.9). Finally, approximately 84% of transfection efficiency was achieved by using protoplasts transfected with EGFP reporter gene. The protoplast transfection experiments using various EGFP-fusion constructs showed this improved protocol as a valuable tool for the protein subcellular localization analysis (Fig. 3.10).

Although both *rbcS* and *PPDK* are encoded in the nucleus, their polypeptides appear to accumulate differentially in the two types of chloroplasts, as demonstrated by the immunoblot study using isolated dimorphic chloroplasts (Offermann et al., 2011). Therefore, their distribution in chlorenchyma cells of *B. sinuspersici* might not be controlled at the transcript level. I expected that *in vivo* protein localization analysis would reveal the level of their regulation in the differential distribution. However, there was no preferential accumulation in the expression levels of EGFP-RbcS and EGFP-PPDK in two chloroplast types regardless of whether full-length or transit-peptide constructs were used (Fig. 3.9H-J). This could be due to the strong 35S promoter which drove expressions of all EGFP constructs. For instance, the constitutive expression of RbcS might overcompensate the rate of its turnover in the PCC. Furthermore, the accumulation of full-length RbcS-EGFP in punctate structures around the

chloroplasts suggest that the localization and/or import of this protein was saturated or overwhelmed by the overexpression level. Therefore subcellular localization analysis of these proteins using their own promoters would be required to elucidate the regulatory mechanisms controlling their distribution.

3.3.5 Chloroplast separation from two compartments and verification

The isolation of two cell or chloroplast types from C_4 plants is indispensable for the study of C_4 photosynthesis. M and BS cells are first isolated from C_4 monocot *Digitaria sanguinalis* by Edwards et al. (1970), and together with current technological progress their efficient isolation enables researchers to conduct a high-throughput analysis of chloroplast proteomes by using two cell types in Kranz-type C_4 species (Majeran et al., 2005, 2008). In the single-cell C_4 species *B. sinuspersici*, a procedure for isolating dimorphic chloroplasts has been established by Offermann et al. (2011). Independently and concamittently, I contributed to a different method successfully isolating the two types of chloroplasts. In the original protocol established by Shiu-Cheung Lung, significant contamination of CCC structures was found during the PCC chloroplast isolation (Fig. 3.15A). Contamination of the CCC also included non-lysed protoplasts ranging from 5 to 15% between experiments. Immunoblot analysis using the RbcL antibody followed by this incomplete purification showed no significant difference in RbcL band intensities between the CCC and PCC chloroplast fractions. Because RbcL accumulates more than 20 times higher in the CCC than PCC chloroplasts as demonstrated in the present immunogold analysis, the contamination of CCC needed to be minimized. Therefore, I further optimized isolation conditions to make this procedure more reliable for future experiments. The final concentration of 20% PEG in the isolation solution facilitated the lysis of protoplasts and prevented the contamination of intact

protoplasts. By further optimizing the centrifugation speed and pH of solutions, the CCC contamination was consistently reduced to less than 1% (Fig. 3.15B). The data obtained using this optimized protocol appeared to correlate well with the results from the immunogold study (Fig. 3.6 and 3.15C). Offerman et al. (2011) reported that the isolated PCC chloroplasts showed 4- to 5-fold more PPDK than the CCC chloroplasts, whereas my results did not exhibit this much difference. The discrepancy between these results might be attributed to differences in growth conditions such as the light intensity (1000 vs 350 µmol sec^{-1} m^{-2}) and temperature (day/night: 35/18 vs 25/18 °C) which probably affected the overall biochemical processes in this species. Similar discrepancies were also observed in $\delta^{13}C$ analysis in studies showing that *B. sinuspersici* plants from natural habitats have a value of -13.8‰ suggesting C_4 photosynthesis, whereas plants grown in a growth chamber under the conditions of approximately 400 µmol sec^{-1} m^{-2} light intensity and 25/15 °C day and night temperatures have a value of -17.4‰ indicating C_4-like photosynthesis (Voznesenskaya et al., 2002; Akhani et al., 2005; Lara et al., 2008). Freitag and Stichler (2002) and Edwards et al. (2004) suggest the plasticity of the photosynthetic mode in *Bienertia* species, depending on growth conditions. Together with my data, the transition of C_3-C_4 of photosynthesis is likely regulated not only developmentally but also environmentally in *B. sinuspersici*, affecting the distribution of C_4 enzymes including PPDK. Our chloroplast separation method will allow for further biochemical and molecular analyses of two types of chloroplasts in *B. sinuspersici*.

3.3.6 Transcript distribution and accumulation

The regulation of key C_4 enzymes and Rubisco expressions has been well studied in Kranz-type C_4 species including maize and *Flaveria bidentis*. It has been shown that nuclear-encoded PEPC,

PPDK, and NADP-ME are primarily regulated at the RNA level, either transcriptionally or post-transcriptionally, in these species (Sheen and Bogorad, 1987b; Langdale et al., 1991; Matsuoka and Numazawa, 1991; Stockhaus et al., 1997; Rosche et al., 1998; Lai et al., 2002; Hibberd and Covshoff, 2010). In contrast, the cell-specific accumulation of Rubisco, both large and small subunits, appears to be predominantly controlled at the post-transcriptional level in *Flaveria* and *Amaranthus* (Patel and Berry, 2008). It has been known that the expressions of RbcL and RbcS are tightly coordinated. For instance, in *Chlamydomonas* a low abundance of RbcS polypeptide inhibits the translation of RbcL in chloroplasts (Rodermel, 2001). On the other hand, the RbcS rapidly degrades in the absence of RbcL polypeptides (Schmidt and Mishkind, 1983). Furthermore, it has been recently reported that unassembled RbcL polypeptides down-regulated RbcL synthesis, regardless of the presence or absence of the RbcS protein (Wostrikoff and Stern, 2007). In *B. sinuspersici*, since the RbcS protein appears to be equally imported to both types of chloroplasts as demonstrated in the *in vivo* protein localization assay using RbcS transit peptides fused with EGFP driven by the 35S promoter (Fig. 3.10H), the differential accumulation of Rubisco might be determined by the amount of RbcL polypeptides in dimorphic chloroplasts. The *in situ* hybridization analysis showed that *rbcL* transcripts appeared to accumulate similarly in the two types of chloroplasts in young and intermediate leaves, whereas they were more abundant in the CCC than in the PCC in mature leaves which is in agreement with the RbcL protein distribution (Fig. 3.4, 3.11, and 3.13). This is further supported by the quantitative real-time PCR result showing approximately 7-fold higher accumulation of *rbcL* transcript in the CCC than in the PCC chloroplasts. These results indicate that the differential RbcL accumulation in distinct chloroplasts was predominantly regulated by transcription and/or mRNA stability.

Transcripts of Rubisco and C_4 enzymes showed higher accumulation in the adaxial side than in the abaxial side in developing leaves (Fig. 3.11 top panels). It has been known that high expressions of photosynthetic genes are induced by light in C_4 plants (Nelson and Langdale, 1992; Furbank and Taylor, 1995; Sheen, 1999; Patel and Berry, 2008). Light is also required for compartmentation of photosynthetic enzymes in another single-cell C_4 species *Suaeda aralocaspica* (Voznesenskaya et al., 2004), Kranz-type C_4 plants maize (Sheen and Bogorad, 1985; Langdale et al., 1988) and *Flaveria* (Shu et al., 1999) but not in *Amaranthus* (Wang et al., 1993a). Since these early stages of developing leaves were observed in shoot tips, the structure of shoot tips might affect this polarized accumulation of transcripts by receiving more light on the adaxial side than on the abaxial side. Furthermore, organelles in chlorenchyma cells in the leaf adaxial side appeared to be more differentiated than those in the abaxial side (Fig. 3.11 top panels). The significant decrease of *rbcS* and *PEPC* transcripts in mature leaves of *B. sinuspersici* after low light treatment has been described by Lara et al. (2008). Collectively, light appeared to participate in the regulation of enzyme distribution as well as in cell differentiation and organelle partitioning in *B. sinuspersici*.

Transcripts of nuclear encoded genes such as *rbcS*, *PEPC*, *PPDK*, and *NAD-ME* were observed in the cytosol and did not show a change in localization throughout the leaf development (Fig. 3.11). Unlike in the Kranz-type C_4 plants, the distribution of these enzymes cannot be controlled at the transcription level in the single-cell C_4 system. Although the spatial enzyme expression by mRNA targeting has been proposed by Edwards et al. (2004), the resolution of the *in situ* hybridization method did not allow the precise subcellular localization of nuclear-encoded transcripts. RT-PCR showed the different accumulation pattern in Rubisco and PPDK transcripts in comparison to their polypeptides as demonstrated by the immunolocalization analysis (Fig. 3.6 and 3.14). Rubisco and C_4 enzymes increased steadily

with age showing the highest amount at the mature stage while their mRNAs increased by 1.0 – 1.2 cm stage but decreased at the mature stage. Similar inconsistency between transcripts and their polypeptides has been observed in maize. In maize, younger cells locate at the base while older cells locate at the tip of a leaf. Langdale et al. (1987 and 1988) described that *rbcL* transcripts decreased but its polypeptides increased from the base to the tip in maize. In this case, the development-dependent regulation appeared to control the accumulation of photosynthetic transcripts and enzymes in *B. sinuspersici* as well as in maize.

The transition from C_3 default to C_4 photosynthesis occurs during leaf development as described for various C_4 species previously (Langdale and Nelson, 1991; Wang et al., 1992; Voznesenskaya et al., 2005). The longitudinal sections hybridized to *rbcL* or *PEPC* antisense mRNA showed gradual accumulation of both transcripts from the base to the tip of intermature leaves, following the basipetal cell development in a leaf (Fig. 3.12). Moreover, *rbcL* transcripts were present in all chloroplasts at the base and middle parts while they were restricted in the CCC chloroplasts at the tip. These results suggest that the transition from C_3 to C_4 photosynthesis occurrs along with the basipetal cell development. In agreement with this observation, Wang et al. (1993b) have reported that the *rbcL* mRNA distribution changed from both M and BS chloroplasts to exclusively BS chloroplasts in the basipetal direction in a single *Amaranthus* leaf.

The accumulation of *psaB* and *psbA* transcripts also showed a developmental change in distribution. Both *psaB* and *psbA* transcripts appeared to accumulate in all chloroplasts of young leaves; they are of similar amounts in the CCC and PCC chloroplasts in intermediate leaves; and there are more in the CCC than PCC chloroplast in mature leaves (Fig. 3.13G-L). The real-time qPCR experiments supported the *in situ* hybridization data showing that the relative amount of *psaB* and *psbA* transcripts in the CCC chloroplasts was approximately 8-folds higher than that in the PCC chloroplasts (Fig. 3.16B, C). I also tried immunolocalization experiments of PsaB and

PsbA proteins, but these were unsuccessful, possibly because of their transmembrane nature. The PsbO immunolocalization result which represented the PSII distribution indicated that CCC chloroplasts contain approximately 50% more PSII than in PCC chloroplasts. Based on this result, *psbA* transcripts appeared to accumulate excessively in the CCC chloroplasts. Moreover, I anticipated that *psaB* transcripts would be low in the CCC because one of PSI proteins PsaD was slightly more abundant in the PCC than in CCC chloroplasts as shown by the immunoblot analysis performed subsequent to the chloroplast separation (Fig. 3.15C). These transcript distribution analyses suggest that the transcription rate of photosynthetic genes in the CCC chloroplasts is higher than that in the PCC in general regardless of the amount of polypeptides in mature leaves of *B. sinuspersici*. Alternatively, chloroplastic transcripts could be degraded at a faster rate in the PCC than in the CCC. The expression of chloroplastic genes has been considered to be regulated primarily at the post-transcriptional level (Marín-Navarro et al., 2007). Especially, *psbA* expression has been suggested to be mainly controlled at translational steps in green algae and higher plants (Marín-Navarro et al., 2007; Mulo et al., 2011). While transcripts of *psbA* highly accumulate because of its strong promoter, the synthesis of PsbA protein is strictly controlled by developmental and environmental signals (Mulo et al., 2011). Moreover, inhibition analysis using the translation inhibitor chloramphenicol shows an increase in mRNA level of *psaB* and *psbA* while *rbcL* transcript levels are unaffected in *Chlamydomonas reinhardtii* (Xu et al., 1993). From these observations, one may assume that the expressions of *psaB* and *psbA* genes are more strictly controlled at the translational step than that of *rbcL*. It is possible that these photosynthetic genes are controlled at multiple levels for fine-tuning of protein accumulation to respond to environmental signals such as light and temperature.

3.3.7 Conclusions

Here, I showed the expression of various key photosynthetic genes in the developing leaf of *B. sinuspersici*. While the single-cell C_4 species mimic Kranz-type C_4 plants in many aspects, their regulatory mechanisms of the protein compartmentation must be very different from those in Kranz-type C_4 plants because of their unique way to perform C_4 photosynthesis. The high resolution quantitative analysis of photosynthetic proteins using TEM-immunolocalization revealed that RbcL accumulates approximately 20-fold higher in the CCC than PCC chloroplasts whereas PPDK exhibits a concentration gradient that is lowest in the CCCI and highest in the PCC chloroplasts in mature *B. sinuspersici* leaves. In addition, the transition from C_3 to C_4 photosynthesis appears to occur during maturation of leaves, between intermature and mature stages. Whether these results are affected when plants are grown under different growth conditions (ie. higher light intensities and temperatures) remain uncertain. The transcript localization analysis by *in situ* hybridization and the quantitative study of the relative transcript amount in dimorphic chloroplasts by real-time qPCR showed that the distribution of *rbcL* transcripts follows that of RbcL proteins, suggesting the differential accumulation of RbcL is regulated at the mRNA level. These findings would help future studies on regulatory mechanisms in the differential distribution of photosynthetic proteins in the single-cell C_4 species.

CHAPTER 4: AMINO ACID AND NUCLEOTIDE SEQUENCE ANALYSES OF RUBISCO LARGE SUBUNIT USING BIOINFORMATIC TOOLS

4.1 Introduction

Multiple sequence alignment tools are software programs commonly used to compare and analyze nucleotide and amino acid sequences. Although ClustalW is probably the most used tool as a general sequence alignment program (Larkin et al., 2007), the use of other programs would be helpful to determine the best choice depending on experimental purposes. MUSCLE (Edgar, 2004) and T-Coffee (Notredame et al., 2000) are multiple sequence alignment programs found in the European Bioinformatics Institute website (http://www.ebi.ac.uk/). Phylogenetic trees can be generated based on results of the sequence alignment by using another function of ClustalW, ClustalW - phylogeny. A general purpose of phylogenetic trees is to show evolutionary relationships among various species (Soltis and Soltis, 2003). Because the accuracy of phylogenetic trees depends on the results of multiple sequence alignment, the choice of reliable programs is important. In addition, the reliability of phylogenetic trees is also affected depending on the source of sequence, either nucleotides or amino acids.

Secondary structures of RNA affect various processes, such as mRNA stability, translation rates, protein binding, and enzymatic reactions (Svoboda and Cara, 2006). Computer software such as Mfold (Zuker, 2003) and RNAfold (Hofacker, 2003) are two bioinformatic tools commonly used for the prediction of RNA secondary structures. Mfold was first produced in late 1980's using the minimum free energy algorithm developed by Zuker and Stiegler (1981). Mfold has been cited in many articles and presently represents the landmark of RNA secondary

structure prediction tools. Because free energies of RNA nucleotide base pairing have been updated, a current version of Mfold (v3.0) uses nearest-neighbour thermodynamic parameters described by Mathews et al. (1999). RNAfold is one of the programs found in the Vienna RNA secondary structure package (http://www.tbi.univie.ac.at/RNA/). RNAfold was established by Hofacker et al. in 1994 and uses the same prediction algorithm and thermodynamic parameters as Mfold (Hofacker, 2003). One advantage of RNAfold is that this program can calculate equilibrium base pairing probabilities and present them in different colours. Another useful program in the same package is Alifold which predicts consensus secondary structure from aligned sequences (Hofacker et al., 2002). Alifold uses a covariance for aligned sequence integrated into Zuker and Stieglers' (1981) dynamic programming. These tools were used to predict potential secondary structures in *rbcL* transcripts.

Rubisco is a key photosynthetic enzyme for all photoautotrophic organisms. In C_4 plants, this enzyme specifically accumulates in the BS chloroplasts in Kranz type C_4 plants or in the CCC chloroplasts in *Bienertia*-type single-cell C_4 plants (Hatch, 1987; Voznesenskaya et al., 2002; Chuong et al., 2006). As discussed in Chapter 3, the differential accumulation of RbcL in dimorphic chloroplasts of *B. sinuspersici* appears to be regulated by transcription and/or mRNA stability. It is possible that the stability of *rbcL* mRNA might be controlled by alternative processing of *rbcL* transcripts in each chloroplast type. The *rbcL* transcripts are considered to be processed into three different forms with different 5'UTR lengths: the premature form (5'UTR with approximately 180 bp); the intermediate form (approximately 100 bp); and the mature form (approximately 60 bp) (Reinbothe et al., 1993; Serino and Maliga, 1998; McCormac et al., 2001). Among these forms, the mature form is considered to be effective for translation, while the intermediate form might be untranslatable or unstable (Reinbothe et al., 1993). Based on these studies, I hypothesized that *rbcL* transcripts could be differentially processed in the CCC and

PCC chloroplasts, and the conformation of *rbcL* mRNA secondary structures might be altered depending on the lengths of transcripts, affecting the mRNA stability.

In this chapter, sequence alignment analysis and secondary structure prediction of *rbcL* transcripts in various plant species including *B. sinuspersici* are discussed. All mRNA sequence alignments and secondary structure predictions were performed using corresponding genomic sequences obtained from the Genebank Database. These bioinformatic tools were used to predict the secondary structures present in the 5'UTR of *rbcL*; which might be helpful in elucidating the possible mechanisms regulating the differential accumulation of *rbcL* transcripts in the two types of chloroplasts of *B. sinuspersici*.

4.2 Results

4.2.1 Multiple sequence alignment and phylogenetic trees of amino acids and mRNA coding sequences of RbcL in different programs

To identify conserved regions in RbcL protein and transcript, RbcL sequences from various species including C_3 and C_4 plants for both monocots and dicots, green and red algae, and cyanobacteria, amino acid sequences were aligned using ClustalW (Larkin et al., 2007), T-Coffee (Notredame et al., 2000), and MUSCLE (Edgar, 2004). Since almost no differences were observed among the three programs, only data from ClustalW is shown (Fig. 4.1). Based on AlignX program in Vector NTI (Invitrogen), RbcL amino acid sequences showed 42.5% identity and 96.2% similarity among the eight species examined. This result suggested that RbcL amino acid sequence is highly conserved among various photosynthetic species. The sequence alignment data from ClustalW, T-Coffee, and MUSCLE were also used to generate phylogenetic trees. Again, only the result from ClustalW is shown since they were all nearly identical (Fig.

4.2). This tree accurately described relationships among different species except for *Arabidopsis*. Based on the phylogenetic analysis, Rubisco can be classified into two groups, "green" and "red-like" Rubisco subgroups (Ninomiya et al., 2008). Rubisco of green algae (GARbcL) and higher plants is believed to be derived from cyanobacteria (CyRbcL), whereas that of red algae (RARbcL) originated from purple eubacteria. When compared among green-like RbcL excluding red algae, the polypeptide sequences 62.2% identical, increasing to 81.2% between green algae and higher plants, and 86.8% within higher plants.

The coding regions of *rbcL* mRNA were also aligned using ClustalW, T-Coffee and MUSCLE (Fig. 4.3A, B and C, respectively). This analysis was useful to determine the best program among the three. Only MUSCLE was able to align both start codons (ATG) and stop codons (TAG, TGA, or TAA) properly. T-Coffee aligned the start codons but not the stop codons while ClustalW failed to align either of them. Phylogenetic trees were generated based on the data of *rbcL* coding sequence alignment from ClustalW, T-Coffee, and MUSCLE. Because all three programs generated very similar trees despite differences in results of the multiple sequence alignment, only the phylogenetic tree generated by MUSCLE is shown (Fig. 4.4). Unlike the phylogenetic tree generated from amino acid sequences, the tree based on the mRNA sequence alignment showed a reasonable position for *Arabidopsis*. Since *Arabidopsis*, *Amaranthus*, and *B. sinuspersici* are all dicot plants, they were expected to group into the same cluster. AlignX showed 37.6% identity and 93.4% similarity in these *rbcL* mRNA coding sequences. Sequence identities in green-like species excluding red algae, green algae and higher plants, and higher plants alone were 50.7%, 66.5%, and 77.8%, respectively. These results indicated that the nucleotide sequences of *rbcL* coding region are highly conserved as well.

Figure 4.1 Amino acid sequence alignment of RbcL from various organisms by ClustalW

Amino acid sequences of RbcL in C_4 monocot maize (*Zea mays*), C_3 monocot rice (*Oryza satiba*), C_4 dicot *Amaranthus hypochondriacus*, single-cell C_4 species *B. sinuspersici*, C_3 dicot *Arabidopsis thaliana*, green algae *Chlamydomonas reinhardtii*, cyanobacteria *Synechococcus sp.*, and red algae *Galdieria partita* were aligned by a multiple sequence alignment program ClustalW. Asterisks indicate identical amino acids. One and two dots indicate weak and strong consensus amino acids, respectively. Zm, maize; Os, rice; Ah, *Amaranthus*; Bs, *Bienertia sinuspersici*; At, *Arabidopsis*; GA, green algae; Cy, cyanobacteria; RA, red algae.

```
ZmRbcL          MSPQTETK--------ASVGFKAGVKDYKLT-YYTPEYETKDTDILAAFRVTPQLGVPPE 51
OsRbcL          MSPQTETK--------ASVGFKAGVKDYKLT-YYTPEYETKDTDILAAFRVTPQPGVPPE 51
AhRbcL          MSPQTETK--------ASVGFKAGVKDYRLT-YYTPEYETQDTDILAAFRVSPQPGVPPE 51
BsRbcL          MSPQTETK--------ASVGFKAGVKDYKLT-YYTPEYETKDTDILAAFRVSPQPGVPPE 51
AtRbcL          MSPQTETK--------ASVGFKAGVKEYKLT-YYTPEYETKDTDILAAFRVTPQPGVPPE 51
GARbcL          MVPQTETK--------AGAGFKAGVKDYRLT-YYTPDYVVRDTDILAAFRMTPQLGVPPE 51
CyRbcL          ----------------MSKKYDAGVKEYRDT-YWTPDYVPLDTDLLACFKCTGQEGVPKE 43
RARbcL          MSQSIEEKSVQERTRIKNSRYESGVIPYAKMGYWNPDYQVKDTDVLALFRVTPQPGVDPI 60
                                .  :.:**  *    *:.*:*   ***:** *: : * **

ZmRbcL          EAGAAVAAESSTGTWTTVWTDGLTSLDRYKGRCYHIEPVPGDPDQYICYVAYPLDLFEEG 111
OsRbcL          EAGAAVAAESSTGTWTTVWTDGLTSLDRYKGRCYHIEPVVGEDNQYIAYVAYPLDLFEEG 111
AhRbcL          EAGAAVAAESSTGTWTSVWTDGLTNLDRYKGRCYNIEPVAGEENQYICYVAYPLDLFEEG 111
BsRbcL          EAGAAVAAESSTGTWTTVWTDGLTSLDRYKGRCYHIEPVAGEENQYICYVAYPLDLFEEG 111
AtRbcL          EAGAAVAAESSTGTWTTVWTDGLTSLDRYKGRCYHIEPVPGEETQFIAYVAYPLDLFEEG 111
GARbcL          ECGAAVAAESSTGTWTTVWTDGLTSLDRYKGRCYDIEPVPGEDNQYIAYVAYPIDLFEEG 111
CyRbcL          EVAAAVAAESSTGTWSTVWSELLTDLDFYKGRCYRIEDVPGDKEAFYAFIAYPLDLFEEG 103
RARbcL          EAAAAVAGESSTATWTVVWTDLLTAADLYRAKAYKVDQVPNNPEQYFAYIAYELDLFEEG 120
                * .****.****.**: **:: **  * *:.:.* :: * .:   : .::** :******

ZmRbcL          SVTNMFTSIVGNVFGFKALRALRLEDLRIPPAYSKTFQGPPHGIQVERDKLNKYGRPLLG 171
OsRbcL          SVTNMFTSIVGNVFGFKALRALRLEDLRIPPTYSKTFQGPPHGIQVERDKLNKYGRPLLG 171
AhRbcL          SVTNMFTSIVGNVFGFKALRALRLEDLRIPVAYVKTFQGPPHGIQVERDKLNKYGRPLLG 171
BsRbcL          SVTNMFTSIVGNVFGFKALRALRLEDLRIPVSYIKTFQGPPHGIQVERDKLNKYGRPLLG 171
AtRbcL          SVTNMFTSIVGNVFGFKALAALRLEDLRIPPAYTKTFQGPPHGIQVERDKLNKYGRPLLG 171
GARbcL          SVTNMFTSIVGNVFGFKALRALRLEDLRIPPAYVKTFVGPPHGIQVERDKLNKYGRGLLG 171
CyRbcL          SITNVLTSLVGNVFGFKALRHLRLEDIRFPIAFIKCCAGPPNGIAVERDRMNKYGRPLLG 163
RARbcL          SIANLTASIIGNVFGFKAVKALRLEDMRLPLAYLKTFQGPATGVILERERLDKFGRPLLG 180
                *::*: :*::********:  *****:*:* :: *   **. *: :**::::*:** ***

ZmRbcL          CTIKPKLGLSAKNYGRACYECLRGGLDFTKDDENVNSQPFMRWRDRFVFCAEAIYKAQAE 231
OsRbcL          CTIKPKLGLSAKNYGRACYECLRGGLDFTKDDENVNSQPFMRWRDRFVFCAEAIYKSQAE 231
AhRbcL          CTIKPKLGLSAKNYGRACYECLRGGLDFTKDDENVNSQPFMRWRDRFLFCAEAIYKSQAE 231
BsRbcL          CTIKPKLGLSAKNYGRAVYECLRGGLDFTKDDENVNSQPFMRWRDRFLFCAEAIYKAQAE 231
AtRbcL          CTIKPKLGLSAKNYGRAVYECLRGGLDFTKDDENVNSQPFMRWRDRFLFCAEAIYKSQAE 231
GARbcL          CTIKPKLGLSAKNYGRAVYECLRGGLDFTKDDENVNSQPFMRWRDRFLFVAEAIYKAQAE 231
CyRbcL          CTIKPKLGLSGKNYGRVVYECLRGGLDFTKDDENINSQPFQRWQNRFEFVAEAIKLAEQE 223
RARbcL          CTTKPKLGLSGKNYGRVVYEALKGGLDFVKDDENINSQPFMRWRERYLFTMEAVNKASAA 240
                ** *******.*****. **.*:*****.*****:***** **::*: *  **:  :.

ZmRbcL          TGEIKGHYLNATAGTCEEMIKRAVFARELGVPIVMHDYLTGGFTANTTLSHYCRDNGLLL 291
OsRbcL          TGEIKGHYLNATAGTCEEMIKRAVFARELGVPIVMHDYLTGGFTANTSLAHYCRDNGLLL 291
AhRbcL          TGEIKGHYLNATAGTCEEMIKRAVFARELGVPIVMHDYLTGGFTANTSLSQYCRDNGLLL 291
BsRbcL          TGEIKGHYLNATAGTCEDMMKRAVFARELGAPIVMHDYITGGFTANTSLAHYCRDNGLLL 291
AtRbcL          TGEIKGHYLNATAGTCEEMIKRAVFARELGVPIVMHDYLTGGFTANTSLSHYCRDNGLLL 291
GARbcL          TGEVKGHYLNATAGTCEEMMKRAVCAKELGVPIIMHDYLTGGFTANTSLAIYCRDNGLLL 291
CyRbcL          TGERKGHYLNVTANTPEEMYERAEFAKELNQPIIMHDFITGGFTANTGLSKWCRANGMLL 283
RARbcL          TGEVKGHYLNVTAATMEEMYARANFAKELGSVIIMIDLVIG-YTAIQTMAKWARDNDMIL 299
                *** ******.** * *:*  **  *:**.  *:* * : * :**   :: :.* *.::*

ZmRbcL          HIHRAMHAVIDRQKNHGMHFRVLAKALRMSGGDHIHSGTVVGKLEGEREITLGFVDLLRD 351
OsRbcL          HIHRAMHAVIDRQKNHGMHFRVLAKALRMSGGDHIHAGTVVGKLEGEREMTLGFVDLLRD 351
AhRbcL          HIHVAMHAVIDRQKNHGMHFRVLAKALRLSGGDHIHSGTVVGKLEGERDITLGFVDLLRD 351
BsRbcL          HIHRAMHAVIDRQKNHGMHFRVLAKALRLSGGDHIHAGTVVGKLEGERDITLGFVDLLRD 351
AtRbcL          HIHRAMHAVIDRQKNHGMHFRVLAKALRLSGGDHIHAGTVVGKLEGDRESTLGFVDLLRD 351
GARbcL          HIHRAMHAVIDRQRNHGIHFRVLAKALRMSGGDHLHSGTVVGKLEGEREVTLGFVDLMRD 351
CyRbcL          HIHRAMHAVIDRHPKHGIHFRVLAKCLRLSGGDQLHTGTVVGKLEGDRQTTLGYIDQLRE 343
RARbcL          HLHRAGNSTYSRQKNHGMNFRVICKWMRMAGVDHIHAGTVVGKLEGDPIITRGFYKTLLL 359
                *:* * ::. .*: :**::***:.* :*::* *::*:**********:   * *: . :

ZmRbcL          DFIEKDRSRGIFFTQDWVSMPGVIPVASGGIHVWHMPALTEIFGDDSVLQFGGGTLGHPW 411
OsRbcL          DFIEKDRARGIFFTQDWVSMPGVIPVASGGIHVWHMPALTEIFGDDSVLQFGGGTLGHPW 411
AhRbcL          DYTEKDRCRGIFFTQSWVSTPGVLPVASGGIHVWHMPALTEIFGDDSVLQFGGGTLGHPW 411
BsRbcL          DYTEKDRSRGIYFTQSWVSTPGVLPVASGGIHVWHMPALTEIFGDDSVLQFGGGTLGHPW 411
AtRbcL          DYVEKDRSRGIFFTQDWVSLPGVLPVASGGIHVWHMPALTEIFGDDSVLQFGGGTLGHPW 411
GARbcL          DYVEKDRSRGIYFTQDWCSMPGVMPVASGGIHVWHMPALVEIFGDDACLQFGGGTLGHPW 411
CyRbcL          SFVPEDRSRGNFFDQDWGSMPGVFAVASGGIHVWHMPALVAIFGDDSVLQFGGGTHGHPW 403
RARbcL          PKLERNLQEGLFFDMEWASLRKVMPVASGGIHAGQMHQLIHYLGEDVVLQFGGGTIGHPD 419
                    .:  .* :*  .* *   *:.*******. :*  *   :*:*  ******* ***

ZmRbcL          GNAPGAAANRVALEACVQARNEGRDLAREGNEIIKAACKWSAELAAACEIWKEIKFDGFK 471
OsRbcL          GNAPGAAANRVALEACVQARNEGRDLAREGNEIIRSACKWSPELAAACEIWKAIKFE-FE 470
AhRbcL          GNAPGAVANRVALEACVQARNEGRDLAREGNTIIREAAKWSPELAAACEVWKEIKFE-FP 470
BsRbcL          GNAPGAVANRVALEACVQARNEGRDLASEGNTIIREAAKWSPELAAACEVWKEIKFE-FP 470
AtRbcL          GNAPGAVANRVALEACVQARNEGRDLAVEGNEIIREACKWSPELAAACEVWKEITFN-FP 470
GARbcL          GNAPGAAANRVALEACTQARNEGRDLAREGGDVIRSACKWSPELAAACEVWKEIKFE-FD 470
CyRbcL          GSAAGAAANRVALEACVKARNAGREIEKESRDILMEAGKHSPELAIALETWKEIKFE-FD 462
RARbcL          GIQAGATANRVALEAMILARNENRDYLTEGPEILREAAKTCGALRTALDLWKDITFN-YT 478
                *  .**.********   *** .*:   *.  ::  * * .  *  * : ** *.*: :

ZmRbcL          AMDTI---------- 476
OsRbcL          PVDKLDS-------- 477
AhRbcL          AMDTI---------- 475
BsRbcL          AMDTV---------- 475
AtRbcL          TIDKLDGQE------ 479
GARbcL          TIDKL---------- 475
CyRbcL          TVDKLDVQ------- 470
RARbcL          STDTSDFVETPTANI 493
                . *.
```

Figure 4.2 Phylogenetic analysis of RbcL amino acid sequenses from various species

Phylogenetic tree was generated from ClustalW sequence alignment results by the neighbour-joining method using ClustalW-Phylogeny. RbcL amino acid sequences were used for the sequence alignment. An asterisk indicates *Arabidopsis* RbcL, which was not included in the dicot clade. Numbers refer to distance of each node. Zm, maize; Os, rice; Ah, *Amaranthus*; Bs, *B. sinuspersici*; At, *Arabidopsis*; GA, green algae; Cy, cyanobacteria; RA, red algae.

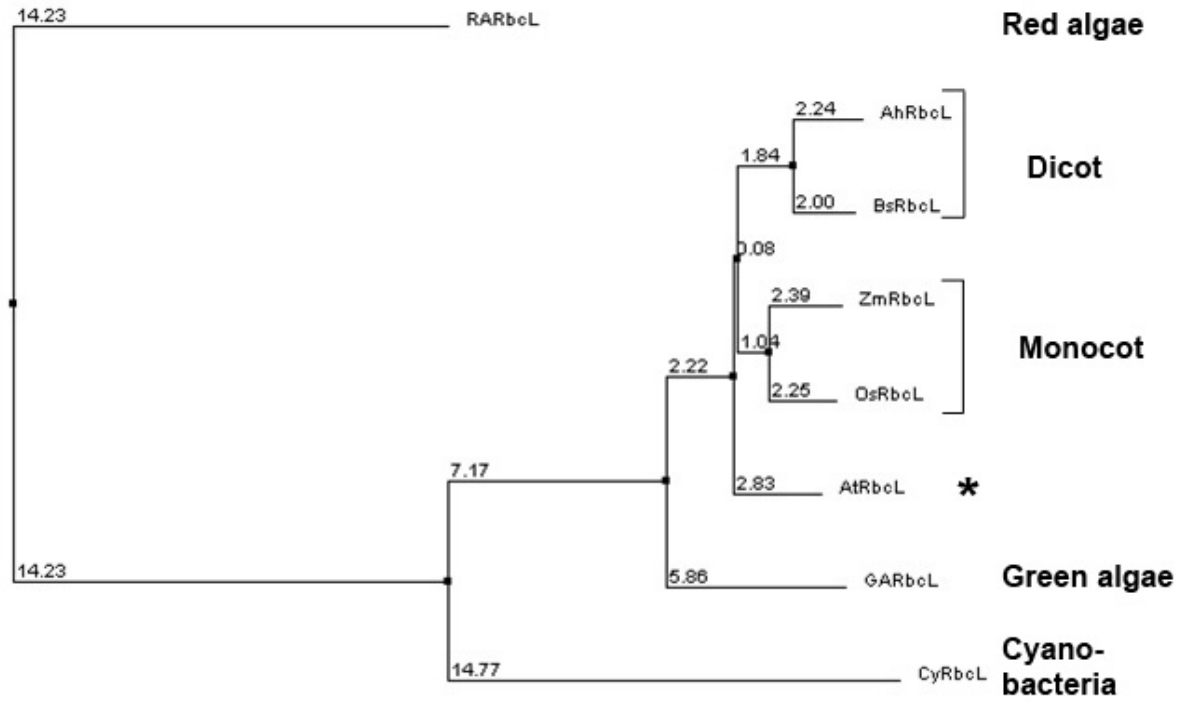
14.23
RARbcL
Red algae
2.24
AhRbcL
1.84
Dicot
2.00
BsRbcL
0.08
2.39
ZmRbcL
Monocot
1.04
2.22
2.25
OsRbcL
7.17
2.83
AtRbcL
*
14.23
5.86
GARbcL
Green algae
Cyano-
bacteria
14.77
CyRbcL

Figure 4.3 Comparison of multiple sequence alignment programs in the alignment of 5' and 3' region of *rbcL* coding sequences from various species

Coding sequences of *rbcL* mRNA in C_4 monocot maize (*Z. mays*), C_3 monocot rice (*O. satiba*), C_4 dicot *A. hypochondriacus*, single-cell C_4 species *B. sinuspersici*, C_3 dicot *A. thaliana*, green algae *C. reinhardtii*, cyanobacteria *Synechococcus sp.*, and red algae *G. partita* were aligned by a multiple sequence alignment program ClustalW **(A)**, T-Coffee **(B)**, or MUSCLE **(C)**. Start and stop codons are boxed in red and blue color, respectively. Zm, maize; Os, rice; Ah, *Amaranthus*; Bs, *B. sinuspersici*; At, *Arabidopsis*; GA, green algae; Cy, cyanobacteria; RA, red algae.

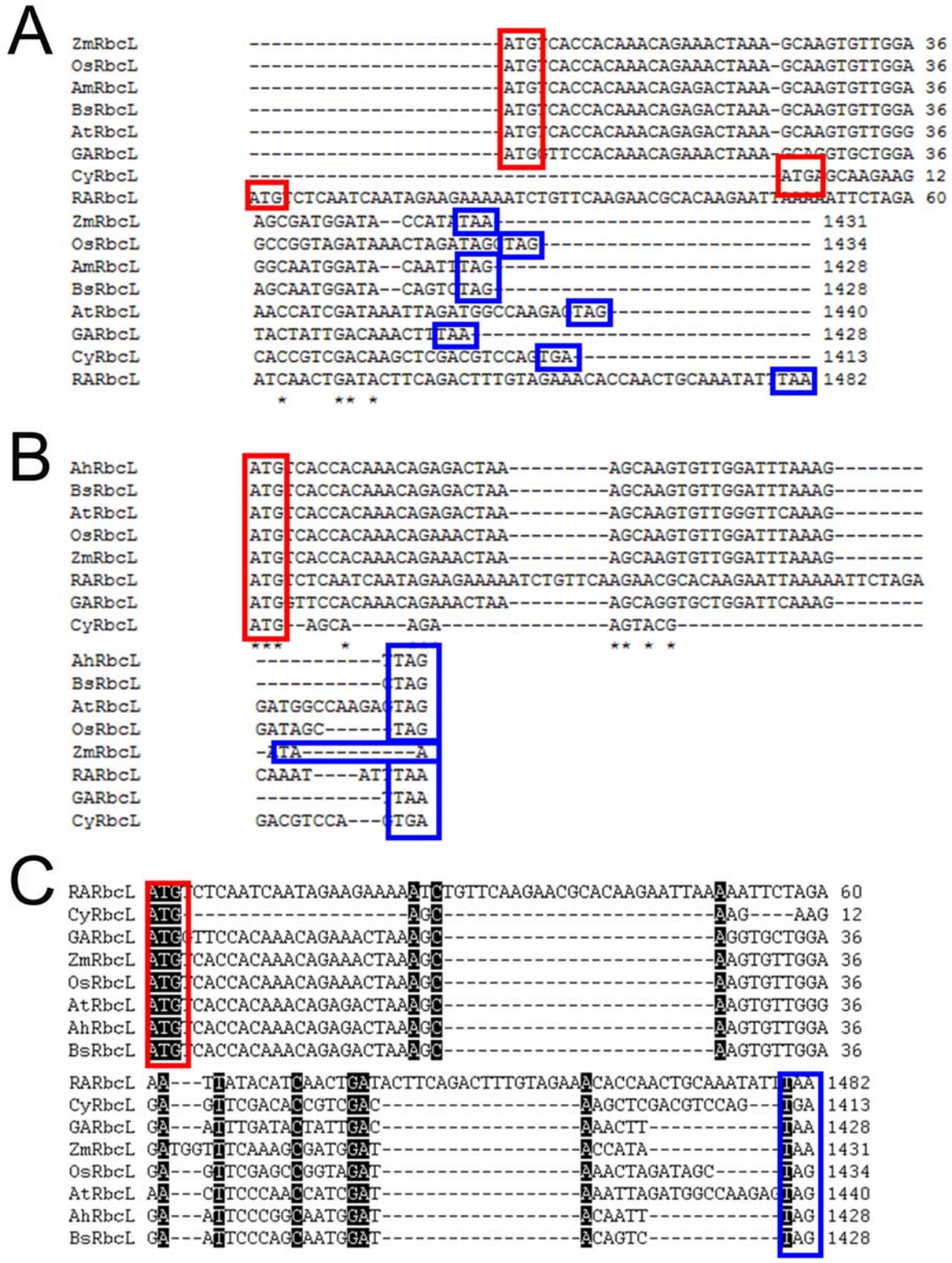
A
ZmRbcL ATGTCACCACAAACAGAAACTAAA-GCAAGTGTTGGA 36
OsRbcL ATGTCACCACAAACAGAAACTAAA-GCAAGTGTTGGA 36
AmRbcL ATGTCACCACAAACAGAGACTAAA-GCAAGTGTTGGA 36
BsRbcL ATGTCACCACAAACAGAGACTAAA-GCAAGTGTTGGA 36
AtRbcL ATGTCACCACAAACAGAGACTAAA-GCAAGTGTTGGG 36
GARbcL ATGGTTCCACAAACAGAAACTAAA-GCAGGTGCTGGA 36
CyRbcL ATGAGCAAGAAG 12
RARbcL ATGTCTCAATCAATAGAAGAAAAATCTGTTCAAGAACGCACAAGAATTAAAAATTCTAGA 60
ZmRbcL AGCGATGGATA--CCATATAA 1431
OsRbcL GCCGGTAGATAAACTAGATAGCTAG 1434
AmRbcL GGCAATGGATA--CAATTTAG 1428
BsRbcL AGCAATGGATA--CAGTCTAG 1428
AtRbcL AACCATCGATAAATTAGATGGCCAAGAGTAG 1440
GARbcL TACTATTGACAAACTTTAA 1428
CyRbcL CACCGTCGACAAGCTCGACGTCCAGTGA 1413
RARbcL ATCAACTGATACTTCAGACTTTGTAGAAACACCAACTGCAAATATTTAA 1482
B
AhRbcL ATGTCACCACAAACAGAGACTAA---------AGCAAGTGTTGGATTTAAAG--------
BsRbcL ATGTCACCACAAACAGAGACTAA---------AGCAAGTGTTGGATTTAAAG--------
AtRbcL ATGTCACCACAAACAGAGACTAA---------AGCAAGTGTTGGGTTCAAAG--------
OsRbcL ATGTCACCACAAACAGAAACTAA---------AGCAAGTGTTGGATTTAAAG--------
ZmRbcL ATGTCACCACAAACAGAAACTAA---------AGCAAGTGTTGGATTTAAAG--------
RARbcL ATGTCTCAATCAATAGAAGAAAAATCTGTTCAAGAACGCACAAGAATTAAAAATTCTAGA
GARbcL ATGGTTCCACAAACAGAAACTAA---------AGCAGGTGCTGGATTCAAAG--------
CyRbcL ATG--AGCA-----AGA---------------AGTACG----------------------
AhRbcL ----------TTAG
BsRbcL ----------CTAG
AtRbcL GATGGCCAAGAGTAG
OsRbcL GATAGC------TAG
ZmRbcL -ATA----------A
RARbcL CAAAT----ATTTAA
GARbcL ----------TTAA
CyRbcL GACGTCCA---GTGA
C
RARbcL ATGTCTCAATCAATAGAAGAAAAATCTGTTCAAGAACGCACAAGAATTAAAAATTCTAGA 60
CyRbcL ATG----------AGC----------AAG----AAG 12
GARbcL ATGGTTCCACAAACAGAAACTAAAGC----------AGGTGCTGGA 36
ZmRbcL ATGTCACCACAAACAGAAACTAAAGC----------AAGTGTTGGA 36
OsRbcL ATGTCACCACAAACAGAAACTAAAGC----------AAGTGTTGGA 36
AtRbcL ATGTCACCACAAACAGAGACTAAAGC----------AAGTGTTGGG 36
AhRbcL ATGTCACCACAAACAGAGACTAAAGC----------AAGTGTTGGA 36
BsRbcL ATGTCACCACAAACAGAGACTAAAGC----------AAGTGTTGGA 36
RARbcL AA---TTATACATCAACTGATACTTCAGACTTTGTAGAAACACCAACTGCAAATATTTAA 1482
CyRbcL GA---GTTCGACACCGTCGAC----------AAGCTCGACGTCCAG---TGA 1413
GARbcL GA---ATTTGATACTATTGAC----------AAACTT----------TAA 1428
ZmRbcL GATGGTTTCAAAGCGATGGAT----------ACCATA----------TAA 1431
OsRbcL GA---GTTCGAGCCGGTAGAT----------AAACTAGATAGC------TAG 1434
AtRbcL AA---CTTCCCAACCATCGAT----------AAATTAGATGGCCAAGAGTAG 1440
AhRbcL GA---ATTCCCGGCAATGGAT----------ACAATT----------TAG 1428
BsRbcL GA---ATTCCCAGCAATGGAT----------ACAGTC----------TAG 1428

Figure 4.4 Phylogenetic analysis of *rbcL* coding sequences from various species

Phylogenetic tree was generated from the MUSCLE sequence alignment results by the neighbour-joining method using ClustalW-Phylogeny. The *rbcL* coding sequences were used for the sequence alignment. An asterisk indicates *Arabidopsis rbcL*, which was classified into the dicot clade. Numbers refer to distance of each node. Zm, maize; Os, rice; Ah, *Amaranthus*; Bs, *B. sinuspersici*; At, *Arabidopsis*; GA, green algae; Cy, cyanobacteria; RA, red algae.

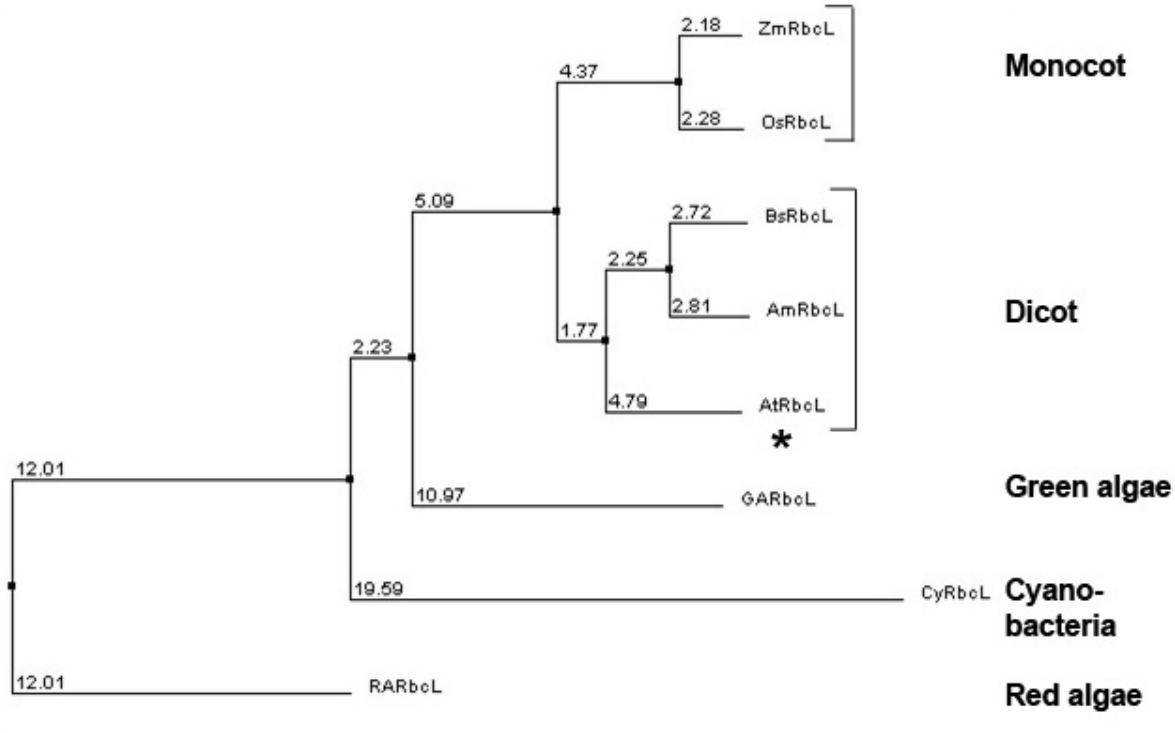
2.18
ZmRbcL
4.37
2.28
OsRbcL
Monocot
5.09
2.72
BsRbcL
2.25
2.81
AmRbcL
Dicot
2.23
1.77
4.79
AtRbcL
*
12.01
10.97
GARbcL
Green algae
19.59
CyRbcL
Cyano-
bacteria
12.01
RARbcL
Red algae

4.2.2 Sequence alignment and secondary structure prediction of *rbcL* UTR

The regulatory elements and structures responsible for mRNA stability and translation efficiency are often present in the UTR regions. Both the 5' and 3'UTR of *rbcL* mRNA sequences in various higher plants were aligned using the MUSCLE program, and their secondary structures were predicted using Mfold (Zuker, 2003) and RNAfold (Hofacker, 2003) to identify conserved sequences and structures. From the secondary structure analysis of *rbcL* 3'UTR, a highly conserved stem-loop structure was found (Fig. 4.5). Multiple sequence alignments revealed that this structure was formed by long inverted repeat sequences from the 46th to the 79th nucleotide after the stop codon of *B. sinuspersici rbcL* mRNA (Fig. 4.6). The 5' end of the 5'UTR also showed a conserved stem-loop structure (Fig. 4.7). The inverted repeats form the structure started from the transcription initiation site to the 23rd nucleotide in *B. sinuspersici* (Fig. 4.8). Kuroda and Maliga (2001) have reported that the coding sequence of *rbcL* mRNA is important for efficient translation. They used 59 nucleotides in the 3' end of *rbcL* 5'UTR and 42 nucleotides in the coding region which contained up to eleven silent mutations. When compared to the wildtype, transgenic tobacco plants expressing the mutant constructs show a 35-fold decrease in *rbcL* translation. It is possible that the coding sequence of *rbcL* may form secondary structures with 5'UTR which could easily be disrupted by the mutations. To test this hypothesis bioinformatically, secondary structures of *rbcL* 5'UTR with 60 nucleotides in the coding sequence were predicted and analysed. The prediction results showed that there was a stable stem-loop structure around the initiation codon (Fig. 4.9). In this structure, the last two guanine of the Shine-Dalgarno sequence (GGAGG) were a part of the stem with exceptions in some species (Fig. 4.9E and F), and the +1 adenine and +2 uracil of the start codon (AUG) were

Figure 4.5 Predicted secondary structures of *rbcL* mRNA 3'UTR sequences from various higher plants

Potential secondary structures of *rbcL* mRNA 3'UTR in maize **(A)**, barley **(B)**, *Arabidopsis* **(C)**, *B. sinuspersici* **(D)**, and tobacco **(E)** were predicted by RNAfold. The consensus secondary structure **(F)** was predicted by Alifold after the sequences were aligned by MUSCLE. Background colors around nucleotide indicate probabilities of folding from the highest (red) to the lowest (purple).

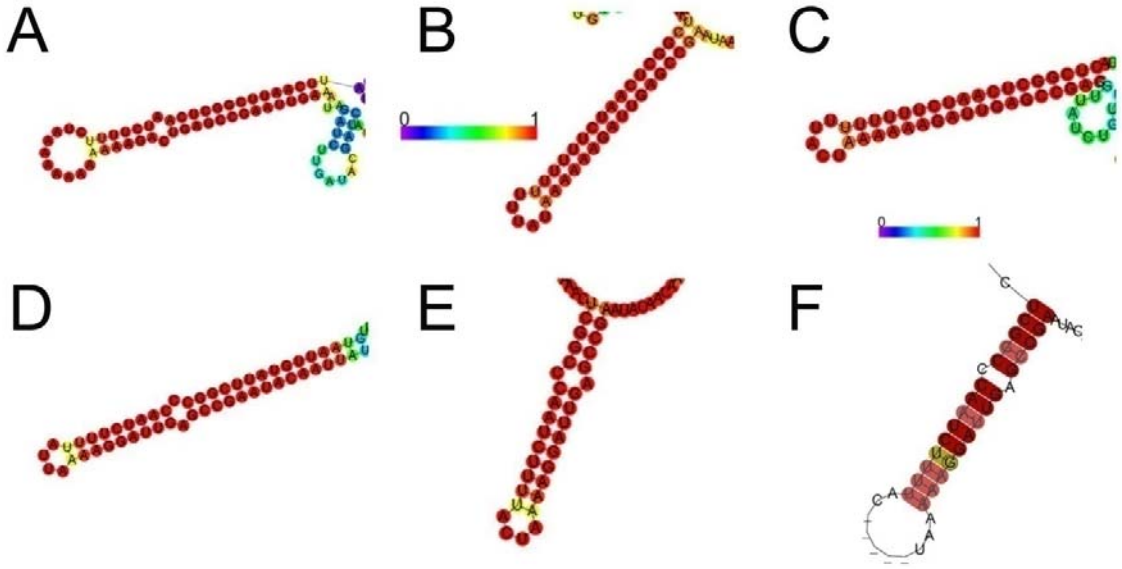
A
B
0
1
C
0
1
D
E
F

Figure 4.6 S**equence alignment of *rbcL* 3'UTR from various higher plants by MUSCLE**

Nucleotide sequences of *rbcL* 3'UTR in maize, rice, barley, *B. sinuspersici*, *Amaranthus*, spinach, *Arabidopsis*, potato, and tobacco were aligned by a multiple sequence alignment program MUSCLE. White letters in black background show nucleotide sequences conserved in at least 8 out of 9 species. Arrows indicate the inverted repeat predicted to form a stem-loop structure by RNAfold. Zm, maize; Os, rice; Hv, barley; Bs, *B. sinuspersici*; Ah, *Amaranthus*; So, spinach; At, *Arabidopsis*; St, potato; Nt, tobacco.


ZmRbcL
OsRbcL
HvRbcL
AtRbcL
StRbcL
NtRbcL
AhRbcL
BsRbcL
SoRbcL

Figure 4.7 Predicted secondary structures of *rbcL* mRNA 5'UTR from various higher plants

Potential secondary structures of *rbcL* mRNA 5'UTR of rice **(A)**, barley **(B)**, *B. sinuspersici* **(C)**, spinach **(D)**, and potato **(E)** were predicted by RNAfold. The consensus secondary structure **(F)** was predicted by Alifold after the sequences were aligned by MUSCLE. Background colors around nucleotides indicate probabilities of folding from the highest (red) to the lowest (purple).

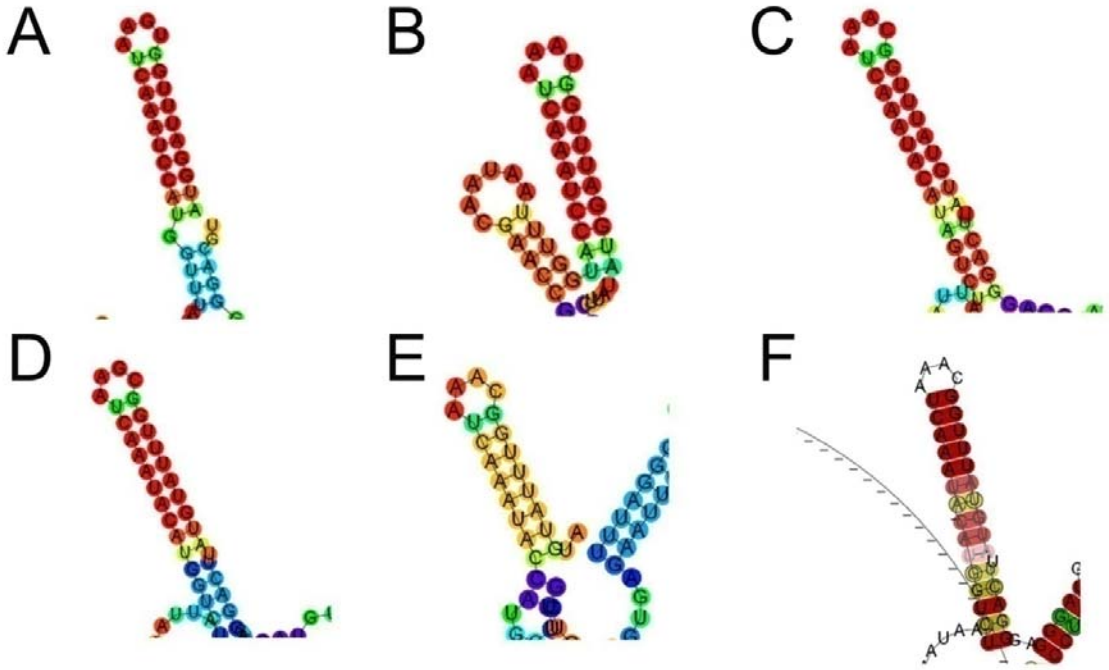
A
B
C
D
E
F

Figure 4.8 Sequence alignment of the 5' sequence of *rbcL* 5'UTR from various higher plants by MUSCLE

The first half nucleotide sequences of *rbcL* 5'UTR in maize, rice, barley, *B. sinuspersici*, *Amaranthus*, spinach, *Arabidopsis*, potato, and tobacco were aligned by a multiple sequence alignment program MUSCLE. White letters in black background show nucleotide sequences conserved in at least 8 out of 9 species. Arrows indicate the inverted repeat which was predicted to form a stem-loop structure by RNAfold. Zm, maize; Os, rice; Hv, barley; Bs, *B. sinuspersici*; Ah, *Amaranthus*; So, spinach; At, *Arabidopsis*; St, potato; Nt, tobacco.

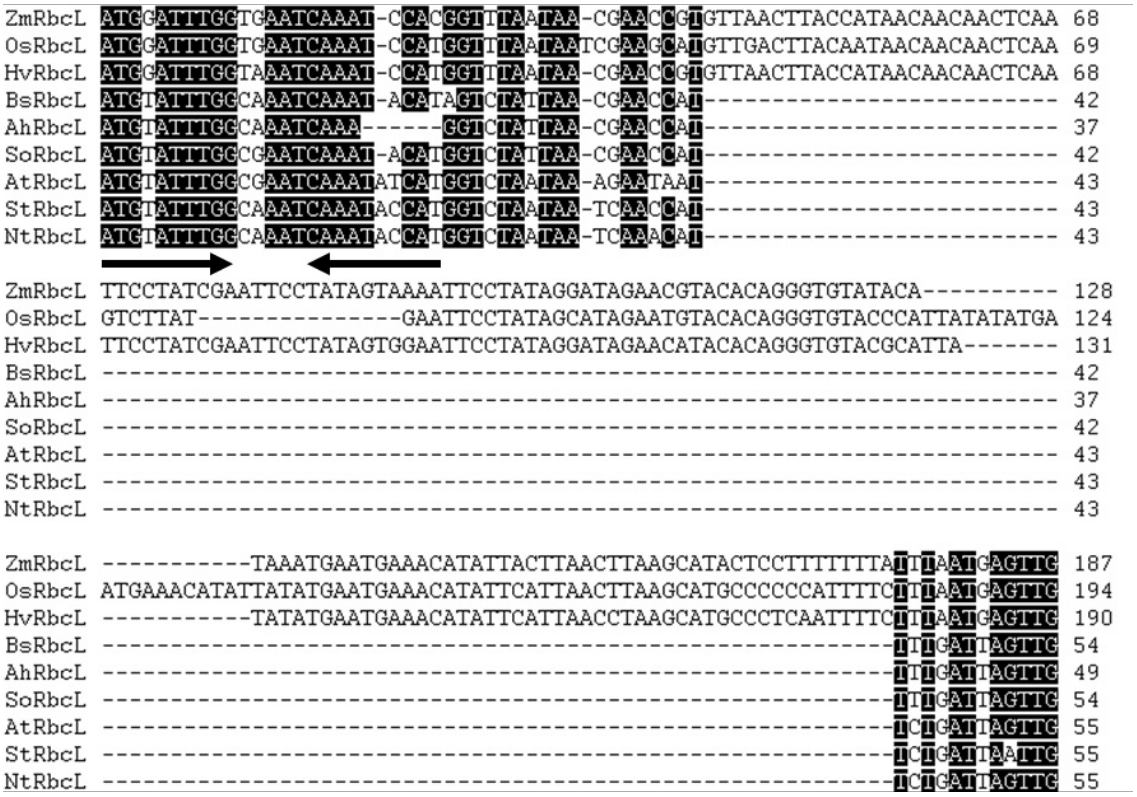
ZmRbcL ATGGATTTGGTGAATCAAAT-CCACGGTTTAATAA-CGAACCGTGTTAACTTACCATAACAACAACTCAA 68
OsRbcL ATGGATTTGGTGAATCAAAT-CCATGGTTTAATAATCGAAGCATGTTGACTTACAATAACAACAACTCAA 69
HvRbcL ATGGATTTGGTAAATCAAAT-CCATGGTTTAATAA-CGAACCGTGTTAACTTACCATAACAACAACTCAA 68
BsRbcL ATGTATTTGGCAAATCAAAT-ACATAGTCTATTAA-CGAACCATG---------- 42
AhRbcL ATGTATTTGGCAAATCAAA------GGTCTATTAA-CGAACCATG---------- 37
SoRbcL ATGTATTTGGCGAATCAAAT-ACATGGTCTATTAA-CGAACCATG---------- 42
AtRbcL ATGTATTTGGCGAATCAAATATCATGGTCTAATAA-AGAATAATG---------- 43
StRbcL ATGTATTTGGCAAATCAAATACCATGGTCTAATAA-TCAACCATG---------- 43
NtRbcL ATGTATTTGGCAAATCAAATACCATGGTCTAATAA-TCAAACATG---------- 43
ZmRbcL TTCCTATCGAATTCCTATAGTAAAATTCCTATAGGATAGAACGTACACAGGGTGTATACA---------- 128
OsRbcL GTCTTAT---------------GAATTCCTATAGCATAGAATGTACACAGGGTGTACCCATTATATATGA 124
HvRbcL TTCCTATCGAATTCCTATAGTGGAATTCCTATAGGATAGAACATACACAGGGTGTACGCATTA------- 131
BsRbcL ---------- 42
AhRbcL ---------- 37
SoRbcL ---------- 42
AtRbcL ---------- 43
StRbcL ---------- 43
NtRbcL ---------- 43
ZmRbcL ----------TAAATGAATGAAACATATTACTTAACTTAAGCATACTCCTTTTTTTATTTAATGAGTTG 187
OsRbcL ATGAAACATATTATATGAATGAAACATATTCATTAACTTAAGCATGCCCCCCATTTTCTTTAATGAGTTG 194
HvRbcL ----------TATATGAATGAAACATATTCATTAACCTAAGCATGCCCTCAATTTTCTTTAATGAGTTG 190
BsRbcL ----------TTTGATTAGTTG 54
AhRbcL ----------TTTGATTAGTTG 49
SoRbcL ----------TTTGATTAGTTG 54
AtRbcL ----------TCTGATTAGTTG 55
StRbcL ----------TCTGATTAATTG 55
NtRbcL ----------TCTGATTAGTTG 55

Figure 4.9 Predicted secondary structures of *rbcL* mRNA 5'UTR and coding sequence proximal to the translation initiation codon (AUG) from various higher plants

Potential *rbcL* mRNA secondary structures of *rbcL* mRNA 5'UTR and coding sequences in maize **(A)**, rice **(B)**, *B. sinuspersici* **(C)**, *Amaranthus* **(D)**, and potato **(E)** were predicted by RNAfold. Only secondary structures around initiation codons are shown. The consensus secondary structure **(F)** was predicted by Alifold after the sequences were aligned by MUSCLE. Initiation codons and Shine-Dalgarno sequences are marked by black and blue circles, respectively. Background colors around nucleotides indicate probabilities of folding from the highest (red) to the lowest (purple).

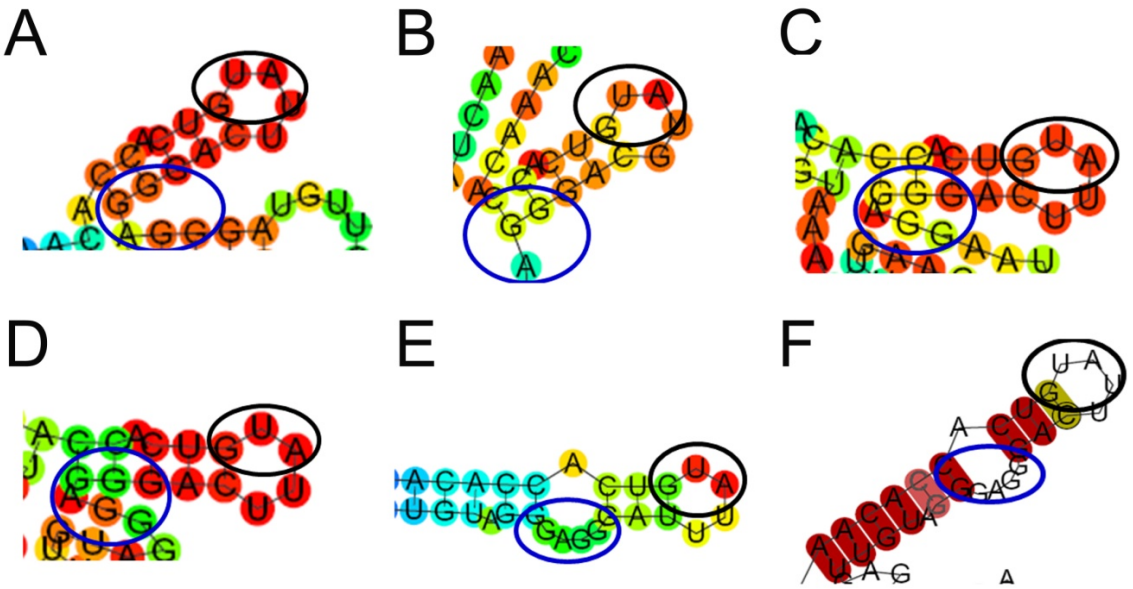
A
B
C
D
E
F

always in the loop. Interestingly, the adenine at the position +6 formed a bulge structure in all tested species.

RNA processing in plastids may be required for efficient translation and mRNA stability of *rbcL*, as proposed by Reinbothe et al. (1993). To determine whether the length of *rbcL* 5'UTR affects secondary structure formation, the secondary structures of 5'UTR of different lengths were predicted. The lengths of mature and intermediate *rbcL* mRNAs varied slightly between species because of their approximate lengths of -60 and -100 5'UTR, respectively. These 5'UTR lengths together with +60 coding sequence were also analyzed. A conserved stem-loop structure was predicted in -60 5'UTR with +60 coding sequence (Fig. 4.10A-F). This structure was in the coding sequence from +42 to +51 nucleotides (Fig. 4.11). The loop part of the structure consisted of UGGU nucleotide sequence. This stem-loop structure, however, was disrupted when -100 5'UTR combined with +60 coding sequence was used (Fig. 4.12). The UGGU sequence that formed a loop in the mature mRNA was partially or totally hybridized to the complement sequence. There was no conserved structure other than that found near the translation initiation site in the intermediate mRNA. Therefore, the only structural difference predicted between *rbcL* mature and intermediate mRNA was that the mature form contained another conserved stem-loop that was absent in the intermediate form.

4.3 Discussion

4.3.1 Identification of the suitable sequence alignment tool and phylogenetic trees of RbcL

RbcL is a plastid genome-encoded protein in algae and higher plants. Green algae and higher plants have the green-like or type I Rubisco consisting of eight RbcLs and eight RbcSs

originating from cyanobacteria. On the other hand, red algae and some brown algae have the red-like or type II Rubisco consisting of only two large subunits derived from purple bacteria. Multiple sequence alignment and phylogenetic tree of RbcL clearly showed the evolutionary relationships among various photosynthetic organisms (Fig. 4.1-4.4). Although the amino acid-based phylogenetic tree showed a distinct location for the C_3 dicot *Arabidopsis* (Fig. 4.2), it was corrected in the nucleotide-based tree (Fig. 4.4). These results suggested that the phylogenetic tree generated from the nucleotide sequence was more reliable than that from the amino acid sequence. Multiple sequence alignment analysis also revealed the accuracy of the programs. MUSCLE was the only program that aligns the start codon (ATG) and stop codon (TAG, TGA, or TAA) of *rbcL* homologous genes (Fig. 4.3A-C). Furthermore, MUSCLE was able to generate alignment data faster than ClustalW and T-Coffee. Therefore, MUSCLE was chosen for the subsequent analysis of *rbcL* transcript.

4.3.2 Regulation of Rubisco transcript and secondary structure predictions

Transcription mechanisms of plastid genes are similar to those of prokaryotes. For instance, bacterial type RNA polymerase including sigma factors are used for transcription in plastid (Troxler et al., 1994). Unlike nuclear-encoded genes, the expression of many plastid genes including *rbcL* is mainly regulated at the post-transcriptional and translational levels (Patel and Berry, 2008). mRNA processing is one of the major post-transcriptional regulations controlling expressions of chloroplastic genes (Marin-Navarro et al., 2007). There are at least two forms of *rbcL* transcripts of different length found in barley (Reinbothe et al., 1993), green algae (Shapira et al., 1997), tobacco (Serino and Maliga, 1998), and *Amaranthus* (McCormac et al., 2001).

Figure 4.10 Predicted secondary structures of the -60 5'UTR and +60 coding sequence of *rbcL* mRNA from various higher plants

Potential secondary structures of *rbcL* mRNA including the mature form (-60) of 5'UTR and 5' region (+60) of coding sequences in barley **(A)**, *B. sinuspersici* **(B)**, *Amaranthus* **(C)**, *Arabidopsis* **(D)**, and spinach **(E)** were predicted by RNAfold. The consensus secondary structure **(F)** was predicted by Alifold after the sequences were aligned by MUSCLE. Background colours around nucleotides indicate probabilities of folding from the highest (red) to the lowest (purple).

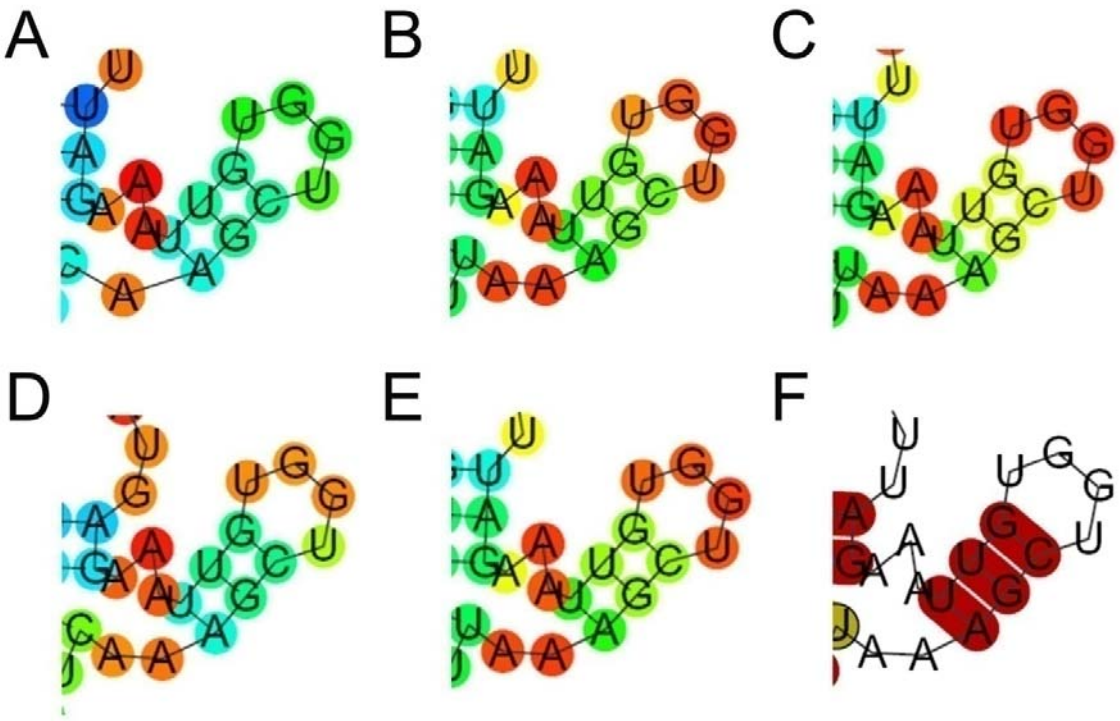
A
B
C
D
E
F

Figure 4.11 Sequence alignment of the 3' sequence of *rbcL* 5'UTR and +60 coding sequence from various higher plants by MUSCLE

Nucleotide sequences of *rbcL* mRNA including the mature form (-60) of 5'UTR and 5' region (+60) of coding sequences in maize, rice, barley, *B. sinuspersici*, *Amaranthus*, spinach, *Arabidopsis*, potato, and tobacco were aligned by a multiple sequence alignment program MUSCLE. Green and blue arrows indicate intermediate (around -100) and mature processing (around -60) site, respectively. Red and orange boxes indicate Shine-Dalgarno sequence and translation initiation codon (ATG), respectively. Black arrows show nucleotide sequences of the stem-loop structure predicted in -60 5'UTR with +60 coding region. Zm, maize; Os, rice; Hv, barley; Bs, *B. sinuspersici*; Ah, *Amaranthus*; So, spinach; At, *Arabidopsis*; St, potato; Nt, tobacco.

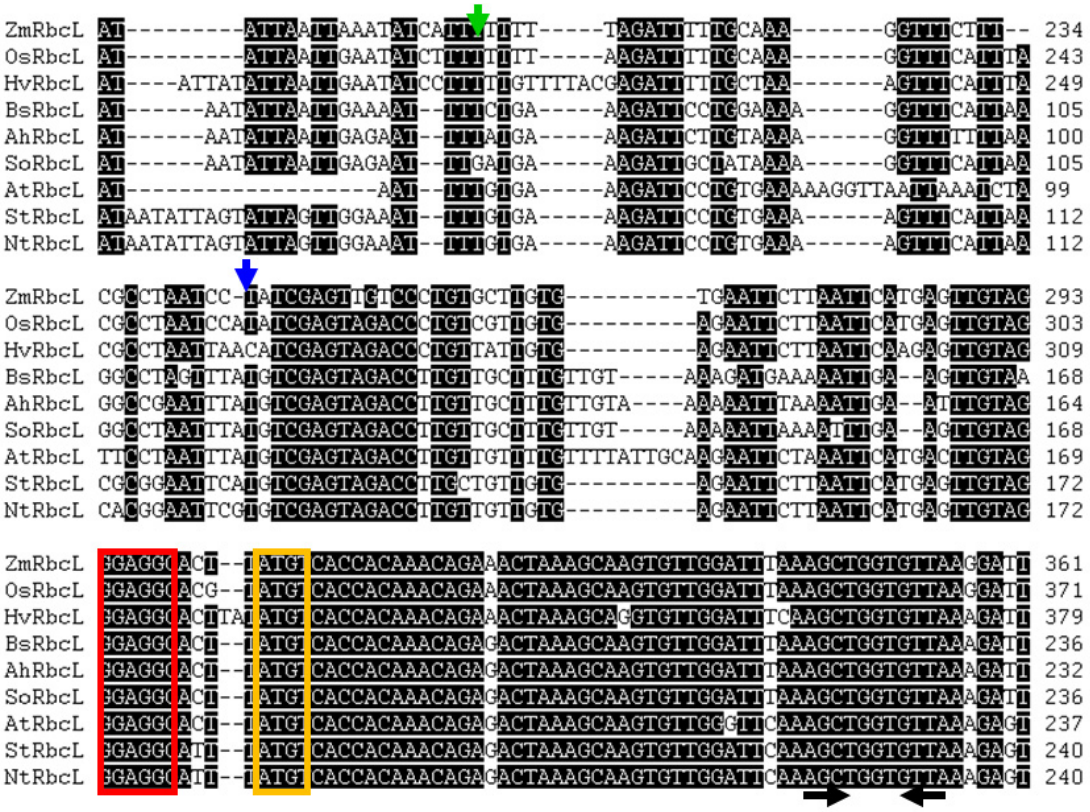
ZmRbcL
OsRbcL
HvRbcL
BsRbcL
AhRbcL
SoRbcL
AtRbcL
StRbcL
NtRbcL

Figure 4.12 Predicted secondary structures of the -100 5'UTR and +60 coding sequence of *rbcL* mRNA from various higher plants

Potential secondary structures of *rbcL* mRNA including the intermediate form (-100) of 5'UTR and 5' region (+60) of coding sequences in barley **(A)**, *B. sinuspersici* **(B)**, *Amaranthus* **(C)**, *Arabidopsis* **(D)**, spinach **(E)**, and tobacco **(F)** were predicted by RNAfold. Background colour around nucleotide indicates probabilities of folding from the highest (red) to the lowest (purple). Nucleotides consisting of the predicted stem-loop structure in the mature form of *rbcL* mRNA are marked by black circles.

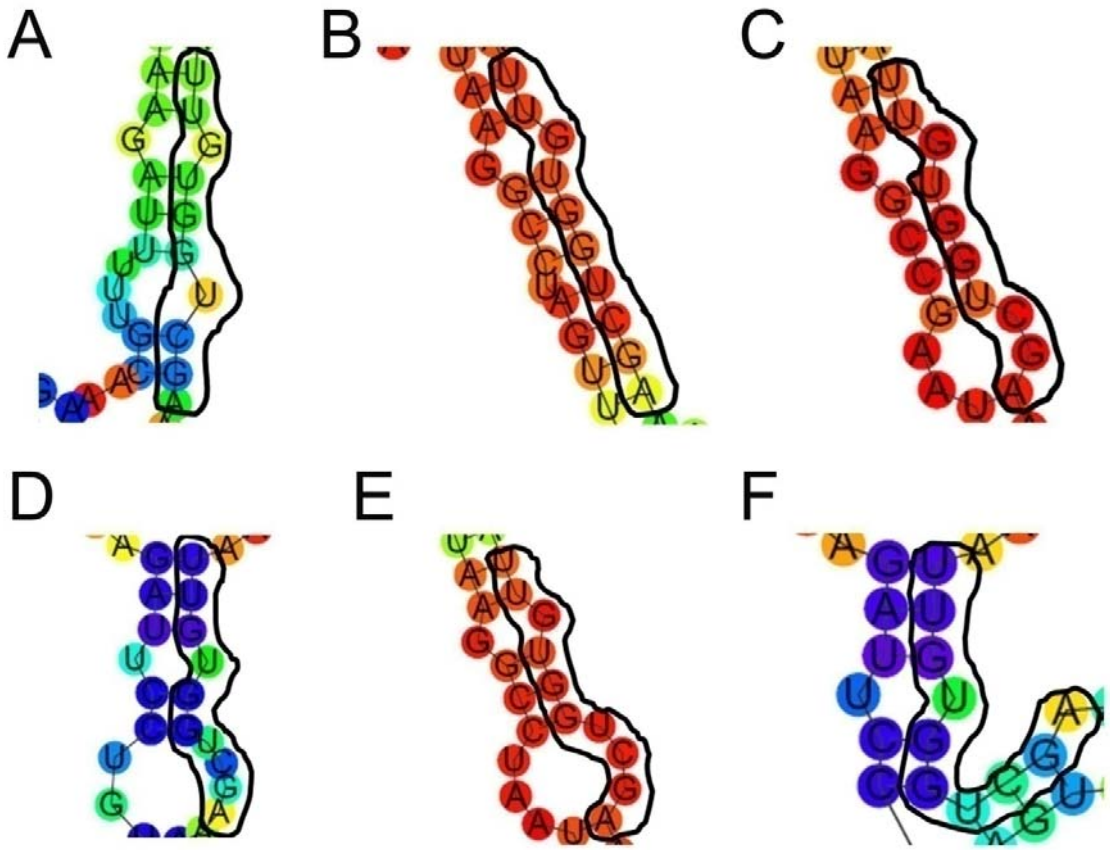
A
B
C
D
E
F

Although *in vitro* translation study in tobacco shows that two different lengths in *rbcL* 5'UTR do not affect translation (Yukawa et al., 2007), it has been suggested that the length of transcripts affects translational efficiency. In addition to the transcript length, secondary structures of the UTR have been proposed to play key roles in the regulation of translation and mRNA stability (Duan et al., 2003; Kim and Mullet, 2003; Meisner et al., 2004).

Plastid mRNAs usually contain inverted repeats in their 3'UTR, forming a stem-loop structure (Stern et al., 1989). The function of the stem-loop structure at the 3'UTR is to stabilize mRNA preventing exonucleolytic degradation (Stern and Kindle, 1993). In spinach, a 155 kDa protein complex binds to the stem-loop in the 3'UTR of chloroplast *petD* mRNA, and interferes with the binding of a 28 kD exonuclease (Hayes et al., 1996). The stem-loop structure in *rbcL* 3'UTR may also function as mRNA stabilizer (Fig. 4.5; Stern and Kindle, 1993).

The functions of the 5'UTR of plastid mRNAs have been less well characterized than those of the 3'UTR. The function of the stem-loop structure predicted at the transcription initiation site of *rbcL* remains unknown (Fig. 4.7, 4.8). Since plastid mRNAs do not have 5'-caps, one can speculate that this stem-loop might function in stabilizing mRNA and facilitating its translation. Similarly, the functions of the stem-loop near the translation initiation site have not been completely characterized either (Fig. 4.9). This stem-loop might also act to recruit the 30S and 50S chloroplastic translation initiation complexes because the Shine-Dalgarno sequence is a part of the stem loop structure. The adenine at +6 positions formed a bulge structure in all higher plants examined and is the third nucleotide in the second codon of *rbcL* (Fig. 4.10, 4.11). The nucleotide sequence around the translation initiation site is highly conserved including the +6 adenine despite the codon redundancy suggesting these nucleotides themselves could have important functions *in vivo*. To determine if this structure relates to

polysome association, this could be tested by generating a point mutation at the site with a polysome association assay and *in vitro* translation analysis.

The secondary structures of the 5'UTR could change because of differential processing, and this change might affect protein binding. Kuroda and Maliga (2001) have described that not only the 5'UTR but the coding sequence also affect RbcL translation efficiency. On the other hand, Whitney and Sharwood (2008) reported that adding the first nine nucleotides of *rbcL* coding region to the 5'UTR in a chimeric construct do not improve translation rates. Although the first nine nucleotides are sufficient to form a stem-loop structure at the translation initiation site, this secondary structure alone might not be enough for efficient translation. These studies implicate that a nucleotide sequence longer than nine bases in the coding sequence is required to generate an additional regulatory element. Therefore, the first 60 bp of the *rbcL* coding sequence were included in addition to the 5'UTR for the secondary structure prediction. Interestingly, the RNA-fold program predicted another stem-loop structure in the mature (-60 with +60) *rbcL* transcript sequence, which was disrupted in the intermediate (-100 with +60) sequence (Fig. 4.12). The consensus structure in mature mRNA sequence (Fig. 4.10) might function in mediating polysome association. This could explain the inefficient translation of the intermediate mRNA in barley (Reinbothe et al., 1993). Alternatively, this secondary structure could be necessary for stabilizing *rbcL* transcripts. It is also possible that the *rbcL* 5'UTR contains unknown *cis*-acting elements that were not determined by the secondary structure prediction programs. Moreover, formation of secondary structures *in vivo* that are distinct from those predicted by the programs cannot be ruled out.

4.3.3 Conclusions

The coding and UTR sequences of *rbcL* from various species were examined by bioinformatic tools. Most notably, one of the stem-loop structures at *rbcL* 5'UTR was predicted to change the conformation depending on the length of *rbcL* transcripts. It is possible to speculate that *rbcL* transcripts become unstable or untranslatable in the PCC chloroplasts of *B. sinuspersici* chlorenchyma cells because they are processed to the intermediate form, in which a potential secondary structure at the 5'UTR is disrupted. This hypothesis needs to be experimentally verified in the future. Nevertheless, predictions using bioinformatics tools would be helpful for the future studies examining the regulation of gene expression in the single-cell C_4 species.

CHAPTER 5: DEGRADATION OF STROMAL PROTEINS THROUGH AUTOPHAGY AND CONTRIBUTION OF STROMULE IN AUTOPHAGY

5.1 Introduction

As described in Chapter 1, autophagy is a complex intracellular process responsible for the degradation of cytosolic and organellar materials, for nutrient recycling and removal of undesirable components in eukaryotic cells. In the autophagic pathways, macroautophagy involves the sequestration of a portion of cytoplasm and organelles into a double membrane structure called an autophagosome which is subsequently transported to the lysosome in mammals or the vacuole in yeast and plants for breakdown. In plants, chloroplastic proteins has been shown to be degraded, at least partially, through autophagic pathways. TEM analysis of senescing wheat revealed that Rubisco is localized in small double-membrane vesicles named Rubisco-containing bodies (RCBs) in the cytosol and vacuole (Chiba et al. 2003). RCBs are also detected in senescing Arabidopsis leaves, however they are absent in the *autophagy-related 5* (*atg5*) mutant (Ishida et al., 2008). Authors proposed that RCBs are formed from stromules and transported into the vacuole through the ATG-dependent autophagic pathway. Based on these studies, I hypothesized that the degradation of stromal proteins might contribute to the differential distribution of enzyme as a post-translational regulation in *B. sinuspersici*. In addition, I was interested in whether stromules participate in autophagy. To test these hypotheses, the response of chloroplasts in mature leaves to oxidative stress was examined using immunolocalization with anti-RbcL and anti-PPDK antibodies. In addition, the *in vivo* localization of autophagosomes and autophagic vacuoles was illustrated by green fluorescent

protein (GFP) fused to AUTOPHGY-RELATED 8 (ATG8), one of autophagosome marker proteins, and the vacuolar dye neutral red (NR), respectively. The results suggest that autophagy is involved in the degradation of proteins including photosynthetic enzymes, which in turn might participate in the regulation in the differential protein accumulation in dimorphic chloroplasts in *B. sinuspersici*.

5.2 Results

5.2.1 Autophagy in stress-induced chlorenchyma cells of *B. sinuspersici* leaves

A previous study using *Arabidopsis* seedlings shows that autophagy is induced by ROS (Xiong et al., 2007b). In order to determine whether this would occur in cells within mature leaves, isolated chlorenchyma cells of *Bienertia sinuspersici* leaves were treated with 20 mM H_2O_2 for 2 h, fixed and observed under a transmission electron microscope (TEM) (Fig. 5.1). When viewed at low resolution, the CCC chloroplasts appeared to be unaffected whereas some PCC chloroplasts became dilated and rounded while others retained their normal oblong shape (Fig. 5.1A). However, at a higher resolution, autophagosomes and autophagic vacuoles were observed in addition to chloroplasts and mitochondria in the CCC (Fig. 5.1B). Moreover, autophagic bodies were occasionally found in the central vacuole in some cells (Fig. 5.1C, D). Autophagic bodies were mainly oval in shape with diameters ranging from 0.4 to 2.5 μm. In autophagosomes, cytoplasmic components including mitochondria were found surrounded by multiple membranes in both the CCC and PCC (Fig. 5.1E, F). Autophagic vacuoles, which were electron transparent, were also observed in the CCC and PCC along with partially degraded cellular components (Fig. 5.1G, H). These results suggest that autophagy was induced by H_2O_2 in chlorenchyma cells of mature *B. sinuspersici* leaves.

Figure 5.1 Transmission electron micrographs of *B. sinuspersici* chlorenchyma cells under oxidative stress

Chlorenchyma cells from mature leaves of *B. sinuspersici* were treated with 20 mM hydrogen peroxide for two hours and observed using transmission electron microscopy (TEM). Images are an entire chlorenchyma cell **(A)**, various organelles in the CCC **(B)**, autophagic bodies in central vacuole **(C, D)**, an autophagosome containing a mitochondrion surrounded by autophagic vacuoles associated with chloroplasts **(E)**, an autophagosome associated with the PCC chloroplast **(F)**, an autophagic vacuole formed in close proximity to chloroplasts in the CCC **(G)**, and autophagic vacuoles in the PCC **(H)**. CCC, central cytoplasmic compartment; PCC, peripheral cytoplasmic compartment; cv, central vacuole; PCh, PCC chloroplast; ap, autophagosome; av, autophagic vacuole; Ch, chloroplast; s, starch grain; m, mitochondrion; ab, autophagic body; cw, cell wall. Bars = 10 μm in **(A)**, 2 μm in **(B)**, 1 μm in **(C, H)**, 500 nm in **(D-G)**.

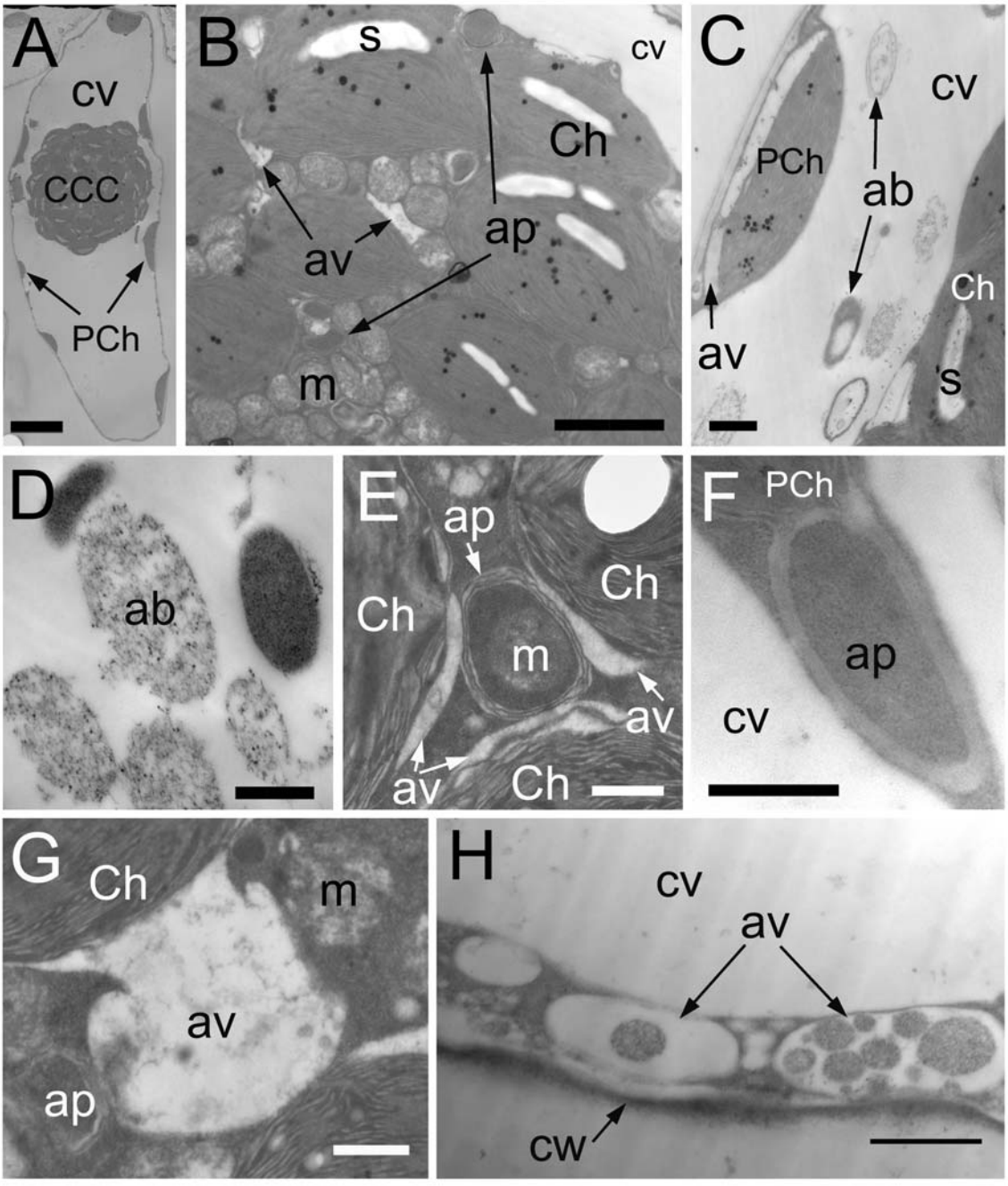
A
cv
CCC
PCh
B
s
cv
Ch
av
ap
m
C
cv
PCh
ab
Ch
av
s
D
ab
E
ap
Ch
Ch
m
av
av
Ch
F
PCh
ap
cv
G
Ch
m
av
ap
H
cv
av
cw

5.2.2 Stromules in control and stressed cells

It has been reported that chloroplasts change their morphology under some stress conditions. Holzinger et al. (2007) described that chloroplast protrusions appear at high temperature (35°C) while they are not detected at 5°C in *Arabidopsis* M chloroplasts. To observe such changes under the oxidative stress, stromal proteins RbcL or PPDK were immunolabeled in chlorenchyma cells and observed under TEM (Fig. 5.2). In the CCC of control cells, dilation and elongation of chloroplast envelopes containing stroma were infrequently observed (Fig. 5.2A, B). Small vesicles with diameters in the range of 90 – 240 nm containing stromal proteins were detected mostly in the PCC and the peripheral region of the CCC along the central vacuole (Fig. 5.2C). Although these vesicles appear similar to the RCBs described in previous studies (Chiba et al., 2003; Ishida et al., 2008), I called these stroma-containing vesicles (SCVs) because they contained PPDK as well as RbcL. Only SCVs of a spherical shape were chosen and measured to prevent the inclusion of stromules in the analysis. Some of these vesicles appeared to be releasing the content to the central vacuole. On the other hand, stress-treated cells showed stromules at a higher frequency (Fig. 5.2D, E), with variable sizes and shapes. Some stromules were detected in autophagic vacuoles with partially degraded contents (Fig. 5.2E arrowhead). Stromules were also observed in cytoplasmic strands connecting the CCC and PCC (Fig. 5.2F). In previous and present studies, we have shown that RbcL mostly accumulates in the CCC chloroplasts but is scarce in the PCC chloroplasts of mature *B. sinuspersici* leaves (Chuong et al., 2006; Chapter 3 in this thesis). The densely-labeled stromule by RbcL antibody suggest that it extends from the CCC chloroplasts to the PCC through the cytoplasmic strand. Although chloroplast protrusions, stromules, and SCVs were found in chlorenchyma cells under the control conditions, they were more abundant in H_2O_2-treated cells.

Figure 5.2 Various forms and localization of stromules detected by immunolocalization analysis

Leaf cross-sections were prepared from non-treated **(A-C)** and treated with hydrogen peroxide **(D-F)** mature *B. sinuspersici* leaves. Sections were probed with RbcL or PPDK antiserum and then gold-conjugated secondary antibody. Images are transmission electron micrographs showing specific reaction of RbcL **(A, D-F)** or PPDK **(B, C)** antibody. Stromules are extending from chloroplasts in CCC **(A, B)**. A stroma-containing vesicle (SCV) located in the PCC cytosol between the chloroplast and central vacuole appeared to be releasing stromal contents in the central vacuole **(C)**. Numerous oval-shaped stromules and autophagosomes in the CCC are detected, with many of them surrounded by autophagic vacuoles **(D)**. Branched stromule, autophagic vacuole degrading stromule, and autophagosome surrounded by autophagic vacuoles are observed **(E)**. A stromule densely labelled by RbcL antibody is detected in the cytoplasmic strand connecting the CCC and the PCC **(F)**. Ch, chloroplast; st, stromule, m, mitochondrion; cv, central vacuole; ap, autophagosome; av, autophagic vacuole; cv, central vacuole; CCC, central cytoplasmic compartment; PCC, peripheral cytoplasmic compartment; PCh, PCC chloroplast; cs, cytoplasmic strand. Bars = 200 nm in **(A, B)**, 100 nm in **(C)**, 500 nm in **(D-F)**.

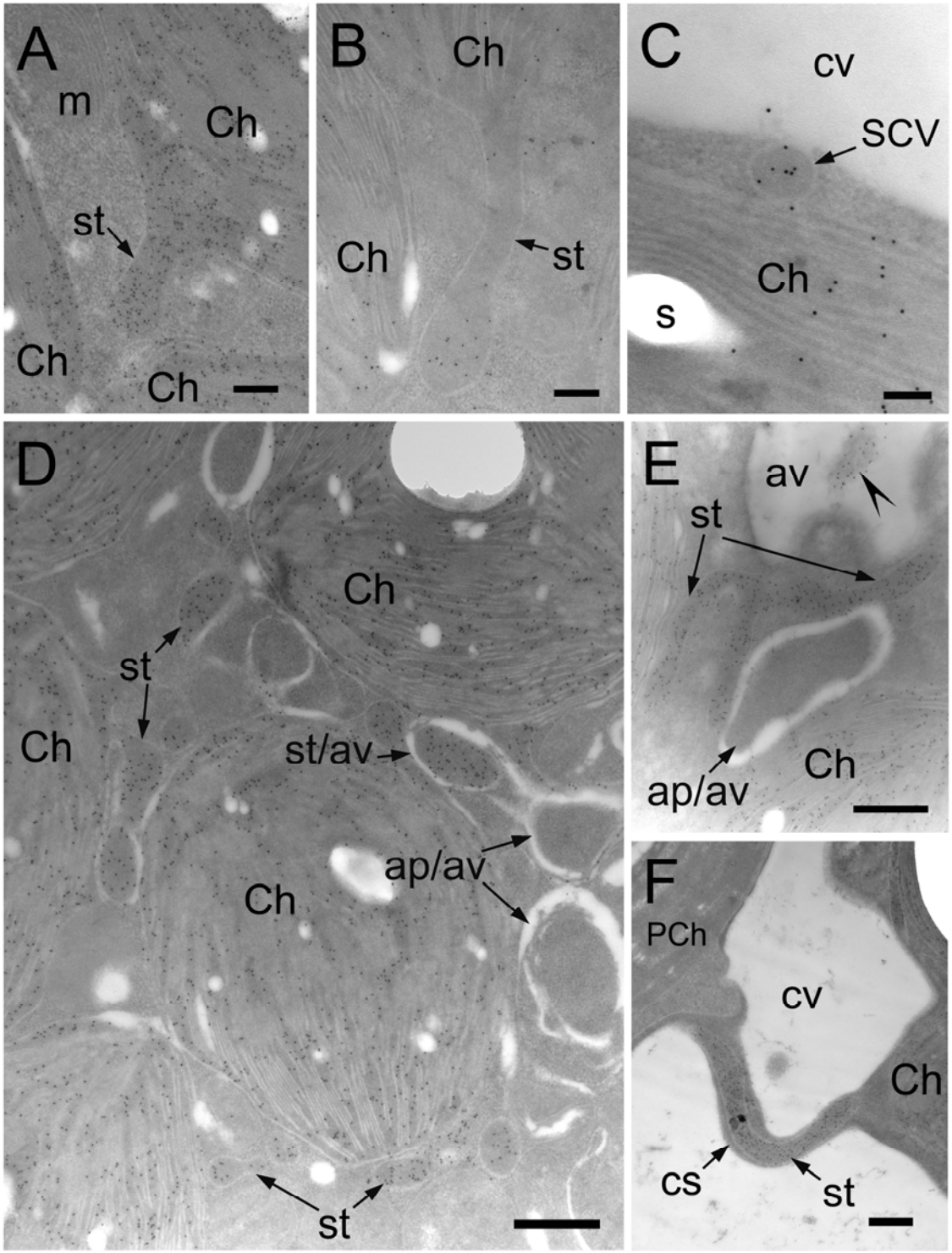
A
m
Ch
st
Ch
Ch
B
Ch
Ch
st
C
cv
SCV
Ch
s
D
Ch
st
Ch
st/av
ap/av
Ch
st
E
av
st
ap/av
Ch
F
PCh
cv
Ch
cs
st

5.3.1 Contribution of stromules in autophagosome formation

I have successfully captured images showing very narrow stromules with diameters ranging from 30 to 50 nm (including membranes and excluding base and tip parts of stromules), originating from chloroplasts and encapsulating portions of the cytoplasm (Fig. 5.3A-D). Careful observation revealed that labelling for stromal proteins was detected between autophagosome membranes in both CCC and PCC of *B. sinuspersici* chlorenchyma cells (Fig. 5.3E-G). The labelling for stromal proteins was also found in a narrow and electron-dense region in between the white membranes of the autophagosome usually observed near chloroplasts. The diameter of the stromal part of stromules was 10 – 20 nm with some exceptions (Fig. 5.4A, B). Although autophagosomes are generally surrounded by two apparent membranes, some were enclosed by multiple membranes (Fig. 5.4C, D). In addition, membranes of autophagosomes were often disrupted and became transparent as seen in Figure 5.2D and E.

5.3.2 Identification of autophagosome contents

The contents of autophagosomes surrounded by stromules seemed to vary based on their appearance. To identify the contents, immunolabelling experiments using various antibodies were performed (Fig. 5.5). For example, labelling for catalase was found inside the autophagosome, indicating a peroxisome was enclosed by membranes (Fig. 5.5A). The RbcL antibody labelled a SCV and its surrounding stromules (Fig. 5.5B). In addition, labelling for the cytosolic marker phosphoenolpyruvate carboxylase (PEPC) revealed that cytosolic content along with other organelles was also captured by autophagosomes (Fig. 5.5C and D).

Figure 5.3 Narrow stromules surrounding autophagosomes

Cross-sections were prepared from H_2O_2-treated leaves. Sections were probed with RbcL or PPDK antiserum and then gold-conjugated secondary antibody. Images are transmission electron micrographs showing specific reaction of RbcL or PPDK antibody. Narrow stromules with diameters in the range of 30 - 50 nm are extending from chloroplasts **(A-D)**. Some stromules appear to be sequestering a portion of cytoplasm **(C, D)**. The membrane part of autophagosomes associated with CCC chloroplasts consists of narrow stromules showing specific reactivity to RbcL **(E, F)** and PPDK in the PCC **(G)**. White arrows indicate gold particles specifically for RbcL **(A-F)** or PPDK **(G)**. CCC, central cytoplasmic compartment; PCC, peripheral cytoplasmic compartment; Ch, chloroplast; st, stromule; ap, autophagosome; m, mitochondrion; PCh, PCC chloroplast; cw, cell wall. Bars = 200 nm in **(A-F)**, 500 nm in **(G)**.

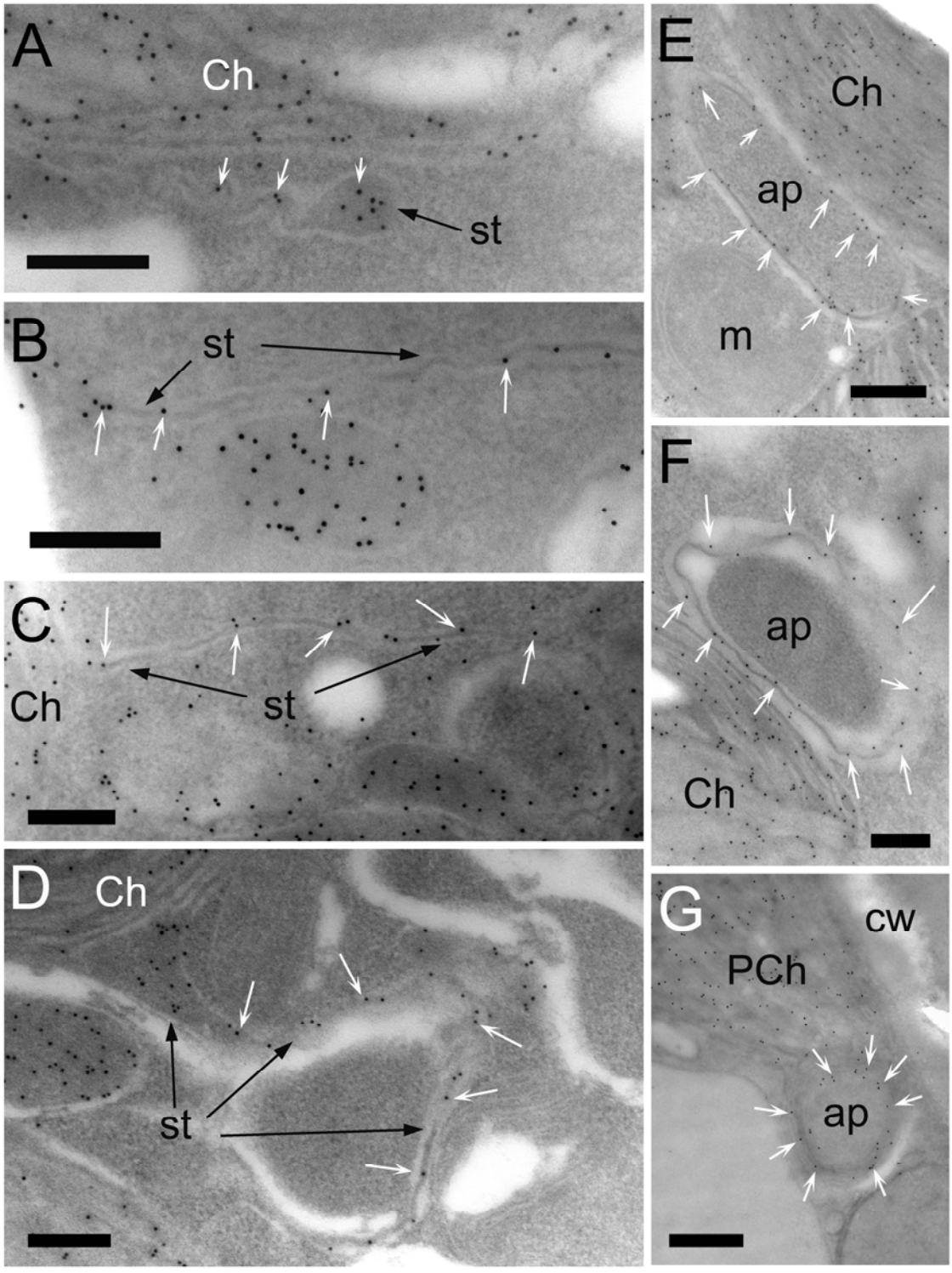
A
Ch
st
B
st
C
Ch
st
D
Ch
st
E
Ch
ap
m
F
ap
Ch
G
cw
PCh
ap

Figure 5.4 Various forms of autophagosome membrane

TEM images of autophagosomes with different membrane morphologies are shown. Cross-sections were prepared from mature leaves treated with hydrogen peroxide. Sections were probed with RbcL antiserum and then gold-conjugated secondary antibody **(A, B)**. Autophagosomes are surrounded by stromules having narrow and thick regions detected by specific reaction of RbcL in the CCC **(A, B)**. Arrow heads indicate gold particles. Numerous membranes are observed on autophagosomes associated with PCC chloroplasts **(C, D)**. st, stromule; ap, autophagosome; Ch, chloroplast; s, starch grain; av, autophagic vacuole; CCC, central cytoplasmic compartment; PCC, peripheral cytoplasmic compartment; PCh, PCC chloroplast. Bars = 200 nm in **(A)**, 500 nm in **(B, D)**, 1 μm in **(C)**.

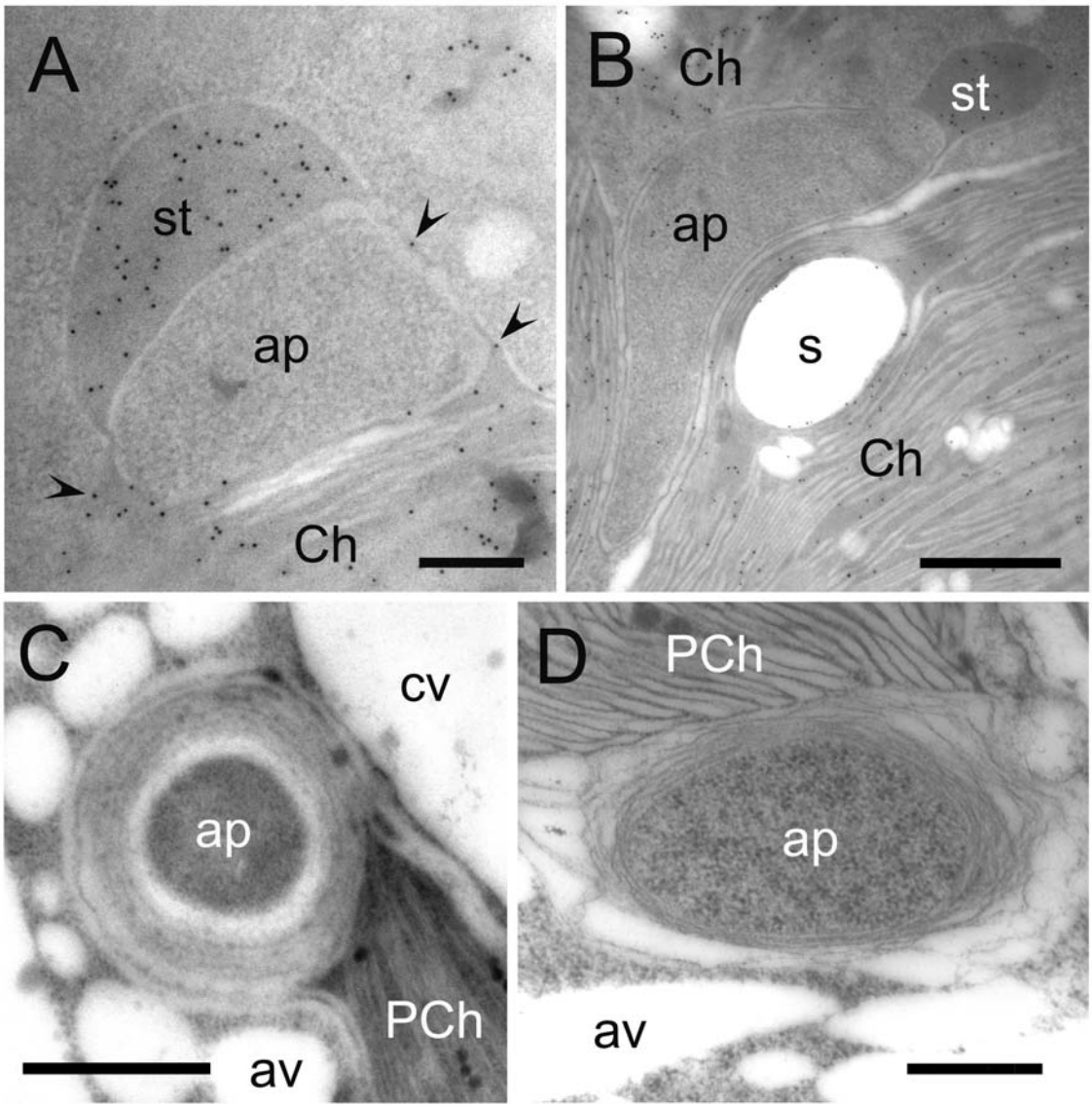
A
st
ap
Ch
B
Ch
st
ap
s
Ch
C
cv
ap
PCh
av
D
PCh
ap
av

Figure 5.5 Identification of various contents in autophagosomes

Cross-sections were prepared from mature leaves treated with hydrogen peroxide. Sections were probed with antiserum raised against catalase **(A)**, RbcL **(B)**, or PEPC **(C, D)** as a marker of peroxisome, stroma of chloroplast, or cytosol, respectively. Sections were further probed with gold-conjugated secondary antibody and observed using TEM. Micrographs show specific locations of these enzymes. White arrows indicate gold particles specifically bound to RbcL in the narrow stromule surrounding a cytoplasmic portion. ap, autophagosome; av, autophagic vacuole; cv, central vacuole; Ch, chloroplast; SCV, stroma-containing vesicle; PCh, PCC chloroplast; cw, cell wall. Bars = 500 nm in **(A, B, D)**, 200 nm in **(C)**.

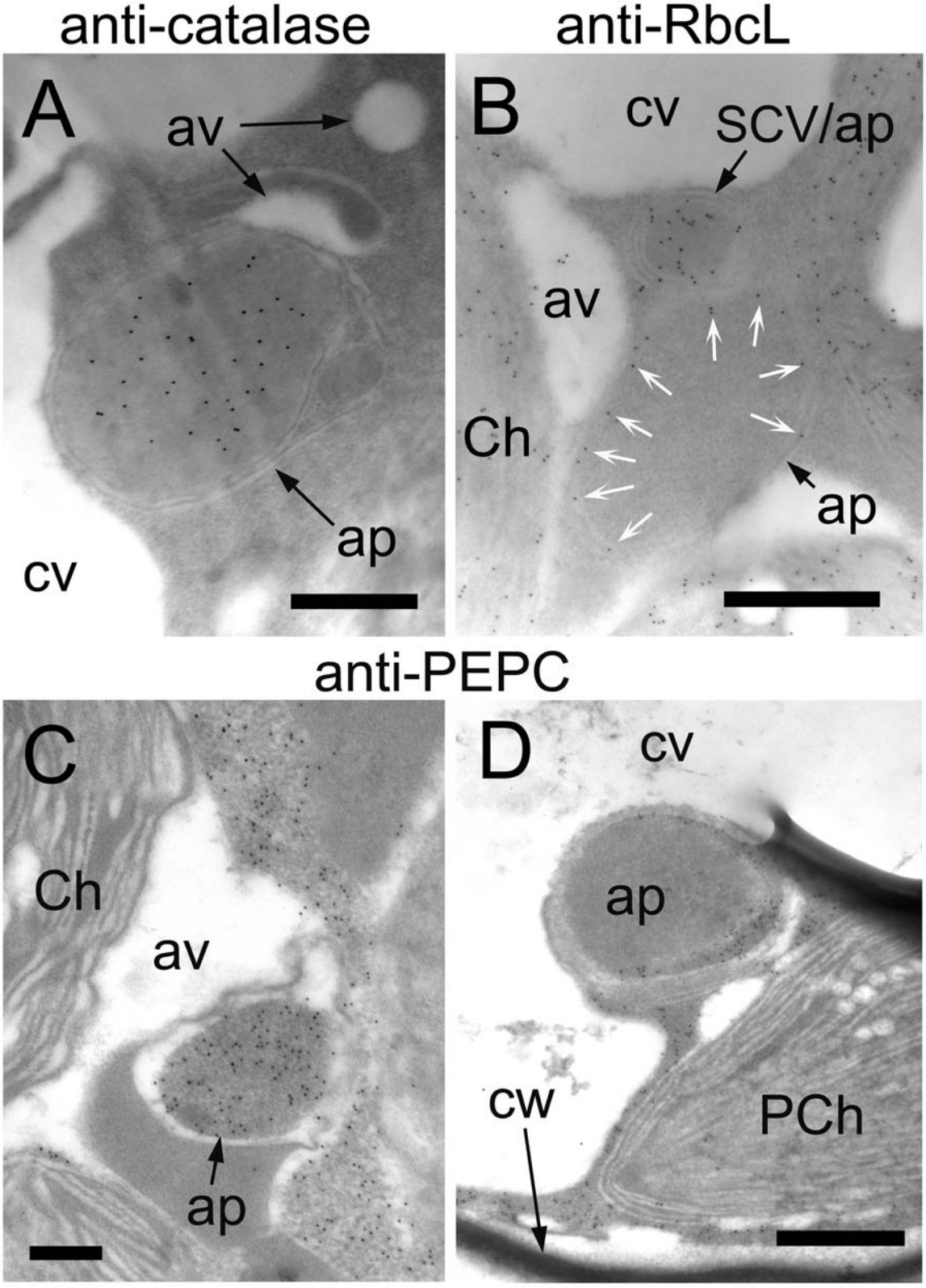
anti-catalase
anti-RbcL
A
av
ap
cv
B
cv
SCV/ap
av
Ch
ap
anti-PEPC
C
Ch
av
ap
D
cv
ap
cw
PCh

Together with the autophagosome containing mitochondria shown in Figure 5.1E, autophagosomes induced by the stress treatment appeared to be generated in a non-selective manner. Furthermore, autophagosomes were often found in close proximity to either the central vacuole or autophagic vacuoles.

5.3.3 Localization of autophagic vacuoles

Neutral red (NR), which stains acidic compartments, is a common dye used to visualize autophagic vacuoles in *Arabidopsis* and tobacco (Otegui et al., 2005; Inoue et al., 2006; Yano et al., 2007; Martinez et al., 2008). To understand how autophagic vacuoles form, chlorenchyma cells isolated from healthy, naturally senescing, and H_2O_2-treated *B. sinuspersici* leaves were stained with NR and observed under a confocal microscope (Fig. 5.6A-C). In control cells, NR mainly accumulated around chloroplasts (Fig 5.6A). Interestingly, higher levels of NR accumulated in the PCC chloroplasts occasionally associated with autophagosomes in some control cells, suggesting that acidic autophagosomes formed in the PCC under normal growth conditions. Naturally senescing and stress-induced cells showed localized accumulation of NR often having more than one punctate structure associated with each chloroplast (Fig. 5.B, C). The preferential accumulation of NR along chloroplasts in all cell types suggested a potential relationship between the formation of autophagic vacuole and chloroplasts. The electron micrograph of the CCC in the H_2O_2-treated cell further supported this idea, showing autophagic vacuole formation on chloroplast envelopes and autophagosome membranes which are perhaps derived from chloroplasts (Fig. 5.6D). In addition, similar patterns in the autophagic vacuole formation between naturally senescing and H_2O_2-treated chlorenchyma cells indicated that cell death was induced by oxidative stress.

Figure 5.6 Formation, localization, and property of autophagic vacuoles

Autophagic vacuoles are observed in mature chlorenchyma cells of *B. sinuspersici* using confocal laser scanning microscopy and TEM. Chlorenchyma cells isolated from healthy **(A)**, senescing **(B)**, or H_2O_2-treated **(C)** leaves were stained with an autophagic vacuole marker neutral red. Some autophagic vacuoles associated with PCC chloroplasts are detected in the control cell (arrows) and increased in senescing and H_2O_2 treated cells in both PCC and CCC. Sections were prepared from leaves treated with H_2O_2 for TEM analyses. Autophagic vacuoles formed in close proximity to chloroplasts and autophagosomes **(D)**. Partially degraded mitochondria and stromules are detected in autophagic vacuoles **(E, F)**. av, autophagic vacuoles; ap, autophagosomes. Bars = 10 μm in **(A-C)**, 2 μm in **(D)**, 500 nm **(E, F)**.

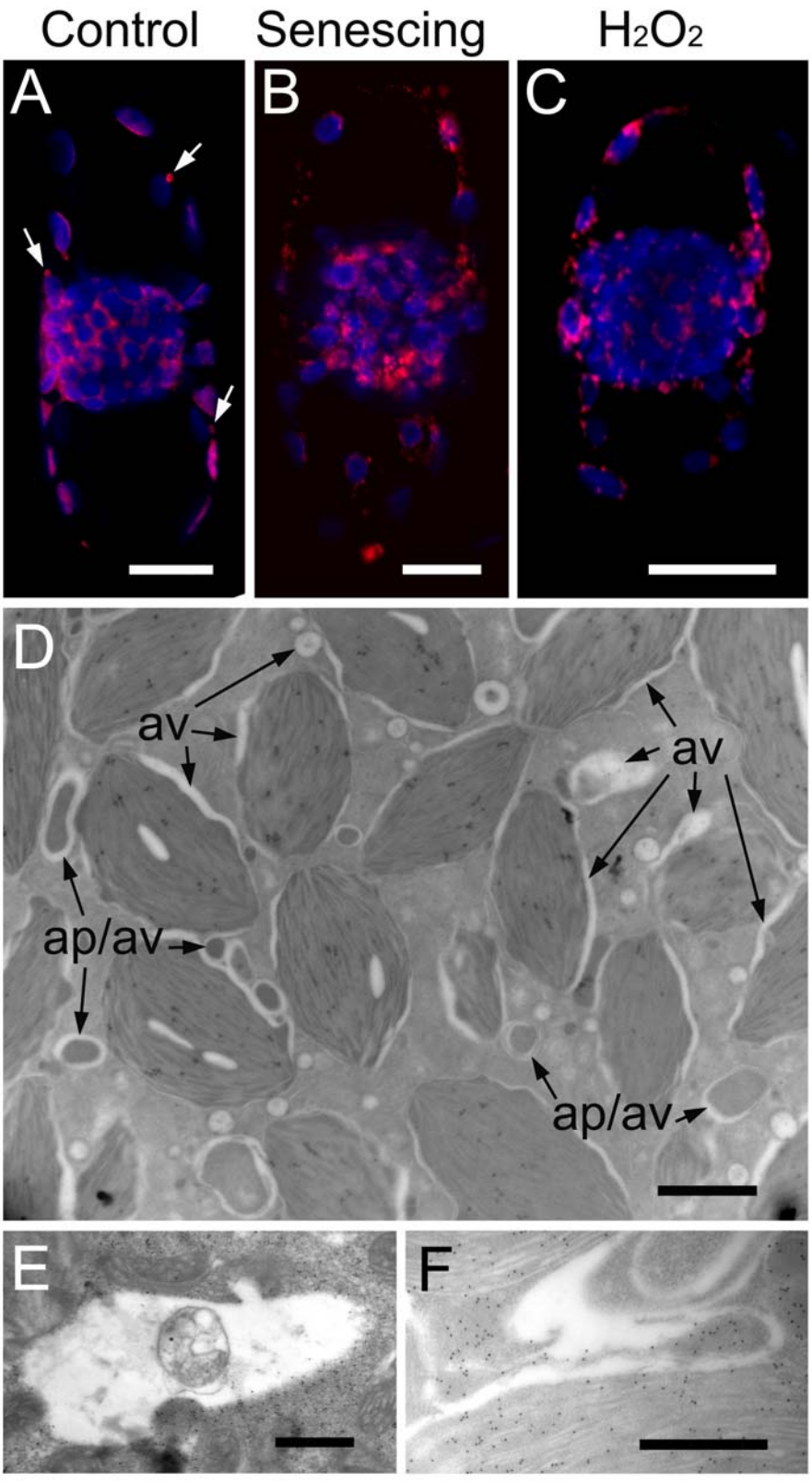
Control
Senescing
H2O2
A
B
C
D
av
av
ap/av
ap/av
E
F

Furthermore, partially degraded cytoplasmic components including mitochondria and stromules in autophagic vacuoles suggested that these newly formed vacuoles contained hydrolase activity (Fig. 5.6E, F).

5.3.4 Autophagosome and autophagic vacuole formation

Autophagosomes and autophagic vacuoles were often observed in close proximity to each other. To investigate the relationship between these autophagic organelles under stress condition (H_2O_2 treatment), the localization of an autophagosome marker protein ATG8 and an autophagic vacuole marker NR were analyzed. First, an ATG8-EGFP fusion construct was transiently expressed in *Arabidopsis* M protoplasts by the PEG -mediated transfection method (Yoo et al., 2007). In control non-stressed protoplasts, ATG8-EGFP was expressed in cytosol and nucleus whereas it accumulated in vesicles in H_2O_2-treated protoplasts (Fig. 5.7A, B). Protoplasts were stained with NR to visualize autophagic vacuoles. NR fluorescence was detected around chloroplasts in control protoplasts whereas it was localized as punctate structures in H_2O_2-treated protoplasts (Fig. 5.7C, D). When ATG8-EGFP expressing protoplasts were stained by NR to compare the localization of the fluorescent signals, the majority of the signals overlapped in cytosol of non-treated control protoplasts. On the other hand, some signals were independent of each other in H_2O_2-treated protoplasts although other signals were overlapped in punctate structures (Fig. 5.7E-L). The distinct signals of EGFP and NR indicated that the formation of autophagosomes and autophagic vacuoles derived from an independent path whereas the overlapped signals in punctate structures suggested the conversion from autophagosomes to autophagic vacuoles.

Figure 5.7 *In vivo* localization analyses of autophagosomes and autophagic vacuoles in *Arabidopsis* mesophyll protoplasts

Localization of autophagosomes and autophagic vacuoles are detected by using a transient expression of the EGFP-ATG8 plasmid construct driven by the 35S promoter and the fluorescent dye neutral red (NR) in *Arabidopsis* mesophyll protoplasts. Protoplasts were incubated in the presence (H_2O_2) or absence (Control) of 5 mM hydrogen peroxide for two hours. Images were taken by using confocal laser scanning microscopy. The EGFP-ATG8 fluorescent (green) and chlorophyll autofluorescent (blue) signals are shown **(A)**. The NR fluorescent (red) and chlorophyll autofluorescent (blue) signals are shown **(B)**. The EGFP-ATG8 expressing protoplasts were stained with NR. The EGFP-ATG8 (green), NR (red), and chlorophyll (blue) fluorescent signals, and merged images are shown **(C)**. Arrows indicate co-localization of EGFP-ATG8 and NR signals whereas arrowheads indicate that EGFP-ATG8 and NR signals are independently localized. Bars = 10 μm.

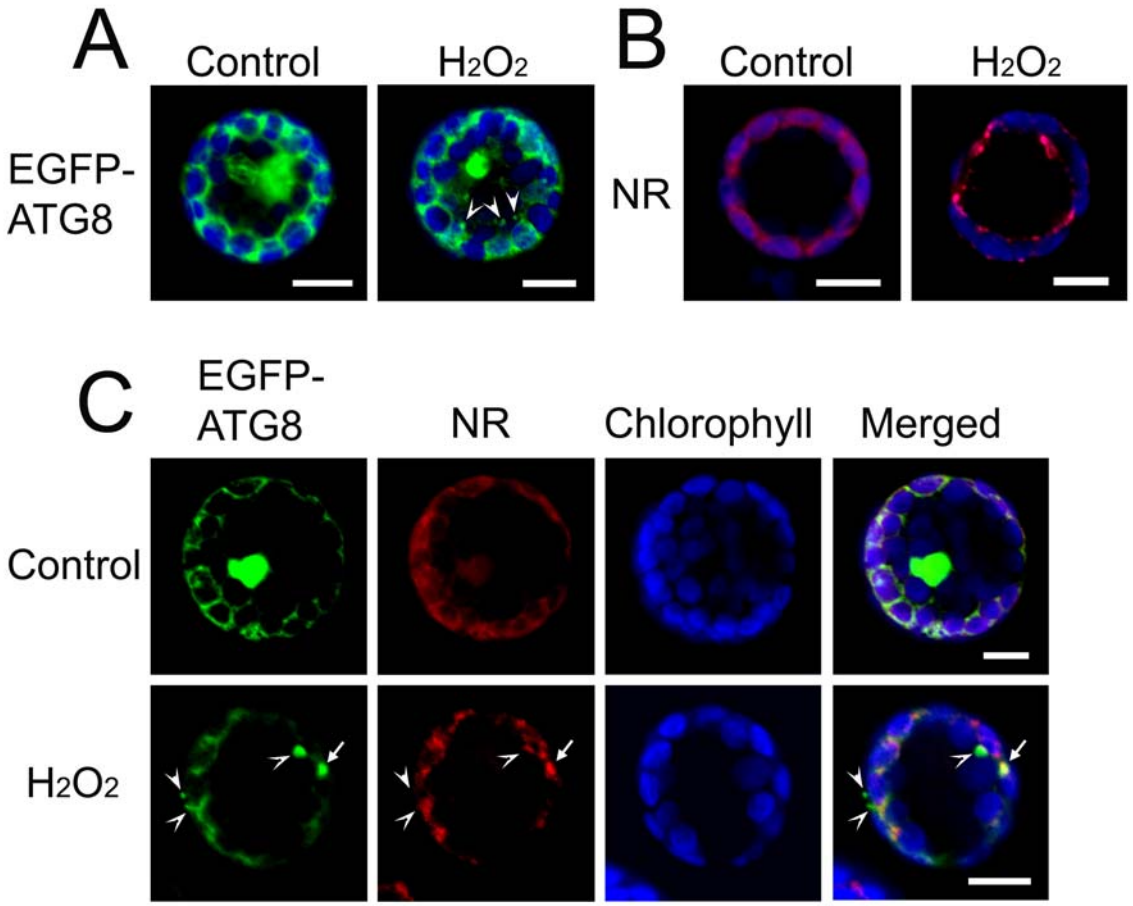
A
Control
H2O2
EGFP-
ATG8
B
Control
H2O2
NR
C
EGFP-
ATG8
NR
Chlorophyll
Merged
Control
H2O2

Moreover, electron micrographs of autophagosomes and autophagic vacuoles with different morphologies and contents further supported the potential autophagosome/autophagic vacuole transformation (Fig. 5.8).

5.3.5 Contribution of stromules in autophagy in *Arabidopsis* mesophyll cells

In this study, autophagosomes surrounded by chloroplast-derived stromules were observed in H_2O_2-treated chlorenchyma cells of mature *B. sinuspersici*. To determine whether this process is conserved in other plant species, *Arabidopsis* was used for EGFP expression and immunogold analyses. First, *Arabidopsis* protoplasts were transfected with RbcS-EGFP plasmid DNA and treated with H_2O_2 to observe chloroplast morphology. The RbcS-EGFP signal was observed mostly in chloroplasts of non-treated protoplasts, whereas it was also found in vesicles attached to or away from chlorophyll autofluorescent signals in H_2O_2-treated protoplasts (Fig. 5.9). Next, *Arabidopsis* leaves were treated with H_2O_2, immunolabelled with anti-RbcL antibody, and observed under TEM microscopy (Fig. 5.10). Cytoplasmic components including SCVs were observed in the central vacuole in H_2O_2-treated cells (Fig. 5.10A, B). Specific reactions to RbcL were also found in stromules encircling portions of cytoplasmic region. Some autophagosomes surrounded by stromules appeared to be releasing their contents into the central vacuole (Fig. 5.10C) while others appeared to contain degraded cellular components (Fig. 5.10D-F). The size of autophagosomes excluding stromules ranged between 0.4 – 1 μm in diameter. However, stromules sequestering larger area of the cytoplasm were occasionally observed (Fig. 5.10G). Chloroplast invagination of cytoplasmic materials was also observed in H_2O_2-treated *Arabidopsis* leaves (Fig 5.10H-J).

Figure 5.8 Transmission electron micrographs indicating potential transformation from autophagosome to autophagic vacuole

Cross-sections were prepared from mature leaves treated with hydrogen peroxide. TEM micrograph shows an autophagosome associated with stromules detected by specific RbcL reactivity (arrowheads) **(A)**. An autophagosome with thick membranes (arrows) is observed **(B)**. A possible intermediate form of autophagosome and autophagic vacuole is detected with partially degraded contents in the lumen although autophagosome membranes remain **(C)**. Another autophagic vacuole with partially degraded contents in the lumen is also observed but its membranes are not visible **(D)**. Ch, chloroplast; st, stromule. Bars = 200 nm in **(A)**, 500 nm in **(B-D)**.

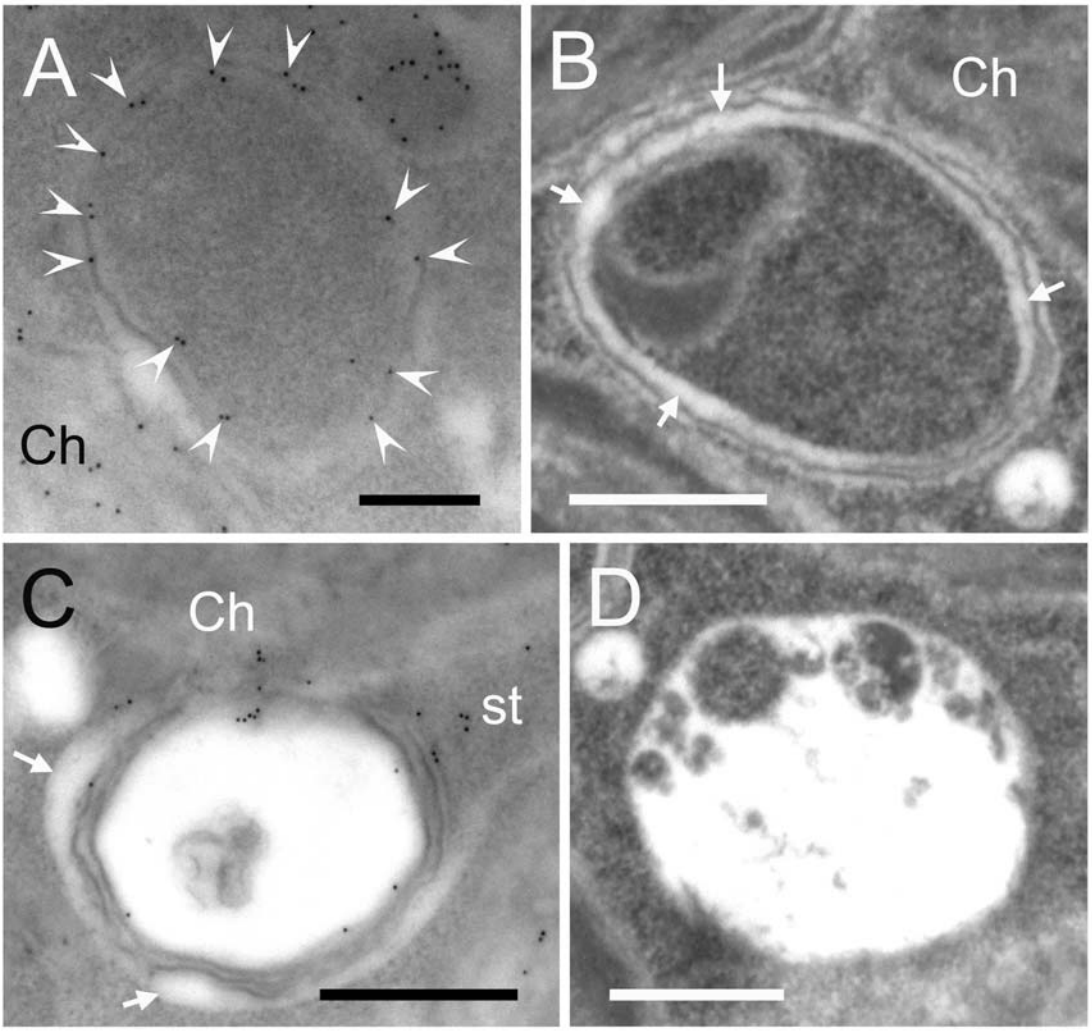
A
Ch
B
Ch
C
Ch
st
D

Figure 5.9 Change in the chloroplast morphology under oxidative stress in *Arabidopsis* mesophyll protoplasts

Arabidopsis mesophyll protoplasts were transfected with the stroma targeting RbcS-EGFP plasmid construct, incubated with (H_2O_2) or without (Control) 5 mM hydrogen peroxide for two hours, and observed using confocal laser scanning microscopy. Micrographs are the RbcS-EGFP fluorescent (green) and chlorophyll autofluorescent (blue) signals, and merged images. Arrowheads indicate the RbcS-EGFP fluorescent signals localized in vesicles. Bars = 10 μm.

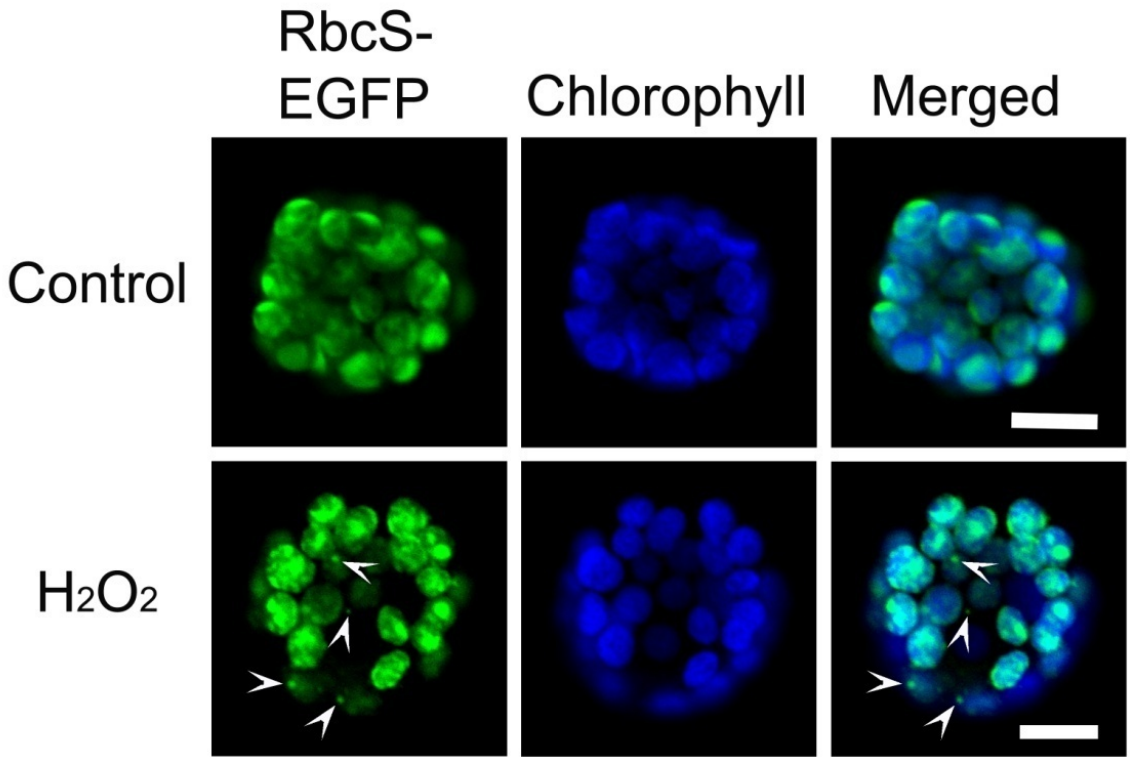
RbcS-
EGFP
Chlorophyll
Merged
Control
H2O2

Figure 5.10 Contribution of stromules in autophagosome and autophagic vacuole formation detected by immunolocalization of RbcL in H_2O_2-treated *Arabidopsis* leaves

Cross-sections were prepared from *Arabidopsis* leaves treated with 10 mM hydrogen peroxide for two hours. Sections were probed with RbcL antiserum and then gold-conjugated secondary antibody. Images are transmission electron micrographs showing specific reaction of the RbcL antibody. Autophagic bodies (arrows) are detected in the central vacuole in close proximity to the chloroplastic cavity (arrowhead) **(A)**. A stroma-containing vesicle (SCV; arrow) localized in the central vacuole is also found near the chloroplastic cavity (arrowhead) **(B)**. Autophagic bodies (arrows) and ring-shaped stromules (arrowheads) are shown. The ring-shaped stromules are either attached to or away from the chloroplast **(C)**. Stromules surround multiple cytoplasmic regions, and possibly generate autophagic vacuoles **(D)**. Stromules sequester a portion of cytoplasm, forming an autophagosome and an autophagic vacuole **(E)**. Autophagic vacuole is surrounded by stromules **(F)**. A stromule extending from a chloroplast is sequestering a large area of cytoplasm **(G)**. Arrows indicate specific reactions to RbcL in the stromule. A portion of cytoplasm is observed in the chloroplast stroma, and its partial degradation is also detected **(H-J)**. ab, autophagic body; Ch, chloroplast; cv, central vacuole; av, autophagic vacuole; st, stromule; ap, autophagosome. Bars = 500 nm in **(A-E, G and I)**, 200 nm in **(H, J)**, 100 nm in **(F)**.

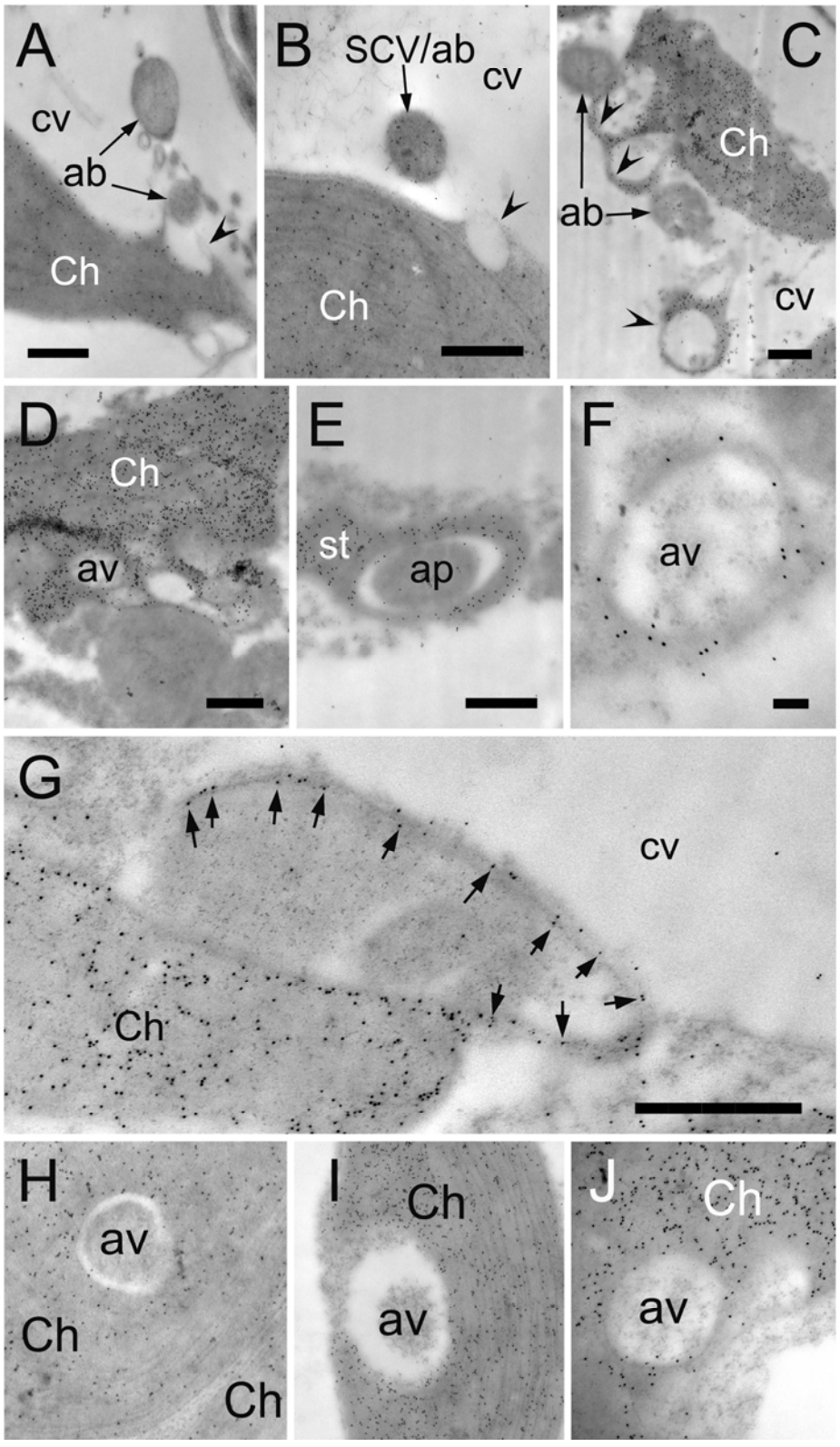
A
cv
ab
Ch
B
SCV/ab
cv
Ch
C
Ch
ab
cv
D
Ch
av
E
st
ap
F
av
G
cv
Ch
H
av
Ch
Ch
I
Ch
av
J
Ch
av

The engulfed contents appeared to be degraded in autophagic vacuoles formed within chloroplasts. These results indicated that stromules and chloroplasts contributed to autophagy in H_2O_2-treated M cells of *Arabidopsis* as well as in those of *B. sinuspersici*.

5.3 Discussion

Previous studies suggest that the degradation of chloroplastic proteins occurs at least partially through autophagic organelles (Chiba et al., 2003; Otegui et al., 2005; Ishida et al., 2008; Martinez et al., 2008; Prins et al., 2008; Wada et al., 2009; Izumi et al., 2010). Although some of the autophagic organelles such as autophagosomes and RCBs have been observed to be surrounded by isolation membranes, the identity of the membrane origin remained undetermined in plants. Here, I investigate the localization of stromal proteins in leaf M cells under H_2O_2-induced stress. My data suggest the involvement of stromules with autophagosome formation.

5.3.1 Participation of stromules in autophagosome formation

Under oxidative stress, numerous stromules and SVCs were induced in chlorenchyma cells of *B. sinuspersici* (Fig. 5.2D-F). In this study, the size of stromules was 0.1 – 0.3 μm in diameter which is somewhat narrower than typical stromules with diameter from 0.3 to 0.8 μm as determined in other studies (Gray et al., 2001; Hanson and Sattarzadeh, 2011). In addition, stromules ranged between 30 - 50 nm in diameter were occasionally observed (Fig. 5.3A-D). I observed the labelling for stromal proteins in a 10 – 20 nm wide gap between membranes with white appearance indicating stromal portion of stromules. Thin stromules of diameter less than

100 nm have also been reported in tomato and *Arabidopsis* (Pyke and Howells, 2002; Holzinger et al., 2008). My immuno-EM analysis revealed thin stromules surrounding portions of cytoplasmic components and forming autophagosomes often associated with chloroplasts in both *B. sinuspersici* and *Arabidopsis* (Fig. 5.3E-G, 5.10G). Ishida et al. (2008) reported that a strong GFP-ATG8 signal in chloroplast protrusions co-localizes with stromal DsRed signals in *Arabidopsis* leaves which correlates with my observation. Moreover, similar observations on the enclosure of intracellular components by stromules have been made in previous studies, some performed more than 40 years ago, in tobacco, tomato, *Deschampsia antarctica*, and green algae suggesting that the participation of stromules in autophagy is conserved in photosynthetic organisms (Weier and Thomson, 1962; Shalla, 1964; Park et al., 1999; Gielwanowska et al., 2005).

The stromule-bounded autophagosome is a multilamellar structure composed of a central body part containing cytoplasmic components and a stromal part between membranes of a stromule. Chiba et al. (2003) demonstrated that RCBs having double membranes are further surrounded by other membranes which is also consistent with our data showing that SCVs were confined by stromules (Fig. 5.5B). Furthermore, autophagosomes having more than two apparent membranes were often found in *B. sinuspersici* indicating that multilamellar autophagosomes might be a common characteristic in photosynthetic cells (Fig. 5.1E, F, 5.4C, D).

5.3.2 Organelle degradation via autophagy

Autophagy is generally defined as a non-selective process of degrading cellular materials. However, selective autophagy digesting certain organelles have been described and named based on the organelle subjected to degradation: for instance, pexophagy for peroxisomes and

mitophagy for mitochondria (Dunn et al., 2005; Sakai et al., 2006; Youle and Narendra, 2011). So far, only one possible selective autophagy has been reported in plants (Izumi et al., 2010). The authors described that a large number of RCBs is detected in *Arabidopsis* starchless mutants while fewere RCBs are observed under carbon rich conditions and in the starch-excess mutants. Whole chloroplast degradation via autophagy has also been observed in senescence-induced *Arabidopsis* leaves (Wada et al., 2009). However, the degradation pathways for peroxisomes and mitochondria have not been described in plants. The results from this study demonstrated that autophagosomes formed in response to H_2O_2 treatment contained various intracellular components including peroxisomes, mitochondria, SVCs, and cytosol (Fig. 5.1E, 5.5). These data suggested that oxidative stress induced autophagy is responsible for the non-selective degradation of cytoplasmic components, and also indicated that the degradation of peroxisomes and mitochondria occurred, at least partially, via the autophagosome mediated pathway in plants. In addition, SCVs were also found in non-stress-treated cells of *B. sinuspersici* (Fig. 5.2C). This is in agreement with the findings provided by Prins et al. (2008) describing that Rubisco containing vesicles are observed in mature tobacco leaves under stress and optimal conditions as well as in young leaves. Whether this pathway is specifically regulated by nutrient conditions remained to be determined in this study. However, the chloroplastic protein degradation through autophagic pathway appears to occur under normal growth conditions. The differential accumulation of photosynthetic enzymes could be partially regulated by the turnover of stromal proteins through the SCV pathway in *B. sinuspersici*.

5.3.3 Biogenesis of autophagosome and autophagic vacuole

In mammals, an autophagosome fuses with a lysosome forming an autolysosome where the degradation of sequestered contents takes place (Mizushima et al., 2002). In yeast and plants, vacuoles are analogous to animal lysosomes having the lytic activity. In plants, most of the volume of the mature cell is occupied by a large central vacuole which has multiple functions, including maintenance of turgor pressure and storage of metabolites as well as digestion of cellular constituents (Marty, 1999). In addition to a central vacuole, autophagic vacuoles have been observed in various plant tissues and cells (Swanson et al., 1998; Moriyasu et al., 2003; Gielwanowska et al., 2005; Otegui et al., 2005, Rose et al., 2006; Yano et al., 2007). In *B. sinuspersici* chlorenchyma cells, the CCC is composed of cytosol and numerous organelles which are packed together to form a ball-like structure surrounded by a central vacuole (Akhani et al., 2005; Chuong et al., 2006; Park et al., 2009). When an autophagosome is formed in the outer region of the CCC, it appeared to be easily transported to the central vacuole (Fig. 5.5A). On the other hand, an autophagosome formed deep inside of the CCC seemed to be engulfed by or transform into autophagic vacuoles (Fig. 5.5C). In the PCC, autophagosomes usually associated with chloroplasts (Fig. 5,4C-D). *In vivo* localization analysis of autophagic vacuoles showed the high level of NR accumulation in these autophagosomes, suggesting that the transformation of autophagosomes to autophagic vacuoles (arrows in Fig. 5.6A). Moreover, the presence of autophagic vacuoles in non-stressed *B. sinuspersici* cells indicated the occurrence of autophagy in regular growth conditions.

Findings from this study suggest two autophagic pathways in the digestion of cell materials: one involved in the transportation of cellular materials to the lumen of the central vacuole while the other utilized autophagic vacuoles synthesized *de novo*. However, it is still

possible that autophagic vacuoles could also participate in the first pathway. After the formation of an autophagosome near the central vacuole, autophagic vacuoles generated in close proximity to the autophagosome could fuse with the central vacuole making the autophagosome protruding into the vacuolar lumen to facilitate a subsequent release (Fig. 5.5A, B, D). The second pathway appears to involve the transformation of an autophagosome into an autophagic vacuole: first, stromules sequester cytoplasmic materials generating an autophagosome (Fig. 5.8A); second, autophagosome membranes start deteriorating (Fig. 5.8B); third, the cellular materials are digested in the lumen of the autophagic vacuole (Fig. 5.8C); finally, all contents including internal membranes are degraded leaving only one boundary membrane (Fig. 5.8D). The co-localization study of EGFP-ATG8 and NR signals in *Arabidopsis* protoplasts also suggested that the two types of autophagic organelles partially overlapped in punctate structures under H_2O_2-treated condition (Fig. 5.7C). Interestingly, similar events in the autophagic vacuole formation have been observed in non-photosynthetic cells including *Arabidopsis* suspension-cultured cells (Rose et al., 2006) and root meristematic cells in tobacco (Zheng and Staehelin, 2011). Rose et al. (2006) observed various forms of autophagic vacuoles in dark-grown cells in sucrose-free media, and classified them into three sequential steps. Zheng and Staehelin (2011) described that the membrane extension originating from the protein storage vacuole encloses an area of cytoplasm forming multilamellar autophagosomes in the inner cortex and the vascular cylinder cells of a tobacco root. The authors also mentioned that the luminal space of the extensive membrane differentiates into pre-lytic vacuoles by ‘reinflation’ which expanded and engulfed an entire autophagosome, and eventually the whole domain transformed into a lytic vacuole. The similarities in various cell types in different conditions suggest the plasticity of the autophagosome and autophagic vacuole biogenesis, with supplied membranes originating from different organelles.

The generation of autophagic vacuoles has been indicated to be independent of, at least, early steps of macroautophagy (Otegui et al., 2005; Yano et al., 2007). Autophagic vacuoles were electron-translucent, and they occasionally contained partially degraded cellular materials (Fig. 5.6E, F). The generation of autophagic vacuole appeared to initiate along with chloroplast envelopes including those of stromules (Fig. 5.1E, G, 5.2D, 5.6D). The contribution of chloroplast envelopes without an extension in the autophagic vacuole formation indicated that the autophagosome formation is not essential for the generation of autophagic vacuoles. This idea is further supported by chloroplast invaginations of cellular components followed by the on-site generation of autophagic vacuoles without forming autophagosomes (Fig. 5.10H-J).

5.3.4 *B. sinuspersici* as a model plant in autophagy research

Since the discovery of the three terrestrial single-cell C_4 species, a number of studies have focused on understanding how this novel photosynthetic system develops (Akhani et al., 2005; Chuong et al., 2006; Lara et al., 2008; Park et al., 2009; Offermann et al., 2011). However, as shown here, *B. sinuspersici* also serves as a suitable model species for the autophagy study in M cells. Unlike mature photosynthetic cells in typical plant species, where most of the cellular space is occupied by a large central vacuole and the cytoplasm is limited to the periphery of the cell, *B. sinuspersici* chlorenchyma cells contain a large cytoplasmic area in the CCC (Fig. 5.1B, 5.6B; Chuong et al., 2006; Lara et al., 2008; Park et al., 2009). This is advantageous, especially, when ultra-thin sections are made for the TEM analysis. In addition, the compartmentation of organelles can be exploited for studying the selective degradation of particular organelles. For instance, mitochondria are exclusively located in the CCC whereas peroxisomes are found in both compartments (Fig. 5.1B, 5.5A, D; Chapter 3 in this thesis). The recently established

transient gene expression protocol in *B. sinuspersici* chlorenchyma protoplasts showed a comparable efficiency to those previously reported for *Arabidopsis* and rice (Chen et al., 2006; Yoo et al., 2007; Lung et al., 2011). Although most genes involved in the process remained to be identified, this protocol would make it feasible to analyze the localization of autophagy-related proteins such as ATGs.

5.3.5 The new function of stromules in autophagy

I have provided data implicating an important role of stromules in photosynthetic cells in the generation of autophagosome by sequestering other cellular components including mitochondria, peroxisomes and cytosol. The interactions between stromules and other organells such as nuclei, mitochondria and peroxisomes have been reported in previous studies (Kwok and Hanson, 2004b; Sage and Sage, 2009). Recently, the close association of stromules and ER in leaf epidermal cells of *Nicotiana benthamiana* has been documented by Schattat et al. (2011). The authors described that the movement of extending stromules is led by an ER channel contacting only at certain points where possibly lipids and proteins are exchanged. Together with my data, it is possible to speculate that ER participates in the autophagosome formation by guiding membrane extensions from various organelles to sequester cytoplasmic compartments and by supplying lipids to the extensions. Whether plastids in non-photosynthetic cells are involved in autophagosome biogenesis needs to be determined in future study. Nevertheless, plants seemed to have established a novel strategy to generate autophagosomes by using chloroplast envelopes as a source of membrane via stromules.

5.3.6 Conclusions

In this Chapter, the localization of stromal proteins such as RbcL and PPDK was examined in leaf mesophyll cells under oxidative stress. The distribution of autophagic organelles was also investigated using GFP-ATG8 and NR. The presence of SCVs and autophagic vacuoles associated with PCC chloroplasts in non-stress-treated *B. sinuspersici* chlorenchyma cells suggest that the turnover of stromal proteins occurs under normal growth conditions. Electron micrographs implied stromule-like structures surrounding portions of cytoplasmic area, possibly generating autophagosomes. In addition, the preferential accumulation of NR around chloroplasts together with TEM observations suggested a potential relationship between chloroplast envelopes and autophagic vacuole formation. I believe that these findings offer a new perspective on autophagy in plants.

CHAPTER 6: SUMMARY AND FUTURE DIRECTIONS

6.1 Summary

B. sinuspersici performs single-cell C_4 photosynthesis by compartmentation of organelles and photosynthetic enzymes. In this thesis, experiments were conducted in an attempt to understand the regulation of differential enzyme distribution and the function of stromules.

Chapter 3 describes the distribution of photosynthetic enzymes at the TEM level and that of their transcripts in dimorphic chloroplasts in developing leaves of *B. sinuspersici*. In mature leaves, RbcL accumulated approximately 20-fold more in the CCC than PCC chloroplasts, whereas PPDK accumulated approximately 2- and 6-fold more in the PCC chloroplasts than in the CCCO and CCCI chloroplasts, respectively, under our growth conditions. This enzyme distribution was completed during the late stage of leaf development, from intermature (1.0 – 1.2 cm in leaf length) to mature (>2 cm) stages. This suggests that the transition from C_3 to C_4 photosynthesis occurs in these late stages under our growth conditions. The analysis of transcript distribution and quantification revealed that the differential *rbcL* accumulation in the two types of chloroplasts appeared to be regulated by transcription and/or mRNA stability. In addition to these findings, two useful protocols for studies in *B. sinuspersici*, PEG-mediated protoplast transfection and dimorphic chloroplast isolation method were empirically optimized. In the former protocol, transfection efficiency was improved from less than 5% to approximately 84%. In the latter protocol, significant contamination of the CCC chloroplasts in 'isolated' PCC chloroplasts was successfully reduced.

In Chapter 4, secondary structures of *rbcL* transcripts were predicted using bioinformatic tools. Transcripts of *rbcL* have been suggested to be processed to different forms: the intermediate and mature form (Reinbothe et al., 1993; Serino and Maliga, 1998; McCormac et al., 2001). The mature form of *rbcL* mRNA is required for the efficient translation while the intermediate form may be unstable or untranslatable. One of the stem-loop structures in *rbcL* 5'UTR was predicted to form in the mature form, but it was disrupted in the intermediate form. It is possible that *rbcL* transcripts in the PCC chloroplasts are preferentially processed to the intermediate form, and therefore the stem-loop structure is disrupted, rendering *rbcL* transcripts unstable or untranslatable. This hypothesis needs to be verified experimentally in the future.

Chapter 5 describes the participation of stromules in autophagosome biogenesis. The identification of the membrane origin has long been unclear since the discovery of autophagy. However, recent studies suggest the involvement of multiple organelles such as ER, mitochondria, and plasma membranes in the formation of autophagosome (Axe et al., 2008; Hailey et al., 2010; Ravikumar et al., 2010). My immunogold analysis using RbcL and PPDK antibodies showed narrow stromules with diameter ranging from 30 to 50 nm sequestering a portion of cytoplasm in *B. sinuspersici* chlorenchyma cells in response to H_2O_2 treatments. The autophagosomes enclosed by stromule-like structures were also found in *Arabidopsis* M cells implying that the contribution of stromules in autophagosome formation is a general phenomenon in chloroplast-containing cells in plants. Moreover, relationships between autophagosomes and autophagic vacuoles were shown using fluorescent markers for autophagosome and autophagic vacuole, ATG8-GFP and NR, respectively. This analysis and TEM micrographs of H_2O_2-treated chlorenchyma cells suggest that the generation of these two autophagic organelles was independent but an autophagosome could transform to an autophagic vacuole. The participation of chloroplast envelopes including those on stromules in the

autophagic vacuole formation was also indicated. Immunolocalization of RbcL and PPDK also showed that these proteins were confined in SCVs, which appeared to originate from chloroplasts and the contens released to the vacuolar lumen. The presence of SCVs in both H_2O_2-treated and control leaves suggests that the degradation of stromal proteins through SCVs is a housekeeping process.

6.2 Future work

In Chapter 3, the distribution of photosynthetic proteins and transcripts in the single-cell C_4 species *B. sinuspersici* was described. The distribution of RbcL proteins appeared to be regulated predominantly at the transcriptional and/or mRNA stability levels. To further determine the level of regulation, chloroplast run-on transcription assays could be employed using isolated dimorphic chloroplasts. Proteins associated with the photosystem, especially PsaB and PsbA appeared to be regulated at translational and/or post-translational levels, and this could be examined using *in vitro* translation systems with purified CCC and PCC chloroplasts. For example, isolated chloroplasts are mixed with amino acids, including radio-labeled methionine to detect newly synthesized polypeptides (pulse labelling). Unlabeled methionine is then applied to the mixture (chase labelling). Proteins are extracted from the membrane fraction of chloroplasts and separated on an acrylamide gel. Intensities of proteins from pulse-labeled chloroplasts would represent translational rates while those from chase-labeled chloroplasts would exhibit post-translational turnover rates. It is hypothesized that PsaB could be translated at higher rates in the PCC than in CCC chloroplasts or degraded faster in the CCC than in PCC chloroplasts, whereas PsbA might be controlled the opposite way. In addition to chloroplast-encoded proteins, nuclear-encoded proteins such as PPDK and RbcS are differentially accumulated. However,

transient expression studies using EGFP fused to the transit peptide sequence of PPDK or RbcS showed similar accumulation of reporter EGFP proteins in both types of chloroplasts indicating there may be no preferential import of these proteins. However, in order to accurately determine the EGFP-fusion proteins accumulation in each chloroplast type, native promoters need to be used in place of the constitutive 35S promoter, which could lead to mislocalization artifacts (Bleckmann et al., 2010). Our newly developed protocols for the protoplast transfection and the ease of dimorphic chloroplast isolation would facilitate other biochemical and molecular experiments in *B. sinuspersici*. The only problem associated with the dimorphic chloroplast isolation technique is that the yield of each purified chloroplast per leaf is very low. This procedure might require further optimization to obtain large amount of RNAs and proteins required for large-scale analyses such as microarray and proteomics. As discussed in Chapter 4, the role of the secondary structures of *rbcL* 5'UTR predicted by bioinformatic tools can be tested by using *in vitro* run-on transcription and translation systems with chloroplasts transformed with vector plasmids containing different length of 5'UTR. However, a reliable protocol for the chloroplast gene transformation in *B. sinuspersici* has yet to be developed.

A potential function for stromules as a membrane source of autophagosomes in leaf M cells was described in Chapter 5. Stromules in non-photosynthetic cells could have a similar function. For instance, stroma-targeting GFP shows that the fluorescence signal in bead-like structures appear to be away from the main plastid body in trichomes of tomato (Pyke and Howells, 2002). Immunogold studies using suitable antibodies would reveal whether stromules participate in autophagosome biogenesis in non-green cells. The conversion from autophagosomes to autophagic vacuoles could be further analyzed by a time-course *in vivo* fluorescent experiments using markers specific for these two autophagic organelles. However, I found that NR appeared to be toxic to cells and altered the localization of other fluorescent

markers such as EGFP-ATG8. Although this issue was resolved by the immediate fixation of cells after the NR staining, an alternative non-toxic marker for autophagic vacuoles may be invaluable for *in vivo* experiments involving live-cell imaging. The biogenesis of autophagic vacuoles is another topic of great interest. My results indicated the contribution of chloroplast envelopes in autophagic vacuole formation in leaf M cells. The process could be monitored by time-course experiments as described above. Unfortunately, a suitable marker for the autophagic vacuole in M cells has yet to be identified. In roots, α-tonoplast intrinsic protein (α-TIP) has been found to be a specific marker of autophagic vacuoles (Moriyasu et al., 2003). Although I have tested the α-TIP antibody in H_2O_2-treated *Arabidopsis* by immunoblot analysis, no detectable signal was observed suggesting little or no expression of this protein in leaves. On the other hand, the labelling for γ-TIP is heavily bound to the tonoplast of central vacuole but did not label the SAV in leaf (Otegui et al., 2005), which appears to have anatomical features similar to those of the autophagic vacuole observed in this thesis. The identification of a specific marker for autophagic vacuoles in M cells would provide information on the mechanisms involved in their formation. The degradation of photosynthetic proteins via SCVs could contribute to the enzyme compartmentation in single-cell C_4 photosynthesis. The careful quantification of each of these proteins in SCVs in each compartment by using immunolocalization would validate this hypothesis.

6.3 Concluding remarks

The data obtained in this thesis indicate that:

1. RbcL accumulates over 20-fold more in the CCC chloroplasts than in the PCC chloroplasts, whereas PPDK shows a concentration gradient such that it is high in the PCC chloroplasts and low in the CCCI chloroplasts.

2. The distribution of RbcL in mature chlorenchyma cells is at least partially regulated at the transcriptional and/or mRNA stability level.

3. A stem-loop structure is predicted to form at 5'UTR of the mature *rbcL* mRNA but it is disrupted in the intermediate *rbcL* mRNA; this structural change might play a role in the differential distribution of *rbcL* transcripts.

4. Stromules appear to participate in autophagosome biogenesis by supplying the membranes.

5. Formation of autophagosomes and autophagic vacuoles is likely independent events, however, autophagosomes might be able to transform to autophagic vacuoles.

6. Chloroplast envelopes may contribute in autophagic vacuole generation.

7. *B. sinuspersici* can serve as a model species suitable not only for examining C_4 photosynthetic gene expression in a single cell but also for the development of autophagy in M cells.

8. The differential accumulation of photosynthetic enzymes including Rubisco and PPDK in dimorphic chloroplasts in *B. sinuspersici* could be partially controlled by the post-translational regulation through the protein turnover via SCVs.

REFERENCES

Adam, Z., Charuvi, D., Tsabari, O, Knopf, R.R. and Reich, Z. (2010). Biogenesis of thylakoid networks in angiosperms: knowns and unknowns. *Plant Mol. Biol. 76, 221-234*.

Akhani, H., Barroca, J., Koteeva, N., Voznesenskaya, E., Franceschi, V., Edwards, G., Ghaffari, S.M. and Ziegler H. (2005). *Bienertia sinuspersici* (Chenopodiaceae): A new species from southwest Asia and discovery of a third terrestrial C_4 plant without Kranz anatomy. *Systematic Bot. 30, 290-301*.

Anderson, J.M. (1999). Insights into the consequences of grana stacking of thylakoid membranes in vascular plants: a personal perspective. *Aust. J. Plant Physiol. 26, 625-639*.

Andersson, B. and Anderson, J.M. (1980). Lateral heterogeneity in the distribution of chlorophyll-protein complexes of the thylakoid membranes of spinach chloroplasts. *Biochim. Biophys. Acta 593, 427-440*.

Andersson, I. (2008). Catalysis and regulation in Rubisco. *J. Exp. Bot. 59, 1555-1568*.

Arimura, S., Hirai, A. and Tsutsumi, N. (2001). Numerous and highly developed tubular projections from plastids observed in Tobacco epidermal cells. *Plant Sci. 160, 449-454*.

Aubert, S., Gout, E., Bligny, R., Marty-Mazars, D., Barrieu, F., Alabouvette, J., Marty, F. and Douce, R. (1996). Ultrastructral and biochemical characterization of autophagy in higher plant cells subjected to carbon deprivation: control by the supply of mitochondria with respiratory substrates. *J. Cell Biol. 133, 1251-1263*.

Axe, E.L., Walker, S.A., Manifava, M., Chandra, P., Roderick, H.L., Habermann, A., Griffiths, G. and Ktistakis, N.T. (2008). Autophagosome formation from membrane compartments enriched in phosphatidylinositol 3-phosphate and dynamically connected to the endoplasmic reticulum. *J. Cell Biol. 182, 685-701*.

Bassham, D.C. (2007). Plant autophagy – more than a starvation response. *Curr. Opin. Plant Biol. 10, 587-593*.

Bassham, D.C. (2009). Function and regulation of macroautophagy in plants. *Biochim. Biophys. Acta 1793, 1397-1403*.

Bassham, D.C., Laporte, M., Marty, F., Moriyasu, Y., Ohsumi, Y., Olsen, L.J. and Yoshimoto, K. (2006). Autophagy in development and stress responses of plants. *Autophagy 2, 2-11*.

Bleckmann, A., Weidtkamp-Peters, S., Seidel, C.A.M. and Simon, R. (2010) Stem ccell signalling in Arabidopsis requires CRN to localize CLV_2 to the plasma membrane. *Plant Physiol. 152, 166-176*.

Bräutigam, A., Kajala, K., Wullenweber, J., Sommer, M., Gagneul, D., Weber, K.L., Carr, K.M., Gowik, U., Maß, J., Lercher, M.J., Westhoff, P., Hibberd, J.M. and Weber, A.P.M. (2011). An mRNA blueprint for C_4 photosynthesis derived from comparative transcriptomics of closely related C_3 and C_4 species. *Plant Physiol. 155, 142-156*.

Brooks, A. And Farquhar, G.D. (1985). Effect of temperature on the CO2/O2 specificity of ribulose-1,5-bisphosphate carboxylase/oxygenase and the rate of respiration in the light. *Planta 165, 397-406*.

Brown, N.J., Parsley, K. and Hibberd, J.M. (2005). The future of C_4 research – maize, *Flaveria* or *Cleome*? *Trends Plant Sci. 10, 215-219*.

Chen, S., Tao, L., Zeng, L., Vega-Sanchez, M., Umemura, K. and Wang, G. (2006). A highly efficient transient protoplast system for analyzing defence gene expression and protein-protein interactions in rice. *Mol. Plant Pathol. 7, 417–427*.

Chiba, A., Ishida, H., Nishizawa, N.K., Makino, A. and Mae, T. (2003). Exclusion of Ribulose-1,5-bisphosphate carboxylase/oxygenase from chloroplasts by specific bodies in naturally senescing leaves of wheat. *Plant Cell Physiol. 44, 914-921*.

Chung S.M., Frankman E.L. and Tzfira T. (2005). A versatile vector system for multiple gene expression in plants. *Trends Plant Sci. 10, 357-361*.

Chuong, S.D.X., Franceschi, V.R. and Edwards, G.E. (2006). The cytoskelton maintains organelle partitioning required for single-cell C_4 photosynthesis in Chenopodiaceae species. *Plant Cell. 18, 2207-2223*.

Cohen, I., Knopf, J.A., Irihimovitch, V. and Shapira, M. (2005). A proposed mechanism for the inhibitory effects of oxidative stress on Rubisco assembly and and its subunit expression. *Plant Physiol. 137, 738-746*.

Danker, T., Dreesen, B., Offermann, S., Horst, I. and Peterhansel, C. (2008). Developmental information but not promoter activity controls the methylation state of histone H3 lysine 4 on two photosynthetic genes in maize. *Plant J*. 53, 465–74.

del Rio, L.A., Sandalio, L.M., Corpas, F.J., Palma, J.M. and Barroso, J.B. (2006). Reactive oxygen species and reactive nitrogen species in peroxisomes. Production, scavenging, and role in cell signalling. *Plant Physiol. 141, 330-335*.

Demmig-Adams, B. and Adams III, W.W. (1992). Photoprotection and other responses of plants to high light stress. *Annu. Rev. Physiol. Plant Mol. Biol. 43, 599-626*.

Dengler, N.G., Dengler, R.E., Donnelly, P.M. and Filosa, M.F. (1995). Expression of the C_4 pattern of photosynthetic enzyme accumulation during leaf development in *Atriplex rosea* (Chenopodiaceae). *Am. J. Bot. 82, 318-327.*

Dengler, N.G. and Taylor, W.C. (2000). Developmental aspects of C_4 photosynthesis. In *Photosynthesis: Physiology and metabolism*., eds. Leegood, R.C., Sharkey, T.D. and von Caemmerer, S.: pp 471-495. The Netherlands: Kluwer.

DeRocher, E.J., Quigley, F., Mache, R. and Bohnert, H.J. The six genes of the Rubisco small subunit multigene family from *Mesembryanthemum crystallinum*, a facultative CAM plant. *Mol. Gen. Genet. 239, 450-462*.

Desimone, M., Henke, A. and Wagner, E. (1996). Oxidative stress induces partial degradation of the large subunint of ribulose-1,5-bisphosphate carboxylase/oxygenase in isolated chloroplasts of barley. *Plant Physiol. 111, 789-796*.

Doelling, J.H., Walker, J.M., Friedman, E.M., Thompson, A.R. and Vierstra, R.D. (2002). The APG8/12-activating enzyme APG7 is required for proper nutrient recycling and senescence in *Arabidopsis thaliana*. *J. Biol. Chem. 277, 33105-33114*.

Doubnerová, V. and Ryšlavá, H. (2011). What can enzymes of C_4 photosynthesis do for C_3 plants under stress? *Plant Sci. 180, 575-583*.

Duan, J., Wainwright, M.S., Comeron, J.M., Saito, N., Sanders, A.R., Gelernter, J. and Gejman, P.V. (2003). Synonymous mutations in the human *dopamine receptor D2 (DRD2)* affect mRNA stability and synthesis of the receptor. *Hum. Mol. Genet. 12, 205-216*.

Dunn, W.A. Jr., Cregg, J.M., Kiel, J.A., van der Klei, I.J., Oku, M., Sakai, Y., Sibirny, A.A., Stasyk, O.V. and Veenhuis, M. (2005). Pexophagy: the selective autophagy of peroxisomes. *Autophagy 1, 75-83*.

Edgar, R. C. (2004). MUSCLE: multiple sequence alignment with high accuracy and high throughput. *Nucl. Acid Res. 32, 1792-1797*.

Edwards, G.E., Franceschi, V.R., Ku, M.S.B., Voznesenskaya, E.V., Pyankov, V.I. and Andreo, C.S. (2001) Compartmentation of photosynthesis in cells and tissues of C_4 plants. *J. Exp. Bot. 52, 577-590*.

Edwards, G.E., Franceschi, V.R. and Voznesenskaya, E.V. (2004). Single-cell C4 photosynthesis versus the dual-cell (Kranz) paradigm. *Annu. Rev. Plant Biol. 55, 173-196*.

Edwards, G.E., Lee, S.S., Chen, T.M. and Black, C.C. (1970). Carboxylation reactions and photosynthesis of carbon conpounds in isolated mesophyll and bundle sheath cells of *Digitaria sanguinalis* (L.) Scop. *Biochem. Biophys. Res. Commun. 39, 389-395*.

Emanuelsson, O., Nielsen, H. and von Hijne, G. (1999). ChloroP, a neural network-based method for predicting chloroplast transit peptides and their cleavage sites. *Protein Sci. 8, 978-984*.

Freitag, H. and Stichler, W. (2000). A remarkable new leaf type with unusual photosynthetic tissue in a central Asiatic genus of Chenopodiacea. *Plant Biol. 2, 154-160.*

Freitag, H. and Stichler, W. (2002). *Bienertia cycloptera* Bunge ex Boiss., Chenopodiaceae, another C_4 plant without Kranz tissues. *Plant Biol. 4, 121-132*.

Friso, G., Majeran, W., Huang, M., Sun, Q. and Wijk, K.J. (2010). Reconstruction of metabolic pathways, protein expression, and homeostasis machineries across maize bundle sheath and mesophyll chloroplast: large-scale quantitative proteomics using the first maize genome assembly. Plant Physiol. 152, 1219-1250.

Fukayama, H., Tsuchida, H., Agarie, S., Nomura, M., Onodera, H., Ono, K., Lee, B., Hirose, S., Toki, S., Ku, M.S.B., Makino, A., Matsuoka, M. and Miyao, M. (2001). Significant accumulation of C_4-specific pyruvate, orthophosphate dikinase in a C_3 plant, rice. *Plant physiol. 127, 1136-1146.*

Furbank, R.T. (2011). Evolution of the C4 photosynthetic mechanism: are there really three C4 acid decarboxylation types? *J. Exp. Bot. 62, 3103-3108*.

Furbank, R.T. and Taylor, W.C. (1995). Regulation of photosynthesis in C_3 and C_4 plants: A molecular approach. *Plant Cell 7, 797-807*.

Gielwanowska, I., Szczuka, E., Bednara, J. and Górecki, R. (2005). Anatomical features and ultrastructure of *Deschampsis antarctica* (Poaceae) leaves from different growing habitats. *Ann. Bot. 96, 1109-1119*.

Gillon, J. and Yakir, D. (2001). Influence of carbonic anhydrase activity in terrestrial vegetation on the ^{18}O content of atmospheric CO_2. *Science 291, 2584-2587.*

Goldfarb, D.S., Gariepy, J., Schoolnik, G. and Kornberg, R.D. (1986). Synthetic peptides as nuclear localization signals. *Nature 322, 641-644*.

Gould, S.J., Keller, G.A., Hosken, N., Wilkinson, J. and Subramani, S. (1989). A conserved tripeptide sorts proteins to peroxisomes. *J. Cell Biol. 108, 1657-1664*.

Gray, J.C., Hanson, M.R., Shaw, D.J., Graham, K., Dale, R., Smallman, P., Natesan, S.K.A., and Newell, C.A. (2012). Plastid stromules are induced by stress treatments acting through abscisic acid. *Plant J. 69, 387-398*.

Gray, J.C., Sullivan, J.A., Hibberd, J.M. and Hansen, M.R. (2001). Stromules: Mobile protrusions and interconnections between plastids. *Plant Biol. 3, 223-233*.

Gunning, B.E.S. (2005). Plastid stromules: video microscopy of their outgrowth, retraction, tensioning, anchoring, branching, bridging, and tip-shedding. *Protoplasma 225, 33-42*.

Hailey, D.W., Rambold, A.S., Satpute-Krishnan, P., Mitra, K., Sougrat, R., Kim, P.K. and Lippincott-Schwartz, J. (2010). Mitochondria supply membranes for autopagosome biogenesis during starvation. *Cell 141, 656-667*.

Hanaoka, H., Noda, T., Shirano, Y., Kato, T., Hayashi, H., Shibata, D., Tabata, S. and Ohsumi, Y. (2002). Leaf senescence and starvation-induced chlorosis are accelerated by the disruption of an *Arabidopsis* autophagy gene. *Plant Physiol. 129, 1181-1193*.

Hanson, M.R. and Sattarzadeh, A. (2011). Stromules: Recent insights into a long neglected feature of plastid morphology and function. *Plant Physiol. 155, 1486-1492*.

Hatch, M.D. (1987). C_4 photosynthesis: a unique blend of modified biochemistry, anatomy and ultrastructure. *Biochim. Biophys. Acta 895, 81-106*.

Hayashi-Nishino, M., Fujita, N., Noda, T., Yamaguchi, A., Yoshimori, T. and Yamamoto, A. (2009). A subdomain of the endoplasmic reticulum forms a cradle for autophagosome formation. *Nat. Cell Biol. 11, 1433-1437.*

Hayes, R., Kudla, J., Schuster, G., Gabay, L., Maliga, P. and Gruissem, W. (1996). Chloroplast mRNA 3'-end processing by ahigh molecular weight protein complex is regulated by nuclear encoded RNA binding proteins. *EMBO J. 15, 1132-1141*.

Häusler, R.E., Hirsch, H., Kreuzaler, F. and Peterhansel, C. (2002). Overexpression of C_4-cycle enzymes in transgenic C_3 plants: a biotechnological approach to improve C_3-photosynthesis. *J. Exp. Bot. 53, 591-607*.

Hibberd, J.M. and Covshoff, S. (2010). The regulation of gene expression required for C_4 photosynthesis. *Annu. Rev. Plant Biol. 61, 181-207*.

Hofacker, I. L. (2003). Vienna RNA secondary structure server. *Nucl. Acids Res. 31, 3429-3431*.

Hofacker, I. L., Fekete, M. and Stadler, P. F. (2002). Secondary structure prediction for aligned RNA sequences. *J. Mol. Biol. 319, 1059-1066*.

Hofacker, I. L., Fekete, M., Stadler, P. F., Bonhoeffer, S., Tacker, M. and Schuster, P. (1994). Fast folding and comparison of RNA secondary structures. *Monatsh. Chem. 125, 167-188*.

Holzinger, A., Buchner, O., Lutz, C. and Hanson, M.R. (2007). Temperature-sensitive formation of chloroplast protrusions and stromules in mesophyll cells of *Arabidopsis thaliana*. *Protoplasma 230, 23-30*.

Holzinger, A., Kwok, E.Y. and Hanson, M.R. (2008). Effects of *arc3*, *arc5* and *arc6* mutations on plastid morphology and stromule formation in green and nongreen tissues of *Arabidopsis thaliana*. *J. Photochem. Photobiol. 84, 1324-1335*

Inoue, Y., Suzuki, T., Hattori, M., Yoshimoto, K., Ohsumi, Y. and Moriyasu, Y. (2006). *AtATG* genes, homologs of yeast autophagy genes, are involved in constitutive autophagy in *Arabidopsis* Root tip cells. *Plant Cell Physiol. 47, 1641-1652*.

Irihimovitch, V. and Shapira, M. (2000). Glutathione redox potential modulated by reactive oxygen species regulates translation of Rubisco large subunit in the chloroplast. *J. Biol. Chem. 275, 16289-16295*.

Ishida, H., Makino, A. and Mae, T. (1999). Fragmentation of the large subunit of ribulose-1,5-bisphosphate carboxylase by reactive oxygen species occurs near Gly-329. *J. Biol. Chem. 274, 5222-5226*.

Ishida, H., Nishimori, Y., Sugisawa, M., Makino, A. and Mae, T. (1997). The large subunit of ribulose-1,5-bisphosphate carboxylase/oxygenase is fragmented into 37-kDa and 16-kDa polypeptides by active oxygen in the lysates of chloroplasts from primary leaves of wheat. *Plant Cell Physiol. 38, 471-479*.

Ishida, H., Shimizu, S., Makino, A. and Mae, T. (1998). Light-dependent fragmentation of the large subunit of ribulose-1,5-bisphosphate carboxylase/oxygenase in chloroplasts isolated from wheat leaves. *Planta 204, 305-309*.

Ishida, H., Yoshimoto, K., Izumi, M., Reisen D., Yano, Y., Makino, A., Ohsumi, Y., Hanson, M.R. and Mae, T. (2008). Mobilization of Rubisco and stroma-localized fluorescent proteins of chloroplasts to the vacuole by and ATG gene-dependent autophagic precess. *Plant Physiol. 148, 142-155*.

Izumi, M., Wada, S., Makino, A. and Ishida, H. (2010). The autophagic degradation of chloroplasts via Rubisco-containing bodies is specifically linked to leaf carbon status but not nitrogen status in Arabidopsis. *Plant Physiol. 154, 1196-1209*.

Johansen, T., and Lamark, T. (2011). Selective autophagy mediated by autophagic adapter proteins. *Autophagy 7, 279–296*.

Kawamata, T., Kamada, Y., Kabeya, Y., Sekito, T. and Ohsumi, Y. (2008). Organization of the pre-autophagosomal structure responsible for autophagosome formation. *Mol. Biol. Cell 19, 2039-2050*.

Khrebtukova, I. and Spreitzer, R.J. (1996). Elimination of the *Chlamydomonas* gene family that encodes the small subunit of ribulose-1.5-bisphospate carboxylase/oxygenase. *Proc. Natl. Acad. Sci. 93, 13689-13693*.

Kim, J. and Mullet, J.E. (2003). A echanism for light-induced translation of the *rbcL* mRNA encoding the large subunit of ribulose-1,5-bisphosphate carboxylase in barley chloroplasts. *Plant Cell Physiol. 44, 491-499*.

Kokubun, N., Ishida, H., Makino, A. and Mae, T. (2002). The degradation of the large subunit of ribulose-1,5-bisphosphate carboxylase/oxygenase into the 44-kDa fragment in the lysates of chloroplasts incubated in darkness. Plant Cell Physiol. 43, 1390-1395.

Kost, B., Spielhofer, P., and Chua, N.H. (1998). A GFP-mouse talin fusion protein labels plant actin filaments *in vivo* and visualizes the actin cytoskeleton in growing pollen tubes. *Plant J. 16, 393-401.*

Köhler, R.H., Cao, J., Zipfel, W.R., Webb, W.W. and Hanson, M.R. (1997). Exchange of protein molecules through connections between higher plant plastids. *Science 276, 2039-2042*.

Köhler, R.H. and Hanson, M.R. (2000). Plastid tubules of higher plants are tissue-specific and developmentally regulated. *J. Cell Sci. 113, 81-89*.

Ku, M.S.B., Agarie, S., Nomura, M., Fukayama, H., Tsuchida, H., Ono, K., Hirose, S., Toki, S., Miyao, M., Matsuoka, M. (1999). High-level expression of maize phosp.hoenolpyruvate carboxylase in transgenic rice plants. *Nature Biotech. 17, 76-80.*

Ku, M.S.B., Kano-Murakami, Y. and Matsuoka, M. (1996). Evolution and expression of C_4 photosynthesis genes. *Plant Physiol. 111, 949-957.*

Ku, S.B. and Edwards, G.E. (1977). Oxygen inhibition of photosynthesis. I. Temperature dependence and relation to O2/Co2 solubility ratio. *Plant Physiol. 59, 986-990.*

Kuroda, H. and Maliga, P. (2001). Sequences downstream of the translation initiation codon are important determinants of translation efficiency in chloroplasts. *Plant Physiol. 125, 430-436*.

Kwok, E.Y. and Hanson, M.R. (2003). Microfilaments and microtubules control the morphology and movement of non-green plastids and stromules in *Nicotiana tabacum*. *Plant J. 35, 16-26*.

Kwok, E.Y. and Hanson, M.R. (2004a). In vivo analysis of interactions between GFP-labeled microfilaments and plastid stromules. *BMC Plant Biol. 4:2, doi: 10.1186/1471-2229-4-2*.

Kwok, E.Y. and Hanson, M.R. (2004b). Plastids and stromules interact with the nucleus and cell membrane in vascular plants. *Plant Cell Rep. 23, 188-195*.

Kwok, E.Y. and Hanson, M.R. (2004c). GFP-labelled Rubisco and aspartate aminotransferase are present in plastid stromules and traffic between plastids. *J. Exp. Bot. 55, 595-604*.

Kwon, S.I. and Park, O.K. (2008). Autophagy in plants. *J. Plant Biol. 51, 313-320*.

Lai, L.B., Wang, L. and Nelson, T.M. (2002). Distinct but conserved functions for two chloroplastic NADP-Malic enzyme isoforms in C_3 and C_4 Flaveria species. *Plant Physiol. 128, 125-139*.

Langdale, J.A., Metzler, M.C. and Nelson, T. (1987). The *Argentia* mutation dilays normal development of photosynthetic cell-types in *Zea mays*. *Dev. Biol. 122, 243-255.*

Langdale, J.A. and Nelson, T. (1991). Spatial regulation of photosynthetic development in C_4 plants. *Trends Genet. 7, 191-196.*

Langdale, J.A., Rothermel, B.A. and Nelson, T. (1988). Cellular pattern of photosynthetic gene expression in developing maize leaves. *Genes Dev. 2, 106-115.*

Langdale, J.A., Taylor, W.C. and Nelson, T. (1991). Cell-specific accumulation of maize phospho*enol*pyruvate carboxylase is correlated with demethylation at a specific site greater than 3 kb upstream of the gene. *Mol. Gen. Genet. 225, 49-55.*

Langdale, J.A., Zelitch, I., Miller, E. and Nelson, T. (1988). Cell position and light influence C_4 versus C_3 patterns of photosynthetic gene expression in maize. *EMBO J. 7, 3643-3651*.

Lara, M.V., Offermann, S., Smith, M., Okita, T.W., Andreo, C.S. and Edwards, G.E. (2008). Leaf development in the single-cell C_4 system in *Bienertia sinuspersici*: expression of genes and peptide levels for C_4 metabolism in relation to chlorenchyma structure under different light conditions. *Plant Physiol. 148, 593-610*.

Larkin, M. A., Blackshields, G., Brown, N. P., Chenna, R., McGettigan, P. A., McWilliam, H., Valentin, F., Wallace, I. M., Wilm, A., Lopez, R., Thompson, J. D., Gibson, T. J. and Higgins D. G. (2007). ClustalW and ClustalX version 2. *Bioinformatics 23, 2947-2948*.

Leister, D. (2003). Chloroplast research in the genomic age. *Trends Genet. 19, 47-56*.

Levanony, H., Rubin, R., Altschuler, Y., and Galili, G. (1992). Evidence for a novel route of wheat storage proteins to vacuoles. *J. Cell. Biol. 119, 1117-1128*.

Li, P., Ponnala, L., Gandotra, N., Wang, L., Si, Y., Tausta, S.L., Kebrom, T.H., Provart, N., Patel, R., Myers, G.R., Reidel, E.J., Turgeon, R., Liu, P., Sun, Q., Nelson, T. and Brutnell, T.P. (2010). The developmental dynamics of the maize leaf transcriptome. *Nat. Genet. 42, 1060-1067*.

Liu, Y., Schiff, M., Czymmek, K., Talloczy, Z., Levine, B. and Dinesh-Kumar, S.P. (2005). Autophagy regulates programmed cell death during the plant innate immune response. *Cell 121, 567-577*.

Long, J.J. and Berry, J.O. (1996). Tissue-specific and light-mediated expression of the C_4 photosynthetic NAD-dependent malic enzyme of amaranth mitochondria. *Plant Physiol. 112, 473-482.*

Lung, S.C., Yanagisawa, M. and Chuong, S.D.X. (2011). Protoplast isolation and transient gene expression in the single-cell C_4 species, *Bienertia sinuspersici*. *Plant Cell Rep. 30, 473-484*.

Lung, S.C., Yanagisawa, M. and Chuong, S.D.X. (2012). Isolation of dimorphic chloroplasts from the single-cell C_4 species *Bienertia sinuspersici*. *Plant Method* In press.

Majeran, W., Cai, Y., Sun, Q. and van Wijk, K.J. (2005). Functional differentiation of bundle sheath and mesophyll maize chloroplasts. *Plant Cell 17, 3111-3140*.

Majeran, W., Friso, G., Ponnala, L., Connolly, B., Huang, M., Reidel, E., Zhang, C., Asakura, Y., Bhuiyan, N.H., Sun, Q., Turgeon, R. And van Wijk, K.J. (2010). Structural and metabolic transitions of C_4 leaf development and differentiation defined by microscopy and quantitative proteomics in maize. *Plant Cell 22, 3509-3542*.

Majeran, W., Zybailov, B., Ytterberg, J.A., Dunsmore, J., Sun, Q. and van Wijk, K.J. (2008). Consequences of C_4 differentiation for chloroplast membrene proteomes in maize mesophyll and bundle sheath cells. *Mol. Cell Proteomics 7, 1609-1638*.

Marc, J., Granger, C.L., Brincat, J., Fisher, D.D., Kao, T.H., McCubbin, A.G., Cyr, R.J. (1998). A *GFP-MAP4* reporter gene for visualizing cortical microtubule rearrangements in living epidermal cells. *Plant Cell 10, 1927-1940*.

Marin-Navarro, J., Manuell, L., Wu J. and Mayfield, S.P. (2007). Chloroplast translation regulation. *Photosynth. Res. 94, 359-374.*

Martineau, B. and Taylor, W.C. (1985). Photosynthetic gene expression and cellular differentiation in developing maize leaves. *Plant Physiol. 78, 399-404.*

Martinez, D.E., Costa, M.L., Gomez, F.M., Otegui, M.S. and Guiamet, J.J. (2008). 'Senescence-associated vacuoles' are involved in the degradation of chloroplast proteins in tobacco leaves. *Plant J. 56, 196-206*.

Marty, F. (1999). Plant vacuoles. *Plant Cell 11, 587-599*.

Mathews, D., Sabina, J., Zucker, M. and Turner, H. (1999). Expanded sequence dependence of thermodynamic parameters improves prediction of RNA secondary structure. *J. Mol. Biol. 288, 911-940*.

Matsuoka, M., Furbank, R.T., Fukayama, H. and Miyao, M. (2001). Molecular engineering of C_4 photosynthesis. *Annu. Rev. Plant Physiol. Plant Mol. Biol. 52, 297-314*.

Matsuoka, M. and Numazawa, T. (1991). Cis-acting elements in the pyruvate, orthophosphate dikinase gene from maize. *Mol Gen Genet. 228, 143-152*.

McCormac, D.J., Litz, H., Wang, J., Gollnick, P.D. and Berry, J.O. (2001). Light-associated and processing-dependent protein binding to 5' regions of rbcL mRNA in the Chloroplasts of a C_4 plant. *J. Biol. Chem. 276, 3476-3483.*

Meijer, W.H., van der Klei, I., Veenhuis, M. and Kiel, J.A.K.W. (2007). ATG genes involved in non-selective autophagy are conserved from yeast to man, but the selective Cvt and pexophagy pathways also require organism-specific genes. *Autophagy 3, 106-116*.

Meisner, N.C., Hackermüller, J., Uhl, V., Aszódi, A., Jaritz, M. and Auer, M. (2004). mRNA openers and closers: Modulating AU-rich element-controlled mRNA stability by a molecular switch in mRNA secondary structure. *ChemBioChem, 5, 1432-1447*.

Miyao, M. (2003). Molecular evolution and genetic engineering of C_4 photosynthetic enzymes. *J. Exp. Bot. 54, 179-189*.

Miyao, M., Masumoto, C., Miyazawa, S. and Fukayama, H. (2011). Lessons from engineering a single-cell C4 photosynthetic pathway into rice. *J. Exp. Bot. 62, 3021-3029*.

Mizushima, N. (2007). Autophagy: process and function. *Genes Dev. 21, 2861-2873*.

Mizushima, N., Ohsumi, Y. and Yoshimori, T. (2002). Autophagosome formation in mammalian cells. *Cell Struct. Funct. 27, 421-429*.

Moriyasu, Y., Hattori, M., Jauh, G.Y. and Rogers, J.C. (2003). Alpha tonoplast intrinsic protein is specifically associated with vacuole membrane involved in an autophagic process. *Plant Cell Physiol. 44, 795-802*.

Moriyasu, Y. and Ohsumi, Y. (1996). Autophagy in tobacco suspension-cultured cells in response to sucrose starvation. *Plant Physiol. 111, 1233-1241*.

Mortz, E., Krogh, T.N., Vorum, H. and Gorg, A. (2001). Improved silver staining protocols for high sensitivity protein identification using matrix-assisted laser desorption/ionization-time of flight analysis. *Proteomics 1, 1359-1363*.

Murashige, T. and Skoog, F. (1962). A revised medium for rapid growth and bioassay with tobacco tissue cultures. *Physiol. Plant. 15, 473-497*.

Mulo, P., Sakurai, I. and Aro, E.M. (2011). Strategies for psbA gene expression in cyanobacteria, green algae and higher plants: From transcription to PSII repair. *Biochim. Biophys. Acta* in press.

Nakano, R., Ishida, H., Makino, A. and Mae, T. (2006). In vivo fragmentation of the large subunit of ribulose-1,5-bisphosphate carboxylase by reactive oxygen species in and intact leaf of cucumber under chilling-light conditions. *Plant Cell Physiol. 47, 270-276*.

Natesan, S.K.A., Sullivan, J.A. and Gray, J.C. (2005). Stromules: a characteristic cell-specific feature of plastid morphology. *J. Exp. Bot. 56, 787-797*.

Nelson, T. and Langdale, J.A. (1992). Developmental genetics of C_4 photosynthesis. *Annu. Rev. Plant Physiol. Plant Mol. Biol. 43, 25-47*.

Newell, C.A., Natesan, S.K.A., Sullivan, J.A., Jouhet, J. Kavanagh, T.A. and Gray, J.C. (2012). Exclusion of plastid nucleoids and ribosomes from stromules in tobacco and Arabidopsis. *Plant J. 69, 399-410*.

Ninomiya, N., Ashida, H. and Yokota, A. (2008). Improvement of cyanobacterial Rubisco by introducing the latch structure involved in high affinity for CO_2 in red algae Rubisco. In J. F. Allen, E. Gantt, J. H. Golbeck and B. Osmond (eds.), *Photosynthesis. Energy from the Sun: 14th International Congress on Photosynthesis*, 867-870. *Springer*.

Noda, T. and Ohsumi, Y. (1998). Tor, a phosphatidylinositol kinase homologue, controls autophagy in yeast. *J. Biol. Chem. 273, 3963-3966*.

Nomura, M., Sentoku, N., Nishimura, A., Lin, J.H., Honda, C., Taniguchi, M., Ishida, Y., Ohta, S., Komari, T., Miyao-Tokutomi, M., Kano-Murakami, Y., Tajima, S. Ku, M.S.B. and Matsuoka, M. (2000). The evolution of C_4 plants: acquisition of *cis*-regulatory sequences in the promoter of C_4-type pyruvate, orthophosphate dikinase gene. *Plant J. 22, 211–21*.

Notredame, C., Higgins, D. and Heringa, J. (2000). T-Coffee: a novel method for multiple sequence alignment. *J. Mol. Biol. 302, 205-217*.

Offermann, S., Okita, T.W. and Edwards, G.E., (2011). Resolving the compartmentation and function of C_4 photosynthesis in the single-cell C_4 species *Bienertia sinuspersici*. *Plant Physiol. 155, 1612-1628*.

Oldenburg D.J. and Bendich, A.J. (2004). Most chloroplast DNA of maize seedlings in linear molecules with defined ends and branched forms. *J Mol Biol.* 335, 953-970.

Otegui, M.S., Noh, Y.-S., Martínez, D.E., Petroff, M.G.V., Staehelin, L.A., Amasino, R.M. and Guiamet, J.J. (2005). Senescence-associated vacuoles with intense proteolytic activity develop in leaves of Arabidopsis and soybean. *Plant J. 41, 831-844*.

Park, H., Eggink, L.L., Roberson, R.W. and Hoober, K.J. (1999). Transfer of proteins from the chloroplast to vacuoles in *Chlamydomonas reinhardtii* (Chlorophyta): A pathway for degradation. *J. Phycol. 35, 528-538*.

Park, J., Knoblauch, M., Okita, T.W. and Edwards, G.E. (2009). Structual changes in the vacuole and Cytoskeleton are key to development of the two cytoplasmic domains supporting single-cell C_4 photosynthesis in *Bienertia sinuspersici*. *Planta 229, 369-382*.

Parry, M. A. J., Andralojc, P. J., Mitchell, R. A. C., Madgwick, P. J. and Keys, A. J. (2003). Manipulation of Rubisco: the amount, activity, function and regulation. *J. Exp. Bot. 54, 1321-1333*.

Parry, M. A. J., Keys, A. J., Madgwick, P. J., Carmo-Silva, A. E. and Andralojc P. J. (2008). Rubisco regulation: a role for inhibitors. *J. Exp. Bot. 59, 1569-1580*.

Patel, M., Siegel, A.J. and Berry, J.O. (2006). Untranslated regions of *FbRbc*S1 mRNA mediate bundle sheath cell-specific gene expression in leaves of a C_4 plant. *J. Biol. Chem. 281, 25485-25491*.

Patel, M. and Berry, J.O. (2008). Rubisco gene expression in C_4 plants. *J Exp Bot. 59, 1625-1634*.

Patel, S. and Dinesh-Kumar, S. (2008). *Arabidopsis* ATG6 is required to limit the pathogen associated cell death response. *Autopagy 4, 20-27*.

Peterhansel, C. (2011). Best practice procedures for the establishment of a C_4 cycle in transgenic C_3 plants. *J. Exp. Bot. 62, 3011-3019*.

Pfaffl, M.W. A new mathematical model for relative quantification in real-time RT-PCR. *Nucl Acids Res, 29, 2002-2007*, (2001).

Prins, A., van Heerden, P.D.R., Olmos, E., Kunert, K.J., Foyer, C.H. (2008). Cysteine proteinases regulate chloroplast protein content and composition in tobacco leaves: a model for dynamic interactions with ribulose-1,5-bisphosphate carboxylase/oxygenase (Rubisco) vesicular bodies. *J. Exp. Bot. 59, 1935-1950*.

Pyke, K.A. and Howells, C.A. (2002). Plastid and stromules morphogenesis in tomato. *Ann. Bot. 90, 559-566*.

Rabinowitz, J.D. and White, E. (2010). Autophagy and metabolism. *Sience, 330, 1344-1348*.

Raines, C.A. (2006). Transgenic approaches to manipulate the environmental responses of the C_3 carbon fixation cycle. *Plant Cell Environ. 29, 331-339*.

Ramsperger, V.C., Summers, R.G. and Berry, J.O. (1996). Photosynthetic gene expression in meristems and during initial leaf development in a C_4 dicotyledonous plant. *Plant Physiol. 111, 999-1010.*

Ravikumar, B., Moreau, K., Jahreiss, L., Puri, C. and Rubinsztein, D.C. (2010). Plasma membrane contributes to the formation of pre-autophagosomal structures. *Nat. Cell Biol. 12, 747-757*.

Reinbothe, S., Reinbothe, C., Heintzen, C., Seidenbecher, C. and Parthier, B. (1993). A methyl jasmonate-induced shift in the length of the 5' untranslated region impairs translation of the plastid rbcL transcript in barley. *EMBO J. 12, 1505-1512.*

Reumann, S., Voitsekhovskaja, O. and Lillo, C. (2010). From signal transduction to autophagy of plant cell organelles: lessons from yeast and mammals and plant-specific features. *Protoplasma 247, 233-256*.

Riedl, J., Crevenna, A.H., Kessenbrock, K., Yu, J.H., Neukirchen, D., Bista, M., Bradke, F., Jenne, D., Holak, T.A., Werb, Z., Sixt, M. and Wedlich-Soldner, R. (2008). Lifeact: a versatile marker to visualize f-actin. *Nature Methods 5, 605-607*.

Rivas, J.D.L., Lozano, J.J. and Ortiz, A.R. (2002). Comparative analysis of chloroplast genemes: Functional annotation, genome-based phylogeny, and deduced evolutionary patterns. *Genome Res. 12, 567-583*.

Rodermel, S. (2001). Pathways of plastid-to-nucleus signalling. *Trends Plant Sci. 6, 471-478*.

Rosche, E., Chitty, J., Westhoff, P. and Taylor, W.C. (1998). Analysis of promoter activity for the gene encoding pyruvate orthophospate dikinase in stably transformed C_4 *Flaveria* species. *Plant Physiol. 117, 821-829*.

Rose, T.L., Bonneau, L., Der, C., Marty-Mazar, D. and Marty, F. (2006). Starvation-induced expression of autophagy-related genes in Arabidopsis. *Biol. Cell 98, 53-67*.

Sage, T.L. and Sage R.F. (2009). The functional anatomy of rice leaves: implications for refixation of photorespiratory CO_2 and efforts to engineer C_4 photosynthesis into rice. *Plant Cell Physiol. 50, 756-772*.

Sage, R.F. (2004). The evolution of C_4 photosynthesis. *New Phytologist 161, 341-370*.

Sakai, Y., Oku, M., van der Klei, I.J. and Kiel, J.A. (2006). Pexophagy: autophagic degradation of peroxisomes. *Biochim. Biophys. Acta 1763, 1767-1775*.

Sambrook, J., Fritsch, E.F. and Maniatis, T. (1989). Molecular Cloning, A Laboratory Manual, Second Edition. Cold Spring Harbor Laboratory Press. Plainview, NY.

Sattarzadeh, A., Krahmer, J., Germain, A.D. and Hanson, M.R. (2009). A myosin XI tail domain homologous to the yeast myosin vacuole-binding domain interacts with plastids and stromules in *Nicotiana benthamiana*. *Mol. Plant 2, 1351-1358*.

Schattat, M., Barton, K., Baudisch, B., Klösgen, R.B. and Mathur, J. (2011). Plastid stromule branching concides with contiguous endoplasmic reticulum dynamics. *Plant Physiol. 155, 1667-1677*.

Schmidt, G.W. and Mishkind, M.L. (1983). Rapid degradation of unassembled ribulose 1,5-bisphosphate carboxylase small subunits in chloroplasts. *Proc. Natl. Acad. Sci. 80, 2632-2636*.

Schwarte, S. and Tiedemann, R. (2011). A gene duplication/loss event in the ribulose-1.5-bisphosphate-carboxylase/oxygenase (Rubisco) small subunit gene family among accessions of *Arabidopsis thaliana*. *Mol. Biol. Evol. 28, 1861-1876*.

Serino, G. and Maliga, P. (1998). RNA polymerase subunits encoded by the plastid *rpo* genes are not shared with the nucleus-encoded plastid enzyme. *Plant Physiol. 117, 1165-1170*.

Shalla, T.A. (1964). Assembly and aggregation of tobacco mosaic virus in tomato leaflets. *J. Cell Biol. 21, 253-264*.

Shapira, M., Lers, A., Heifetz, P.B., Irihimovitz, V., Osmond, C.B., Gillham, N.W. and Boynton J.E. (1997). Differential regulation of chloroplast gene expression in *Chlamydomonas reinhardtii* during photoacclimation: light stress transiently suppresses synthesis of the Rubisco LSU protein while enhancing synthesis of the PS II D1 protein. *Plant Mol. Biol. 33, 1001-1011.*

Sheahan, M.B., Staiger, C.J., Rose, R.J. and McCurdy, D.W. (2004). A green fluorescent protein fusion to actin-binding domain 2 of *Arabidopsis* fimbrin highlights new features of a dynamic actin cytoskelton in live plant cells. *Plant Physiol. 136, 3968-3978.*

Sheehy, J.E., Mitchell, P.L. and Hardy B., eds. (2000). Redesigning rice photosynthesis to improve yield. Amsterdam, the Netherlands: Elsevier.

Sheen, J. (1999). C_4 gene expression. *Annu Rev Plant Physiol. Plant Mol. Biol. 50, 187-217.*

Sheen, J.Y. and Bogorad, L. (1985). Differential expression of the ribulose bisphosphate carboxylase large subunit gene in bundle sheath and mesophyll cells of developing maize leaves is influenced by light. *Plant Physiol. 79, 1072-1076*.

Sheen, J.Y. and Bogorad, L. (1987a). Differential expression of C_4 pathway genes in mesophyll and bundle sheath cells of greening maize leaves. *J. Biol. Chem. 262, 11726-11730.*

Sheen, J.Y. and Bogorad, L. (1987b). Regulation of levels of nuclear transcripts for C_4 photosynthesis in bundle sheath and mesophyll cells of maize leaves. *Plant Mol Biol. 8, 227-238*.

Shiina, T. Hayashi, K., Ishii, N., Morikawa, K. and Toyoshima, Y. (2000). Chloroplast tubules visualized in transplastomic plants expressing green fluorescent protein. *Plant Cell Physiol. 41, 367-371*.

Shu, G., Pontieri, V., Dengler, N. G. and Mets, L. J. (1999). Light induction of cell type differentialtion and cell-type-specific gene expression in cotyledons of a C_4 plant, *Flaveria trinervia. Plant Physiol. 121, 731-741.*

Soltis, D.E. and Soltis, P.S. (2003). The role of Phylogenetics in comparative Genetics. *Plant Physiol. 132, 1790-1800*.

Spreitzer, R. J. and Salvucci, M. E. (2002). Rubisco: Structure, regulatory interactions, and possibilities for a better enzyme. *Annu. Rev. Plant Biol. 53, 449-475*.

Stern, D. B., Jones, H. and Gruissem, W. (1989). Function of plastid mRNA 3' inverted repeats: RNA stabilization and gene-specific protein binding. *J. Biol. Chem. 264, 18742-18750*.

Stern, D. B. and Kindle, K. (1993). 3' end maturation of the Chlamydomonas reinhardtii chloroplast atpB mRNA is a two stem process. *Mol. Cell. Biol. 13, 2277-2285*.

Stockhaus, J., Schlue, U., Koczor, M., Chitty, J.A., Taylor, W.C. and Westhoff, P. (1997). The promoter of the gene encoding the C_4 form of phosphonenolpyruvate carboxylase directs mesophyll-specific expression in transgenic C_4 *Flaveria* spp. *Plant Cell 9, 479-489*.

Stothard, P. (2000). The Sequence Manipulation Suite: JavaScript programs for analyzing and formatting protein and DNA sequences. *Biotechniques 28, 1102-1104*.

Sugiura, M. (1995). The chloroplast genome. *Essays Biochem. 30, 49-57*.

Suzuki, K., Kirisako, T., Kamada, Y., Mizushima, N., Noda, T. and Ohsumi, Y. (2001). The pre-autophagosomal structure organized by concerted functions of *APG* genes in essential for autophagosome formation. *EMBO J. 20, 5971-5981*.

Suzuki, K. and Ohsumi, Y. (2010). Current knowledge of the pre-autophagosomal structure (PAS). *FEBS Lett. 584, 1280-1286*.

Svoboda, P. and Cara, D. (2006). Hairpin RNA: a secondary structure of primary importance. *Cell. Mol. Life Sci. 63, 901-918*.

Swanson, S.J., Bethke, P.C. and Jones, R.L. (1998). Barley aleurone cells contain two types of vacuoles: characterization of lytic organelles by use of fluorescent probes. *Plant Cell 10, 685-698*.

Takeuchi, Y., Akagi, H., Kamasawa, N., Osumi, M. and Honda, H. (2000). Aberrant chloroplasts in transgenic rice plants expressing a high level of maize NADP-dependent malic enzyme. *Planta 211, 265-274.*

Taniguchi, M., Izawa, K., Ku, M.S.B., Lin, J.H., Saito H, Ishida, Y., Ohta, S., Komari, T., Matsuoka, M. and Sugiyama, T. (2000). Binding of cell type-specific nuclear proteins to the 5'-flanking region of maize C4 phospho*enol*pyruvate carboxylase gene confers its differential transcription in mesophyll cells. *Plant Mol. Biol.* 44, 543–57.

Thompson, A.R., Vierstra, R.D. (2005). Autophagic recycling: lessons from yeast help define the process in plants. *Curr. Opin. Plant Biol. 8, 165-173*.

Tirlapur, U.K., Dahse, I., Reiss, B., Meurer, J. and Oelmüller, R. (1999). Characterization of the activity of a plastid-targeted green fluorescent protein in *Arabidopsis*. *Eur. J. Cell Biol. 78, 233-240*.

Toyooka, K., Okamoto, T., and Minamikawa, T. (2001). Cotyledon cells of *Vigna mungo* seedlings use at least two distinct autophagic machineries for degradation of starch granules and cellular components. *J. Cell Biol. 154, 973-982*.

Troxler, R. F., Zhang, F., Hu, J. and Bogorad, L. (1994). Evidence that sigma factors are components of chloroplast RNA polymerase. *Plant Physiol. 104, 753-759*.

Vanhee, C., Zapotoczny, G., Masquelier, D., Ghislain, M., and Batoko, H. (2011). The Arabidopsis multistress regulator TSPO is a heme binding membrane protein and a potential scavenger of porphyrinsvia an autophagy-dependent degradation mechanism. *Plant Cell 23, 785–805*.

Voznesenskaya, E.V., Edwards, G.E., Kirats, O., Artyusheva, E.G. and Francheschi, V.R. (2003). Development of biochemical specialization and organelle partitioning in the single-cell C_4 system in leaves of *Borszczowia aralocaspica* (Chenopodiaceae). *Am. J. Bot. 90, 1669-1680.*

Voznesenskaya, E.V., Franceschi, V.R. and Edwards, G.E. (2004). Light-dependent development of single cell C_4 photosynthesis in cotyledons of *Borszczowia aralocaspica* (Chenopodiaceae) during transformation from a storage to a photosynthetic organ. *Ann. Bot. 93, 177-187*

Voznesenskaya, E.V., Franceschi, V.R., Kiirats, O., Artyusheva, E.G., Freitag, H. and Edwards, G.E. (2002). Proof of C_4 photosynthesis without Kranz anatomy in *Bienertia cycloptera* (Chenopodiaceae). *Plant J. 31, 649-662.*

Voznesenskaya, E.V., Franceschi, V.R., Kiirats, O., Freitag, H and Edwards, G.E. (2001). Kranz anatomy is not essential for terrestrial C_4 plant photosynthesis. *Nature 414, 543-546.*

Voznesenskaya, E.V., Koteyeva, N.K., Chuong, S.D.X., Akhani, H., Edwards, G.E. and Franceschi, V.R. (2005). Differentiation of cellular and biochemical features of the single-cell C_4 syndrome during leaf development in *Bienertia cycroptera* (Chenopodiaceae). *Am. J. Bot. 92, (1784-1795).*

Wada, S., Ishida, H., Izumi, M., Yoshimoto, K., Ohsumi, Y., Mae, T. and Makino, A. (2009). Autophagy plays a role in chloroplast degradation during senescence in individually darkened leaves. *Plant Physiol. 149, 885-893*.

Wang, R. and Brattain, M.G. (2007). The maximal size of protein to diffuse through the nuclear pore is larger than 60 kDa. *FEBS Lett. 581, 3164-3170*.

Wang, J.L., Kessig, D.F. and Berry, J.O. (1992). Regulation of C_4 gene expression in developing amaranth leaves. *Plant Cell 4, 173-184.*

Wang, J.L., Long, J.J., Hotchkiss, T. and Berry, J.O. (1993a). C_4 photosynthetic gene expression in light- and dark-grown amaranth cotyledons. *Plant Physiol. 102, 1085-1093.*

Wang, J.L., Turgeon, R., Carr, J.P. and Berry, J.O. (1993b). Carbon sink-to-source transition is coordinated with establishment of cell-specific gene expression in a C_4 plant. *Plant Cell 5, 289-296.*

Waters, M.T., Fray, R.G. and Pyke, K.A. (2004). Stromules formation is dependent upon plastid size, plastid differentiation status and the density of plastids within the cell. *Plant J. 39, 655-667*.

Weidberg, H., Shvets, E. and Elazar, Z. (2011). Biogenesis and cargo selectivity of autophagosomes. *Annu. Rev. Biochem. 80, 125-156*.

Weier, T.E. and Thomson, W.W. (1962). Membranes of mesophyll cells of *Nicotiana rustica* and *Phaseolus vulgaris* with paticular reference to the chloroplast. *Am. J. Bot. 49, 807-820*.

Westhoff, P. and Gowik, U. (2010). Evolution of C4 photosynthesis-lokking for the master switch. *Plant Physiol. 154, 598-601*.

Whitney, S. M. and Sharwood, R. E. (2008). Construction of a tobacco master line to improve Rubisco engineering in chloroplasts. *J. Exp. Bot. 59, 1909-1921*.

Wildman, S.G., Hongladarom, T. and Honda, S.I. Chloroplasts and mitochondria in living plant cells: Cinephotomicrographic studies. *Science, 138, 434-436*.

Woodson, J.D. and Chory, J. (2008). Coordination of gene expression between organellar and nuclear genomes. *Nat. Rev. Genet. 9, 383-395*.

Wostrikoff, K., and Stern, D. (2007). Rubisco large-subunit translation is autoregulated in response to its assembly sate in tobacco chloroplasts. *Proc. Natl. Acad. Sci. 104, 6466-6471*.

Xiong, Y., Contento, A.L. and Bassham, D.C. (2007a). Disruption of autophagy results in constitutive oxidative stress in Arabidopsis. *Autophagy 3, 257-258*.

Xiong, Y., Contento, A.L., Nguyen, P.Q. and Bassham, D.C. (2007b). Degradation of oxidized proteins by autophagy during oxidative stress in Arabidopsis. *Plant Physiol. 143, 291-299*.

Xu, R., Bingham, S.E. and Webber, A.N. (1993). Increased mRNA accumulation in a *psaB* frame-shift mutation of *Chlamydomonas reinhardtii* suggests a role for translation in *psaB* mRNA stability. *Plant Mol. Biol. 22, 465-474*.

Yang, Z. and Klionsky, D.J. (2010). Mammalian autophagy: core molecular machinery and signalling regulation. *Curr. Opin. Cell. Biol. 22, 124-131*.

Yano, K., Hattori, M. and Moriyasu, Y. (2007). A novel type of autophagy occurs together with vacuole genesis in miniprotoplasts prepared from tobacco culture cells. *Autophagy 3, 215-221*.

Ylä-Anttila, P., Vihinen, H., Jokitalo, E. and Eskelinen, E.L. (2009). 3D tomography reveals connections between the phagophore and endoplasmic reticulum. *Autophagy 5, 1180-1185*.

Yoo, S.D., Cho, Y.H. and Sheen, J. (2007). *Arabidopsis* mesophyll protoplasts: a versatile cell system for transient gene expression analysis. *Nat. Protoc. 2, 1565-1572.*

Yoshimoto, K., Hanaoka, H., Sato, S., Kato, T., Tabata, S., Noda, T. and Ohsumi, Y. (2004). Processing of ATG8s, ubiquitin-like proteins, and their deconjugation by ATG4s are essential for plant autophagy. *Plant Cell 16, 2967-2983*.

Youle, R.J. and Narendra, D.P. (2011). Mechanisms of mitophagy. *Nat. Rev. Mol. Cell Biol. 12, 9-14*.

Young, A.R.J., Chan, E.Y.W., Hu, X.W., Köchl, R., Crawshaw, S.G., High, S., Hailey, D.W., Lippincott-Schwartz, L. and Tooze, S.A. (2006). Starvation and ULK-dependent cycling of mammalian Atg9 between the TGN and endosomes. *J. Cell Sci. 119, 3888-3900*.

Yukawa, M., Kuroda, H. And Sugiura, M. (2007). A new in vitro translation system for non-radioactive assay from tobacco chloroplasts: effect of pre-mRNA processing on translation in vitro. *Plant J. 49, 367-376*.

Zheng, H. and Staehelin, L.A. (2011). Protein storage vacuoles are transformed into lytic vacuoles in root meristematic cells of germinating seedlings by multiple, cell type-specific mechanisms. *Plant Physiol. 155, 2023-2035*.

Zuker, M. (2003). Mfold web server for nucleic acid folding and hybridization prediction. *Nucl. Acids Res. 31, 3406-3415*.

Zuker, M. and Stiegler, P. (1981). Optimal computer folding of large RNA sequences using thermodynamics and auxiliary information. *Nucl. Acid Res. 9, 133-148*.

Appendix. **List of primer sequences used in this project**

Name	**Sequence (5' to 3')**
RbcL	
-RACE	
BcRbLF3	GCA AGA TCA CGT CCC TCA TT
BcRbLR4	GAA TAC CTC CCG AAG CAA CA
BcRbL5'O	AGG CTC GAT GTG GTA GCA TC
BcRbL3'O	TTG GTG GAG GAA CCT TAG GA
BsRbcL5'O2	AAT AGG GGA CGG CCA TAC TT
BsRbcL3'I2	CGT CTG TCT GGT GGA GAT CA
-Subcloning	
BsRbcLcdsF2BamH1	CGC GGA TCC ATG TCA CCA CAA ACA GAG ACT AAA
BsRbcLcdsR2Sal1	CGC GTC GAC AAA TTT GAT TTC CTT CCA TAC CT
-Semi-quantitative RT-PCR	
BsRbcL3'I2	CGT CTG TCT GGT GGA GAT CA
BsRbLStop	CTA GAC TGT ATC CAT TGC TGG GAA
-Real-time qPCR	
BsqRbcLF1	TGT TCT GCC TGT TGC TTC GGG A
BsqRbcLR1	CGG TGC ATT TCC CCA AGG GTG T
RbcS	
-RACE	

BcRbSF2	ATC CTT GTT GCG TGA GAT CC
BsRbSR2	AGG CTT TTG GGT AAG CCT TC
BsRbS5'O	GGG GTG GAA GGT AAG AAA GG
BsRbS5'I	CAA TTG GTG GCC ATA CCT G
-Subcloning	
BsRbcScdsF1EcoRI	CGC GAA TTC ATG GCT TCT AGT TTG ATG TCC AG
BsRbcScdsF3NcoI	CGC CCA TGG CAA TGG CTT CTA GTT TGA TGT CCA G
BsRbcScdsR1HindIII	CGC AAG CTT ATT AGT AGC CTG GGG GCT TG
BsRbcSTPR2Sal	CGC GTC GAC CGC ATT GGA CTT TTC CAC CGT T
BsRbcSMatR2BamHI	AGA GGA TCC TGT AGC CTG GGG GCT TGT AG
AtRbcSF1NcoI	AGA CCA TGG CTT CCT CTA TGC TCT CTT
AtRbcSR1BamHI	ATA GGA TCC ACC GGT GAA GCT TGG TGG
-Semi-quantitative RT-PCR	
BsRbcSRTF1	ATG GCT TCT AGT TTG ATG TCC AG
BsRbcSRTR2	CAT AAA CGG TTG GAC CGA AT

PEPC

-RACE

BsPEPC5'I	AAC ATG TCT CCC AGC TCC TC
BsPEPC3'I	GTG CCA AGC CTA CAC CCT AA
- Subcloning	
BsPCcdsF4SacI	CGC GAG CTC AAT GGC TAG TGG GAA GTT GGA
BsPCcdsR4KpnI	CGC GGT ACC CTA AAC CGG TGT TCT GCA TTC
BsPEPCcdsF1ClaI	CGC ATC GAT GCA CTT GTC TTT CTT CTT CTT CAA

BsPEPCcdsR1SalI	CGC GTC GAC AAG GAA GAA AAA CGC CGA AT

- Semi-quantitative RT-PCR

BsPEPCRTF1	GCA CTT GTC TTT CTT CTT CTT CAA
BsPEPC5'I	AAC ATG TCT CCC AGC TCC TC

PPDK

-RACE

BsPPDKF4	CAC AAG GGA AGA GTG CCA TT
BsPPDKR4	CAT TGT TTC TTG CTG CCA AA
BsPPDK5'O	CTG CAG CAT GAG ACG TCA TT
BsPPDK3'O	TTT GGC AGC AAG AAA CAA TG
BsPPDK3'I	TTG GAC TTT GTA GGA CTG AGC A
BsPPDKR5	TTG CAA CGC TTC GTA TCA AA
BsPPDK5'I2	TTC TTT GGA TCA GCA GGA AA
BsPPDK5'O3	CAA GGA TTT CCT CCC ACA GA
BsPPDKF7	TGT TGG GAG GTA AAG GAG CA
BsPPDKF8	CTG TGG GAG GAA ATC CTT GA

- Subcloning

BsPKTPF2NcoI	AGA CCA TGG CAA TGG CAT TAT GTT TCA AAG GAA
BsPPDKcdsF3BamHI	CGC GGA TCC CTC CCT TTG ATC TCT GGA GGA
BsPPDKcdsR3SalI	CGC GTC GAC AAT TCA AAC CGC AAC TTG AGC
BsPKMatR3BamHI	CGC GGA TCC GAA TTA AAA CCG CAA CTT GAG C

- Semi-quantitative RT-PCR

BsPPDKRTF1	CTC CCT TTG ATC TCT GGA GGA

BsPPDK5'O3	CAA GGA TTT CCT CCC ACA GA

NAD-ME

-RACE

BsNADF2	GAA AGC CCA CTT GGT CTG AA
BsNADR3	TAC AAC TGG CCT GCT GAA CA
BsNAD5'O	TTC AGA CCA AGT GGG CTT TC
BsNAD3'O	CCC TAG ATC TCC AAG ACC TAA AA
BsNAD5'O2	GGC CAA CGT GTA AAA ACA GC
BsNAD3'O2	CTG GGA TAA ATC CGC AAA GA
BsNAD3'I3	CCC TGA AGA CGC ATT CTC TA
BsNADF3	CCG ACT GCA TGA CAG AAA TG
SaNADF1	AGC TGC TTT TGA GAG TGC AA
SaNADR1	CGG ACC TCG GGG TCT ATA TC
BsNADR4	TAG CCT TCT GCA AGG TCC TC

- Subcloning

BsMEcdsF4NcoI	CGC CCA TGG CAA TGT CGA TGA TTT GTA ATC GGA GT
BsMETPR1BamHI	ATA GGA TCC CAC GAT GAC CTT CAG AAG TAG TAA ACG
BsNADcdsF2Cla1	CGC ATC GAT AAA TTC TGC AAC CAT TCA AAA
BsNADcdsR2Sal1	CGC GTC GAC GCA TTT CTT TGG CCT CAA AT

- Semi-quantitative RT-PCR

BsNADRTF2	AAG CCC CCA AAT TAT TCT CAA
BsNAD5'O2	GGC CAA CGT GTA AAA ACA GC

---

psaB

- Subcloning

BspsaBF2XhoI	CGC CTC GAG TTA ACC GAA TTT GCC CGA TG
BspsaBR2EcoRI	CGC GAA TTC ATG GCA TTA AGA TTT CCA AGG

-Real-time qPCR

BsqpsaBF1	TCG CTA TTC CCG GAG CCA GAG G
BsqpsaBR1	AGT TCC CGC TCC TTG GGA GGT

---

psbA

- Subcloning

BspsbAF1XbaI	CGC TCT AGA TTA TCC ATT TGT AGA TGG AGC TT
BspsbAR1BamHI	CGC GGA TCC ATG ACT GCA ATT TTA GAG AGA CG

-Real-time qPCR

BsqpsbAF1	TGG AGG AGC AGC AAT GAA CGC T
BsqpsbAR1	AGA CGC GAA AGC GAA AGC CT

16SrRNA

- Subcloning

Bs16SF2XhoI	ACA CTC GAG CCG CAC AAG CGG TGG AGC AT
Bs16SR2BamHI	CGC GGA TCC GTG ATC CAG CCG CAC CTT

-Real-time qPCR

Bsq16SF2	GGA GCT GGC CAT GCC CGA AG
Bsq16SR2	GGT GAT CCA GCC GCA CCT TCC

18SrRNA

- Semi-quantitative RT-PCR

18SrRNAF2	GCA TTT GCC AAG GAT GTT TT
18S rRNA	CAC CAC CAC CCA TAG AAT CAA G

ATG8

- Subcloning

AtATG8aSalIF1	AGA GTC GAC ATG GCT AAG AGT TCC TTC AAG AT
AtATG8aBamHIR1	AGA GGA TCC TCA AGC AAC GGT AAG AGA TCC

ABD2

- Subcloning

AtfABD2F1NcoI	ATA CCA TGG CAG ATC CTC TTG AAA GAG CTG AAT TG
AtfABD2R1BamHI	ATA GGA TCC ATT CGA TGG ATG CTT CCT CTG

NLS

- Subcloning

NLS-GFP-NcoI	ATC CAT GGT GCC AAA AAA GAA GAG AAA GGT AGA AGA CCC CGT GAT GGT GAG CAA GGG CGA
EGFPR2NotI	CGCGCGGCCGCGTCACTGGATTTTGGTT

Lifeact

- Subcloning

Lifeact-GFP-NcoI	ATC CAT GGG TGT CGC AGA TTT GAT CAA GAA ATT CGA AAG CAT CTC AAA GGA AGA AGT GAG CAA GGG CGA GGA
EGFPR2NotI	CGCGCGGCCGCGTCACTGGATTTTGGTT

PTS1

- Subcloning

EGFPfowardC1	AAA CCA TGG TGA GCA AGG GCG AG
SKLreverse	AAA GGA TCC CTA CAG CTT GCT CTT GTA CAG CTC GTC CAT GC